Département de Chimie
Université de Fribourg (Suisse)

ELECTRON-DRIVEN CHEMISTRY OF SATURATED COMPOUNDS CONTAINING OXYGEN OR NITROGEN ATOMS

THESE

présentée à la Faculté des Sciences de l'Université de Fribourg (Suisse)
pour l'obtention du grade de *Doctor rerum naturalium*

par
Bogdan Cătălin Ibănescu
de Iaşi (Romania)

Numero de la thèse: 1628
Uniprint
2009

Acceptée par la Faculté des Sciences de l'Université de Fribourg (Suisse) sur la proposition du jury:

Prof. Peter BELSER, Université de Fribourg, présidente du jury,
Prof. Michael ALLAN, Université de Fribourg, directeur de thèse,
Prof. Petra SWIDEREK, Universitt Bremen, Institute of Applied and Physical Chemistry,
Prof. Thomas BALLY, Université de Fribourg.
Fribourg, le 20 mars 2009.

Le Directeur de thèse:

Prof. Michael ALLAN

Le Doyen:

Prof. Titus JENNY

To my loving wife, Catalina,
and
to my parents.

Contents

Résumé

L'objectif de ce travail est d'améliorer notre compréhension concernant les processus d'attachement dissociatif par impact éléctronique engendrés par des résonances Feshbach.

L'attachement dissociatif représente une classe importante des processus dus à la réaction avec des éléctrons. Dépendant de la nature de la résonance (l'ion négatif temporel) qui engendre les processus d'attachement dissociatif, ces-derniers peuvent être divisés en plusieurs types. Les processus dus à des résonances Feshbach sont probablement les moins compris. Ils apparaissent à des energies situées entre 6-15eV et sont très importants, car ils apparaissent dans la plupart des composés où les processus d'attachement dissociatif ont été étudiés et parce qu'ils ont souvent des sections efficaces substantielles. Généralement très peu est connu concernant l'assignement de ces résonances responsables des bandes d'attachement dissociatif. Encore moins est connu sur les méchanismes de dissociation. De plus, ce groupe de bandes est souvent responsable d'une fraction signifiante de la chimie induite par des électrons. Des bandes dans cette région d'énérgie ont été rapportées dans la domaine des dommages causés à l'ADN par des électrons, laissant supporser que ces résonances de type Feshbach peuvent être responsables également pour de la chimie induite par des éléctrons dans des biomolécules en phase condensée.

Une approche initialement expérimentale a été choisie. Les spectres d'attachement dissociatif ont été mesurrés pour une série de composés similaires, permettant l'identification de tendances dans les types de fragmentation et des phénomènes comme la rélectivité d'état ou de position. Cette approche expérimentale a été accentuée car les résonant théories actuelles ne parviennent de loin pas à décrire avec une précison suffisante les résonances Feshbach pour pouvoir tirer des conclusions sur des mechanismes dissociatifs (avec l'exception d'une série d'études menées récemment au sujet de processus d'attachement dissociatif sur H_2O [1, 2]).

Généralement des composés contenant des hétéroatomes (primairement les alcools et les éthers, mais aussi les amines et les thioalcools) ont été choisis, non seulement à cause du rôle important que ces composés jouent en biologie et dans les applications techniques, mais également à cause de la présence des électrons **lone pair** menant à des résonances Feshbach avec des propriétés intéressantes.

Un deuxième objectif de ce travail a été l'amélioration de la compréhension des méchanismes de fragmentation, en utilisant des calculs théoriques, en particulier la méthode TD-DFT pour analyser les surfaces de potentiel des états Rydberg étant des étaux parentels des résonances Feshbach. De plus la méthode 'R-matrix' a été

utilisée pour étudier les resonances Feshbach directement.

Les résultats spécifiques présentés dans cettes thèse sont :

- Les attachements dissociatifs ont été mesurés pour plus de 60 composés, révélant des tendances et règles, apportant certaines évidences dans l'assignement et les méchanismes des processus d'attachement dissociatif.
- Toutes les bandes dans la région des 6-15eV ont pu être clairement assignées à des résonances Feshbach, primairement en comparaison avec leurs états grand-parental cationic et parental neutre Rydberg.
- L'étude des types de fragmentation a révélé dans beaucoup de molécules, que, dû au large excés d'énergie émis lors de la fragmentation des résonances Feshbach, beaucoup de fragments ioniques sont métastables et continuent souvent à se décomposer en perdant des molécules stables comme par exemple H_2 (parfois même deux molécules H_2), C_2H_4, etc.
- La différence dramatique observée dans les types de fragmentation des éthers linéaires et de l'éther cyclique tetrahydrofurane (THF) a été clarifiée comme étant une conséquence de la métastabilité du fragment primaire. Le processus élémentaire intitial du clivage de la liaison C−O est le même dans les deux cas.
- L'étude du méthanol et de l'éthnaol deutérés révèle un cas de séléctivité d'état et position de la fragmentation. La liaison O−H est cassée par des résonances Feshbach avec un trou dans le **lone pair** de l'atom hétérogène, la liaison C−H est cassé par des résonances Feshbach avec un trou dans l'orbitale sigma du groupe alkyle. Cette observation apporte l'évidence de la localisation spatiale de l'excitation dans certaines parties de la molécule, donnée par la localisation du trou.
- Des études sur l'éthanol avec le β-carbone du group ethyle deuteré démontre que les deux atoms H de la molécule H_2, qui peuvent être séparé après la perte initiale d'un atom H, viennent chaqu'un du α- et β-carbone du groupe ethyl, *i.e.* HD est séparé de $CD_3CH_2O^-$ dans toutes les bandes observées.
- Des bandes d'attachement dissociatif non-rapportées jusqu'à présent, assignées à des résonances de contour ont été découvertes aux alentours de 3eV dans les alcools. Ceci montre un effet isotopique *régulier* fort (*e.g.* la perte de D est plus ou moins 10× moins efficace qu'une perte de H dans le cas du méthanol). Ces bandes sont faibles pour le méthanol et l'éthanol, mais deviennent intenses lorsque la dimension du groupe alkyle augmente. Elles sont même encore beaucoup plus intenses dans les dialcools.
- Des bandes d'attachement dissociatif similaires, assignées à des résonances de contour ont été deécouvertes dans des éthers. Une bandes aux alentours de 3.5 eV est souvent observée. Deux bandes apparaissent dans quelques cas. Pour la bande de plus basse énergie la dissociation semble apparatre au seuil thermochimique de la bande.
- Un faible effet isotopique contraire a été trouvé pour plusieurs résonances Feshbach.
- Une règle très générale a été trouvée dans plusieurs molécules, d'après laquelle les deux résonances les plus basses en énergie $^2(n, 3s^2)$ et $^2(\bar{n}, 3s^2)$ dans des molecules contenant de l'oxygène (i.e. alcools, monoethers, diethers

de létylène glycole, etc.), cassent la liaison O−H, mais pas la liaison O−C. Au contraire, la résonance Feshbach située plus haut en énergie, avec des trous dans les orbitales σ du group alkyle, sépare les deux liaisons O−H et O−C.

- L'observation mentionnée ci-dessus a été rationalisée pour les résonances n et $\bar{n}$ observées dans pour le méthanol et léthanol avec des calculs de surfaces de potentiel des états Rydberg parentaux, où une barrière d'activation a été trouvée pour la dissociation O−C, mais pas pour celle de O−H.
- Un essai a été tenté pour étendre les calculs de surface de potentiel des résonances Feshbach montionnés auparavant en utilisant le code 'R-matrix'. Ces calculs ont confirmé que la courbe de potentiel des résonances Feshbach suit celle des état Rydberg parentiels. Cependant, les résonances ont été calculées trop près des états Rydberg. Des problèmes sont survenues à de larges séparations internucléaires, révélant les limites de la théorie actuelle.
- Des études de composés contenant les deux groupes hydroxyl et ether, démontrent que des ponts d'hydrogène ou la présence des deux atomes d'oxygène dans le fragmente neutre peuvent affecter la règle mentionnée ci-dessus concernant la dissociation de O−C et O−H.
- Des études préliminaires sur des amines indiquent qu'il existe une règle de séléction similaire pour la dissociation des liaisons N−C et N−H.
- Des tendances inéressantes ont été trouvées dans les résonances Feshbach de plus haute énergie (*i.e.* avec des trous dans les groupes alkyle) lorsque la dimension du groupe alkyle augmente. Dans les cas étudiés (20 substances), les énergies des bandes d'attachement dissociatif semblent être déterminées seulement par la nature du groupe alkyle partant, indépendamment du reste de la molécule. Ceci montre que des nombreuses résonances Feshbach avec un trou dans les orbitales σ dans cette région, seules celles localisées sur la moitié alkyl mènent à la dissociation.
- Une étude préliminaire d'attachment dissociatif pour des substances contenant des liaisons S−H a été mené sur l'éthanethiol. Les spectres obtenus pour ces modèles sont complétement différents des spectres des molécules contenant un ou deux atomes d'oxygène. Ils sont dominés par des résonances dans la région de 0-3 eV.
- Une réaction ion-molécule efficace a été découverte, où la base forte O^- (préparée *in situ* par DEA de CO_2) arrache le proton (faiblement acidique) du diacetylène C_4H_2.
- Il a été montré que les produits des réactions ion-molécule peuvent atteindre des intensités similaires aux produits d'attachement dissociatif propres même à des pressions surprenament basses et donc générer des fragments artefacts dans les spectres d'attachement dissociatif. Des exemples sont les réactions de O^- et OH^- avec le méthanol et l'éthanol.

Summary

The broad aim of the present work was to improve our understanding of dissociative electron attachment (DEA) processes mediated by Feshbach resonances.

DEA represents an important class of processes leading to electron-driven chemical change. Depending on the nature of the resonance (the transient negative ion) which mediate it, DEA processes can be divided into several types. Out of these, the DEA processes mediated by Feshbach resonances (FR) are probably the least understood. The FR mediated DEA processes occur at electron energies in the 6-15 eV range, and are very important, both because they occur in most compounds where DEA was studied and because they often have substantial cross sections. Very little is generally known about the specific assignment of the resonances responsible for the these DEA bands, and even less is known about the mechanisms of the dissociation. At the same time this group of DEA bands is often responsible for a significant fraction of the electron-induced chemistry. Bands in this energy range have been reported in the electron-induced damage in DNA, suggesting that these Feshbach-type resonances may be responsible even for electron-induced chemistry in condensed-phase biomolecules.

A primarily experimental approach was chosen, where DEA spectra were measured for many related compounds, permitting the identification of trends in fragmentation patterns and phenomena like site and state selectivity. The experimental approach is emphasized because current resonant theories are far from being able to describe Feshbach resonances in polyatomic molecules with a sufficient accuracy to draw conclusions about dissociation mechanisms (with a notable exception of a recent series of studies on DEA in H_2O [1, 2]).

This study concentrates on saturated compounds, because the absence of low-lying unoccupied valence orbitals in saturated compounds simplifies the identification of Feshbach resonances which involve double occupation of Rydberg-like orbitals. The identification of Feshbach resonances is further guided by comparison with the cationic grandparent states of the Feshbach resonances, revealed by UV photoelectron spectra, many of which were recorded within the current work.

Heteroatom-containing compounds (primarily alcohols and ethers, but also amines and thioalcohols) were chosen, both because of the important role this type of compounds play in biology and technological applications, and because the presence of lone pair of electrons in these compounds leads to Feshbach resonances with interesting properties.

A second objective of this work was to improve the understanding of the fragmentation mechanisms using theoretical techniques, in particular the TD-DFT method to study the potential surfaces of the Rydberg states which are the parent states of the Feshbach resonances, and of the R-matrix method to study the Feshbach resonances directly.

The specific results presented in this thesis are:

- DEA processes were measured for more than 60 compounds, revealing a number of trends and rules, which yielded evidence on the assignments and the mechanisms of the DEA processes.

- All the bands in the 6-15 eV region could be convincingly assigned to Feshbach resonances, primarily by comparison with their grandparent cationic and parent neutral Rydberg states.

- A study of the fragmentation patterns in many molecules revealed that, because of the very large excess energy generally released in the fragmentation of Feshbach resonances, many fragment ions are metastable and often fragment further, by losing stable molecules like H_2 (sometimes even two H_2 molecules), C_2H_4, etc.

- The observed dramatic difference in the fragmentation patterns of linear ethers and the cyclic ether, tetrahydrofuran (THF), was clarified as a consequence of metastability of the primary fragments. The initial elementary process of C−O bond cleavage is the same in both cases.

- The study of deuterated methanol and ethanol revealed a case of site and state selectivity of the fragmentation: The O−H bond is broken *via* Feshbach resonances with a hole in the lone pair of the heteroatom, whereas the C−H bond is broken *via* Feshbach resonances with a hole in the σ orbital of the alkyl group. This observation provides evidence of the spatial localization of the excitation in certain parts of the molecule, given by the localization of the hole.

- The study of ethanol where the β-carbon of the ethyl group carries D-atoms revealed that the two H-atoms of the H_2 molecule which is split off after the initial loss of an H-atom come one each from the α and the β-carbons of the ethyl group, *i.e.*, that HD is lost from $CD_3CH_2O^-$ at all the observed bands.

- A DEA band, assigned to a shape resonance, was discovered around 3 eV in alcohols. It shows a strong *regular* isotope effect (*e.g.*, loss of D is about 10× less efficient than loss of H in methanol). These bands are weak in methanol and ethanol, but become strong with increasing size of the alkyl group and even stronger in diols.

- Similar DEA bands associated with shape resonances were discovered in ethers. A band around 3.5 eV is often observed, but two bands appear in some cases. For the lowest band the dissociations appears to occur at the thermochemical threshold.

- A weaker *inverse* isotope effect was found for several Feshbach resonances.

- A very general rule was discovered in many molecules, whereby the lowest two resonances ($^2(n, 3s^2)$ and $^2(\bar{n}, 3s^2)$) in O-atom containing molecules (*i.e.*, alcohols, ethers, monoethers and diethers of ethylene glycol, etc.) decay by breaking the O−H bond, but not the O−C bond. In contrast, the higher-lying Feshbach resonances, with holes in the σ orbitals of the alkyl groups, split both the O−H and the O−C bonds.

- The above observation was rationalized for the n and the $\bar{n}$ resonances in selected compounds by calculations of the potential surfaces of the parent Rydberg states, where an activation barrier was found for O−C, but not for O−H dissociation.

- An attempt was made to extend the above calculations to potential surfaces of the Feshbach resonances themselves, using the R-matrix code. The calculations confirmed that the Feshbach resonance potential curves closely followed the parent Rydberg states. The resonances are calculated too close to the Rydberg states, however, and problems were encountered at larger internuclear separations, revealing the limits of the current state of the theory.

- Study of compounds containing both hydroxyl and ether groups revealed that hydrogen bridges or the presence of two oxygen atoms in the neutral fragment can affect the above O−C and O−H dissociation selection rule.

- Preliminary studies of amines indicate that a similar dissociation selection rule exists also for the N−C and N−H bonds.

- Interesting trends were found in the energies of the higher Feshbach resonance bands (*i.e.*, with holes on the alkyl groups) when the size of the alkyl groups was increased. In all the cases studied (20 compounds), the energies of the DEA bands were found to be determined by the nature of the leaving alkyl group alone, independent of the rest of the molecule. It shows that out of the many Feshbach resonances with holes in σ orbitals present in this region, only those localized on the alkyl moiety lead to dissociation.

- A preliminary study of dissociative electron attachment for thiols was performed on ethanethiol. The spectra obtained for this model molecule are completely different from the spectra of molecules containing one or two oxygen atoms. They are dominated by resonances in the 0-3 eV region.

- An efficient ion-molecule reaction was discovered, where the strong base O^- (prepared *in-situ* by DEA to CO_2) abstracts the (weakly acidic) proton from diacetylene C_4H_2.

- It was shown that products of ion-molecule reactions are formed in similar yields as the proper DEA products even at surprisingly low pressures and thus lead to artifact fragments in the DEA spectra. Examples are the reactions of O^- and OH^- with methanol and ethanol.

Chapter 1

General Introduction

Electron-molecule and electron-atom collisions either in the gas phase, on surfaces or in the condensed phase, initiate and drive almost all the relevant chemical processes associated with radiation chemistry, atmospheric chemistry, stability of nuclear waste repositories, plasma-enhanced chemical vapor deposition (CVD), plasma processing of materials for microelectronic devices and other applications, and novel light sources for research purposes (e.g., excimer lamps in the extreme ultraviolet) and in everyday lighting applications.

Collisions of electrons with molecules and atoms create the energetic species that drive chemical and physical changes of matter in environments that range from plasmas to living tissue. The molecules used to etch semiconductor materials do not react with silicon surfaces unless they are subjected to electronic collisions in the low-temperature, high-density plasmas used in plasma etching and in CVD.

The life sciences are a field where the important role of electron-driven processes is only now beginning to be recognized. It has been shown [3] that low-energy electrons with energies significantly below the ionization energies of DNA molecules can initiate single and double strand-breaking in DNA molecules (fig. 1.1). Sanche and co-workers [3] identified some of the key mechanisms involved as electron attachment processes.

In the field of technology electron induced reactions underpin most of the modern semiconductor industry since it is the reactive fragments produced by electron impact of etchant gases that react directly with the silicon substrate [4]. It has been demonstrated that direct electron reactions may be performed at the individual molecular level using STM based technology thus introducing the prospect of designed synthesis on the nanoscale [5]. Another recent application for chemical processes induced by free electrons is the Focused Electron Beam Induced Processing (FEBIP) where an electron beam dissociates a precursor gas. Depending on the type of precursor, a structure is grown or the substrate is etched. By moving the electron beam, 2D and 3D patterns can be transferred onto or into the substrate. The dimensions of the final structure depend mainly on the electron beam that is used, and can vary from hundreds of micrometers down to a single nanometer [6].

In the upper atmosphere of the Earth and other planets, inelastic electron

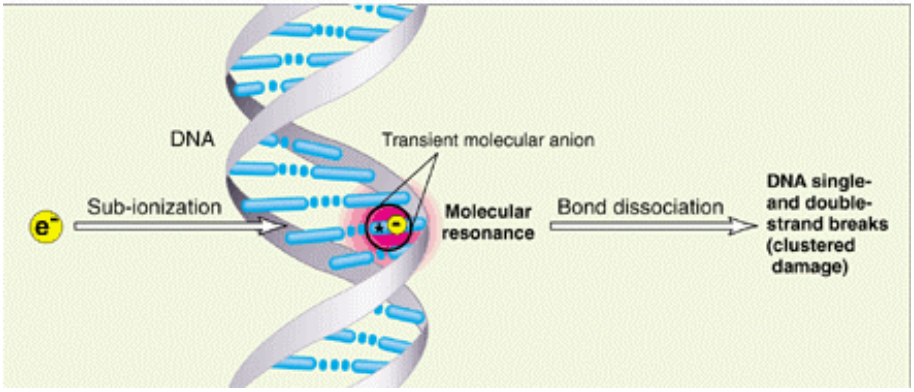

Figure 1.1: DNA single and double strand breaks caused by electrons with energies between 1 eV and 20 eV [3].

molecule collisions lead to thermalization of photoelectrons produced by cosmic-ray or secondary-electron ionization of atmospheric molecules [7, 8]. The Aurora Borealis, which can be seen in the northern sky, occur as a result of ionization of atmospheric molecules by energetic electrons. In the interstellar medium, rotational excitation of molecules in electron collisions is an important mechanism for electron cooling [9, 10, 11]. Electron molecule collisions also play an important role in the physics of supernovae explosions [12]. Electron collision processes such as associative detachment are believed to be responsible for the creation of the hydrogen molecule H_2 at early stages of the universe after the Big Bang. The appearance of H_2 caused an efficient cooling effect of the hot material which eventually led to the creation of stars and galaxies [13].

These are only a few examples of electron-driven processes. However, despite their importance, not all of the physics and chemistry underpinning such processes are well understood and only a few of the required cross sections for electron scattering of the most important molecules are known. To understand any of the above-mentioned chemical and physical changes, the scientific community therefore requires an understanding of the fundamental electron molecule interaction processes that underlie them. The scarcity of experimental data represents an impediment to the development of theory, and the absence of theoretical models makes it impossible to understand the experimental data [14, 15].

At a microscopic level, electron-molecule collisions are much more complicated than electron-atom collisions because of the additional degrees of freedom that are introduced in the target (vibration and rotation of the nuclei) and in the collision process (dissociation of the molecule into two or more fragments). In addition to the dissociation of a molecule into neutral ground-state fragments (neutral molecular dissociation), electron scattering can also result in other dissociative processes such as dissociative excitation, dissociative ionization, and dissociative electron attachment. Dissociation also leads to fragments which are often much more reactive than the parent molecules. This intriguing aspect of electron-molecule collisions gives dissociation processes unprecedented significance in many applications and environ-

ments where the key processes are often initiated by the formation of secondary species *via* a primary dissociative electron-molecule collision.

Electronic collisions are uniquely effective in transferring energy to and from the electronic degrees of freedom of the target atom or molecule. If collisions with photons obey a set of selection rules which is determined primarily by dipole interactions and spin conservation, collisions with electrons can lead to singlet-to-triplet transitions with the same or larger probabilities than singlet-to-singlet or triplet-to-triplet transitions. The reason for this behavior is that the incident electron can be exchanged with those of the target and thereby change its spin state. Thus electron impact can excite more dissociative states of a molecule and thus reduce it to fragments, and this is a key mechanism by which radicals and molecular fragments are produced in many environments ranging from planetary atmospheres to molecular beam sources.

Electron interactions with atoms and molecules in the gas phase have been studied experimentally since the early 20^{th} century. However, the current level of understanding of electron-atom collisions far exceeds our insight into the electron-molecule collision process. Also the vast majority of experiments to date have involved atomic or molecular targets in their electronic ground state and, in the case of excitation, have focused on only a few low-lying excited target states.

The experimental study of electron interactions with ground state atoms has evolved from the Franck-Hertz experiment [16], arguably the first electron-atom collision study, to the realization of the *perfect electron scattering experiment* in which all relevant quantum numbers of the collision complex electron + atom are quantified before and after the collision. The experiment of Frank and Hertz demonstrated the existence of discrete excited states of Hg atoms and helped to confirm the quantum theory that predicted the occupation of discrete energy states by electrons. Since this experiment significant progress has been made in the study of resonances and the effect of electron correlation in electron-atom collisions [14, 15].

1.1 Basic concepts in electron-molecule collisions

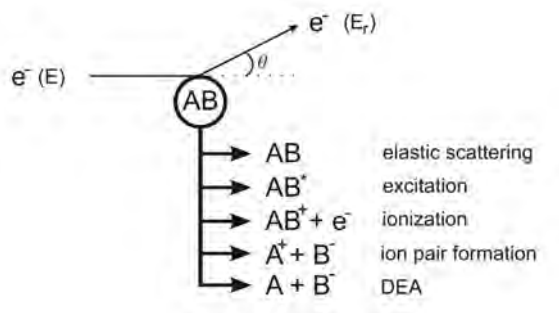

Figure 1.2: Schematic diagram of a collision between an electron with an incident energy E and a target molecule AB.

The collision between an electron and a molecule can lead to the different processes summarized in fig. 1.2. These processes can be divided in two classes: direct scattering and resonant scattering. In the case of direct scattering the electron with the incident energy E collides with a molecule and is scattered at an angle θ with respect to the incident beam, leaving with the residual energy E_r. When the scattered electron has the same energy as the incident electron ($E = E_r$) then the scattering process is called elastic. When energy is transfered to internal degrees of freedom of the target molecule the process is said to be inelastic. Since the mass of the electron is much smaller than that of the target molecule, energy transfer to translational motion is negligible in polyatomic molecules, so the energy distribution of the scattered electrons follows the energy level scheme of the target, that is:

$$\Delta E = E - E_r = E_{el} + E_{vib} + E_{rot} \tag{1.1}$$

where E_{el}, E_{vib} and E_{rot} are the electronic, vibrational, and rotational excitation energies, respectively [17].

If the electron has enough energy then the collision can lead to the ionization of the molecule, dissociative ionization or even ion pair formation is possible:

$$AB + e^- \longrightarrow AB^{+(*)} + 2e^- \tag{1.2}$$

$$AB^{+(*)} \longrightarrow A^{(*)} + B^{+(*)} \tag{1.3}$$

$$AB + e^- \longrightarrow A^+ + B^- + e^- \tag{1.4}$$

This process is used in positive mass spectrometry to produce fragment cations of the target molecule, simply using the electron to provide the necessary energy.

1.2 Resonances in electron-molecule collisions

Non-dissociative, electron-molecule collisions amount to so called resonant scattering. Thereby the electron is trapped for a finite amount of time in the proximity of the molecule, forming a transient negative ion (TNI) with the electron in a quasi-bound state. This state can be regarded as a resonance because it results from an electronic transition from a continuum state ($AB + e^-$) to a quasidiscrete state ($AB^{-\#}$) of the molecular anion.

$$AB + e^-(E_{in}) \longrightarrow AB^{-\#} \tag{1.5}$$

These resonances are characterized by sharp changes in certain scattering cross sections and by transit times that are considerably longer than the normal duration for an electron to pass a molecule. For instance, an electron with a kinetic energy of 2 eV takes 10^{-15} s (1 fs) to travel 10^{-9} m, whereas the lifetime of a resonance is usually much longer than 1 fs. There are several possibilities for the stabilization and decay of the unstable TNI (1.6–1.8):

$$AB^{-\#} \longrightarrow AB^- + h\nu \tag{1.6}$$

$$AB^{-\#} \longrightarrow AB^{(*)} + e^-(E_r) \tag{1.7}$$

$$AB^{-\#} \longrightarrow A^{(*)} + B^{-(*)} \tag{1.8}$$

Reaction (1.6) describes the process of *radiative cooling* in which the anion AB^- is stabilized by the emission of photons. This process is characterized by a lifetime of 10^{-9} s. The second reaction (1.7) is called *autodetachment* where the electron is released from the molecule. The lifetime for this process is in a broad range varying from 10^{-15}s (in the case of small molecules) to 10^{-3}s (for larger molecules). Depending on the energy of the electron released in this process it can either be elastic ($E_{in} = E_r$) or inelastic resonant scattering ($E_{in} > E_r$). The third reaction (1.8) is the *dissociative electron attachment* (DEA). In this process the molecule is stabilized by forming the thermodynamically stable anion B^- and one or more neutral fragments A. In the case of DEA the lifetime is in the range of 10^{-14} – 10^{-12} s.

1.2.1 Classification of resonances

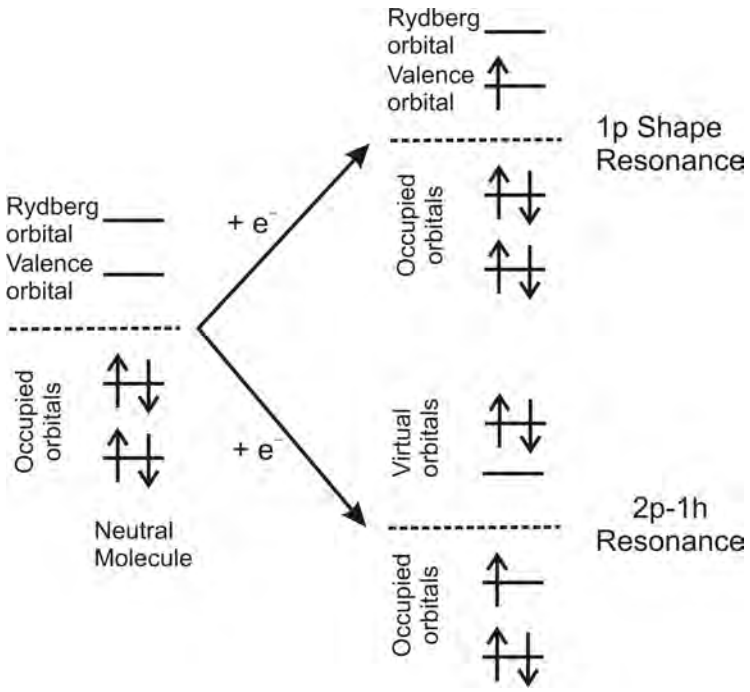

Figure 1.3: Classification of resonances with respect to the capture mechanism.

When classifying resonances, a useful concept is that of the parent state. This is the state of the neutral molecule obtained by a formal removal of the captured electron.

Generally, resonances can be divided into two main groups: single particle (1p) resonances and two particle-one hole (2p-1h) resonances as depicted in fig. 1.3:

- **1p Shape Resonances:** In this case the electron is trapped in a virtual molecular orbital by the *shape* of the potential, which must have a centrifugal barrier. Shape resonances lie energetically above their parent electronic state,

i.e. the ground state of the neutral precursor, to which they can very often decay very efficiently, resulting in a short lifetime.

- **2p-1h Resonances:** The electron can also be trapped by an electronic excitation it has induced in the target molecule. In this case two electrons occupy previously unoccupied orbitals and a hole remains in one of the low lying molecular orbitals. If such a resonance lies energetically below the parent excited state then is called *Feshbach resonance*.

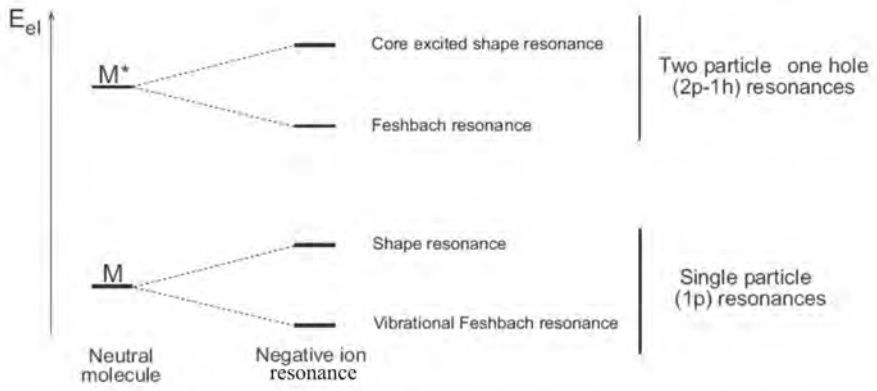

Figure 1.4: Classification of resonances with respect to the energy of the parent state.

A classification of resonances is given in Fig. 1.4. In function of the energy of the resonance relative to the parent state, and the capture mechanism the resonances can be divided in:

- **Shape resonances:** Shape resonances usually occur at energies below 4 eV and have short lifetimes (10^{-15} - 10^{-10} s [18]) because the electron can tunnel through the barrier separating it from the continuum. They are energetically above the parent state and they usually decay through autodetachment. The energies of these resonances can be interpreted in terms of virtual orbital energies and by means of Koopmans' theorem (with empirical scaling), providing valuable information on the unoccupied orbitals of the molecule.

- **Vibrational Feshbach resonances (VFR):** They usually occur at low energies and when vibrational levels of the temporary negative ion are below the corresponding vibrational states of the neutral [19]. VFR are likely to occur in molecules with a large polarizability and a very large dipole moment that leads to a long-range attractive interaction. They may serve as a doorway for dissociation at low energies if they are coupled to a dissociative valence state and can be observed in DEA, as in the case of N_2O [20] and ethylene carbonate [21].

- **Core-excited shape resonances:** They result when the electron capture is accompanied by electronic excitation. The parent is usually a valence state.

They lie energetically above their parent state and often they decay into the parent excited state and can therefore be observed in their excitation functions. These resonances are characterized by small attachment cross sections and thus are only weakly observed in the transmission spectrum.

- **Feshbach resonances (FR):** The parent states of these resonances are usually Rydberg states and they are energetically below their parent states. The decay into the parent state is forbidden resulting usually in longer lifetimes [17]. FR usually have pronounced vibrational structure. The bands of FR associated with Rydberg states of the molecule may have similar band shape as the bands of their parent state and their grandparent state [22] (see section 1.4 for more details).

FR are present in many (perhaps all) molecules. Knowing their dissociation mechanism and the dynamics is important for all molecules, probably even for complex molecules such as DNA. But there are problems in their identification in unsaturated compounds. Therefore much simpler models such as saturated compounds were chosen. The main purpose of the work presented in the following chapters is to understand the dissociation mechanism of FR in saturated compounds. The transferability of the conclusions from saturated to unsaturated compounds is likely to be possible.

1.2.2 Trapping mechanism in shape resonances

This section describes qualitatively the trapping mechanism of the electron in a shape resonance. The purpose is to show the nature of autodetaching electronic states of the anions. A more detailed description can be found in ref. [17].

As the electron approaches the molecule the negative charge induces a dipole in the target molecule. The result is an attractive interaction between the two particles at long distances described by the following potential V_a:

$$V_a(r) = -\frac{\alpha e^2}{2r^4} \tag{1.9}$$

where α is the polarizability of the molecule, e the elementary charge and r the distance between the two particles.

Additionally, a repulsive centrifugal pseudo-potential V_r is generated due to the angular momentum of the electron:

$$V_r(r) = \frac{\hbar^2 \ell(\ell+1)}{2m_e r^2} \tag{1.10}$$

where $\hbar = h/2\pi = 6.6{\cdot}10^{-16}$eV·s, h is the Planck constant, ℓ the angular momentum quantum number of the electron and m_e the mass of the electron.

The effective potential V_{eff} of the interaction is the combination of the attractive and the repulsive potentials:

$$V_{eff}(r) = V_a(r) + V_r(r) = -\frac{\alpha e^2}{2r^4} + \frac{\hbar\ell(\ell+1)}{2m_e r^2} \tag{1.11}$$

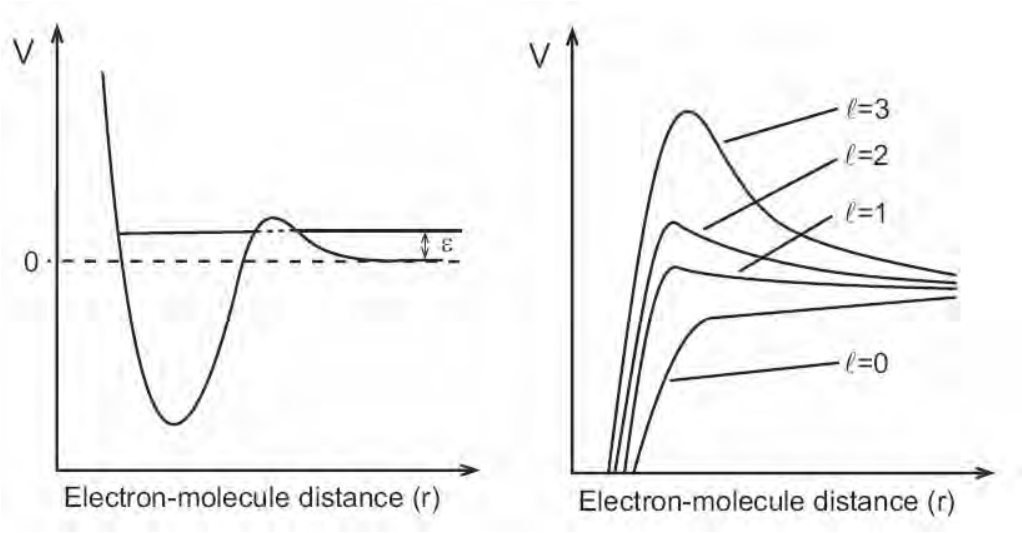

Figure 1.5: Effective potential describing the electron-molecule interaction including Pauli repulsion at small distances (left). On the right the potential barrier for various angular momentum values [17].

The result is a potential barrier for $\ell \neq 0$ as shown in fig. 1.5. The electron has the possibility to tunnel through the barrier and can occupy a quasi-bound state (a discrete electronic state embedded in the continuum) if the molecule has an unoccupied molecular orbital of a symmetry determined by the value of ℓ. At short electron - molecule distances the Pauli repulsion start to become dominant and results in a potential energy curve as shown schematically in fig. 1.5. Due to the fact that the electron is captured by the *shape* of effective interaction potential this resonance is denoted as *shape resonance*. The resonance has a finite lifetime due to back-tunneling of the electron through the barrier formed by the interaction potential.

1.3 Dissociative electron attachment (DEA)

The process of dissociative electron attachment can be explained in more detail using a Born-Oppenheimer potential energy diagram. This representation is complete only for diatomic molecules, whereas for polyatomic molecules it describes a cut through the hyperdimensional surface where Q represents the dissociative reaction coordinate.

In fig. 1.6 such a potential energy diagram is shown for the diatomic molecule AB and the corresponding anion AB^- along the Q(A-B). The capture of the electron is represented by a vertical transition from the ground state of AB to the ground state of AB^-. The potential energy curve for AB^- shown in fig. 1.6 is repulsive in the Franck-Condon region, thus the bond length of the TNI increases spontaneously. The TNI is a thermodynamically unstable species and two competing processes can take place: autodetachment and dissociation. The anionic curve is reached according

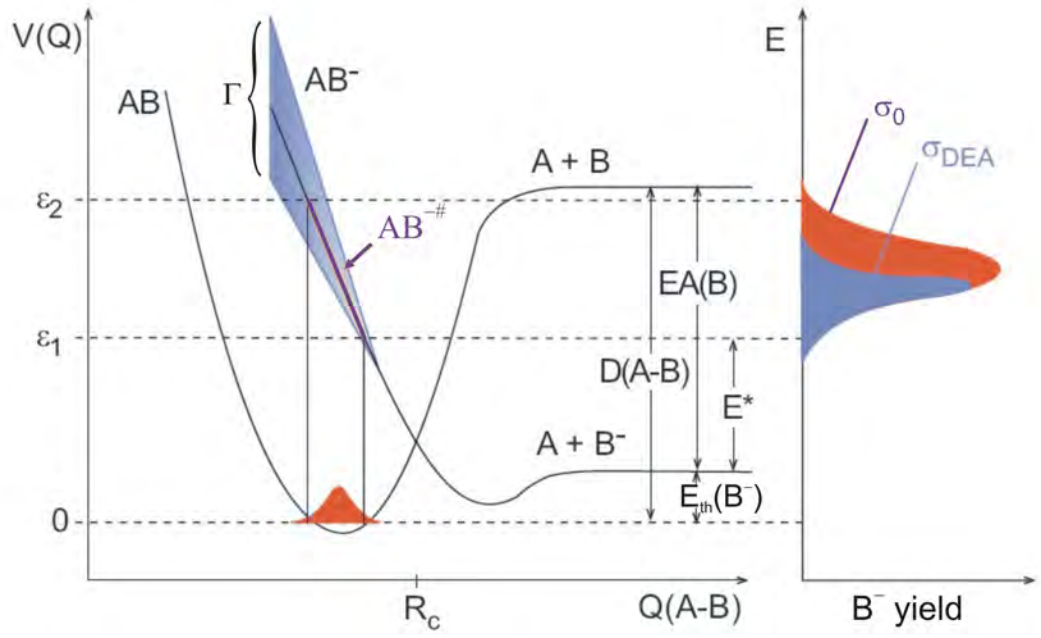

Figure 1.6: Potential energy diagram representing DEA to the target molecule AB. On the right the ion yield is shown. $D(A-B)$ is the dissociation energy of the bond A-B, $EA(B)$ represents the electron affinity of the neutral fragment B, E^* the excess energy and $E_{th}(B^-)$ the thermodynamical threshold for the formation of the B^-

to the energy width of the ground state of AB^- (Γ) and autodetachment is possible until the crossing point R_c where the neutral potential surface is reached. Beyond R_c autodetachment is energetically impossible and dissociation remains the only possible relaxation channel.

The autodetachment lifetime τ is linked to the energy width Γ of the anionic state in accordance with the Heisenberg uncertainty principle:

$$\tau \approx \frac{\hbar}{\Gamma} \tag{1.12}$$

The probability of the anion to survive until R_c is reached depends on the energy and, in general, is higher with lower energy. Additionally τ decreases as the anion approaches the crossing point. Thus the peak maximum of the ion yield is shifted to lower energies as shown on the right side of fig. 1.6 by the blue surface.

The anionic products formed in the dissociation process are usually detected by means of mass spectrometry as a function of the electron energy. The obtained ion yields generally show a resonant profile with a shape that can be considered as a reflection of the initial ground state vibrational wave function at the potential of the anion (*reflection principle*) which is shown on the right side of fig. 1.6. This reflection principle does not take into account autodetachment, but the shape (*i.e.* the width, slope, structures) of the ion yield distribution curve still contains information on

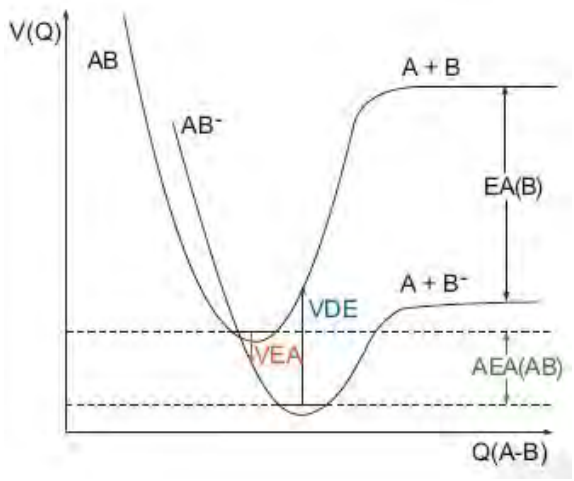

Figure 1.7: Potential energy diagram representing the terms adiabatic electron affinity (AEA), vertical electron affinity (VEA) and vertical detachment energy (VDE).

the nature of the initial Franck-Condon transition and the relative positions of the anionic and neutral potential surfaces.

For the formation of a thermodynamically stable anion the molecule needs to have positive adiabatic electron affinity (AEA). This implies that the ground state of the anion lies below the ground state of the neutral. The energy difference between the neutral ground state and that of the excited state of the anion is denoted as vertical electron affinity. The vertical detachment energy (VDE) is the energy needed to detach an electron from the anion. All these terms are schematically represented in fig. 1.7.

The experimentally observed appearance energy (AE) for the fragment B^- is defined as:

$$AE(B^-) = D(A-B) - EA(B) + E^* \tag{1.13}$$

where $D(A-B)$ is the dissociation energy for the A−B bond, $EA(B)$ the electron affinity of B and E^* the excess energy (as in fig. 1.6).

The thermodynamic threshold energy of the process ($E_{th}(B^-)$) is the minimum energy required for the dissociation of the molecule into $A + B^-$. This is given by the following equation:

$$E_{th}(B^-) = D(A-B) - EA(B) \tag{1.14}$$

The excess energy of the dissociation process can be obtained as the difference between the experimental appearance energy and the thermodynamical threshold for the formation of the corresponding ion. This excess energy is usually transfered either to kinetic energy or it is distributed between various internal degrees of freedom (vibrational, rotational or electronic) of the neutral and anionic fragments.

In conclusion, the *position* of the observed signal in the ion yield curve is dependent on the VEA convoluted with the (energy dependent) probability for disso-

ciation into a particular ion, and the *intensity* of the signal is determined by the autodetachment rate and the Franck-Condon vibrational wavefunction of the initial transition.

1.3.1 The dissociative electron attachment cross section

The efficiency of a DEA process can be expressed by the DEA cross section (σ_{DEA}). DEA can be understood as proceeding in two steps: first the resonance is formed and then dissociation can take place. Therefore, σ_{DEA} can be expressed as:

$$\sigma_{DEA} = \sigma_c(E)P(E) \tag{1.15}$$

where $\sigma_c(E)$ is the electron capture cross section and $P(E)$ is the probability for the resonance to dissociate.

One approximate expression for $P(E)$ is given in ref. [23]:

$$P(E) = e^{-\frac{\tau_{DEA}}{\tau_{AD}}} \tag{1.16}$$

where τ_{DEA} is the time required for the resonance to dissociate and τ_{AD} is the lifetime of the anionic electronic state and can be linked to Γ by the equation (1.12).

From this equation it follows that as the τ_{AD} decreases $P(E)$ exponentially approaches zero. In other words, if τ_{DEA} is much longer than the lifetime of the anion state then the probability for dissociation is very small.

1.4 The link between DEA and PE spectrometry

The present study concentrates on the study of Feshbach resonances in saturated compounds. The identification of such resonances is guided by the comparison with the cationic grandparent states of the Feshbach resonances, revealed by UV photoelectron spectra. This approach in the identification of Feshbach resonances in polyatomic molecules has been first shown by Skalický and Allan [22].

To identify Feshbach resonances we have used the relation between the grandparent cationic state, the parent Rydberg state and the daughter Feshbach resonance. Fig. 1.8 shows this relation on the argon atom [25] because in this case the relation can be followed experimentally. The grandparent states are visible in the photoelectron spectrum, the parent states are observable in the electron energy loss spectrum while the elastic cross section spectrum or the DEA spectrum gives informations concerning the Feshbach resonances.

Adding an electron into a Rydberg orbital around a positive ion core releases about 4 eV of energy – the term value. Another about 0.4 eV, the electron affinity of the Rydberg state, are released when a second electron is added to an $3s$ Rydberg state, leading to a short-lived Feshbach resonance involving two strongly correlated electrons localized on a potential-energy ridge [26]. Both energies are to some degree independent of the molecule because of the weak penetration of the core by the

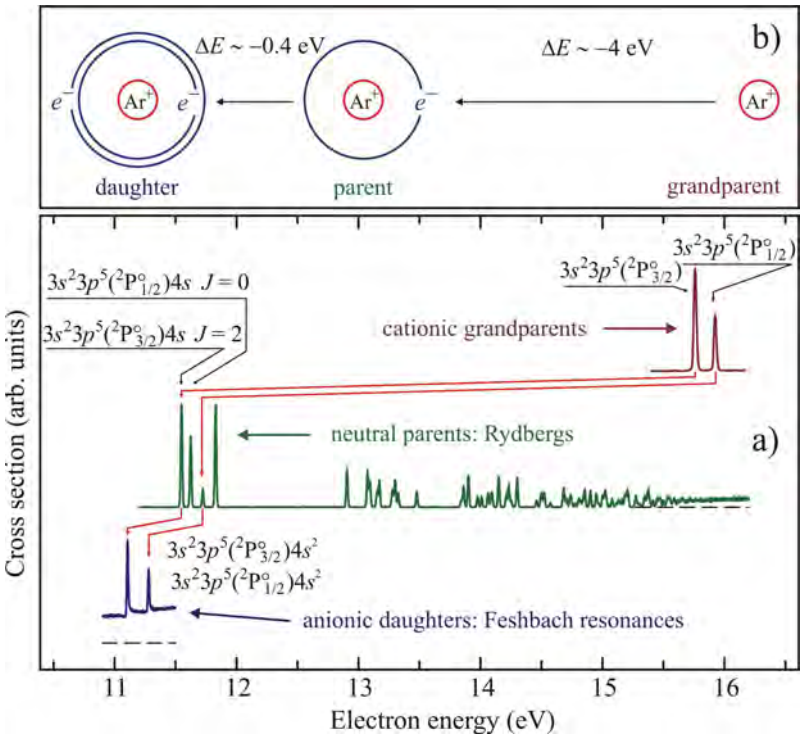

Figure 1.8: Figure illustrating the descendancy relations between the grandparent cation, parent Rydberg and Feshbach anion states on the example of Ar. a) The photoelectron spectrum (top), the electron energy loss spectrum (center), and the elastic cross section [24] (bottom) of argon. (The energy-loss spectrum was recorded at a scattering angle of $\theta = 135°$ and a residual energy of 1 eV, the elastic cross section at $\theta = 117°$.) b) Schematic diagram of the electron configurations, with the daughter Feshbach resonance having two highly correlated electrons moving in a Rydberg-like orbital.

diffuse Rydberg electron cloud, and this fact will be used to predict the energies of the Feshbach resonances from ionization energies determined by photoelectron spectra. The method is important in the case of polyatomic molecules with Feshbach resonances without sharp structures, which can not be detected in elastic cross section or by other means.

A more detailed investigation of many molecules revealed that the $3s$ term values are not entirely constant for different molecules, but decrease with increasing degree of alkylation, because bulky substituents penetrate even a large Rydberg orbital [27]. As an example, the $3s$ term value of ethanol is 3.8 eV, and this value decreases with increasing alkylation until it reaches a limiting value of about 2.8 eV for very bulky alkyl substituents [27]. Likewise, the energy relation between the Rydberg states and the Feshbach resonances has been studied in detail for a number of atoms and molecules [25, 28, 29, 30, 31], and is not entirely independent of the target.

Even with these limitations, the energy relation between the grandparent state

and the daughter Feshbach resonance represent a useful tool for assigning DEA band to Feshbach resonances, as it has been shown by Skalický and Allan [22] and in the present work [32].

1.5 Objectives

For most compounds DEA fragmentations are observed at electron energies in the 6-15 eV range, sometimes with substantial cross sections, but very little is generally known about the assignment of the resonances responsible for the corresponding bands in the DEA spectrum, and even less is known about the mechanisms of the dissociation. These DEA bands are generally assigned as to be of the Feshbach resonance type, with two excited electrons, but only rarely has a specific assignment been given. At the same time DEA bands in the 6-15 eV range is often responsible for a significant fraction of the electron-induced chemistry. Bands in this energy range have been reported in the context of electron-induced damage in DNA [3, 33], suggesting that Feshbach-type resonances may be responsible even for electron-induced chemistry in condensed-phase biomolecules.

The broad objective of the present work is to shed more light on the assignment of DEA bands in the 6-15 eV range, region that has been neglected in the literature, learn more about the properties of the resonances involved, and about the mechanisms of the fragmentation.

In this work, a primarily experimental approach was chosen, *i.e.* DEA spectra were measured for many related compounds, permitting the identification of trends in fragmentation patterns and phenomena like site and state selectivity. The experimental approach was emphasized because current resonant theories are far from being able to describe Feshbach resonances in polyatomic molecules with a sufficient accuracy to draw conclusions about dissociation mechanisms (with the notable exception of a recent series of studies on DEA in H_2O [1] and C_2H_2 [34]).

The present study concentrates on saturated compounds, because Feshbach resonances generally involve double occupation of Rydberg-like orbitals, and the absence of low-lying unoccupied valence orbitals in saturated compounds simplifies the identification of Feshbach resonances. The identification of Feshbach resonances is further guided by comparison with the cationic grandparent states of the Feshbach resonances, revealed by UV photoelectron spectra, many of which needed to be recorded within the current work.

Heteroatom-containing compounds (primarily alcohols and ethers, but also amines and thioalcohols) were chosen, both because of the important role this type of compounds play in biology and technological applications, and because the presence of lone pairs of electrons in these compounds leads to Feshbach resonances with interesting properties.

A second objective of this work was to improve our understanding of the fragmentation mechanisms using theoretical techniques. In particular we used the TD-DFT method to study the potential surfaces of the Rydberg states which are the

parent states of the Feshbach resonances, and the R-matrix method to study the Feshbach resonances directly.

1.6 Layout of the thesis

Chapter 2 describes the experimental methods used to observe the dissociative electron attachment of molecules. Improvements on the experimental setup are also presented. The chapter is concluded with a description of various computational methods used in the work.

In chapter 3 the dissociative electron attachment of substances with one or two hydroxyl groups is presented. The main results are published in ref. [32] reprinted in section 3.2. Additional results, not published in the article, include the DEA spectra of propanols and butanols, the pressure dependence of the anion yield for methanol and ethanol and the relative intensity test for deuterated methanols.

Chapter 4 is dedicated to the study of dissociative electron attachment of different ethers. First, a striking difference is observed between the fragmentation pattern of cyclic ethers, such as tetrahydrofuran, and that of open-chain ethers, such as diethylether or dibutylether. These results are published in ref. [35] and reprinted in section 4.1. Secondly, the analysis of the dissociation *via* Feshbach resonances is performed in various ethers, acetals and ethers of ethylene glycol. The main results are published in ref. [36] and reprinted in section 4.2.

The study of saturated compounds is extended to amines in chapter 5. This chapter shows that the main conclusion noticed in oxygen, namely the use of the methyl group as a protective group, the dependence of the energy for the observed DEA band on the alkyl group and the non-dissociative nature of the $^2(n, 3s^2)$ resonance, are applicable also to compounds with nitrogen, with minor differences. Some special cases are also presented.

In chapter 6, a striking difference is presented between the dissociative electron attachment of alcohols and that of ethers. To explain this difference the relation between the Feshbach resonaces and their parent Rydberg state is used. First, the potential energy surfaces of Rydberg states are calculated using the TD−DFT method. Thereby we could explain the experimental observations, under the assumption that the potential energy surface of the Feshbach resonances are similar to those of the parent Rydberg states. In the last section an attempt to calculate the Feshbach resonances is presented, in order to verify the above mentioned assumption. The main results from this chapter are published in ref. [37], reprinted as section 6.2.

Chapter 7 presents a preliminary study for the dissociative attachment for compounds with S−H bond on the example of ethanethiol. The DEA spectra of this model molecule prove to be completely different from the spectra of oxygen containing compounds.

In chapter 8 the absolute cross sections for dissociative electron attachment in the case of acetylene and diacetylene are determined. The author's contribution to

this work is the determination of relative mass resolved cross sections in the case of acetylene and diacetylene. These results are published as ref. [38] and are reprinted in section 8.1. Additionally, pressure tests have been performed to determine the influence of the calibrating gas on the studied molecules.

In conclusions (chapter 9) the results are summarized and suggestions for improvements of the calculations are given.

Chapter 2

Experimental and theoretical methods

In this chapter we first describe the experimental methods used to observe the dissociative electron attachment of molecules. Improvements on the experimental setup are also presented. The second part of the chapter is dedicated to a description of various calculation used in the work. The last part presents the synthesis of molecules analyzed in this work that were not commercially available.

2.1 Experimental setups

To analyze electron molecule collisions we used two different experimental setups: a dissociative electron attachment spectrometer to obtain negative ion yields as a function of the electron energy, and a photoelectron spectrometer to obtain the ionization spectrum of molecules. Photoelectron spectra are useful in the assignment of Feshbach resonances, as it has been shown in ref. [22].

2.1.1 Dissociative electron attachment spectrometry in gas phase

2.1.1.1 Description of the spectrometer

DEA reactions were studied by means of a crossed electron-quasistatic target gas arrangement, shown in figure. 2.1. It has been described previously [23, 39], but has been improved within the present work. The improvements were made to the calibration procedure, a new set of voltages used to detect the very light H^- and D^- ions and better control of the pressure in the target chamber.

The experimental setup is housed in a stainless steel high-vacuum chamber, pumped by a diffusion pump to a base pressure lower than 10^{-7} mbar. A rotary vane pump backs the diffusion pump.

The dissociative electron spectrometer follows the design principles pioneered

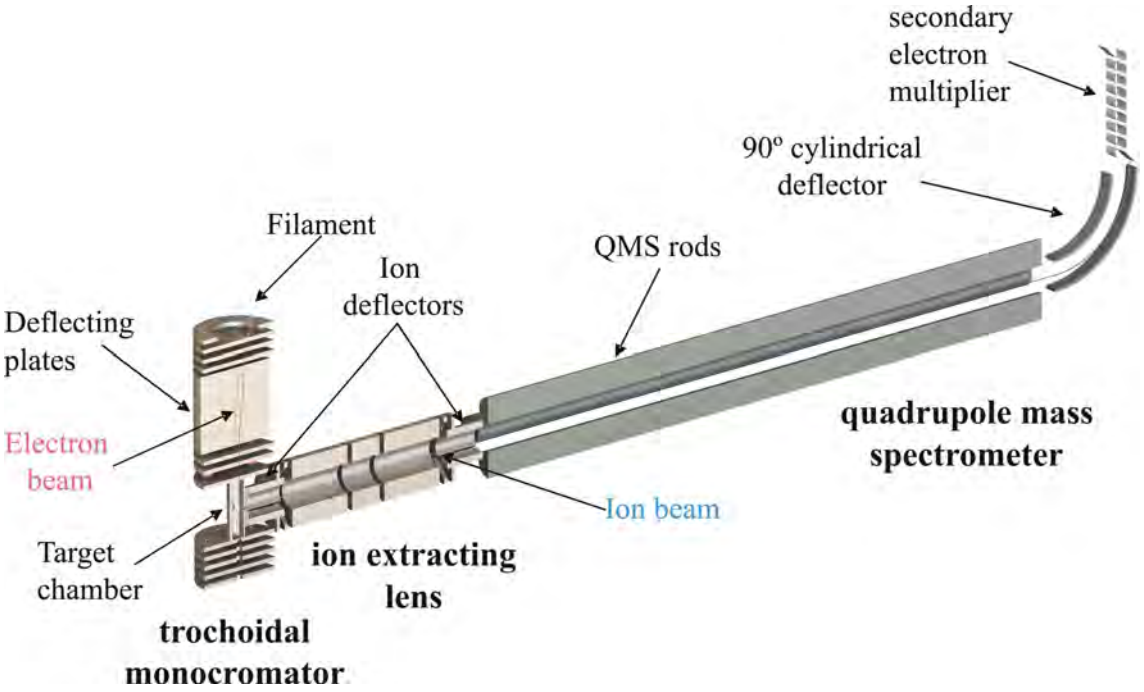

Figure 2.1: Scheme of the experimental setup used for dissociative electron attachment to gas phase molecules.

by Stamatovic and Schulz [40, 41]. It consists of an trochoidal electron monocromator that generates a quasi-monoenergetic electron beam which is directed to a target chamber where it collides with sample molecules, a mass filter and ion detector that is used to mass select and count the ions generated in the dissociative attachment process [23]. To mass-select the ions we used a quadrupole mass filter, with a secondary electron multiplier as the ion detector (fig. 2.1). The rods of the quadrupole mass spectrometer are housed in a separated high-vacuum chamber differentially pumped by a second diffusion pump backed by a rotary vane pump.

The molecules are introduced into the target chamber with the help of a gas-inlet system through a leak valve. The gas inlet system is equipped with two leak valves and a CO_2 gas cylinder, allowing for rapid switching of gases for calibration purposes. Additional connections for gaseous or liquids samples are also present. The system can be pumped out by a rotary vane pump, when switching samples and for the freeze-thaw cycle, and can be heated with a heating band up to 120 °C.

2.1.1.2 Generation of the monoenergetic electron beam

In the current experimental setup the electrons are emitted from a hot filament, supplied with a current of 4.5-4.7 A, through thermionic emission. These electrons are attracted and directed towards the crossed electric and magnetic field region of the trochoidal electron monocromator [40, 41] by two electrodes. The first three electrodes have off-axis apertures and accelerate and guide the electrons into the selection region. The selection region together with the rest of the spectrometer

is immersed in the magnetic field generated by two main coils mounted inside the vacuum chamber. To compensate for any external influences the system includes two additional correction coils. The homogeneous electric field is generated by a parallel-plate capacitor, with two plates, notes as *D-plates*, which are symmetric vertical cut-aways of a cylinder. Due to the presence of both fields the electrons move on trochoidal trajectories with the guiding center moving in a direction (z) perpendicular to both fields. The drift velocity (v_z) depends on the strength of the electric field (E) and the magnetic field (B) according to [40, 41]:

$$v_z = \frac{\left|\vec{E} \times \vec{B}\right|}{B^2} \tag{2.1}$$

The monoenergetic electrons are accelerated to the final energy, by two electrodes and introduced into the target chamber. The first of these two electrodes has two apertures, one off-axis and other one on axis, to aid with the initial alignment. The second electrode has only one aperture on axis. The displacement between the two apertures influences the energy spread $\Delta\omega$ of the electron beam [41]:

$$\Delta\omega = \frac{E^2 L^2 m}{D^3 B^2}\Delta D + eES_1 \tag{2.2}$$

where L is the length of the D-plates, D the displacement between the entrance and exit aperture, ΔD the sum of diameters for the entrance and exit apertures and S_1 the diameter of the entrance aperture. This equation excludes the transverse momentum contribution. During experiments the resolution of the electron beam can be controlled by changing the relative potential on the two D-plates and hence the electric field E.

The transmitted electrons are collected by the final set of electrodes. All the electrodes of the trochoidal electron monochromator and the target chamber, are made of molybdenum (generally considered a good material for working with electron beams of small energy because of its homogeneous surface potential), centered and isolated from each other by ruby balls.

2.1.1.3 Ion detection

The negative ions produced by the dissociative attachment processes are extracted by an electric field produced by an electrode. They are focused by a series of three electrodes on to the entrance of the quadrupole mass spectrometer (QMS). All the electrodes of the ion extracting lens are also made of molybdenum. They are centered and separated by ruby balls. The extracting electrode is separated from the others by a ceramic ring, replacing the ruby balls due to lack of physical space. The ion lens is made from three different sections. They are used to guide and focus the ion beam to the entrance of the QMS. The first and last sections are divided in four pieces to deflect the ions and compensate for the magnetic field.

Voltages are applied to the rods of the QMS with a superposition of alternating voltage (amplitude V) and direct voltage (U) creating an alternating electric

quadrupole field that guides the ions on oscillating trajectories. Depending on the U/V ratio only ions with a certain mass to charge ratio follow stable trajectories. All other ions hit the rods and are neutralized. In relation to metastable ions often encountered in this work it is important that the flight-time of an ion through the quadrupole is approximately 50 μs. Ions that decay within the QMS are not detected either.

The transmitted negative ions are collected by the first dynode of a 16 stage secondary electron multiplier (SEM). By subsequent secondary-electron emission and acceleration to the respective next dynode an electron pulse is generated at the collector. The time resolution given by SEM is in the order of 10^{-8} seconds and the gain is over 10^6. The final pulse is decoupled from the high voltage supplied to SEM by a capacitor, amplified by a preamplifier and then transformed into a TTL pulse by a discriminator with TTL output. The TTL pulse is read by an interface card of a personal computer and displayed as ion counts.

2.1.1.4 Modes of operation

The current software used to record the spectra allows the dissociative attachment spectrometer to be run in three different modes of operation: *electron transmission spectrum* mode, *dissociative electron attachment spectrum* mode and *mass spectrum* mode.

- **Electron transmission spectrum mode**: In this mode the incident electron energy is scanned and the current of transmitted electrons is measured. The transmitted current is plotted against the incident electron energy in a *electron transmission spectrum*. This mode does not make use of the quadrupole mass spectrometer.
- **Dissociative electron attachment spectrum mode**: In this mode the spectra are obtained by scanning the incident electron energy and the ion count is measured at the SEM. The ion count is plotted against the incident electron energy. This mode makes use of the quadrupole mass spectrometer to detect the ions of desired fixed mass.
- **Mass spectrum mode**: In this mode the incident electron energy is kept constant and the ion mass is being scanned. The ion yield is plotted against the ion mass.

2.1.1.5 Calibration of the energy scale

One of the main problems when using an experimental setup such as the current one is the calibration of the energy scale. This an important issue because there are several factors affecting the energy scale. The first factor is that the voltage used by the trochoidal electron monochromator to accelerate the electrons is different from the electron energy. This is the result of the fact that the electron moves axially and transversally with respect to the monochromator, and the applied voltage influences

only the axial motion, leading to uncertainties in the determination of the electron energy. This problem is corrected by the use of a calibrating gas that presents spectroscopic features at precisely defined energies.

Another problem is that the energy scale drifts over time due to changing conditions in the experimental setup over the time of the measurement. These drifts are usually very small and can be compensated by recalibrating the energy scale at defined intervals of time, usually after one day. A third problem is that the electrodes used are quickly covered by a thin isolating film. This is due to the use of diffusion pumps and because the sample is absorbed on the surface during the measurements. Using turbomolecular pumps will decrease the severity of the problem but at the same time would adversely affect the magnetic field in the trochoidal electron monochromator, dramatically reducing the resolution of the spectrometer. The effect of the isolating film is that the electrodes are covered with a small negative charge when the electron beam is used. The charged film then repels the slow electrons. This leads to a cut-off of the transmission spectrum and the spectrum starts artificially at a value different than zero. Such a situation is presented in fig. 7.4 on page 133. This is usually called the *charging effect*.

A similar effect is given by the fact that the entrance and the exit apertures of the target chamber are, after long exposure times, affected by the electron beam and change their chemical structure. This change generates a small isolating film at the entrance and the exit of the target chamber, which in turn generates a small potential barrier for the electron beam, stopping the slow electrons. In a very well maintained spectrometer this effect is usually in the order of several meV and thus negligible.

This effect cumulated with the charging effect are particularly important when recording signals at very low energies, close to 0 eV. Such is the case when the calibration is performed with SF_6. SF_6 forms metastable SF_6^- by s-wave electron capture very close to 0 eV electron energy with a very large cross section. Because of the charging effect the peak at 0 eV can be cut off leading to errors in the calibration of the energy scale. These effects are particularly difficult to correct and the only solution is to disassemble the spectrometer and clean the electrodes.

To reduce such calibration errors, we have calibrated the energy scale using another gas: CO_2. It is well known [42, 43] that dissociation of CO_2 by electrons produces O^- ions at 4.4 eV and 8.2 eV. We used the onset of the first vibrational band at 3.998 eV to calibrate the energy scale.

The shape of the band gives an indication on the resolution of the electron beam. Fig. 2.2 shows the 4.4 eV band of O^-/CO_2 recorded at two different resolutions: 70 meV and 160 meV respectively. To calibrate our energy scale we set 75% of the first vibrational band at 3.998 eV. But this band it is not visible in the transmission spectrum recorded at 160 meV resolution, introducing errors into the calibration of the energy scale. To determine these errors we considered that the spectrum recorded at 70 meV is properly calibrated and shifted the 160 meV curve (red curve in fig. 2.2) until they overlap. The 3.99 eV corresponds to 67% of the observed band and the estimated error in the calibration when the wrong percentage is used

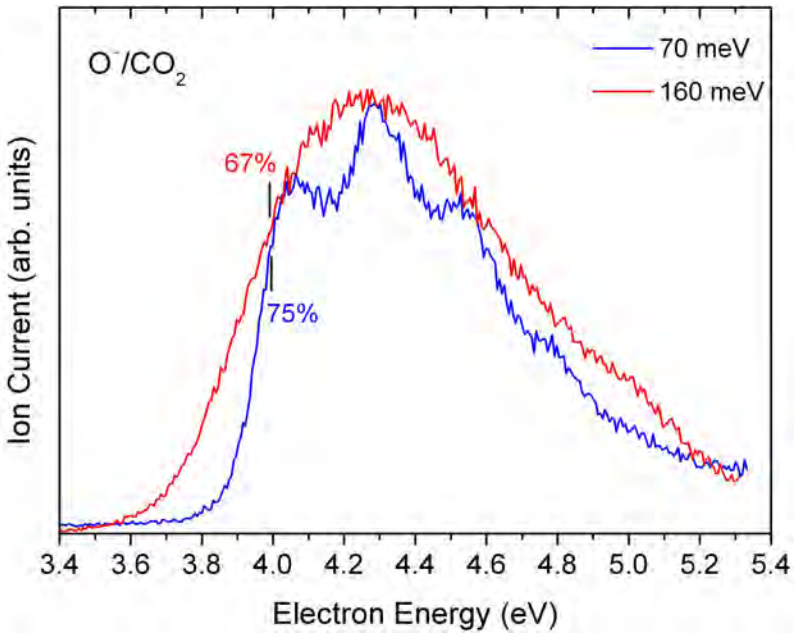

Figure 2.2: The 4.4 eV band of O^-/CO_2 recorded at different electron beam resolutions. The calibration point is also indicated.

is about 0.05 eV.

Most of the DEA processes presented in this work have very low cross sections. This means that a long recording time is required to improve the signal-to-noise ratio. During the recording time the energy scale can drift and the spectra need to be corrected for this drift. A new calibration algorithm has been developed to correct the drift especially for long term measurements.

This algorithm uses the transmission spectra as a tool to detect the drift during the recording time. The initial transmission spectrum is calibrated using the onset of O^-/CO_2 and subsequent transmission spectra are shifted so that the inflexion point is at the same energy in all the spectra. Once the drift has been determined this is applied to the dissociative attachment spectrum associated with the respective transmission spectrum. The transmission and the DEA spectra are recorded alternately at determined intervals. The interval is selected such that the drift between two consecutive spectra is kept to a minimum.

The use of the above-mentioned algorithm improves the resolution for the recorded spectra especially for recording times longer than 8 hours and it is very easy to automatize. Previous calibration techniques were more difficult to automatize since they required the manual introduction of the calibrating gas in the target chamber, and dramatically restricted the recording time. Still, the use of the new algorithm has one disadvantage. Since it uses the transmission spectrum as a tool for calibration, one requirement is that the onset of the spectrum does not change during the recording. This is particularly a problem due to the charging effects of the electrodes induced by the sample and care must be taken to avoid or to compensate for this effect.

2.1.1.6 Detection of the H^- ions

Another improvement done to the experimental setup during this work is the development of a procedure to record the appearance of the very light ions, H^- or D^-. They are particularly difficult to detect in this type of instruments because the magnetic field required for the operation of the trochoidal monochromator is perpendicular to the ion path and deviates the light ions in the ion transporting lens, preventing them from reaching the quadrupole mass spectrometer.

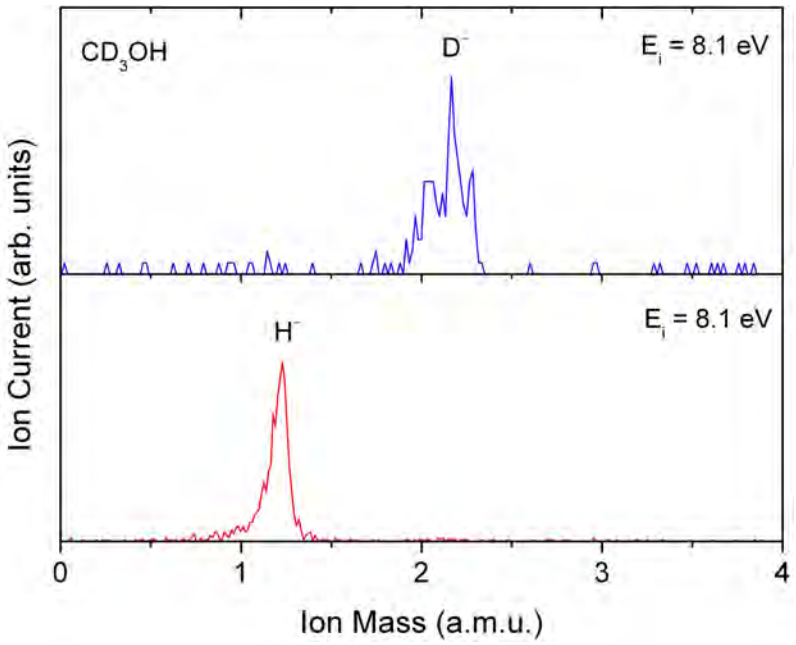

Figure 2.3: Different mass spectra recorded with two sets of voltages for the detection of H^- and D^-, respectively, in the case of methanol-d_3, showing the selectivity of the ion lens.

Thus a new set of voltages have been determined to record these light ions. They are incompatible with the voltages used for the recording of other ions. Thus two new modes have been introduced into the software, one for H^- and D^- ions and a second one for heavier ions. The set of voltages are applied to the electrodes of the ion lens, improving the guiding for H^- and D^- but, at the same time, decreasing the guiding of the other ions.

The usefulness of the new set of parameters is exemplified in fig. 2.3 for the partially deuterated methanol, CD_3OH. In this case both H^- and D^- have been detected. By appropriately compensating the deflection of the magnetic field using the two pairs of x, y deflectors, situated near the entrance and the exit of the ion lens, we can selectively record either H^- or D^-.

2.1.2 Photoelectron spectroscopy

2.1.2.1 General principles

When a high energy photon strikes an atom or molecule (M), photoionization may result and photoelectrons are emitted:

$$M + h\nu \rightarrow M^+ + e^- \tag{2.3}$$

In photoelectron spectroscopy high energy monochromatic radiation, in our case the 58.4 nm (HeI) emission of a He discharge lamp, is directed on a gaseous sample to be studied. The photoelectrons ejected from the sample are detected at a right angle to the light beam and counted as a function of their kinetic energy (K) by an electron energy analyser. That is, the photoelectron spectrometer produces a graph of the number of electrons ejected *vs.* their kinetic energy. Since the relationship between ionization energy, I_j, and K for an atom is simply given by:

$$K = h\nu - I_j \tag{2.4}$$

one can plot the data as number of electrons detected at each energy (counts/sec) *vs.* the ionization energy (eV), and such a plot is called a photoelectron spectrum. If the species is a molecule, there are additional possibilities of vibrational or rotational excitation on ionization, and the energies of the photoelectrons may be reduced:

$$K = h\nu - I_j - E^*_{vib,rot} \tag{2.5}$$

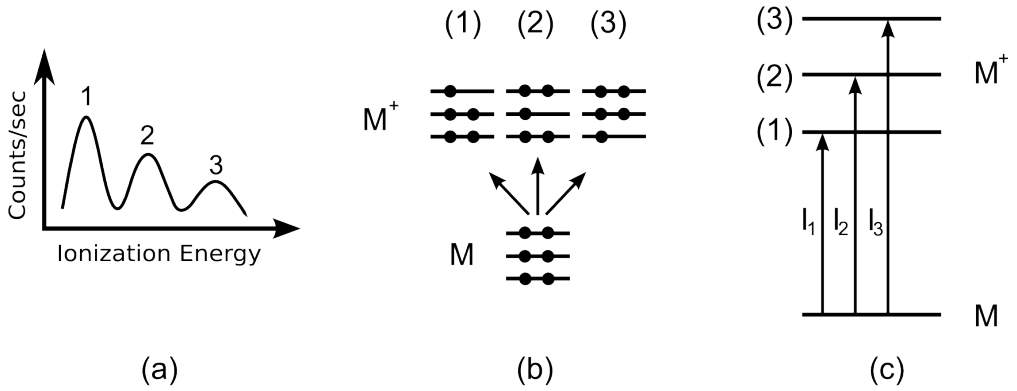

Figure 2.4: Schematic drawings of (a) the photoelectron spectrum showing three ionization bands, (b) the dominant electron configurations of the three lowest Koopmans electronic states (see section 2.1.2.2) of the ion (M^+) formed by photoionization of a closed-shell molecule (M), and (c) the energy level diagram derived from the photoelectron spectrum.

For polyatomic molecules, the spectrum contains many vibrational lines for each electronic state of the ionized molecule, and the system of lines that corresponds to

a single electronic state of the ion constitutes a band. The 58.4 nm photon carries an energy of 21.22 eV, which is sufficient to ionize the valence electrons, that is, the electrons which occupy the orbitals that are involved in chemical bonding and are characterized by the highest principal quantum number of the occupied atomic orbitals [44].

A schematic drawing of a photoelectron spectrum is shown in figure 2.4. The photoelectron bands correspond to the first three Koopmans states (see next section) of the ion. The electron configuration and energy levels are also shown [45].

Two types of ionization energies, *adiabatic* and *vertical*, have to be defined. The adiabatic ionization energy (I_a) is the energy required to ionize a molecule to the vibrational ground state of the ion. On the other hand, the vertical ionization energy (I_v) is the energy to ionize the molecule to a vibrational level of the ion which has the maximum probability of photoionization. In many spectra, vibrational structure is not resolved and only broad bands are observed, and the band maximum corresponds to the vertical ionization energy, while the adiabatic ionization energy can only be estimated as the onset of the band. When using Koopmans' theorem (see next section) it is the vertical energy that is calculated, not the adiabatic one.

The intensities of vibrational peaks are governed by the Franck-Condon factors:

$$q_{v,v'} = \left| \int \psi_v \psi_{v'} d\tau \right|^2 \tag{2.6}$$

which are given by the square of the overlap integral of a vibrational wave function ψ_v of the ground state and a $\psi_{v'}$ of the excited electronic states [44, 45].

2.1.2.2 Koopmans' Theorem

Photoelectron spectroscopy is the study of the energies, abundances and angular distributions of photoelectrons which, within a molecular orbital model, are characteristics of the individual molecular orbitals from which they originate. The quantities measured most directly in photoelectron spectroscopy are the ionization energies for the removal of electrons from different molecular orbitals. According to Koopmans' theorem, each ionization energy, I_j, is equal in magnitude to an orbital energy, ϵ_j, within the Hartree-Fock framework:

$$I_j \cong -\epsilon_j \tag{2.7}$$

This relationship, which is very useful and often used as a good approximation in studying photoelectron spectra (although the limitation of the Hartree-Fock model must be kept in mind when making spectral assignments), means that the photoelectron spectrum of a molecule may be regarded as a direct representation of the molecular orbital energy diagram, and the spectrum gives not only the orbital energies but also, less directly, the changes in the molecular geometry caused by removal of one electron from each orbital. These changes can reveal the character of the orbitals, *i.e.* whether they are bonding, antibonding or non-bonding, and how their bonding power is distributed in the molecules [46].

There are two different types of states that are involved in the photoionization of the molecules:

- **Koopmans states**: They are states where the removal of the photoelectron is not accompanied by additional processes. The orbital energy from where photoelectron is ejected can be determined using the Koopman's theorem, within the Hartree-Fock framework.
- **Non-Koopmans states**: In this case photoelectron interacts with other electrons when departing the atom. For example, it may excite a valence electron to a previously unoccupied molecular orbital (*shake-up* states) or it might transfer sufficient energy to the valence electron to remove it entirely from the atom (*shake-off* states). These states, even though they involve ionization from a molecular orbital are not visible in the photoelectron spectrum but they are visible in other forms of spectroscopy such as electroabsorption (EA) spectroscopy of radical cations.

2.1.2.3 Photoelectron spectrometer

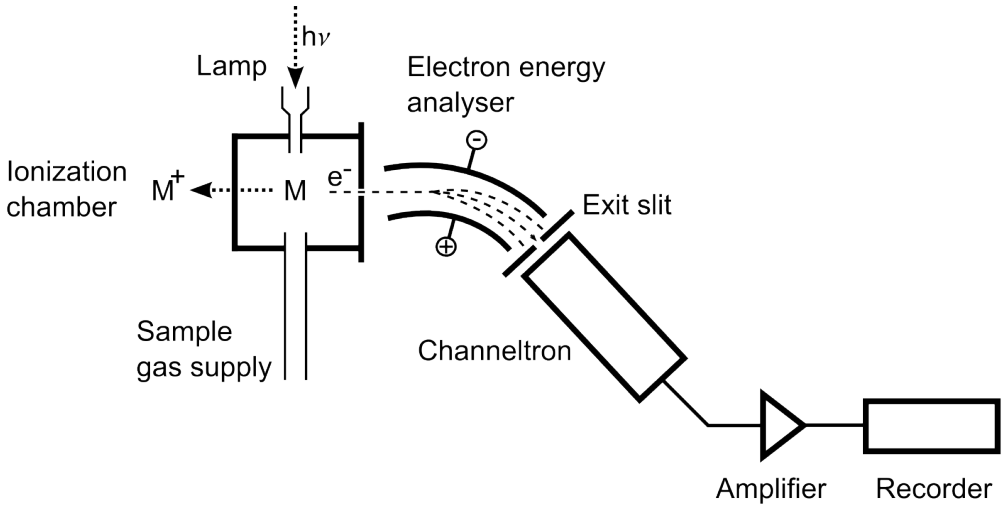

Figure 2.5: Schematic representation of a photoelectron spectrometer.

The HeI photoelectron spectrometer consists of five essential components, a He discharge lamp that produces suitable radiation, a target chamber in which molecules can be ionized at a defined electrical potential, a cylindrical electron energy analyser, a channeltron which detects the electrons and a recorder (figure 2.5). The signal given by the channeltron is amplified and shaped in order to be processed by the recorder. The target chamber, the analyser and the electron detector are located in a vacuum chamber connected to three rotary pumps and one diffusion pump. A photoelectron spectrum is measured by varying the energy of the photoelectrons

allowed to reach the detector and recording the rate at which electrons of each energy arrive [46].

The light source used in the photoelectron spectrometer is a helium discharge lamp operated at such a pressure that one obtains mainly HeI (58.4 nm) emissions. This light is energetic enough to cause ionization of valence electrons and is not accompanied by any lines of lower energy down to about 4 eV. The excited helium atoms are obtained from an electrical discharge of about 2 kV. Other lines (HeIβ 53.7 nm, HeIγ 52.2 nm ...) are present in the output of the He discharge lamp, but at a much weaker intensity. They cause weak side-bands in the photoelectron measurements [45].

The electrons emerging from ionization chamber are energy analysed through an electrostatic 127 ° cylindrical analyser. To provide high resolution and high sensitivity simultaneously, the electron analyser must be designed with focusing properties such that it can accept as large a fraction as possible of electrons produced in a properly matched source, while still giving the desired resolution. The 127 ° cylindrical analyser has a strong first-order focusing in one direction, and is suited as a line source of electrons [46].

The detector used to count the photoelectrons is a continuous dynode secondary electron multiplier, called *channeltron*. In this device, a single electron is accelerated to about 700 V and strikes a conversion electrode (dynode) which causes the emission of two or three secondary electrons which are then attracted and multiplied by several stages of dynodes. Detectors of this type have current amplification factors of 10^4 to 10^8.

During photoelectron measurements, the analyser voltage was constantly set at $\pm$1.0 V and the retarding potential between the inlet slit and the ionization chamber was scanned. The working resolution of the spectrometer was 18-22 meV as measured by the full width at half maximum for the $^2P_{3/2}$ peak of Ar. The sample pressure in the vacuum chamber was kept at (2-4)$\times 10^{-5}$ torr. Calibrations of the ionization energy scale of the spectra were carried out using the two lines of Xe which correspond to 12.130 eV and 13.436 eV in ionization energy and the two bands of Ar which correspond to 15.759 eV and 15.937 eV [46].

2.2 Calculations

The experimental DEA spectra presented in this work are supported by *ab initio* calculations performed using the Gaussian 03 software package [47]. This section presents the computational details for these calculations.

2.2.1 Calculations of the thermodynamical threshold

One set of *ab initio* calculations performed was to determine the thermodynamical thresholds and possible structures of stable fragments for various molecules. These calculations were performed using density-functional theory (DFT). The ge-

ometries of neutral fragments were optimized using B3LYP functional with the 6-311++G(2df,2pd) basis set. The thresholds energies were determined by calculating the difference between total electronic energies of the target molecule and the anionic and neutral fragments. Adiabatic electron affinities of fragment anions were calculated from the difference of neutral and anionic electron energies. All the reported energies have been corrected for zero-point vibrational energy (ZPE) obtained from a frequency calculation.

2.2.2 Calculations of the excited states

In section 6.3 a dramatic difference is observed between DEA spectra of alcohols and that of ethers. To explain this difference we used the TD-DFT method to calculate the excited states of different alcohols and ethers which are the parent states of the Feshbach resonances involved in the electron attachment. The energies of the excited states were calculated as the sum of the electronic ground energy and the excitation energy to the respective excited state. The electronic energy of the ground state of the optimized geometry has been used as a reference, thus setting the origin of the energy scale to zero, and it was subtracted from the energies of the excited states.

A script in the programming language Python was developed for the calculation of 1D and 2D potential energy surfaces. It works on the principle of a *rigid scan*, modifying selected parameters of the geometry of the molecule. The second step is to calculate the values for the electronic ground energy and excitation energies for the selected states. The parameters required for a run are the initial geometry of the molecule, introduced using the Z-matrix description, the bond or the bonds that are modified during the scan, the step and the length of the scan. The script automatically launches the Gaussian 03 program to perform the required set of calculations.

A second Python script has been developed to extract and arrange the calculated values in a convenient manner. This script requires only the list of the files containing the results, which is automatically written by the first script, and the successful completion of all calculations.

In the second phase of development, the scripts were improved so that they also allow the use of angles as coordinates when calculating the potential energy surfaces.

2.3 Synthesis

Most of the compounds presented in this work are commercially available and they were used as provided by the supplier, without any further purification. But some compounds were not commercially available and they were synthesized by the Synthesis Laboratory at Department of Chemistry, University of Fribourg, under the supervision of Anne Schuwey. Their synthesis are presented in this section.

2.3.1 Ethanol-d_3

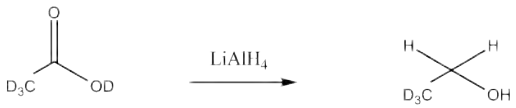

Figure 2.6: Reaction scheme for the synthesis of ethanol-d_3.

Ethanol-d_3 was synthesized starting from deuterated acetic acid as is presented in fig. 2.6.

Reaction steps:

- Put triethyleneglycoldimethylether in a dry apparatus under argon. Carefully add $LiAlH_4$. Carefully add, in drops, solution of deuterated acetic acid in triethyleneglycoldimethylether during 30 minutes, maintaining the reaction mixture at room temperature with a water bath. Keep at room temperature for 5 hours and then heat to 100 °C for 12 hours.
- Quench the reaction by carefully adding tetraethyleneglycol during 1 hour (foam formation and very strong degassing occur).
- Perform a Flash distillation of the product under high vacuum while keeping the reaction mixture at 0 °C.
- 1.6 g of colorless liquid was obtained containing deuterated ethanol, 3% non-deuterated ethanol and a little of triethyleneglycoldimethylether, water and some traces of tetraethyleneglykol. The glycols were not considered to be a problem since their dissociation fragments upon electron collision have a higher mass than those observed from ethanol-d_3. Care must be taken to avoid all contact with water to prevent D-H exchange.

2.3.2 Dibutoxymethane

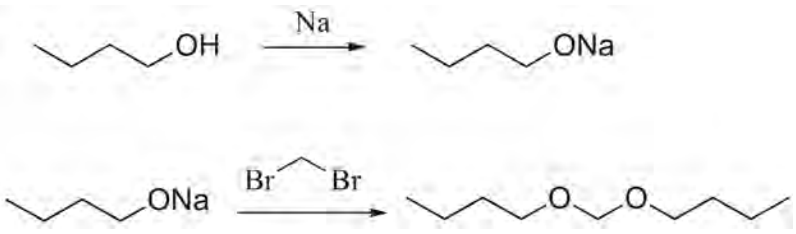

Figure 2.7: Reaction scheme for the synthesis of dibutoxymethane.

Dibutoxymethane was synthesized using the reaction scheme presented in fig 2.7. The total yield of the synthesis was 40 %.

Reaction steps:

- Put *n*-butanol in a dry apparatus under argon. Carefully add sodium in small portions, maintaining a temperature of 40 °C with a water bath. Agitate one night at room temperature and carefully heat to reflux. Agitate under reflux until the metallic sodium disappears completely (around 1 hour). Cool to room temperature, add dibromomethane in drops during around 1 hour. Heat to reflux during 3 hours with the formation of a white precipitate.

- Quench the reaction carefully adding 50 ml of water, under cooling conditions (the precipitate is completely dissolved). Add 20 ml of diethyl ether, separate the phases, and wash the organic phase with 4 × 30 ml of water. Dry on $MgSO_4$, filter and evaporate diethylether.

- Distill the product, first under normal pressure to eliminate the excess of *n*-butanol and then under vacuum (50 mbar) at 80 °C.

Chapter 3

Dissociative electron attachment of aliphatic alcohols

In this chapter, the dissociative electron attachment of molecules with one or two hydroxyl groups is presented. The main results are published in ref. [32] reprinted in section 3.2. Additional results, not published in the article, include the DEA spectra of propanols and butanols, the pressure dependence of the anion yield for methanol and ethanol, and the relative intensity test for deuterated methanols.

3.1 General considerations

The interest in electron-induced chemical processes has been renewed by the discovery that electrons at subionization [3] and even at subexcitation energies [33] damage the DNA molecule. Electron-induced chemistry at subionization energies can proceed either *via* electronic excitation of the target or, particularly at energies too low for electronic excitation, by means of dissociative electron attachment (DEA) [48]. The latter mechanism is particularly important because even a high energy primary electron (or γ photon) impinging on a material or on a biological tissue leads to a "shower" of low energy electrons, providing a large amount of subionization electrons with energies suitable for DEA.

Of particular importance are the studies of DEA of isolated polyatomic molecules in the gas phase, especially molecules of biological interest. In these, the hydroxyl group is particularly important being ubiquitous in living organisms. In this work we present the DEA spectra of several saturated compounds containing one or more hydroxyl groups which can be considered as model compounds for biomolecules.

3.2 Electron-induced chemistry of alcohols

The reprint of the article starts on the next page.

Electron-induced chemistry of alcohols†

Bogdan C. Ibănescu, Olivier May, Angèle Monney and Michael Allan*

Received 28th March 2007, Accepted 24th April 2007
First published as an Advance Article on the web 24th May 2007
DOI: 10.1039/b704656a

We studied dissociative electron attachment to a series of compounds with one or two hydroxyl groups. For the monoalcohols we found, apart from the known fragmentations in the 6–12 eV range proceeding *via* Feshbach resonances, also new weaker processes at lower energies, around 3 eV. They have a steep onset at the dissociation threshold and show a dramatic D/H isotope effect. We assigned them as proceeding *via* shape resonances with temporary occupation of σ^*_{O-H} orbitals. These low energy fragmentations become much stronger in the larger molecules and the strongest DEA process in the compounds with two hydroxyl groups, which thus represent an intermediate case between the behavior of small alcohols and the sugar ribose which was discovered to have strong DEA fragmentations near zero electron energy [S. Ptasińska, S. Denifl, P. Scheier and T. D. Märk, *J. Chem. Phys.*, 2004, **120**, 8505]. Above 6 eV, in the Feshbach resonance regime, the dominant process is a fast loss of a hydrogen atom from the hydroxyl group. In some cases the resulting $(M - 1)^-$ anion (loss of hydrogen atom) is sufficiently energy-rich to further dissociate by loss of stable, closed shell molecules like H_2 or ethene. The fast primary process is state- and site selective in several cases, the negative ion states with a hole in the n_O orbital losing the OH hydrogen, those with a hole in the σ_{C-H} orbitals the alkyl hydrogen.

1. Introduction

The interest in electron-induced chemical processes has recently been renewed by the discovery that electrons at subionization[1] and even subexcitation energies[2] damage DNA and by the emerging applications in materials science.[3] Electron-induced chemistry at subionization energies can proceed either *via* electronic excitation of the target or, particularly at energies too low for electronic excitation, by way of dissociative electron attachment (DEA).[4] The latter mechanism is particularly important because even a high energy primary electron (or γ photon) impinging on a material or on a biological tissue leads to a "shower" of low energy electrons, providing a large amount of subionization electrons with energies suitable for DEA.

These applications renewed the interest in the corresponding elementary step, the DEA to isolated polyatomic molecules in the gas phase and, in particular, to molecules of biological interest with many interesting findings.[5–10] In our earlier work we studied several saturated compounds containing the amino- and the hydroxyl groups which could be considered as model compounds for biomolecules.[11] We used the comparison between the HeI photoelectron spectra and the DEA spectra to identify the Feshbach resonances and to assign the DEA bands and found that all DEA bands could be explained by Feshbach resonances, the low-lying ones being localized on the functional groups. In the present paper we substantially extend the work on the alcohols and report several new findings, in particular, the involvement of shape resonances at low energies, dramatic isotope effects, cases of state and site selective chemistry, and more insight into the mechanism of fragmentation of Feshbach resonances.

The process of DEA has been extensively studied in the past.[4,12] As has been summarized in our earlier paper,[11] many DEA spectra of polyatomic molecules follow the same general pattern. They can be divided into a low energy domain, between zero and about $\sim$5 eV, and a high energy domain, about 5–14 eV.

DEA in the low energy range is generally initiated by an electron capture to form a shape ('one particle') resonance. The initial phase of the DEA is characterized by a competition of a very fast autodetachment and stabilization of the negative ion by a distortion of the molecular frame. The bands in the low energy range can often be assigned by their coincidence in energy with resonances found in the electron transmission spectrum (ETS) or vibrational excitation cross sections. Insight into the mechanism can be gained by comparing the appearance energies of the various fragments with the thermochemical thresholds because generally only few dissociation channels are energetically open. The low energy processes in methyl acetate may serve as typical examples.[13] In addition, vibrational Feshbach resonances (VFR)[14] may serve as doorway states to initiate DEA at very low energies. Representative examples are CH_3I,[15] N_2O[16] and ethylene carbonate.[17] The VFR mechanism has been shown to be operative in uracil and thymine.[7,18]

In virtually all compounds one or several DEA bands are also found in the 5–14 eV range. The assignment of these bands is more difficult because no (or only very weak) corresponding features are found in the other channels of electron scattering, like vibrational excitation or total cross-section (as revealed by the ETS). The situation is complicated

Department of Chemistry, University of Fribourg, Chemin du Musée 9, CH-1700 Fribourg, Switzerland
† The HTML version of this article has been enhanced with colour images.

by the fact that dissociation into many different fragments is energetically possible, and many different fragments often actually occur. It appears that most DEA bands in this energy range are due to Feshbach resonances with double occupation of Rydberg-like orbitals and a positive ion core.[19,20]

An unambiguous assignment of the high energy bands to such resonances has occasionally been possible in small molecules where the DEA bands have sharp vibrational structure which resembles that of a Rydberg excited state of the neutral molecule (the parent state) and that of the photoelectron band of the positive ion (the grandparent state). Examples are ammonia[20] and acetaldehyde.[21,22] In view of the high energy and the competition with fast autodetachment it is somewhat surprising that complex fragmentations involving 'scrambling' are often observed. They indicate that a relatively long time is available for the dissociation. The mechanism involves propagation of the nuclear wave packet on a manifold of the Rydberg-like anion states, possibly predissociated by repulsive valence states, as recently explicitly calculated for water.[23] The analogy to conical intersection[24,25] is involved.

Feshbach resonances with occupation of Rydberg-like orbitals are well known from scattering experiments other than DEA, in particular ETS of rare gases, diatomic and polyatomic molecules[26–29] or in the vibrational excitation cross-sections (for an example see ref. 30). The energies of these Feshbach resonances were found to have a simple relation to the energies of the parent Rydberg states and the grandparent state of the cation. The relation depends only weakly on the molecule in question. The electron affinity of the parent Rydberg state is of the order of 0.3–0.5 eV for the s^2 configuration.[26–29,31] Read expressed the relation with a modified Rydberg–Ritz formula.[32] Spence[33] fitted a linear relationship between the energy of the Feshbach resonance E_F and the first ionization energy I, $E_F = A \cdot I + B$, for many hydrogen- and methyl halides. The slope A had the value of around 1. The constant B had the values -3.9 and -1.8 eV for the s^2 and p^2 configurations, respectively. This means that the s^2 Feshbach resonance was always found $\sim$4 eV below its grandparent state, the ground state of the ion.

For completeness, it should be mentioned that in an intermediate energy range, $\sim$4–7 eV, DEA bands have been found which have nearly the same energy as, and resemble in shape, the low-lying singlet valence excited states of the target molecule. These bands have been found in unsaturated compounds and assigned to resonances where an s-like electron is weakly bound to a valence-excited core. Examples are CS_2 [34] and other molecules (for example, norbornadiene, cyclopentadiene, SO_2).[35]

This paper presents dissociative electron attachment spectra of a series of alcohols and attempts to assign the observed bands to various types of resonances as outlined above. The assignment is guided by a comparison with HeI photoelectron spectra and vibrational excitation cross-sections.

2. Methods

The dissociative electron attachment spectrometer used to measure the yield of mass-selected stable anions as a function of electron energy has been described previously.[17,36] It employs a magnetically collimated trochoidal electron monochromator to prepare a beam of quasi-monoenergetic electrons which is directed into a target chamber filled with a quasi-static sample gas. Fragment anions are extracted at 90° by a three-cylinder lens and directed into a quadrupole mass spectrometer. The energy scale was calibrated on the onset of the O^-/CO_2 signal at 4.0 eV. The electron current was several hundreds of nanoamperes and the resolution about 150 meV.

A common problem with DEA instruments equipped with a trochoidal monochromator is the difficulty of detecting light ions, specifically H^- and D^-, because the magnetic field required for the operation of the trochoidal monochromator is perpendicular to the ion path and deviates the light ions in the ion transporting lens, preventing them from reaching the quadrupole mass spectrometer. (The time-of-flight spectrometer without a magnetic field of Krishnakumar is better in this respect.[10]) Our ion lens has two pairs of x, y deflectors, situated near its entrance and its exit,[17] which were used to compensate the deflection by the magnetic field. The electron beam current and, consequently, the sensitivity have been improved in comparison to our earlier work, permitting the detection of weak bands not reported earlier. Care was taken to make the measurements at sufficiently low pressures as ion–molecule reactions of the type

$$O^- + ROH \rightarrow RO^- + OH$$

were often found to distort the spectra at higher pressures.

The vibrational excitation cross-sections were recorded with a spectrometer using hemispherical electron-energy selectors.[37] The photoelectron spectra were recorded with a modified Perkin Elmer PS18 HeI photoelectron spectrometer.

Threshold energies for various fragmentations were calculated as the differences of the total energies of the products and the targets at 0 K, corrected for the zero point vibrational energy, using the density functional theory (DFT) B3LYP/6-311 + G(2df,2p) model.[38]

3. Results and discussion

The alcohols studied in this work are shown in the following scheme (Scheme 1):

They include the two simple alcohols methanol and ethanol, and a series of alcohols all of which are to some degree related

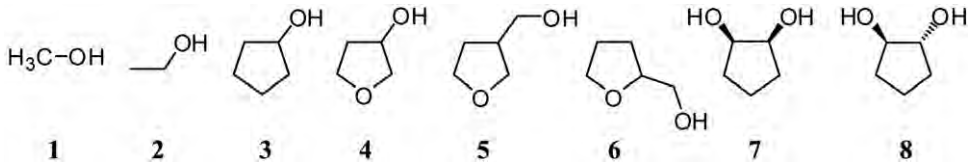

Scheme 1

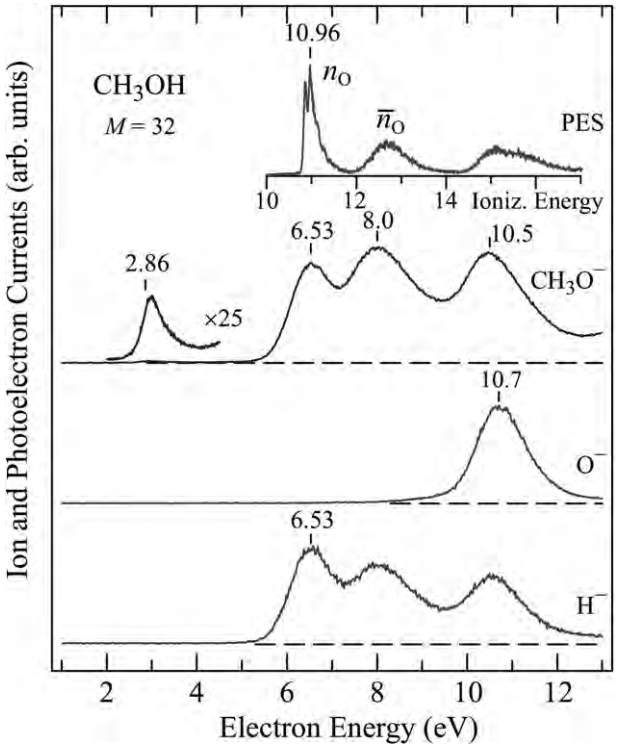

Fig. 1 The HeI photoelectron spectrum (top, shown shifted by −4.5 eV) and the yields of the $(M-1)^-$, H^- and O^- fragments from methanol (**1**).

to tetrahydrofuran and ribose, which have been of interest recently[9,39,40] because of their relevance for DNA.

The figures shown in this paper generally compare the photoelectron spectra, which have been found important for identifying Feshbach resonances, with the yield of the $(M-1)^-$ fragment (loss of hydrogen atom), or $(M-2)^-$ (loss of deuterium)—often the primary fragments in alcohols. (M is the molecular mass and $(M-1)^-$ stands for an anion with a mass of $M-1$.) The complementary fragment, H^- or D^-, and selected fragments considered interesting for the discussion are also shown. Fragments judged less essential for the present work are not shown but are mentioned in the text.

3.1 Methanol (1)

Kühn *et al.*[41] studied dissociative electron attachment to methanol including fully and partially deuterated isotopomers. They also analyzed the translational energies of the ionic fragments. They observed CH_3O^-, OH^- and O^- fragments in three bands in the 5–12 eV range which they assigned to core excited resonances with two electrons in a Rydberg-like MO. The observation of unexpected fragments from the isotopically substituted compounds, *i.e.*, OH^-/CH_3OD or OD^-/CD_3OH revealed hydrogen scrambling for these two fragments, in contrast to the formation of CH_3O^- (and its deuterated analogue), which proceeded without scrambling. Methanol has also been studied by Curtis and Walker,[42] who discovered a substantial kinetic energy release for H^- and compared the Feshbach resonances in the DEA spectra to the parent Rydberg states in the VUV spectrum. They also observed an early indication of site selectivity—D^- originated from the OD group at 5–8 eV, but from both hydroxyl and methyl groups around 10.5 eV. The concept of site selectivity was extended to other compounds and generalized by Prabhudesai *et al.*[10]

Table 1 Threshold energies for the reactions $e^- + ROH \rightarrow RO^- + H$, in eV. The DFT values were calculated as described in section 2. The "therm." values were derived from experimental thermochemical data, in particular the gas phase acidities.[43] The onsets of the DEA bands were taken from the present spectra

Target	E_{thr}		
	DFT	Therm.	Onset of DEA
1	2.82	2.94	2.86
2	2.69	2.81	2.75
3	2.53		2.67
4	2.31		2.50
5	2.35		2.36
6	2.64		2.58
7	1.89		1.94
8	2.43		2.43

Our current spectrum of the CH_3O^- fragment, shown in Fig. 1, is consistent with the earlier spectra but additionally reveals a weaker band peaking at 2.99 eV. Its left side is steep, consistent with a vertical onset at the energetic threshold, calculated from the experimental methanol acidity of 1596 kJ mol^{-1} [43] to be 2.94 eV (Table 1). Since we did not find the required experimental acidities of all the compounds measured in this work, we also used DFT calculations to determine the threshold energies. Comparison of the threshold energies determined from experimental thermochemical data and calculated using quantum chemical methods for methanol and ethanol (Table 1) indicates that the latter is reliable within about ±0.2 eV, sufficient for the present purposes. The observed DEA bands are broadened by the finite resolution of the experiment and possibly also by 'hot bands', signals from thermally vibrationally excited molecules. It is therefore not quite trivial to decide at what position on the observed band the experimental onset should be taken—it depends on the inherent shape of the band. For a step-shaped band the onset should be taken at 50%, for a line-shaped band at 100% of the band height. Since the real band shape is somewhere between these two extremes we adopted the same pragmatic approach as in an earlier work[44] and take the value at 75% of the height. The agreement between calculation and theory obtained with these rules and indicated in Table 1 is satisfactory.

The 2.99 eV band can not be assigned to a core-excited resonance because of lack of suitable parent electronically excited states (both Rydberg and valence). At the same time the energy is too high for an assignment to a dipole-bound resonance or a virtual state. The dissociation must thus proceed *via* a $^2(\sigma^*)$ shape resonance, as will be discussed in more detail below in connection with ethanol. The H^- yield, also shown in Fig. 1, is very similar in shape to the CH_3O^- yield above 6 eV, indicating that the same Feshbach resonances dissociate into both fragments—the charge distribution is not selective. The 2.99 eV band is missing in the H^- yield—this is probably because of the higher threshold for H^- formation. The O^- yield is consistent with earlier results.[41]

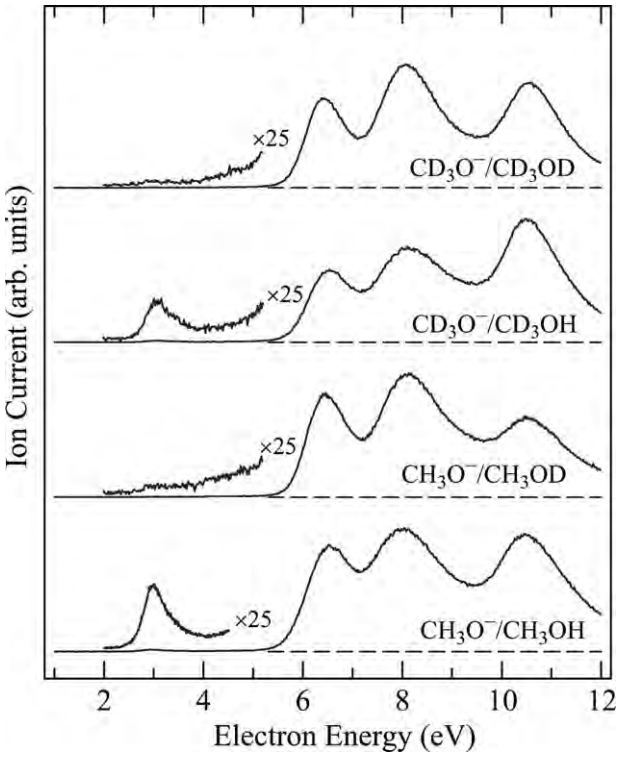

Fig. 2 Yield of the methanolate anion fragment from various isotopically substituted methanols.

Study of the fully and the partially deuterated methanols revealed a strong isotope effect for the 3 eV band (Fig. 2). The signal has dropped below the detectability limit when the hydroxyl group was deuterated, indicating an isotope effect of more than a factor of 10. The process thus resembles the formation of H^- from H_2 where the large width of the $^2\Sigma_u$ σ^* shape resonance ($\Gamma \sim 4$ eV at the H_2 equilibrium internuclear distance in the nonlocal model of Mündel *et al.*[45]) causes an isotope effect of a factor of 200.[46] Physically, the dramatic drop of the cross-section is a consequence of the slower motion of the heavier deuterium compared with the lighter hydrogen, leading to longer dissociation time, and thus less favorable competition of dissociation with the very fast autodetachment.

Our present experiment does not measure absolute cross-sections but we estimated the relative cross-sections for the various methanol isotopomers by recording signal intensities for the same pressure (same Penning gauge reading) and the same electron beam current. These measurements confirmed the strong isotope effect for the 3 eV band mentioned above where the cross-section for breaking the O–H bond is at least 10× larger than that for breaking the O–D bond. Deuteration of the methyl group also has an effect, albeit weaker, on the cross-section for breaking the O–H bond—the cross-section for breaking the O–H bond in CD_3OH appears to be about 2× larger than the cross-section for breaking the O–H bond in CH_3OH. This observation is somewhat surprising because the above argument is not applicable — the O–H bond would be expected to dissociate equally fast whether the methyl group is deuterated or not. The reason could be related to the fact that the C–H modes in the methyl-deuterated compound are, in terms of frequency, better separated from the dissociating

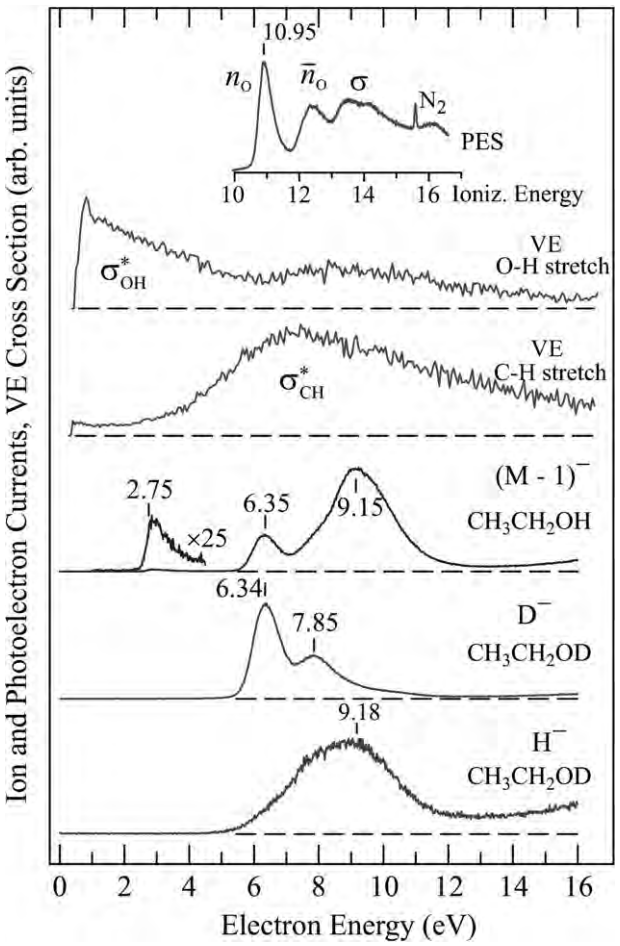

Fig. 3 Comparison of selected DEA spectra with vibrational excitation cross-sections (measured at 135°) and photoelectron spectra for ethanol (**2**). The PE spectrum is shown shifted by −4.65 eV; a weak sharp peak due to a N_2 impurity is marked. D^- and H^- yields from ethanol-d_1 are shown in the bottom two spectra.

(O–H stretch) mode, reducing the possibility of fast intramolecular vibrational redistribution (IVR) which would quench the dissociation.

The pressure-normalized measurements further revealed (weaker) isotope effects for the bands in the Feshbach resonance region. The relative intensities of the three methanolate bands in the 6–12 eV range (*i.e.*, the shape of the spectrum in this energy range) also depend to some degree on deuteration (Fig. 1 and 2). The intensity of the highest band (8.1 eV) increased with deuteration, being about 2× larger in CD_3OD than in CH_3OH. CH_3OD yielded also the CHO^- fragment (loss of D and of H_2).

3.2 Ethanol (2)

Fig. 3 shows the spectra for the major fragments from ethanol. The 6.35 eV band in the $(M - 1)^-$/EtOH and D^-/EtOD spectra can be assigned to a Feshbach resonance with a hole in the n_O oxygen lone pair orbital. The Feshbach resonance with a hole in the $\bar{n}_O$ oxygen lone pair orbital appears as a weaker peak at 7.85 eV in the D^-/EtOD spectrum and as an indistinct shoulder at the same energy in the $(M - 1)^-$/EtOH spectrum.

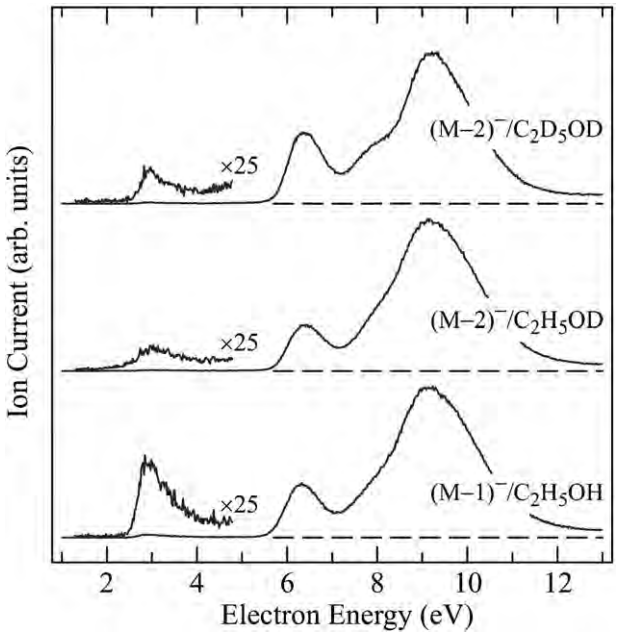

Fig. 4 Yield of the ethanolate anion fragment from various isotopically substituted ethanols.

Finally the photoelectron spectrum shows overlapping bands due to ionization from various C–H and C–C σ orbitals above 13 eV and the broad DA bands appearing around 9.15 eV in the DA spectra can be assigned to the corresponding Feshbach resonances.

A weaker band appears at 2.88 eV in the $(M-1)^-$/EtOH spectrum. It can be assigned to a very short-lived σ^*_{OH} shape resonance, similarly to methanol. The shape of the band is asymmetrical, consistent with a vertical onset at the energetic threshold. The signal onset, taken at 75% of peak height, is at 2.75 eV in good agreement both with the value of 2.81 eV determined from the experimental gas phase acidity of ethanol[43] and the value of 2.69 eV obtained from DFT calculations (Table 1). As in the methanol case, a very short lifetime (large width) of the resonance responsible for the 2.88 eV band is deduced from the very pronounced isotope effect, shown in Fig. 4: the band is about 4× weaker when the hydroxyl hydrogen is replaced by deuterium.

Additional evidence for the identity of resonance processes is provided by the cross-sections for vibrational excitation (VE) because they are generally enhanced by resonances, in particular by shape resonances[47] and by vibrational Feshbach resonances.[14] We therefore compare the DEA spectra to selected VE spectra in Fig. 3. The cross-sections for the excitation of two vibrations are shown. The spectrum for the excitation of the C–H stretch vibration is similar to the C–H stretch excitation in hydrocarbons[48]—it consists of a very broad band peaking around 7.5 eV which could be assigned to a temporary occupation of σ^*_{CH} orbitals, the large width of the band indicating a very large autodetachment width and possibly also several overlapping resonances.

The cross-section for the excitation of the O–H stretch vibration is similar to the cross-section observed in formic acid[49]—it peaks at threshold and then decreases slowly over an energy range of several eV. The electron cloud associated with this resonant process must be located on the O–H bond (because it excites selectively the O–H vibration). The band in the O–H stretch vibrational excitation cross-section is much broader than the band in the $(M-1)^-$ DEA band in Fig. 3, but we propose that both processes are due to the same σ* shape resonance, possibly enhanced by dipole binding at low energies. It is well established that shape resonances with large autodetachment widths can result in relatively narrow DEA bands. The prototype examples are H_2 [50,51] and the halogen halides.[14,52] The H_2 case has in common with the present observation in ethanol also the large isotope effect. The cause of the striking difference of the DEA and the VE band widths in these cases is, on the one hand, the vertical DEA signal rise at the threshold and, on the other hand, the rapid increase of the resonant autodetachment width with energy[50,51] and consequently rapid decrease of the DEA cross-section.

The hydrogen halide resonance phenomena at low energies are the result of a σ* valence state at large internuclear distances and dipole binding of the extra electron at shorter internuclear distances,[14,52] which causes the anion potential curve to bend down before it crosses the potential curve of the neutral molecule. A similar situation has also been identified in uracil and thymine.[18] The dipole moments of methanol (1.7 D) and ethanol (1.5 D) are not much less than that of HF (1.8 D) and it is thus probable that dipole binding also bends the anion potential surface down at stretched O–H distances and

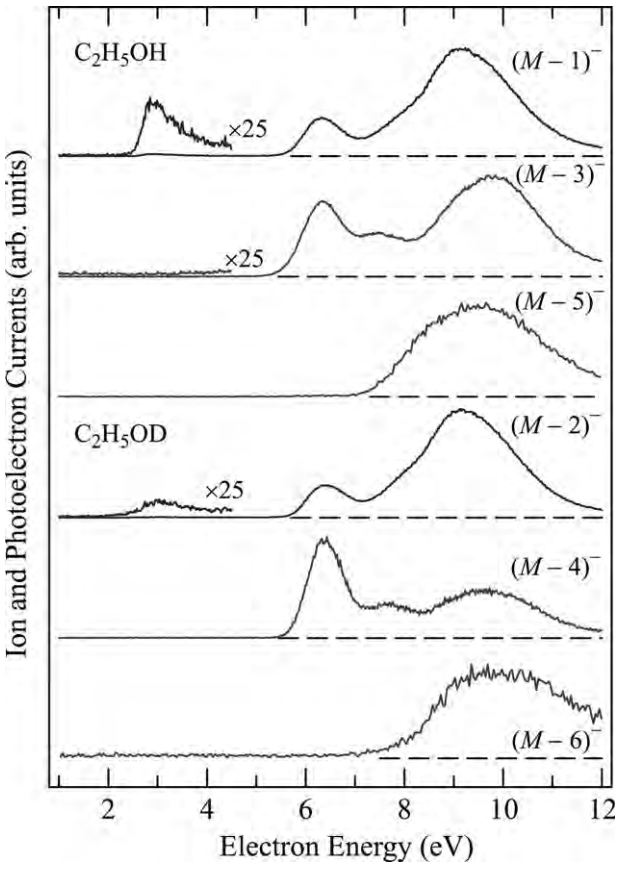

Fig. 5 Yields of fragments resulting from a loss of a hydrogen atom and subsequent losses of one and two hydrogen molecules. The top three spectra refer to C_2H_5OH, the lower three spectra to C_2H_5OD.

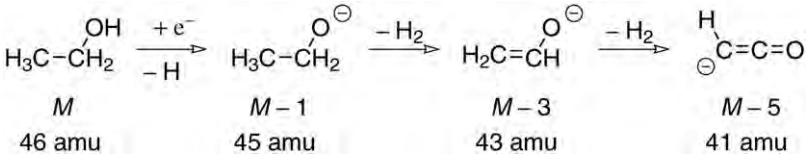

Fig. 6 Tentative reactions leading to fragments with masses $M - 1$, $M - 3$ and $M - 5$ from ethanol (**2**).

affects VE and DEA in the alcohols at low energies. An ultimate proof of vibrational Feshbach resonances are the structures in the VE cross-sections slightly below the vibrational levels of the neutral molecules—like those found in HF or CO_2.[14] We searched but did not find any such structures in methanol and ethanol VE cross-sections, however.

The DEA bands at 6.0, 7.7 and 8.8 eV do not have any obvious analogs in VE (Fig. 3), providing a further evidence that they are due to core excited Feshbach resonances and not to σ* shape resonances.

Fig. 5 shows the yields of the less expected fragments $(M - 3)^-$ and $(M - 5)^-$ from EtOH and the corresponding fragments from EtOD. Fig. 6 shows tentative structures of the products and Table 2 gives the corresponding calculated threshold energies. The $(M - 3)^-$ fragment is presumably the result of a loss of an H atom and an H_2 molecule and its structure could be that of an acetaldehyde deprotonated in the α position—the negative charge is stabilized by delocalization over three atoms which results in the relatively large acidity of the α hydrogen in carbonyl compounds. For this reason it has already been found to be an important fragment in DEA to acetaldehyde.[53] Table 2 indicates that the threshold energy for this fragmentation is surprisingly low, in fact the fragmentation of the $CH_3CH_2O^-$ anion into $H_2 + CH_2CHO^-$ is thermoneutral. This means that the $m/z = 43$ fragment could appear already around 3 eV—the fact that it is not observed there indicates that the fragmentation has an activation barrier and does not proceed without excess energy.

The $(M - 5)^-$ fragment is presumably the result of a loss of an H atom and two H_2 molecules, and its structure could be that of a deprotonated ketene. Deprotonated ketene is a stable anion and has already been observed in DEA to methyl acetate.[44] The calculated threshold energy is well below the actual appearance of this fragment (Fig. 5).

Fig. 3 also illustrates another interesting effect—deuterium atom is lost from CH_3CH_2OD *via* the relatively narrow 6.35 and 7.85 eV Feshbach resonances whereas hydrogen is lost *via* a broad 9.18 eV feature. As already mentioned above, we assign this broad 9.18 eV feature to Feshbach resonances with holes in the σ_{CH} orbitals, that is, we observe that hydrogens are lost from the hydroxyl group for Feshbach resonances located on the hydroxyl group, and hydrogens are lost from the alkyl group for Feshbach resonances located on the alkyl group. The broad $(M - 1)^-$ 8.8 eV band in the undeuterated molecule CH_3CH_2OH is the sum of both processes, in this case indistinguishable. The state selective chemistry observed here is similar to that reported recently in acetic acid by Krishnakumar.[10]

Table 2 Threshold energies for the more complex fragmentations, calculated as described in section 2. See Fig. 6 and 8 for tentative structures some of the polyatomic products

Target	Products	m/z	E_{thr}
2	$H + CH_3CH_2O^-$	45	2.69
	$H + H_2 + CH_2CHO^-$	43	2.67
	$H + H_2 + H_2 + HCCO^-$	41	3.72
3	$H + c\text{-}C_5H_9O^-$	85	2.53
	$H + H_2 + c\text{-}C_5H_7O^-$	83	2.45
	$H + CH_2{=}CH_2 + CH_3C(CH_2)O^-$	57	2.54
6	$H + CH_3\text{-}CH_3 + CH_2{=}CHCOO^-$	71	0.42
	$H_2C\text{–}OH + c\text{–}C_4H_7O^-$	71	3.43

3.3 Cyclopentanol (3)

The spectra are shown in Fig. 7. The larger alkyl group of cyclopentanol as compared to methanol or ethanol has the consequence of many more σ_{C-H} and σ_{C-C} orbitals and many more corresponding cation states which cause the "sigma

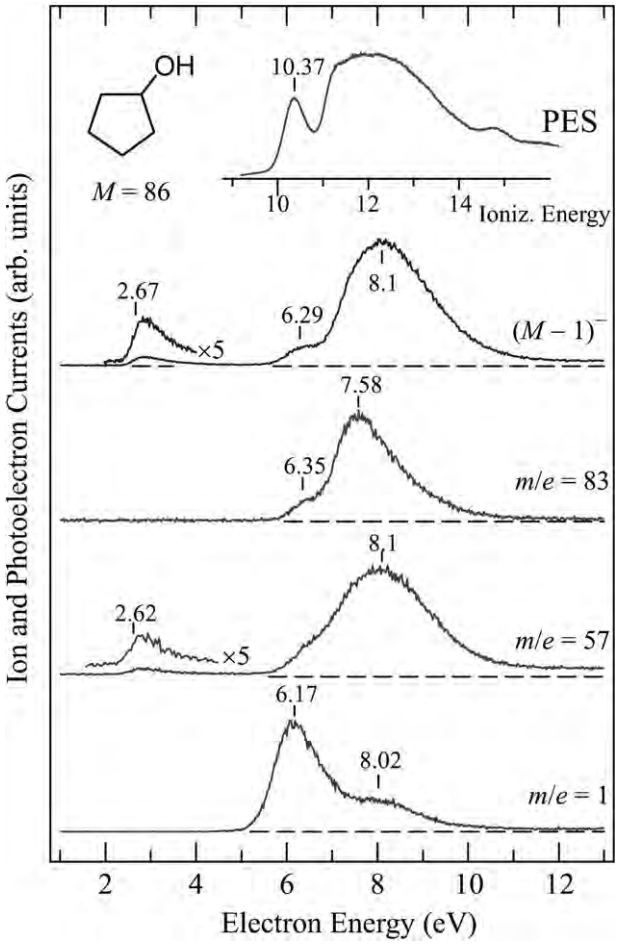

Fig. 7 Photoelectron and DEA spectra of cyclopentanol (**3**). The PE spectrum is shown shifted by −4.25 eV.

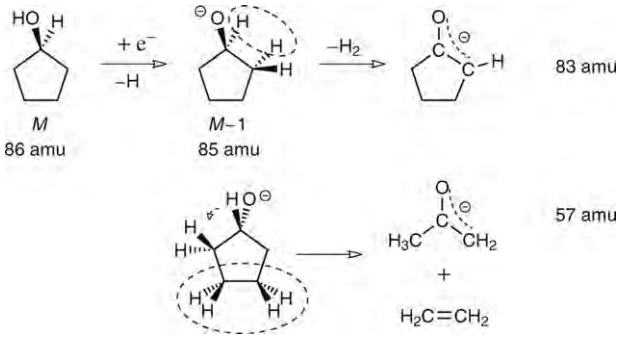

Fig. 8 Tentative equations leading to fragments with $m/z = 57$ and 83 from cyclopentanol.

mountain'' in the 11–14 eV range of the photoelectron spectrum. The first lone pair band n_O is visible as a separate band, but the second lone pair ionization $\bar{n}_O$ overlaps with the σ states. The 6.29 eV shoulder in the $(M - 1)^-$ DEA spectrum can be assigned to a Feshbach resonance with a hole in the n_O lone pair orbital. The 7.58 eV peak in the $m/z = 83$ spectrum could be due to a Feshbach resonance with a hole in the $\bar{n}_O$ lone pair orbital. The broad and unstructured band peaking around 8.1 eV which appears in particular in the $(M - 1)^-$ and the $m/z = 57$ spectra is assigned to several overlapping Feshbach resonances with σ^{-1}_{C-H} and σ^{-1}_{C-C} grandparent states.

DEA to cyclopentanol yields also the less expected fragments with masses with $m/z = 57$ and 83. The mass spectra do not, of course, give any direct evidence of their structures but in the scheme in Fig. 8 we show what we consider to be the most plausible candidates for these fragments. In both cases the short-lived resonance formed by electron attachment is first stabilized by the loss of hydrogen atom to form a cyclopentanolate anion with substantial vibrational energy. This anion can then lose an H_2 molecule and form an α-deprotonated cyclopentanone whose stability is the consequence of charge delocalization over three atoms and the ensuing relatively large acidity of α-hydrogens in carbonyl compounds, as already encountered above in connection with the α-deprotonated acetaldehyde fragment from ethanol. The pentanolate anion can also undergo an intramolecular hydrogen shift and lose an ethene molecule, yielding an α-deprotonated acetone as shown in the lower part of Fig. 8. The loss of ethene appears to be a frequent process. In cyclobutanol ($m/z = 72$) we observed, apart from the $(M - 1)^-$ ion, only one prominent fragment which corresponds to the loss of ethene from the $(M - 1)^-$ ion, yielding an ion with $m/z = 43$, $H_2C{=}CHO^-$, which can be understood as either the vinyl alcoholate ion or as an α-deprotonated acetaldehyde.

Finally, the 2.67 eV band in the $(M - 1)^-$ spectrum in Fig. 7 is assigned to dissociation *via* a shape resonance as in methanol and ethanol. The onset is at a slightly lower energy than in methanol, and this change is reflected in the calculated threshold energy (Table 1).

3.4 Tetrahydrofuran-3-ol (4)

The spectra are shown in Fig. 9. The photoelectron spectrum has a band at 9.98 eV, due to ionization from the ether oxygen lone pair orbital, and a second band at 10.9 eV, due to

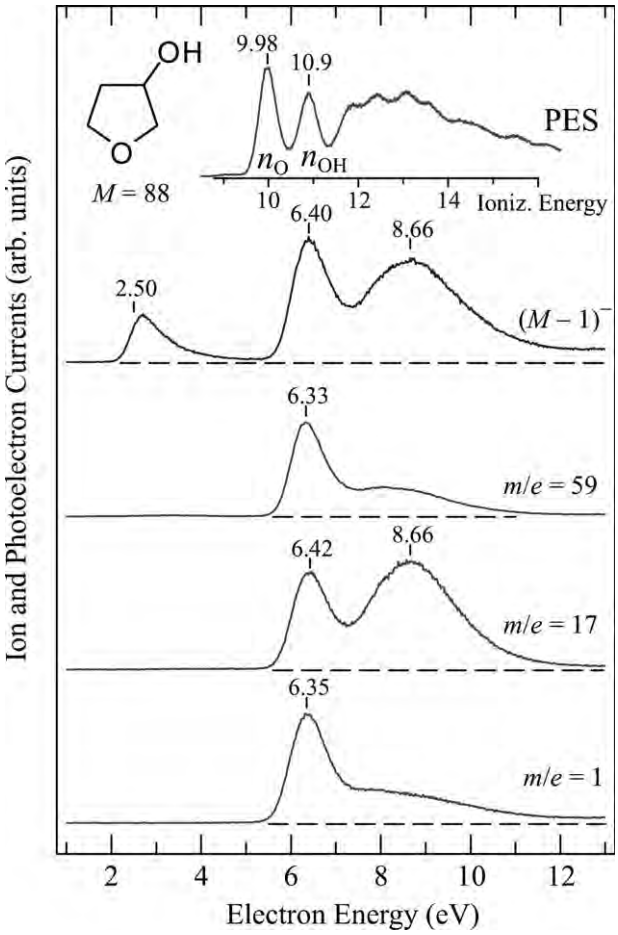

Fig. 9 Photoelectron and DEA spectra of tetrahydrofuran-3-ol (**4**). The PE spectrum is shifted by −4.5 eV.

ionization from the hydroxyl oxygen lone pair orbital. When the PES band is shifted by an amount similar to the other alcohols, the first DEA band at 6.4 eV appears to correspond to the second photoelectron band, that is, to a Feshbach resonance with a hole on the hydroxyl oxygen. The absolute DEA cross-section of **4** (fragments of all masses combined) has been measured by Aflatooni *et al.*[39] who obtained a substantial value of 4.9×10^{-19} cm^2 at the peak of the 6.2 eV band—in contrast to the parent tetrahydrofuran with a peak cross-section of only 0.16×10^{-19} cm^2. The H^- yield in Fig. 9 can be compared to the H^- yield obtained from 10 monolayer thick film of frozen tetrahydrofuran-3-ol by Antic *et al.*[54,55] They observed a shoulder at 7.3 eV followed by a peak at 10 eV, features which probably correspond to the present features at 6.4 and 8.1 eV, but shifted toward higher energies by the surrounding molecules in the condensed phase—an effect similar to the blue shift of Rydberg states of neutral molecules.[56]

A band with an onset at 2.50 eV is observed in the $(M - 1)^-$ spectrum and is assigned to dissociation *via* a σ^*_{O-H} shape resonance as in the preceding alcohols. The onset is at a distinctly lower energy than in methanol, and this change is reflected in the calculated threshold energy (Table 1). The intensity of this band is substantially larger than that for the alcohols discussed so far. This could be a consequence of the

stabilization of the σ* orbitals due to the presence of two electronegative atoms and to the lower energy of the threshold. The broad band at 8.66 eV is presumably due to Feshbach resonances associated with ionization from the σ_{C-C} and σ_{C-H} orbitals.

The fragment with $m/z = 59$ whose spectrum is shown in Fig. 9 corresponds to the loss of an ethene molecule from the $(M - 1)^-$ anion. The structure of the $m/z = 59$ anion could be either the OCH_2CHO^- anion obtained when ethene is split off from tetrahydrofuran-3-ol, or its more stable rearranged form, the acetate anion CH_3COO^-. Also observed, but not shown in Fig. 9, was a fragment with $m/z = 57$, which corresponds to the loss of a formaldehyde molecule from the $(M - 1)^-$ anion. Its structure could be that of an α-deprotonated acetone, isoelectronic with the acetate anion and also stabilized by the delocalization of the charge over three atoms. A fragment with $m/z = 41$, probably deprotonated ketene, is observed with an incident energy of 8 eV. OH^- is presumably the result of direct breaking of the C–OH bond.

3.5 (Tetrahydrofuran-3-yl)methanol (5)

The spectrum in Fig. 10 reveals that the $(M - 1)^-$ fragment is observed with an onset at 2.36 eV, consistent with the calculated threshold (Table 1). Like in tetrahydrofuran-3-ol, the PE-spectrum has two low-lying bands, corresponding to ionization from the ether and the hydroxyl oxygen lone pair orbitals, but only one Feshbach resonance band in the 6–7 eV range. The assignment of the 6.4 eV DEA band to the second PE band appears more probable—the assignment to the first band would require shifting the PE-spectrum by an amount too different from that used for the monoalcohols **1**–**3**. The dominant fragments are $(M - 1)^-$ and H^-; the $m/z = 41$ and OH^- signals are about 5× weaker than the $(M - 1)^-$ signal. Like in the previous section, OH^- is presumably the result of direct breaking of the C–OH bond. The fragment with $m/z = 41$ is presumably deprotonated ketene and results from secondary fragmentation of the $(M - 1)^-$ ion.

3.6 (Tetrahydrofuran-2-yl)methanol (6)

This compound is structurally closely related to the previous one, with the difference that it can build an intramolecular hydrogen bond, not possible in (tetrahydrofuran-3-yl)methanol. This hydrogen bridge slightly stabilizes the neutral target molecule and has the consequence of slightly increasing the threshold for the $(M - 1)^-$ formation. This slight increase is reflected both in the increase of the energy of the $(M - 1)^-$ fragment onset (Fig. 10 and 11) and the calculated threshold energy (Table 1).

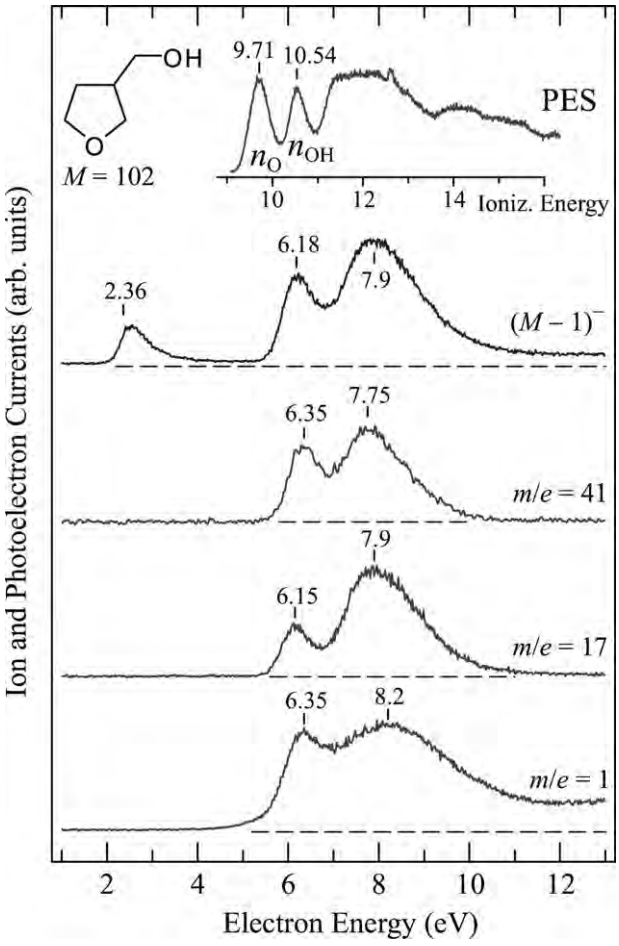

Fig. 10 DEA and PE spectra of (tetrahydrofuran-3-yl)methanol (**5**). The PE spectrum is shown shifted by −4.35 eV.

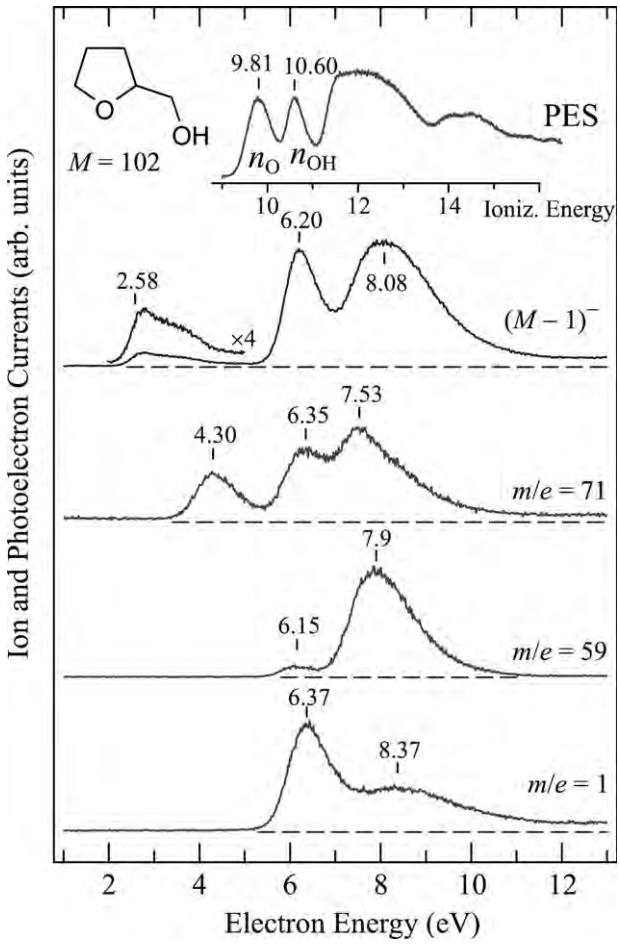

Fig. 11 DEA and PE spectra of (tetrahydrofuran-2-yl)methanol (**6**). The PE spectrum is shown shifted by −4.5 eV.

The fragmentation pattern (Fig. 11) in the Feshbach resonance range closely resembles that of the preceding compound (**5**), with dominant $(M - 1)^-$ and H^- fragments, a weaker OH^- fragment (not shown in Fig. 11), and spectra of similar shapes. New are the fragments with masses 59 and 71. The $m/z = 59$ fragment could correspond to the loss of the ketene molecule from $(M - 1)^-$ and have the propanolate anion structure $C_3H_7O^-$. The $m/z = 71$ fragment is exceptional in the present work in being the only fragment other than $(M - 1)^-$ observed already at energies below the Feshbach resonances, with a band peaking at 4.3 eV in Fig. 11. We propose two mechanisms for its formation: either it could correspond to a simple breaking of a C–C bond to give the CH_2OH + c-$C_4H_7O^-$ fragments with a calculated threshold at 3.43 eV (Table 2) or it could correspond to the loss of the ethane molecule, CH_3CH_3, and have the structure of the conjugate base of the acrylic acid, $CH_2{=}CHCOO^-$. The latter process has a surprisingly low calculated threshold of 0.42 eV (Table 2), but would require a more substantial rearrangement of atoms during the reaction. The onset of this band is above the threshold for both possible explanations, indicating activation energy in the fragmentation. An $m/z = 83$ fragment is weakly observed (but not shown in Fig. 11) and could correspond to the loss of a water molecule from the $(M - 1)^-$ anion and have the structure of an α-deprotonated cyclopentanone.

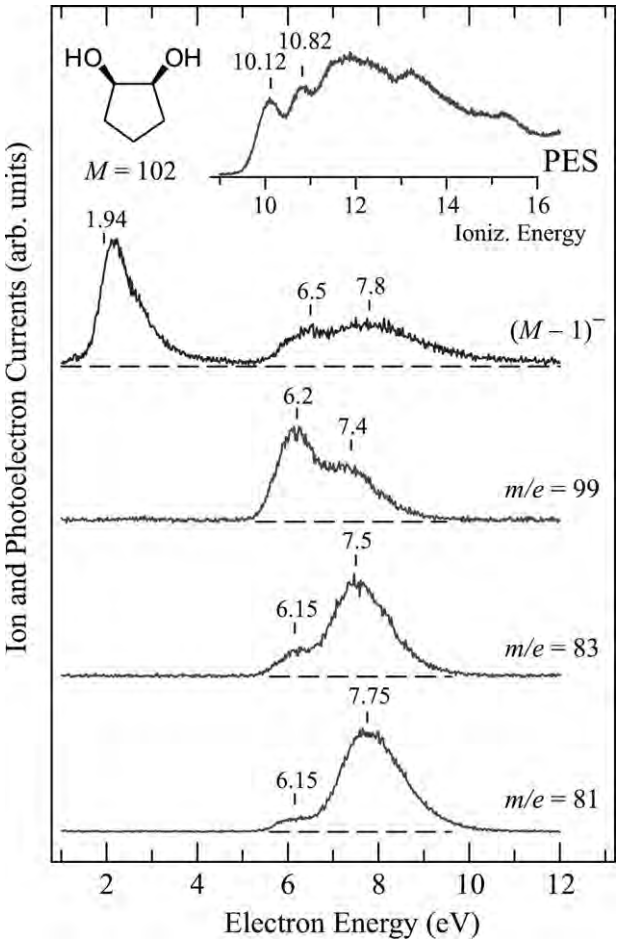

Fig. 12 DEA spectra and the HeI photoelectron spectrum (shown shifted by −4.5 eV) of *cis*-cyclopentane-1,2-diol (**7**).

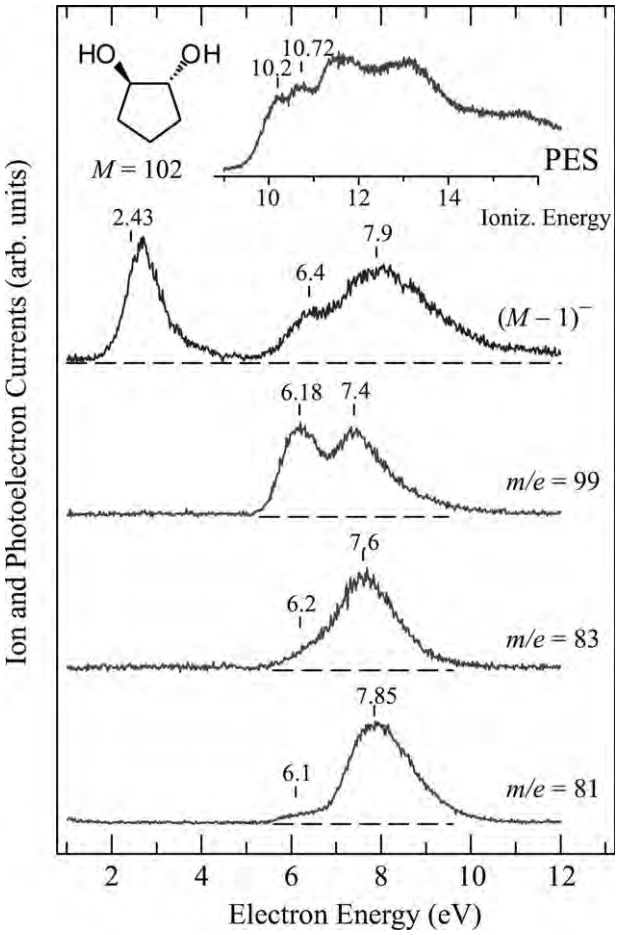

Fig. 13 DEA spectra and the HeI photoelectron spectrum (shown shifted by −4.5 eV) of *trans*-cyclopentane-1,2-diol (**8**).

The H^- yield in Fig. 11 can be compared to the H^- yield obtained from 10 monolayer thick film of frozen (tetrahydrofuran-2-yl)methanol by Antic *et al.*,[54,55] with the same conclusions as reached for tetrahydrofuran-3-ol in section 3.4.

3.7 *Cis*- and *trans*-cyclopentane-1,2-diols (7) and (8)

Fig. 12 and 13 show the PES and DEA spectra of two representative diols. The oxygen lone pair orbitals give rise to two bands in the photoelectron spectrum. MO calculations indicate that charge in the *cis* compound cation is localized to a large degree—the HOMO is essentially the lone pair on the O-atom participating in a hydrogen bridge whereas HOMO-1 is essentially the lone pair on the O-atom not participating in a hydrogen bridge. The OH groups in the *trans* compound are not involved in hydrogen bonds and are thus essentially equivalent. As a consequence, both HOMO and HOMO-1 are delocalized, with equal coefficients on each oxygen lone pair. The two lone pair orbitals in the *trans* compound are too far apart for a through-space interaction, but both are subject to destabilizing through-bond interactions. MO calculations indicate that the through-bond interaction is slightly stronger for the in-phase combination ($n_O + n_{O'}$), which then becomes the HOMO, than for the out-of-phase combination ($n_O - n_{O'}$), which becomes the HOMO-1. The consequence is the 'reverse order' of the cationic states.[57]

The most striking feature of the DEA spectra of the diols is the decreasing energy and increasing relative intensity of the low energy band in comparison to the monoalcohols—they are more intense than the Feshbach resonance bands.

The decreasing thresholds are the result of the increased electron affinity of the fragments, particularly for the *cis* compound where the negative charge is stabilized by a hydrogen bridge. The increase in intensity could be a consequence of decreasing autodetachment width of the lowest σ* resonance as a result of its decreased energy.

These results are potentially interesting in relation with the DEA spectra of deoxyribose, recently studied by Ptasińska *et al.*[58] and of D-ribose, studied by Bald *et al.*[9] Both have a five-membered ring in their furanose form and the former has three, the latter four hydroxyl groups and may thus be considered as a continuation of the present series of mono- and dialcohols. Both in the deoxyribose and the D-ribose intense signals were observed already at 0 eV, in continuation of the trend of increasing intensity of the low energy signals with increasing number of hydroxyl groups reported for mono- and dialcohols in this work. New in the sugars are fragmentation channels with very low thresholds, leading to several stable molecules like H_2O and CO_2,[9,40,58] which we did not observe in the alcohols studied here.

4. Conclusions

We observe two groups of electron-induced dissociations in hydroxyl-containing compounds. At higher energies, in the 5–10 eV range, the chemistry already well-known from smaller alcohols proceeds *via* Feshbach resonances, with a grandparent positive ion core and two electrons in diffuse Rydberg-like orbitals.

Additionally to the dissociations mediated by the Feshbach resonances, we report processes at lower energies, 2–3 eV, which start at their energetic thresholds. Dramatic H/D isotope effects indicate large autodetachment widths of the low-energy resonances, which we assign as shape resonances with temporary occupation of σ^*_{O-H} valence orbitals. The corresponding potential surfaces are likely to acquire a dipole-bound character and to bend down at intermediate O–H distances, similarly to the halogen halide cases.

The importance of the low energy process increases when a second oxygen atom is incorporated in the targets—in the tetrahydrofuran derived molecules—and increases even more when the number of hydroxyl groups is increased from one to two. For the diols the low-energy signal increases when the hydroxyl groups are closer together, that is, when the interaction of the σ^*_{O-H} orbitals of the individual OH groups is increased, therefore increasing the splitting of the two resulting molecular orbitals and stabilizing of the lower σ^*_{O-H} orbital. The trend toward larger intensity of the low-energy processes appears to be continued and further enhanced by the availability of fragmentations with very low thresholds in the sugars (leading to stable molecules like H_2O and CO_2), which have even more OH groups, and where intense signals have already been observed starting at 0 eV.[9,40,58]

Our observations provide indirect insight into the dynamics of the dissociation of the Feshbach resonances—which is not well understood in polyatomic molecules, with the notable exception of the recent detailed theoretical work on H_2O.[23] The mass spectra do not, of course, give indication of the structure of the fragments, but the present work provides indirect evidence by 'chemical' means, by observing the trends in a number of related compounds. The observations made with the present compounds are that:

– The $(M-1)^-$ and H^- fragments are observed in all cases and generally represent the strongest signals.

– These fragments often carry a 'signature' of the Feshbach resonance involved, hydroxyl hydrogens depart from Feshbach resonances with a hole in the oxygen lone pair orbital, alkyl hydrogens depart from Feshbach resonances with a hole in the C–H localized orbitals.

– Fragments other than $(M-1)^-$ and H^- can in most cases be rationalized by subsequent dissociations of the initial $(M-1)^-$ ion into stable structures, generally closed-shell molecules and closed-shell ions, often further stabilized by charge delocalization. These structures are often quite unrelated to the original structure of the target molecule, substantial reorganization of the atoms is required.

These observations can be rationalized by assuming that the primary step in the dissociation of the Feshbach resonances associated with the ionization of the hydroxyl oxygen lone electrons is the loss of the hydroxyl hydrogen, that is, the acidic proton departs, together with the 'extra' electron. For the Feshbach resonances around 8 eV the primary process may be the loss of an alkyl hydrogen. These processes are, because of the low mass of the proton, fast enough to compete with the fast autodetachment of the resonance—this step is 'kinetically driven', on a time scale comparable to or shorter than a classical vibrational period.

The indirect information on the structures of fragments other than $(M-1)^-$ and H^- indicates that their formation is 'thermodynamically driven', with preference for stable fragments. This indicates that these fragments are formed in a slower secondary reaction from the $(M-1)^-$ ion. Some of the $(M-1)^-$ ions formed in the initial fast step are likely to have enough internal energy for the secondary fragmentations. The energy distribution between the kinetic energy of the departing H-atom and the internal degrees of freedom in the initial fast step is to some degree statistical, that is, the $(M-1)^-$ ion is generated with a distribution of internal energies. (The energy distribution of the departing H^- ions has been measured for methanol[42] and a significant release of kinetic energy has been observed.) At least some of the $(M-1)^-$ ions are thus generated hot enough to further dissociate thermally, with preference being given to the most stable fragments, closed shell molecules and ions, which 'boil off' from the primary $(M-1)^-$ ion. $(M-1)^-$ ions which either do not have enough energy to dissociate or where the dissociation takes longer than the passage time through the ion lens and the quadrupole mass filter (about 10 μs) are detected with the $M-1$ mass.

An important difference between small molecules (like H_2O) and the larger molecules is that the latter have many low-lying thresholds corresponding to the loss of stable molecules like ethene, formaldehyde, ketene, water, *etc.*, opening many more fragmentation channels at relatively low energies.

In some cases a second fast primary dissociation appears to be the breaking of a C–O bond leading to loss of OH^- or RO^-.

The low-energy (2–3 eV) processes are limited to the fast dissociations leading to the $(M-1)^-$ ions, without subsequent fragmentations, although calculations indicate that the thresholds for some of the more complex fragmentations would be low enough. It seems that the primary $(M-1)^-$ ions do not have enough energy to overcome activation energies involved in the atom 'scrambling' required for the 'thermodynamically driven' secondary fragmentations.

These findings indicate that care must be taken in porting the results from isolated gas phase molecules to condensed phase, where the initially formed hot ion may be rapidly cooled by the surroundings, quenching further dissociations.

Acknowledgements

This research is part of project No. 200020-113599/1 of the Swiss National Science Foundation.

References

1 B. Boudaiffa, P. Cloutier, D. Hunting, M. A. Huels and L. Sanche, *Science*, 2000, **287**, 1658.
2 F. Martin, P. D. Burrow, Z. Cai, P. Cloutier, D. Hunting and L. Sanche, *Phys. Rev. Lett.*, 2004, **93**, 068101.
3 U. Schmelmer, R. Jordan, W. Geyer, W. Eck, A. Gölzhäuser, M. Grunze and A. Ulman, *Angew. Chem., Int. Ed.*, 2003, **42**, 559.
4 E. Illenbergger and J. Momigny, *Gaseous Molecular Ions*, Steinkopf Verlag, Darmstadt and Springer Verlag, New York, 1992.
5 G. Hanel, B. Gstir, S. Denifl, P. Scheier, M. Probst, M. Farizon, E. Illenberger and T. D. Märk, *Phys. Rev. Lett.*, 2003, **90**, 188104.
6 H. Abdoul-Carime, S. Gohke and E. Illenberger, *Phys. Rev. Lett.*, 2004, **92**, 168103.
7 A. M. Scheer, K. Aflatooni, G. A. Gallup and P. D. Burrow, *Phys. Rev. Lett.*, 2004, **92**, 068102.
8 C. König, J. Kopyra, I. Bald and E. Illenberger, *Phys. Rev. Lett.*, 2006, **97**, 018105.
9 I. Bald, J. Kopyra and E. Illenberger, *Angew. Chem., Int. Ed.*, 2006, **45**, 4851.
10 V. S. Prabhudesai, A. H. Kelkar, D. Nandi and E. Krishnakumar, *Phys. Rev. Lett.*, 2005, **95**, 143202.
11 T. Skalický and M. Allan, *J. Phys. B*, 2004, **37**, 4849.
12 L. G. Christophorou, D. L. McCorkle and A. A. Christodoulides, in *Electron-Molecule Interactions and Their Applications*, ed. L. G. Christophorou, Academic Press, Orlando, 1984, vol. 1, p. 477.
13 Y. Pariat and M. Allan, *Int. J. Mass Spectrom. Ion Processes*, 1991, **103**, 181.
14 H. Hotop, M.-W. Ruf, M. Allan and I. I. Fabrikant, *Adv. At. Mol. Opt. Phys.*, 2003, **49**, 85.
15 A. Schramm, I. I. Fabrikant, J. M. Weber, E. Leber, M. W. Ruf and H. Hotop, *J. Phys. B*, 1999, **32**, 2153.
16 M. Allan and T. Skalický, *J. Phys. B*, 2003, **36**, 3397.
17 M. Stepanović, Y. Pariat and M. Allan, *J. Chem. Phys.*, 1999, **110**, 11376.
18 P. D. Burrow, G. A. Gallup, A. M. Scheer, S. Denifl, S. Ptasińska, T. Mark and P. Scheier, *J. Chem. Phys.*, 2006, **124**, 124310.
19 M. B. Robin, *Higher Excited States of Polyatomic Molecules*, Academic Press, Orlando, 1985.
20 K. L. Stricklett and P. D. Burrow, *J. Phys. B*, 1986, **19**, 4241.
21 R. A. Dressler and M. Allan, *Chem. Phys. Lett.*, 1985, **118**, 93.
22 R. A. Dressler and M. Allan, *J. Electron Spectrosc. Relat. Phenom.*, 1986, **41**, 275.
23 D. J. Haxton, Z. Zhang, H.-D. Meyer, T. N. Rescigno and C. W. McCurdy, *Phys. Rev. A*, 2004, **69**, 062714.
24 H. Estrada, L. S. Cederbaum and W. Domcke, *J. Chem. Phys.*, 1986, **84**, 152.
25 S. Feuerbacher, T. Sommerfeld and L. Cederbaum, *J. Chem. Phys.*, 2004, **120**, 3201.
26 L. Sanche and G. J. Schulz, *Phys. Rev. Lett.*, 1971, **27**, 1333.
27 L. Sanche and G. J. Schulz, *Phys. Rev. A*, 1972, **5**, 1672.
28 L. Sanche and G. J. Schulz, *Phys. Rev. A*, 1972, **6**, 69.
29 L. Sanche and G. J. Schulz, *J. Chem. Phys.*, 1973, **58**, 479.
30 F. Gresteau, R. I. Hall, A. Huetz, D. Vichon and J. Mazeau, *J. Phys. B*, 1979, **12**, 2925.
31 D. Spence, *J. Phys. B*, 1975, **12**, 721.
32 F. H. Read, *J. Phys. B*, 1977, **10**, 449.
33 D. Spence, *J. Chem. Phys.*, 1977, **66**, 669.
34 R. A. Dressler, M. Allan and M. Tronc, *Chem. Phys.*, 1987, **20**, 393.
35 V. I. Khvostenko, A. S. Vorob'yov and O. G. Khvostenko, *J. Phys. B*, 1990, **23**, 1975.
36 R. Dressler and M. Allan, *Chem. Phys.*, 1985, **92**, 449.
37 M. Allan, *J. Phys. B*, 1992, **25**, 1559.
38 M. J. Frisch, G. W. Trucks, H. B. Schlegel, G. E. Scuseria, M. A. Robb, J. R. Cheeseman, J. A. Montgomery, Jr., T. Vreven, K. N. Kudin, J. C. Burant, J. M. Millam, S. S. Iyengar, J. Tomasi, V. Barone, B. Mennucci, M. Cossi, G. Scalmani, N. Rega, G. A. Petersson, H. Nakatsuji, M. Hada, M. Ehara, K. Toyota, R. Fukuda, J. Hasegawa, M. Ishida, T. Nakajima, Y. Honda, O. Kitao, H. Nakai, M. Klene, X. Li, J. E. Knox, H. P. Hratchian, J. B. Cross, V. Bakken, C. Adamo, J. Jaramillo, R. Gomperts, R. E. Stratmann, O. Yazyev, A. J. Austin, R. Cammi, C. Pomelli, J. Ochterski, P. Y. Ayala, K. Morokuma, G. A. Voth, P. Salvador, J. J. Dannenberg, V. G. Zakrzewski, S. Dapprich, A. D. Daniels, M. C. Strain, O. Farkas, D. K. Malick, A. D. Rabuck, K. Raghavachari, J. B. Foresman, J. V. Ortiz, Q. Cui, A. G. Baboul, S. Clifford, J. Cioslowski, B. B. Stefanov, G. Liu, A. Liashenko, P. Piskorz, I. Komaromi, R. L. Martin, D. J. Fox, T. Keith, M. A. Al-Laham, C. Y. Peng, A. Nanayakkara, M. Challacombe, P. M. W. Gill, B. G. Johnson, W. Chen, M. W. Wong, C. Gonzalez and J. A. Pople, *GAUSSIAN 03 (Revision C.02)*, Gaussian, Inc., Wallingford, CT, 2004.
39 A. Aflatooni, A. M. Scheer and P. D. Burrow, *J. Chem. Phys.*, 2006, **125**, 054301.
40 P. Sulzer, S. Ptasińska, F. Zappa, B. Mielewska, A. R. Milosavljević, P. Scheier, T. D. Märk, I. Bald, S. Gohlke, M. A. Huels and E. Illenberger, *J. Chem. Phys.*, 2006, **125**, 044304.
41 A. Kühn, H. P. Fenzlaff and E. Illenberger, *J. Chem. Phys.*, 1988, **88**, 7453.
42 M. G. Curtis and I. C. Walker, *J. Chem. Soc., Faraday Trans.*, 1992, **88**, 2805.
43 NIST Chemistry webbook: http://webbook.nist.gov/chemistry.
44 Y. Pariat and M. Allan, *Int. J. Mass Spectrom. Ion Processes*, 1991, **103**, 181.
45 C. Mündel, M. Berman and W. Domcke, *Phys. Rev. A*, 1985, **32**, 181.
46 G. J. Schulz and R. K. Asundi, *Phys. Rev.*, 1967, **158**, 25.
47 G. J. Schulz, *Rev. Mod. Phys.*, 1973, **45**, 423.
48 I. C. Walker, A. Stamatović and S. F. Wong, *J. Chem. Phys.*, 1978, **69**, 5532.
49 M. Allan, *J. Phys. B*, 2006, **39**, 2939.
50 J. Horáček, M. Čížek, K. Houfek, P. Kolorenč and W. Domcke, *Phys. Rev. A*, 2004, **70**, 052712.
51 J. Horáček, M. Čížek, K. Houfek, P. Kolorenč and W. Domcke, *Phys. Rev. A*, 2006, **73**, 022701.
52 M. Čížek, J. Horáček, M. Allan, A.-C. Sergenton, D. Popović, W. Domcke, T. Leininger and F. X. Gadea, *Phys. Rev. A*, 2001, **63**, 062710.
53 R. Dressler and M. Allan, *J. Electron Spectrosc. Relat. Phenom.*, 1986, **41**, 275.
54 D. Antic, L. Parenteau, M. Lepage and L. Sanche, *J. Phys. Chem. B*, 1999, **103**, 6611.
55 L. Parenteau, D. Antic and L. Sanche, *J. Phys. Chem. B*, 2000, **104**, 4711.
56 M. B. Robin, *Higher Excited States of Polyatomic Molecules*, Academic Press, Orlando, 1985.
57 R. Hoffmann, E. Heilbronner and R. Gleiter, *J. Am. Chem. Soc.*, 1970, **92**, 706.
58 S. Ptasińska, S. Denifl, P. Scheier and T. D. Märk, *J. Chem. Phys.*, 2004, **120**, 8505.

3.3 Dissociative electron attachment of aliphatic alcohols

In this section, the DEA spectra of other alcohols, not published in ref. [32], are discussed. For linear alcohols several structural effects are presented. The influence of the ring size in some alcohols is also discussed.

3.3.1 Propanols

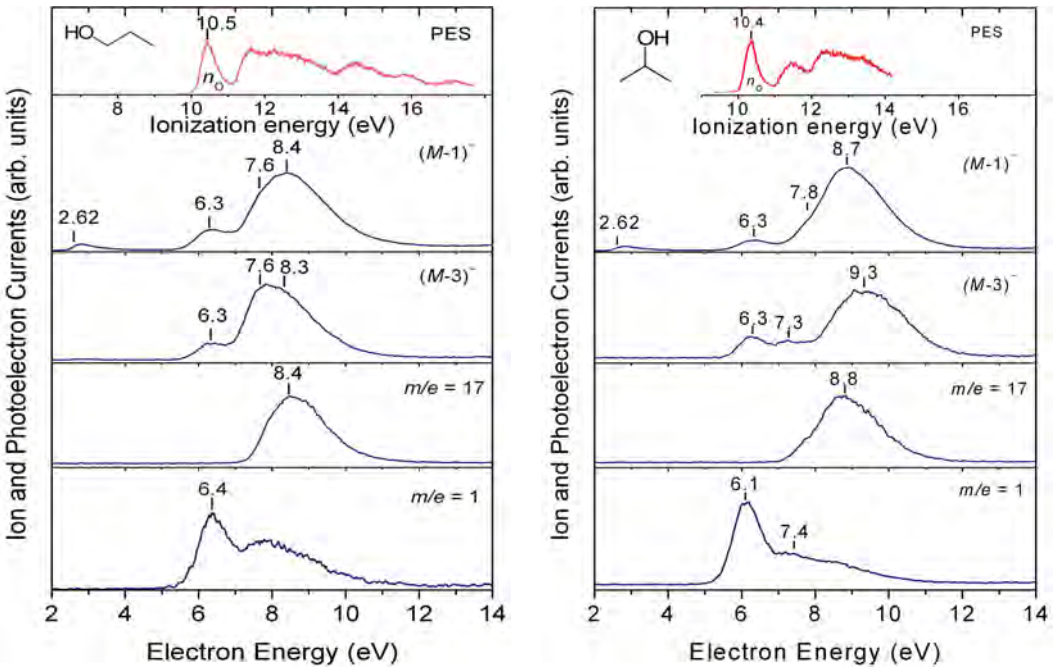

(a) (b)

Figure 3.1: Photoelectron (taken from ref. [45]) and DEA spectra of the two isomers of propanol. The PE spectrum is shown shifted by −4.2 eV for 1-propanol (a) and −4.1 eV for 2-propanol (b).

The DEA spectra of the major fragments from 1-propanol and 2-propanol are presented in fig. 3.1. The $(M\text{-}1)^-$ anion spectrum (loss of a H atom) from both substances is very similar to the corresponding DEA spectra of ethanol and methanol. In all cases a small peak at low energies is detected. Due to the asymmetry of this band and the coincidence of its onset with the threshold energies (shown in table 3.1), we assign this band to a very short-lived σ^*_{OH} shape resonance, similar to those presented in section 3.2. Additionally, we assign the band at 6.3 eV to a Feshbach resonance with a hole in the out-of-plane (n_O) oxygen lone pair orbital. The Feshbach resonance with a hole in the in-plane ($\bar{n}_O$) (see fig. 6.2 on page 86 for details on the notation of molecular orbitals) oxygen lone pair orbital appears as a weak shoulder at 7.6−7.8 eV for both isomers of propanol. The broad band at

around 8 eV is most likely due to one or several Feshbach resonances corresponding to the overlapping bands in the photoelectron spectrum, because of ionization from various C−H and C−C σ orbitals above 12 eV.

Table 3.1: Threshold energies for the reactions $e^- + \mathrm{ROH} \rightarrow \mathrm{RO}^- + \mathrm{H}$, in eV. The DFT values were calculated as described in section 2.2.1. The onset of the DEA bands (taken at 75% of peak height) were taken from the present spectra.

Target	E_{thr}	
	DFT	Onset of DEA
1-propanol	2.66	2.62
2-propanol	2.59	2.62
1-butanol	2.58	2.68
2-butanol	2.53	2.35
cyclobutanol	2.39	2.26
cyclopentanol	2.53	2.67
cyclohexanol	2.57	2.74

The main difference between the two isomers of propanol derives from their classification within different subsets of alcohols: 1-propanol is a primary alcohol while 2-propanol is a secondary alcohol. This difference in the nature of site where the hydroxyl group is attached has some influence on the DEA spectra. The broad band at around 8.4 eV in 1-propanol, associated with Feshbach resonances with holes in $\sigma_{\mathrm{C-H}}$ or $\sigma_{\mathrm{C-C}}$ orbitals, is shifted to higher energies by about 0.3 eV, to 8.7 eV in 2-propanol. The same shift to higher energies is also reflected in the PE band related to this Feshbach resonance, which is changing from 12.25 eV in 1-propanol to 12.58 eV in 2-propanol. Propanol offers the choice of only two isomers and this is not enough to establish a general trend with respect to the nature of the binding site of the hydroxyl group. The next alcohol, butanol, offers a wider choice of isomers and the influence of the nature of the alcohol will be discussed in more detail in the next section.

One of the major fragments formed in the dissociation of the two propanols is the OH^- anion, the result of the O−C bond breaking. In the 0-16 eV energy range, the OH^- yield shows the presence of a broad band at the same energy as the 3^{rd} band in the $(M-1)^-$ spectra. The coincidence of these two bands suggests that they are dissociation products of the same resonance. Interestingly, only the 3rd Feshbach resonance leads to the formation of the OH^- anion, confirming the rule that O−C bond is only broken by resonances associated with $\sigma_{\mathrm{C-H}}$ or $\sigma_{\mathrm{C-C}}$ orbitals. This rule will be extended to ethers in chapter 4 and investigated with *ab initio* calculations in chapter 6.

Another fragment detected from the dissociation of the two isomers of propanol is $(M-3)^-$. This fragment is most likely the result of a loss of an H atom and an H_2 molecule and its structure could be that of an acetaldehyde deprotonated in the α position – the negative charge is stabilized by delocalization over three atoms. Similar fragments have been detected in other compounds with hydroxyl groups [32].

3.3.2 Butanols

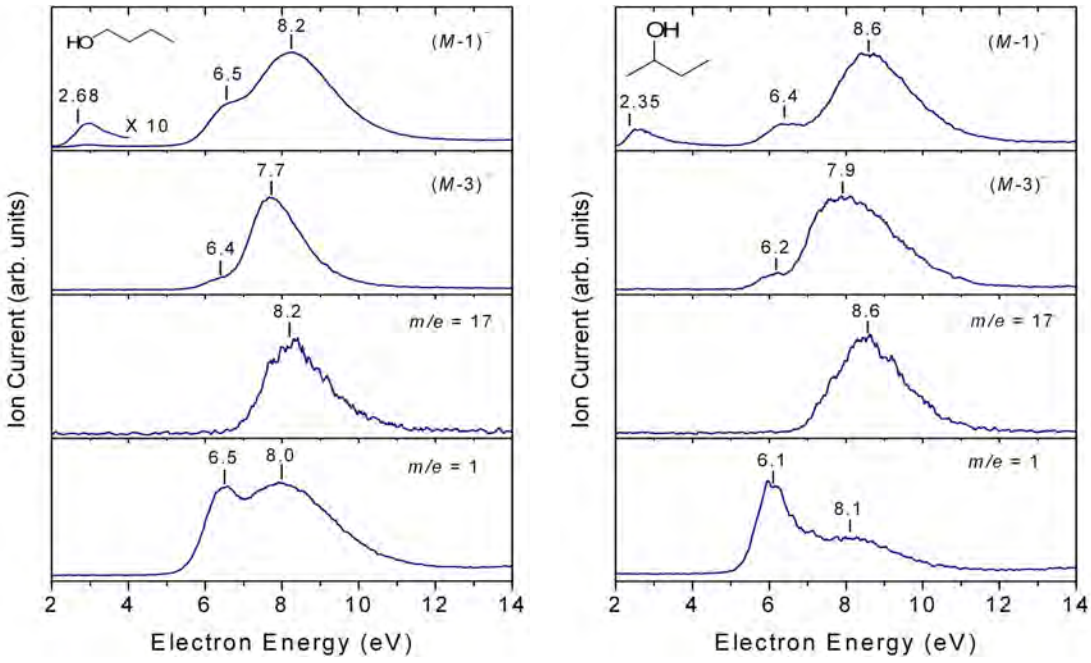

(a) 1-Butanol (b) 2-Butanol

Figure 3.2: DEA spectra of the 1-butanol and 2-butanol.

The spectra for the three isomers of butanol are shown in figs. 3.2 and 3.3. The PE spectrum of 1-butanol [45] shows a band at 10.37 eV due to ionization from the n_O oxygen lone pair orbital. Similarly to the previous cases of alcohols, we assign the 6.5 eV band in the $(M-1)^-$ spectra in all butanols to a Feshbach resonance with a hole in above mentioned orbital. The Feshbach resonance with a hole in the the $\bar{n}_O$ oxygen lone pair orbital is not visible in the $(M-1)^-$ spectra but appears as a distinct band in the $(M-3)^-$ spectra. Finally, we assign the broad band at around 8 eV in the $(M-1)^-$ spectra to Feshbach resonances with holes in the C−H and C−C σ orbitals.

Changing from primary to secondary propanol led to a shift of the broad band at 8-9 eV to higher energies. In butanols the trend can be extended to tertiary alcohols. The main difference in $(M-1)^-$ spectra among the three isomers of butanol is the position of the 3^{rd} Feshbach resonance. This resonance is shifted to higher energies (from 8.2 eV in 1-butanol to 8.6 eV in 2-butanol and, finally, to 8.7 eV in *tert*-butanol) on going from the primary to the tertiary alcohol. The bands at lower energies are not affected by this change.

Even though the shift in energy is small and in some cases in the range of experimental errors, the continuity of the trend in both series of alcohols indicates that the effect is real. The fact that only the broad band at 8-9 eV is affected by where the hydroxyl group is attached, and that this change is reflected in the PE spectrum are an indication on the localization of the orbital associated with the

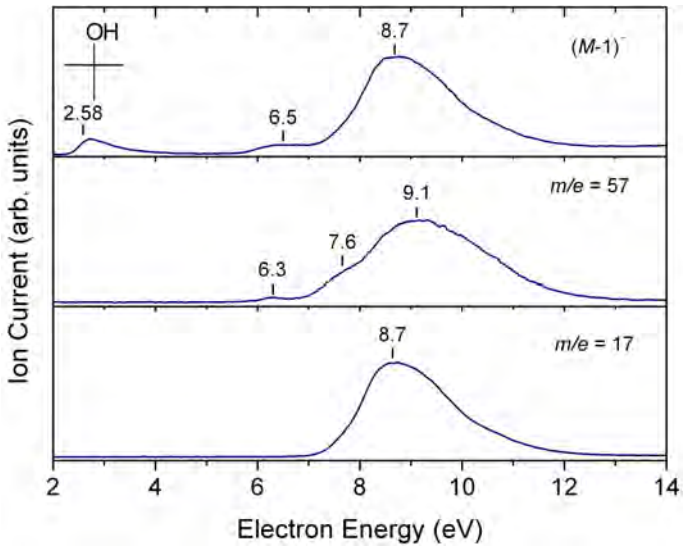

Figure 3.3: DEA spectra of the *tert*-butanol.

Feshbach resonance on the alkyl fragment of the molecule.

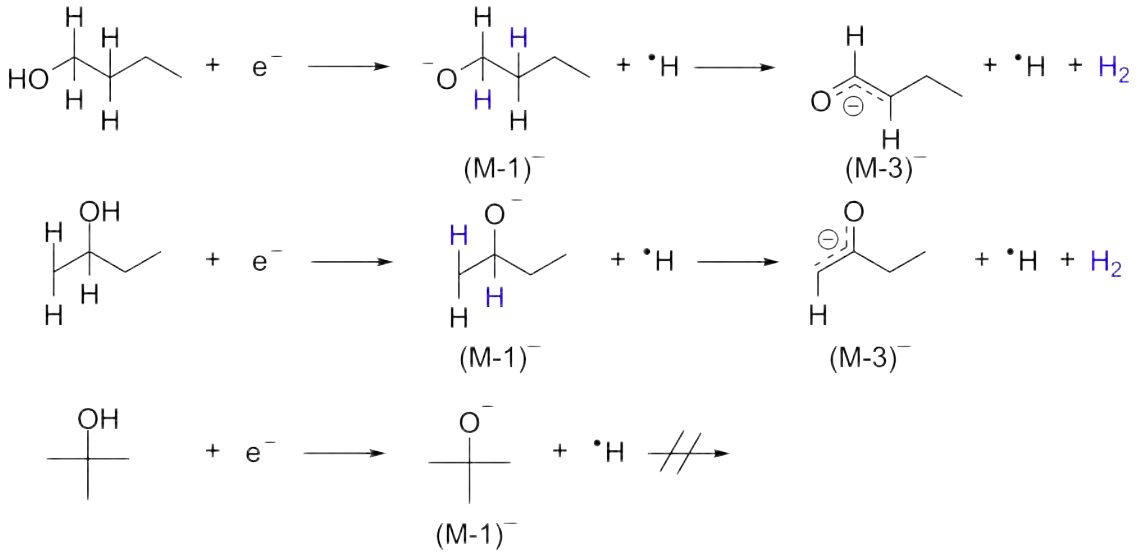

Figure 3.4: Scheme showing the formation of $(M-3)^-$ ion in butanols.

A major fragment detected for butanols is the OH^- anion. The DEA spectra of this anion show the presence of only one broad band at an energy similar to that of the broad 8-9 eV band in the $(M-1)^-$ spectra. We conclude that OH^- is the product of dissociation of the same resonance as $(M-1)^-$, similar to the situation encountered for propanols.

Another fragment detected from the dissociation of the isomers of butanol is $(M-3)^-$. Just as for other alcohols, we suggest that this anion is the result of a loss of an H atom and an H_2 molecule, with a structure of an butyroaldehyde

deprotonated in the α position as shown by the reaction scheme in fig. 3.4. The $(M-3)^-$ anion has not been detected for *tert*-butanol, indicating that the two hydrogens required for the formation of H_2, are lost from neighboring carbons, one of the sites being the α-carbon.

3.3.3 Ali-cyclic alcohols

The spectra of OH^- and $(M-1)^-$ fragments for several ali-cyclic alcohols are shown in fig. 3.5.

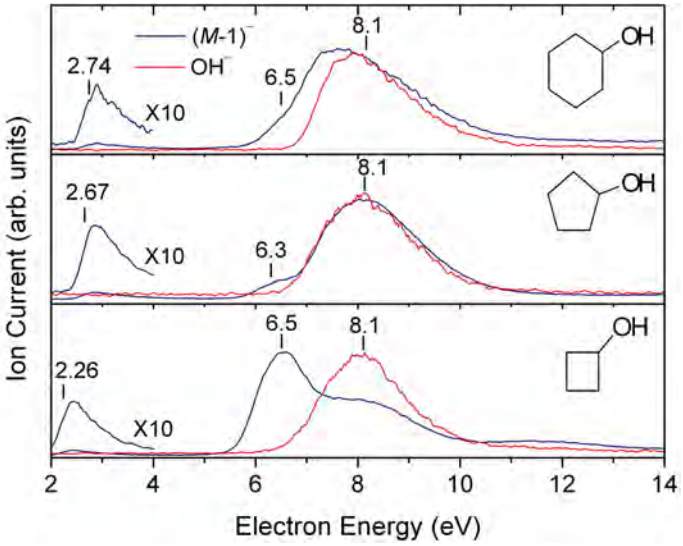

Figure 3.5: DEA spectra of three ali-cyclic alcohols. The spectra of the OH^- anion are represented as red solid lines, while the spectra of the $(M-1)^-$ fragment are represented as blue solid lines.

The size of the cyclo-alkyl ring attached to the hydroxyl group has several influences on the DEA spectra. The $(M-1)^-$ spectra of these alcohols show the presence of a band at low energies, around 2.5 eV. For cyclopentanol the low energy band has been assigned to dissociation *via* a shape resonance (see section 3.2). Similarly, we assign the corresponding band in cyclobutanol and cyclohexanol to shape resonances. The onset of the DEA band associated with the resonance rises in energy as the ring size is increased. This change is also reflected in the calculated threshold energies (Table 3.1). This is most likely due to the increase in the O−H bond strength since the our calculations indicate that the electron affinities of the these alcohols are identical.

In section 3.2 the broad and unstructured band peaking around 8.1 eV which appears in the $(M-1)^-$ spectra for cyclopentanol is assigned to several overlapping Feshbach resonances with σ^{-1}_{C-H} and σ^{-1}_{C-C} grandparent states. A similar band appears at 8.1 eV in the other ali-cyclic alcohols and also in the other alcohols which we have analyzed so far. The position of this band decreases as the length of the alkyl chain is increased. It is at 10.5 eV in methanol and decreases steadily up to 8.2

eV in 1-butanol. But in ali-cyclic alcohols a limit is reached and the position of this band does not decrease below 8.1 eV even if the size of the cyclo-alkyl fragment is increased. This trend in the position of this Feshbach resonance is also reflected in the position of the band in the OH^- spectra. In cyclic alcohols this band is centered at 8.1 eV and it has a similar FWHM value.

Another change induced by the ring size concerns the relative intensity of the bands associated with the Feshbach resonances. In cyclobutanol the 8.1 eV band is the least intense band but, as the size of the alkyl cycle is increased, it dramatically increases in intensity being dominant and the 6.5 eV being present only as a shoulder in cyclohexanol. The increase in intensity is most likely due to the fact that the 8 eV band is the result of several overlapping bands associated with Feshbach resonances with holes in the C−H and C−C σ orbitals. As the ring size is increased so is the number of σ orbitals and the intensity of the band.

Several other fragments have been recorded in the dissociation of the cyclic alcohols. One of these fragments is the $(M-3)^-$ anion. As in the case of cyclopentanol, discussed in section 3.2, we propose that $(M-3)^-$ is the result of an additional loss of an H_2 molecule from $(M-1)^-$ anion, forming an anion whose stability is a consequence of the charge delocalization over three atoms.

3.3.4 Ethanol-d_3

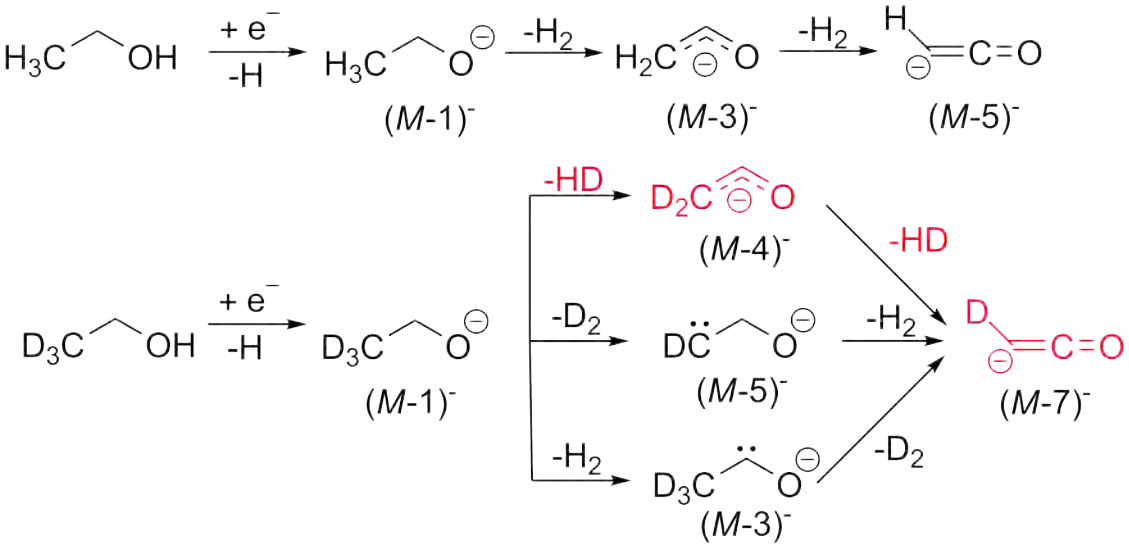

Figure 3.6: Reaction scheme for the formation of $(M-1)^-$, $(M-3)^-$, $(M-5)^-$ ions in ethanol and $(M-1)^-$, $(M-3)^-$, $(M-4)^-$, $(M-5)^-$, $(M-7)^-$ ions in ethanol-d_3. The reactions observed experimentally are marked in red.

One frequent dissociation reaction undergone by alcohols reported in section 3.2 is the loss of an hydrogen atom, followed by an additional loss of H_2 molecule with the formation of a $(M-3)^-$ anion as shown in fig. 3.6 for ethanol. H_2 could in

principle be lost from the same carbon atom or from two neighboring atoms. The partially deuterated isotopomer of ethanol, ethanol-d_3, CD_3CH_2OH, is used here to distinguish between these two possibilities and determine from which site the two hydrogen atoms are lost. If both hydrogens were lost from the α-carbon then $(M-3)^-$ should be observed, while loss from the β-carbon would yield $(M-5)^-$. But if one hydrogen were lost from α-carbon and the other from β-carbon then $(M-4)^-$ should be detected, as is shown in fig. 3.6. Ethanol-d_3 is not commercially available and it was synthesized using the following reaction (see section 2.3.1 for more details):

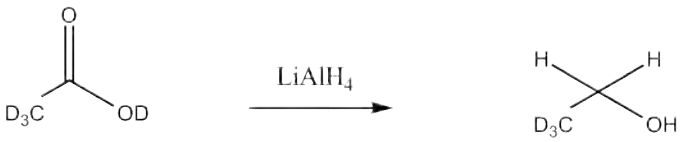

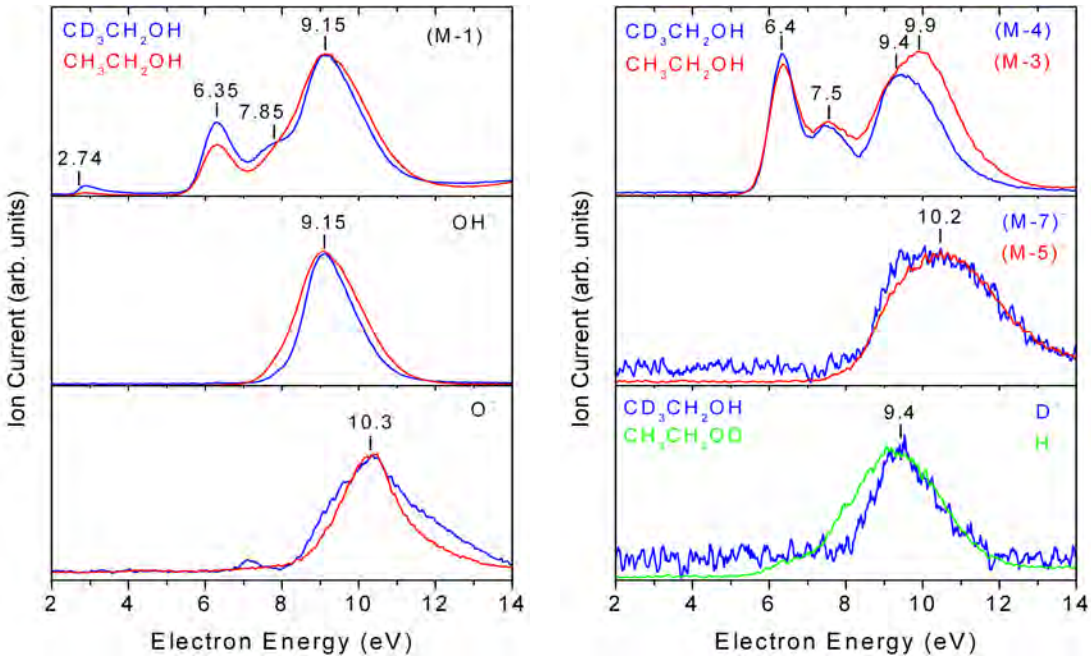

Figure 3.7: DEA spectra of various fragments from ethanol-d_3 (solid blue lines), undeuterated ethanol (solid red lines), ethanol-d_1 (solid green lines).

The DEA spectra of ethanol-d_3 are shown in fig. 3.7. The molecular weight of ethanol-d_3 is 49. No DEA signal has been detected at $(M-3)^-$ (loss of three hydrogen atoms) or $(M-5)^-$ (loss of one hydrogen atom and D_2). But a DEA spectrum has been recorded at $(M-4)^-$ (loss of a hydrogen atom and an HD molecule). This is an indication that one hydrogen is lost from the α-carbon and the other one is lost from the β-carbon. in addition, a comparison between the DEA spectra of $(M-3)^-$ ion from undeuterated ethanol and $(M-4)^-$ ion from ethanol-d_3 indicates that they are formed through the same process. These observations

indicate that during the formation of the $(M-3)^-$ anion from undeuterated ethanols, the hydrogens are lost from two neighboring carbon atoms.

Apart from the loss of a H and H_2 with the formation of the $(M-3)^-$ ion, the loss of H and two H_2 molecules has been observed in ethanol (section 3.2). Ethanol-d_3 sheds some light on this process as well. The $(M-5)^-$ ion observed from undeuterated ethanol is formed from the dehydrogenation of the $(M-3)^-$ ion. Consequently the observation of a $(M-7)^-$ ion from ethanol-d_3 is an indication of a similar process with an additional loss of an HD molecule from the $(M-4)^-$ ion. This conclusion is supported by the remarkable similarity of DEA spectra of the $(M-5)^-$ ion from undeuterated ethanol and $(M-7)^-$ ion from ethanol-d_3 (fig. 3.7).

Finally, fig. 3.7 shows a comparison between the DEA spectrum for the formation of D^- from ethanol-d_3 and that of H^- from ethanol-d_1 and it reveals the presence of state selective chemistry. Both spectra show the presence of a broad unstructured band at around 9 eV. The onset of the band in the H^-/EtOD spectrum is around 5 eV while the onset in the D^-/ethanol-d_3 spectrum is around 8 eV. This may be due to the fact that, while H^- can be lost from both carbon atoms [32], D^-/ethanol-d_3 can only be lost from the terminal methyl site. It is also worth noting that the 9.4 eV band in the D^-/ethanol-d_3 spectrum coincides in energy and FWHM value with the 9.4 eV band in the $(M-4)^-$/ethanol-d_3 spectrum, indicating that they are the product of dissociation of the same resonance.

No H^- has been detected as a result of electron-molecule collision in ethanol-d_3. This is in contrast to the undeuterated ethanol where H^- ion was observed. This means that the distribution of the negative charge between the $(M-1)^-$ and H fragment is not selective for the dissociation of the Feshbach resonances with the formation of both $(M-1)^-$ and H^- ions in undeuterated ethanol. But, in ethanol-d_3, the charge distribution between the two fragments is selective since the dissociation of the Feshbach resonances results only in the formation of the $(M-1)^-$ ion.

3.4 Relative band intensity studies on deuterated alcohols

The present experimental setup does not allow to measure absolute cross-sections but the relative cross-sections can be determined for various methanol and ethanol isotopomers by recording signal intensities for the same pressure (same Penning gauge reading) and the same electron beam current. The spectra for various fragments are normalized to the highest yield. The results are presented in fig. 3.8 for methanol isotopomers and in fig. 3.9 for ethanol isotopomers. They show a comparison of the yield of the same type of fragment (*e.g.*, for the top left corner in fig. 3.8 the methanolate anion) from different isotopomers. The errors in determining the relative cross-sections are estimated to be about 30%.

The analysis of the fragment yields as a function of deuteration reveals some interesting isotope effects for the bands in the region where Feshbach resonances

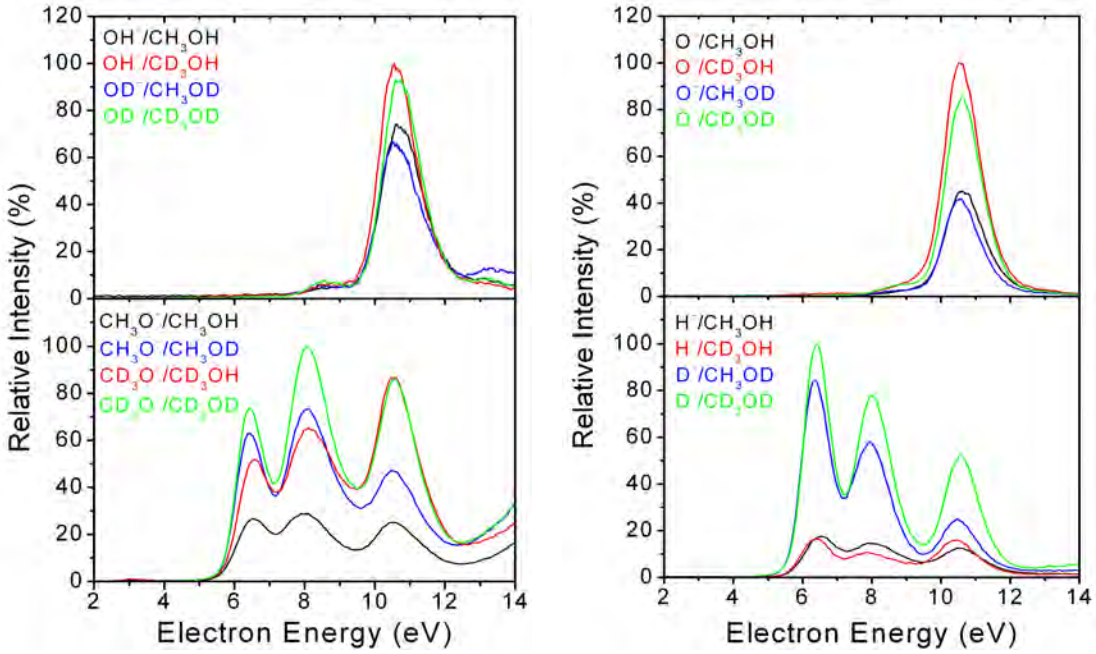

Figure 3.8: Relative yield of various fragments from the isotopically substituted methanols. The spectra are normalized with respect to the highest ion signal.

have been detected in methanol. The formation of the O^- and OH^- fragments occurs only through the third observed Feshbach resonance. For these anions we observe that deuterating the hydroxyl group (a change from the black curve to the blue curve and from red curve to the green curve in fig. 3.8) has no effect on the ion yield while deuterating the methyl group (a change from the black curve to the red curve and from the blue curve to the green curve in fig. 3.8) leads to an inversed isotope effect. O^- shows a more pronounced increase on deuteration of the methyl group than OH^-. These observations would support the idea that the hole in this Feshbach resonance is largely localized on the methyl group since deuteration of this group leads to a change in ion yield. This idea will be explored more in detail in the chapter dedicated to ethers (chapter 4).

The relative yields presented in fig. 3.8 shed some light into the formation dynamics of the O^- ion. The formation of the O^- requires the breaking of both bonds on the oxygen atom and it seems that the determining step for the formation of this anion is the breaking of the O−C bond since a higher yield is observed when the methyl group is deuterated.

The analysis is more complicated for the methanolate and hydrogen (deuterium) anions since these ions are the product of dissociation of three Feshbach resonances. In the first two resonances the electrons are removed from the nonbonding orbitals, while in the third resonance the electron is removed from a σ orbital [22]. This leads to different isotope effects for the observed resonances. For the formation of the methanolate anion we observe an inverse isotope effect. This effect varies less with the deuteration site for the first two resonances than for the third resonance.

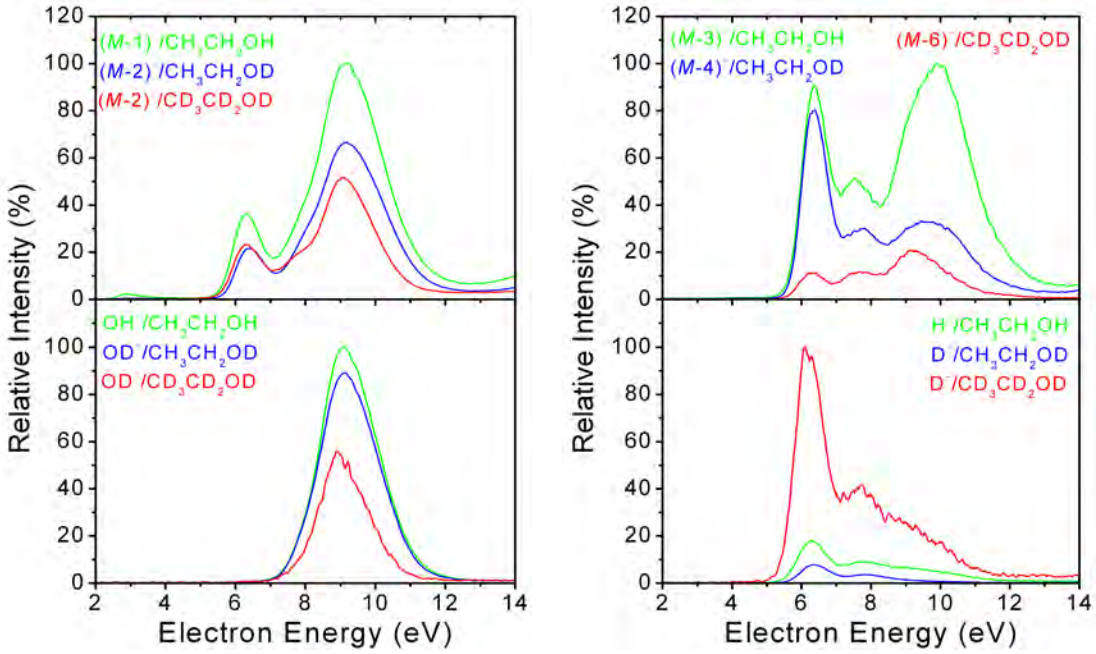

Figure 3.9: Relative yield of various fragments from selected isotopically substituted ethanols. The spectra are normalized to the highest ion signal.

For this resonance an isotope effect is obtained only when methyl is deuterated, a situation similar to that encountered for the O^- and OH^- ions.

An inverse isotope effect is also observed for the H^- (D^-) ion. However, this effect is only noticed when the hydroxyl group is deuterated, while deuteration of the methyl group does not lead to significant change in the observed ion yield.

The inverse isotope effects can be rationalized by considering that the deuterated groups have a higher mass than their undeuterated counterparts. For the methanolate anion the increase in mass increases the possibility of fast intramolecular vibrational redistribution (IVR) in the anion which stabilizes the anion and thus endows it with a longer lifetime. This reasoning cannot be used to explain the isotope effect for the third observed Feshbach resonance. For this resonance deuteration of the methyl group leads to an increase in the yields of all ions with the exception of H^-. The reason could be related to the fact that C−D modes are, in terms of their frequencies, better separated from the dissociating (O−H stretch) mode, thus reducing the possibility of fast intramolecular vibrational redistribution (IVR) of the temporary negative ion.

For ethanol we observe a strong (normal) isotope effect for the main fragments, as shown in fig. 3.9. In all cases the increase of the amount of deuteration leads to a decrease in the yield with H^-/D^- being the only exception. For the formation of ethanolate anion, the strongest effect is provided by deuteration of the hydroxyl group (a change from the green curve to the other two in fig. 3.9). Additional deuteration of the alkyl chain (a change from the blue curve to the red curve in fig. 3.9) leads to weaker isotope effect. For this anion the isotope effect is not

different for the observed resonances as in the case of methanol. The hydroxylate anion is in ethanol, as in methanol, only obtained as the product of dissociation of the third observed Feshbach resonance. And, as in methanol, the isotope effect is inverse and introduced by the deuteration of the alkyl chain but only weakly by the deuteration of the hydroxyl group. Also this effect sheds some light on the dissociation dynamics of the resonance at 9 eV. Most likely the resonance is a Feshbach resonance where the hole is on an orbital localized on the alkyl chain.

One ion that does not appear in methanol, but appears in ethanol is $(M-3)^-$ or $(M-6)^-$ in ethanol-d_6. This anion is obtained as product of dissociation of three Feshbach resonance. For the first observed resonance an isotope effect is noticed when the ethyl is deuterated and only very weakly when hydroxyl is deuterated. For the second resonance both steps of deuteration introduce roughly equal amounts of isotope effect while for the third observed resonance most of the isotope effect is introduced by deuteration on the hydroxyl group.

For H^- or D^- ion we observe an inverse isotope effect. This can be the result of the fact that, for this ion, the change in mass is more pronounced upon deuteration than for the other ions. Thus competing processes, such as autodetachment, are affected more strongly leading to a more dramatic effect.

3.5 Pressure dependence of ion yields in alcohols

In the study of electron-molecule collisions two experimental regimes are encountered. In the first regime the mean free path between the molecules is long enough so that the collisions between them are rare during the lifetime of the anions. This is called *single collision regime* and is predominant if the pressure in the target chamber is low. But, as the pressure in the target chamber is increased another regime becomes predominant. In this regime the mean free path between the molecules and the ions is relatively short and collisions between them become possible. This regime is called *ion-molecule regime*. Ion-molecule reactions are not a desired effect in the measurement of dissociative electron attachment since they are secondary processes. Thus it is important to study the influence of pressure on the DEA spectra.

In the single collision regime the ion yield increases linearly with the increase in pressure. But, as ion-molecule reactions become a predominant factor, the dependence of the ion yield on pressure becomes more and more non-linear.

The DEA spectra of alcohols and that of many polyatomic molecules, can be divided into a low energy domain, between zero and about 5 eV where dissociation is dominated by shape resonances, and a high energy domain, about $5-14$ eV where dissociation occurs mostly through Feshbach resonances. Because of the difference in the mechanism of the electron capture, the pressure dependence will be presented separately for the two energy domains.

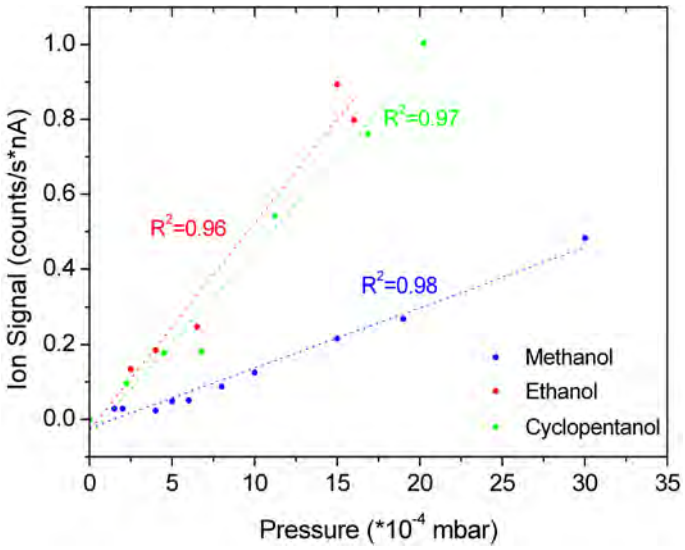

Figure 3.10: Ion yield at the peak of the first DEA band for three alcohols as a function of pressure. The experimental values are represented by points, while the dashed lines represent the values obtained with a linear fit.

3.5.1 The 0-5 eV energy domain

In the low energy domain the DEA spectra of alcohols show the presence of processes that start at their thermodynamic energy thresholds. These processes are assigned to shape resonances with temporary occupation of $\sigma^*_{\mathrm{O-H}}$ valence orbitals. In this energy range only one negative fragment has been detected as the result of electron-molecule reaction. This anion is the result of the loss of a hydrogen atom and has been labeled as $(M-1)^-$ (see section 3.2 for more details).

Fig. 3.10 shows the ion yield of the $(M-1)^-$ anion for methanol, ethanol and cyclopentanol at the peak of the DEA band as a function of the pressure in the main chamber. The yield is recorded at the same electron current. The pressure measurements in the main chamber are made using a recently installed capacitance manometer and are independentof the type of gas. The experimental values are compared with a linear dependence (dashed lines in fig. 3.10) and the correlation coefficients (R^2) are indicated in the figure.

For all molecules a value of R^2 higher than 0.95 has been obtained for the correlation coefficients and no systematic deviation was observed, indicating a linear dependence between the ion yield for the $(M-1)^-$ anion and the pressure in the target chamber. Also, no other ions were detected at these low energies. We conclude that the band associated with the shape resonance is not affected by ion-molecule reactions. The only possible collisions are between the $(M-1)^-$ ion and the neutral molecule resulting in the inelastic scattering of the ion and subsequent cooling. Also the ion has very little kinetic energy prior to collision. Overall these processes have no observable impact on the ion yield.

3.5.2 The 5-16 eV energy domain

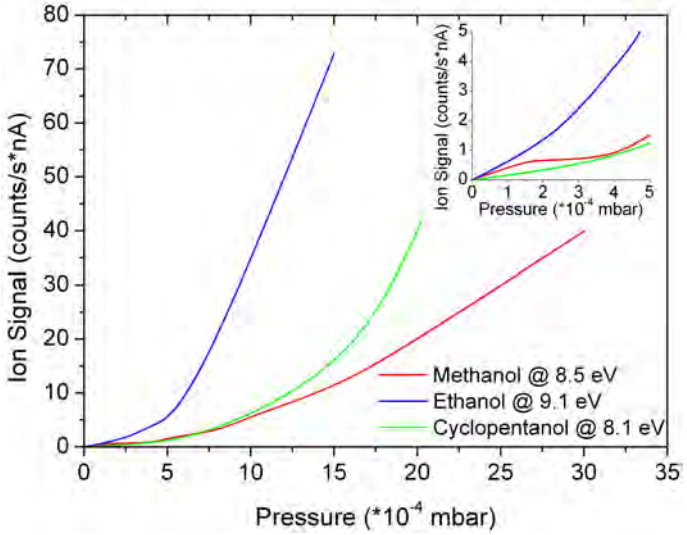

Figure 3.11: Ion yield at highest DEA band of the $(M-1)^-$ fragment for several alcohols as a function of pressure. A blow-out of the $0-5\cdot10^{-4}$ mbar is presented in the inset.

To understand the pressure dependence in this energy range one has to consider the dissociation characteristics of the alcohols. In the 5-16 eV energy domain the DEA spectra of alcohols are dominated by the presence of several Feshbach resonances with occupation of Rydberg-like orbitals. In this energy range dissociation proceeds with the formation of several fragments, the most common of which is, as in the 0-5 eV domain, the $(M-1)^-$.

Fig. 3.11 shows the yield of the $(M-1)^-$ ion as a function of pressure in the target chamber. The ion yield is recorded at the energy of the most intense DEA band for all alcohols (8.5 eV for methanol, 9.1 eV for ethanol and 8.1 eV for cyclopentanol) and for the same electron beam current. A comparison with a similar graph, recorded for the 0-5 eV energy range (fig. 3.10), reveals that the dependence of the ion yield of the $(M-1)^-$ fragment on pressure is non-linear for the 5-16 eV energy range already above $1.5\cdot10^{-4}$ mbar. We conclude that above this pressure there are secondary ion-molecule reactions that cause the dependence on pressure to deviate from linearity. It is thus important to determine what are these secondary ion-molecule reactions.

Fig. 3.12(a) shows the relative intensity of the DEA bands in the $(M-1)^-$ spectrum as a function of pressure in the target chamber. This is calculated by normalizing the signal intensity at the same electron beam current to that of the highest DEA band. For methanol three DEA bands have been detected, with the 8.5 eV band being the most intense, while for ethanol the 7.8 eV band is present only as a shoulder for the 9.1 eV band and it is thus difficult to determine the relative intensity of this band. The highest signal for ethanol is for the 9.1 eV band. The errors in the determination of the relative intensity are estimated to be about 20%.

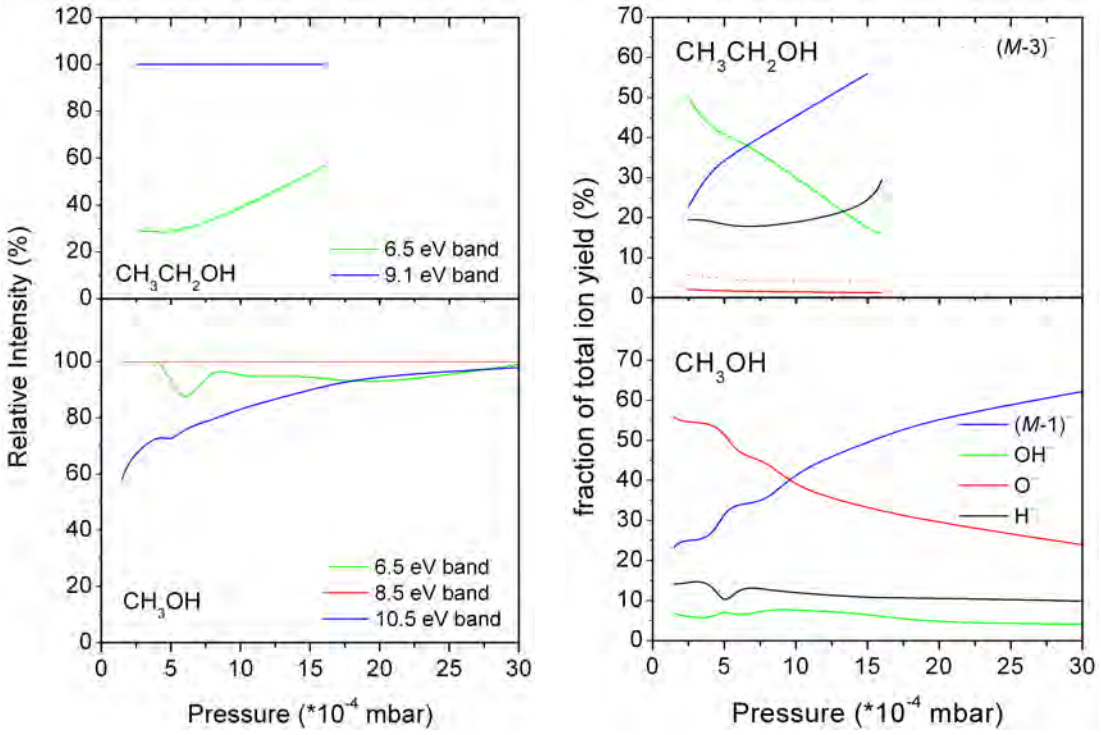

(a) (b)

Figure 3.12: (a) Relative yield of $(M-1)^-$ (see text for more details) from different Feshbach resonances for methanol and ethanol as a function of pressure; (b) Fraction of the total ion yield for different fragments from methanol and ethanol as a function of pressure. The $(M-3)^-$ ion specific to fragmentation of ethanol is shown as dotted line.

If no secondary ion-molecule reaction take place then the relative intensity of all the bands should remain constant at all pressures. In methanol the 6.5 eV band has always the same intensity as the 8.5 eV band at all pressures, but for the band at 10.5 eV the relative intensity increases as the pressure is increased. Thus ion-molecule reactions must affect in particular the 10.5 eV resonance and generate additional $(M-1)^-$ anions.

To establish the reactions taking place we used the fraction of a certain anion yield in the total ion signal, calculated using the following relation:

$$f(Ion) = \frac{I(Ion)}{\sum_{i=1}^{n} I_i(Ion)} \tag{3.1}$$

where: $f(Ion)$ = the fraction of anion yield in the total ion yield; $I(Ion)$ = signal intensity of the anion; $\sum I_i(Ion)$ = sum of signal intensities for all detected anions.

Under single collision conditions the signal intensity of the ions increases linearly with the pressure and thus the fraction of a particular ion yield in the total ion signal

remains at a constant value. In methanol this condition is fulfilled for H^- and OH^- anions (fig. 3.12(b)). But for O^- the fraction decreases as the pressure is increased, while for the CH_3O^- anion it increases. We conclude that O^- is consumed while CH_3O^- is generated in ion-molecule reactions. Since O^- is highly basic we conclude that the most probable reaction is that O^- abstracts a proton from the neutral methanol forming CH_3O^- , according to the following reaction:

$$O^- + CH_3OH \longrightarrow OH^{\cdot} + CH_3O^-$$

Figure 3.13: Reaction Scheme for the ion-molecule reaction between methanol and O^-.

The variation of the fraction of a certain anion in the total ion yield gives limited evidence for the reactions that take place. The above reaction can account for the steeper increase of the 10.5 eV band compared to the other bands (fig. 3.12(a)) since O^- is only produced at this electron energy. But it does not account for the non-linear increase of the other bands (fig. 3.11). This problem will be addressed in the last part of this section together with ethanol.

The signal intensity for the ethanolate anion in the studied energy range is also affected by ion-molecule reactions. This can be observed in the non-linear increase of the ion yield as a function of pressure (fig. 3.11). The signal intensity at 6.5 eV has a higher increase rate than at higher energies (fig. 3.12(a)). Additional information is provided by the analysis of the fraction of ion yield as a function of pressure (fig. 3.12(b)). For the O^- and H^- anions their fraction of the total ion yield remains constant or it varies slightly, within the error range. This suggests that they are not involved in ion-molecule reactions. But for the ethanolate anion the fraction increases as the pressure increases, while the fraction of the hydroxyl anion decreases. The variation of the relative yield for these two anion shows that they are involved in ion-molecule reactions. The most likely reaction is the removal of a proton from ethanol by the OH^- with the formation of the ethanolate anion:

$$OH^- + CH_3CH_2OH \longrightarrow H_2O + CH_3CH_2O^-$$

Figure 3.14: Reaction Scheme for the ion-molecule reaction between ethanol and OH^-.

Just as for methanol where a similar reaction involving O^- has been surmised to occur, this reaction can only account for the increase of the 9.1 eV band, energy at which the OH^- ions are produced, and not for the increase of the other bands.

Similar reactions have already been reported to occur in the gas phase between alcohols and O^- and OH^- ions [50, 51]. Houriet *et al.* have reported that the reaction of OH^- with alcohols with the formation of the alkoxide anion is exothermic by about 68 kJ/mol. At the same time the reaction of O^- with alcohols is less exothermic than the reaction with OH^- by about 33 kJ/mol [51]. The gas phase acidities are given in table 3.2.

Table 3.2: Gas phase acidities ($\Delta_f H^\circ$) for different molecules (Ref. [49]). The values are in kJ/mol.

Molecule	$\Delta_f H^\circ$
$\mathbf{CH_3CH_2OH}$	1586
$\mathbf{CH_3OH}$	1596
OH	1601
$\mathbf{H_2O}$	1633

Interestingly, while O^- and OH^- are present in both methanol and ethanol, O^- reacts, through ion-molecule reactions, with methanol forming $(M-1)^-$ ion and OH^- does not react with methanol. In ethanol, is OH^- that is involved in ion-molecule reactions and not O^-. In ethanol this is expected since OH^- is more reactive than O^- [51]. But, paradoxically, in methanol it is O^- that reacts and not OH^- suggesting that perhaps the reaction of methanol with O^- is not going directly as described by the reaction in fig. 3.13 but through an intermediate as suggested in fig. 3.15.

$$O^- + CH_3OH \longrightarrow HO^- + CH_3O^\cdot$$
$$OH^- + CH_3OH \longrightarrow H_2O + CH_3O^-$$

Figure 3.15: Proposed reaction scheme for the ion-molecule reaction between methanol and O^-.

The highest increase of ion signal with pressure is obtained for ethanol. For this molecule the dependence of ion signal with pressure is already non-linear at $5 \cdot 10^{-4}$ mbar, indicating the presence of secondary reactions and possible results are affected by them. Unfortunately it is almost impossible to work with ethanol as such low pressures in the target chamber, due to very low ion signal.

To explain the non-linear increase of the $(M-1)^-$ ion as a function of pressure at 6.5 eV and 8.5 eV for methanol, and at 6.5 eV for ethanol, it is necessary to determine the mean free path of the gas in the target chamber at that pressure. The mean free path (λ) can be calculated if the molecular diameter (d) and the pressure (p) are known, using the following relation:

$$\lambda = \frac{kT}{(\sqrt{2}\,\pi d^2)p} \tag{3.2}$$

Unfortunately there is no data available in the literature concerning the molecular diameter for our molecules of interest. Consequently we used the available data for hydrogen, nitrogen, benzene and cyclohexane as reference values to estimate λ for our molecules. The results for a pressure in the target chamber of $3 \cdot 10^{-3}$ mbar (the maximum pressure in our tests) and a temperature of 363.15 °K are presented in table 3.3.

The data presented in table 3.3 shows that the mean free path decreases from 40

Table 3.3: Mean free path (λ) for different molecules at a pressure of $3 \cdot 10^{-3}$ mbar and a temperature of 363.15 °K.

Molecule	d(Å^2)	λ(mm)	ref.
hydrogen	2.97	42.7	[52, 53, 54]
nitrogen	3.68	27.8	[52, 53, 54]
benzene	5.47	12.6	[52, 55]
cyclohexane	6.46	9.0	[52, 56]

mm for a small molecule up to 9 mm for a bulky molecule. λ for methanol, ethanol and cyclopentanol are most likely between these two extremes. Considering that the ions are obtained in the middle of the target chamber and that the distance to the first electrode of the ion lens is 3 mm, we conclude that λ is, for our molecules, larger than the distance until the electrode. This indicates that ion-molecule reactions are unlikely to occur in the target chamber after the electron-molecule collisions. They must take place in the ion extracting lens whose length is equal or larger than λ.

Another reason for the non-linear dependence observed for methanol and ethanol is that the cross section for ion-molecule reactions is much larger than the molecular diameter. The cross section for electron collision with polar molecules increases exponentially as the energy of the electron approaches zero [19]. The reason is that a very slow electron is strongly deflected even by a molecule with a small dipole moment. The same is true for anions with very little kinetic energy. They could very easily be involved in ion-molecule reactions even though, initially, they are far from the molecule.

This conclusion has important consequences for dissociative electron attachment measurements. One needs to work at low pressures and always check the pressure dependence. Also, ion-molecule reactions could be responsible for some of the discrepancies between DEA data measured by different research groups.

Chapter 4

Dissociative electron attachment of ethers

In this chapter the dissociative electron attachment of different alkyl ethers is studied. First, a striking difference is observed between the fragmentation pattern of cyclic ethers, such as tetrahydrofuran, and that of linear ethers, such as diethylether or dibutylether. This observation is rationalized based on the fact that in open-chain ethers the excess energy is partitioned between the (internal and kinetic) energies of two fragments, resulting in an ion cool enough to be observed. The ion resulting from cleavage of the CO bond in THF contains the entire excess energy (more than 6 eV at an electron energy of 7.65 eV) and is too short-lived with respect to further dissociation and thermal autodetachment to be detected in a mass spectrometer. These results are published in ref. [35] and reprinted in section 4.1. Secondly the analysis of the dissociation *via* Feshbach resonances is analyzed in various molecules with C−O bonds. We conclude that the involved Feshbach resonances are mostly localized on alkyl chains and that the energy of the resonance depends strongly on the structure of the alkyl chain. The main results will be published in ref. [36] and reprinted here in section 4.2.

4.1 Cleavage of the ether bond by electron impact: differences between linear ethers and tetrahydrofuran

The reprint of the article starts on the next page.

Cleavage of the ether bond by electron impact: differences between linear ethers and tetrahydrofuran†

Bogdan C. Ibănescu, Olivier May and Michael Allan

Received 23rd November 2007, Accepted 4th January 2008
First published as an Advance Article on the web 24th January 2008
DOI: 10.1039/b718130b

Dissociative electron attachment (DEA) to diethyl ether yielded primarily the $C_2H_5O^-$ ion, with a strong Feshbach resonance band at 9.1 eV and a weaker shape resonance band at 3.89 eV. Very similar spectra were obtained for dibutyl ether, with $C_4H_9O^-$ bands at 8.0 and 3.6 eV. Some of these primary ions subsequently lost H_2 and yielded weaker signals of the $C_2H_3O^-$ and $C_4H_7O^-$ ions. In contrast, DEA to the cyclic ether tetrahydrofuran (THF) yielded mainly a fragment of mass 41, presumably deprotonated ketene, at 7.65 eV. The low-energy band was missing in THF. H^- with two bands at 6.88 and 8.61 eV, and an ion of mass 43 (presumably deprotonated acetaldehyde) with two bands at 6.7 and 8.50 eV were also observed. We propose that in the primary DEA step the C–O bond is cleaved in both the open-chain and the cyclic ethers. In the open-chain ethers the excess energy is partitioned between the (internal and kinetic) energies of two fragments, resulting in an RO^- ion cool enough to be observed. The $^{\bullet}CH_2(CH_2)_3O^-$ ion resulting from cleavage of the C–O bond in THF contains the entire excess energy (more than 6 eV at an electron energy of 7.65 eV) and is too short-lived with respect to further dissociation and thermal autodetachment to be detected in a mass spectrometer. These findings imply that there could be a substantial difference between the fragmentation in the gas phase described here and fragmentation in the condensed phase where the initially formed fragments can be rapidly cooled by the environment.

1. Introduction

Electron interactions with the cyclic ether tetrahydrofuran (THF) have been studied because THF serves as a convenient model for the sugar ring in the DNA backbone in connection with radiation damage.[1] Of particular importance in respect to this application are studies in the condensed phase. Lepage *et al.*[2] studied resonances (*i.e.*, temporary anion states which act as intermediates in the electron-induced degradation) in THF by means of resonant vibrational excitation (VE) in thin-film THF and detected at least three resonances, located near 4, 7.5, and 10 eV. Antic *et al.*[1] studied the electron-induced yield of negative ions from frozen THF and observed formation of H^- at 10 eV, attributed to a core excited resonance. Electron energy loss spectra (EELS), in particular the observation of an (n,π*) transition, revealed neutral degradation products containing carbonyl groups. Antic *et al.*[3] reported a resonance at 23 eV which decayed into a highly excited state undergoing a further dipolar dissociation. The formation of aldehydes from THF frozen on a Kr substrate was studied in detail by Breton *et al.*[4] and Jäggle *et al.*[5] by means of vibrational and electronic EELS of the products. A strong rise of aldehyde production was observed from about 6 eV upward and was correlated to (n,σ^*_{CO}) electronic excitation threshold of THF, together with core-excited resonances around 9 and 10 eV. The absolute cross section reached a value of ~6000 pm^2 above 11 eV. A small feature found around 3 eV was proposed to result from a σ* shape resonance. The formation of olefins and CO were identified in the later study. Electron trapping processes in condensed THF were studied quantitatively by Park *et al.*[6] The charge trapping cross section for 6–9 eV electrons was found to have an upper limit of 40 pm^2, much smaller than the aldehyde production cross section mentioned above, leading to the conclusion that the major part of THF degradation has electronic excitation and not dissociative electron attachment (DEA) as the primary step. A much larger trapping cross section (~4000 pm^2 for 2 monolayers), strongly dependent on the quantity of deposited THF, and proceeding *via* intermolecular stabilization, was found in the 0–0.1 eV range.

The condensed phase work was complemented by gas phase DEA fragmentation studies performed by Sulzer *et al.*[7] Of particular importance is the quantitative study of Aflatooni *et al.*[8] who found two DEA bands, at 6.2 and 8 eV, with a surprisingly small cross section, 1.5 pm^2, about a factor 30 less than that in the 3-hydroxy substituted THF.

Indispensable for the global understanding of the electron-induced processes are also gas phase studies not directly involving chemical change. Zecca *et al.*[9] and Możejko *et al.*[10] measured the absolute total cross section for electron scattering by gas-phase THF (Zecca *et al.* reported also the positron cross section). The elastic and/or vibrational excitation differential cross sections were measured by Milosavljević *et al.*,[11] Colyer *et al.*,[12] Dampc *et al.*[13,14] and in this laboratory.[15] The studies identified broad resonant bands around 6.2

Department of Chemistry, University of Fribourg, Chemin du Musée, 9, CH-1700 Fribourg, Switzerland
† The HTML version of this article has been enhanced with colour images.

and 10.8 eV, assigned to two or more overlapping shape resonances. Indication of an additional resonant process around 2.6 eV was reported in the last study.

High-level scattering calculations of the elastic and/or momentum-transfer cross sections in THF were reported by Trevisan *et al.*,[16] Winstead and McKoy[17] and Tonzani and Greene.[18] Bouchiha *et al.*[19] also calculated the electronically inelastic cross section and the energies of a number of core-excited (Feshbach) resonances.

The present work reports DEA spectra of diethyl ether, dibutyl ether and THF with the aim of gaining insight into how susceptible is the ether bond to cleavage by electron impact, and understanding the differences between cyclic and open-chain ethers. The similarities of, and differences between, the cleavage of the bond O–C in ethers, and the O–C and O–H bonds in alcohols are also discussed.

2. Methods

The dissociative electron attachment spectrometer used to measure the yield of mass-selected stable anions as a function of electron energy has been described previously.[20–22] It employs a magnetically collimated trochoidal electron monochromator[23] to prepare a beam of quasi-monoenergetic electrons, which is directed into a target chamber filled with a quasi-static sample gas. Fragment anions are extracted at 90° by a three-cylinder lens and directed into a quadrupole mass spectrometer. The energy scale was calibrated on the onset of the O^-/CO_2 signal at 4.0 eV. The electron current was around 200 nA and the resolution about 150 meV. Photoelectron (PE) spectra were recorded with a modified Perkin Elmer PS18 HeI photoelectron spectrometer. Threshold energies for various fragmentations were calculated as the differences of the total energies of the products and the targets at 0 K, corrected for the zero point vibrational energy, using the density functional theory (DFT) B3LYP/6-311 + G(2df,2p) model,[24] applied already in our previous study of alcohols.[22]

3. Results and discussion

Fig. 1–3 show the DEA spectra of THF and two linear ethers related to it. Diethyl ether has the same total number of carbon atoms as THF. Dibutyl ether is in a certain sense even closer related to THF because the alkyl group is four carbon atoms long for both. Qualitative indications of the relative signal intensities are given by the count rates, which were normalized to a current of 200 nA and a main chamber pressure of 2×10^{-6} mbar. The pressure is an uncorrected Penning gauge reading, but the gauge sensitivity may be expected to be comparable for the compound studied here, particularly for diethyl ether and THF, which have the same number of heavy atoms. The relative intensities may thus be compared qualitatively even between the compounds. The vacuum chamber is equipped with a liquid nitrogen trap, which was generally filled during the measurements, resulting in a main chamber pressure between 1×10^{-7} and 5×10^{-7} mbar—barely measurable with the Penning gauge. The count rate measurements were consequently taken without liquid nitrogen in the trap to yield higher, more accurate pressure readings. The H^- intensity can not be compared with the intensity of the other fragments, however, because the transmissivity of the ion lens and the quadrupole mass filter may be expected to be substantially different for this very light ion, which is harder to guide in the magnetic field of the trochoidal monochromator.

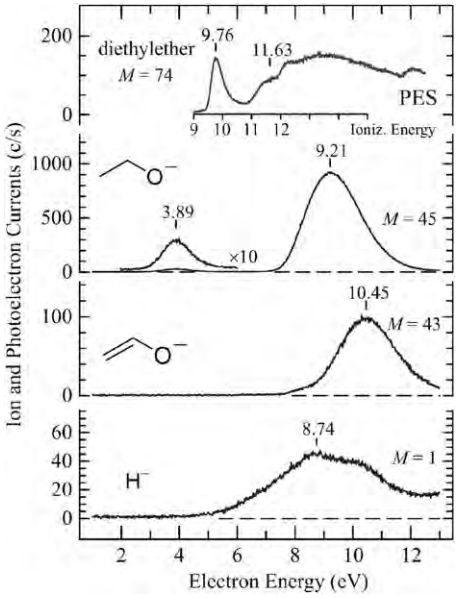

Fig. 1 The HeI photoelectron spectrum (top, shown shifted by −4.5 eV), and the yields of the fragments with the masses indicated, for diethyl ether.

The strongest signal from diethyl ether has the mass of 45, and may be assigned with confidence to the ethanolate anion $CH_3CH_2O^-$, resulting from the cleavage of one C–O bond. The process is thus related to the C–O bond cleavage in many alcohols (leading to OH^- formation), with a band at a similar energy.[22,25,26]

An indication of the expected energies of Feshbach resonances can be obtained from ionization energies, measured by photoelectron (PE) spectroscopy. The prediction is based on the observation that the energy difference between the $^2(\psi_i^{-1})$ grandparent cation state (where ψ_i is the i-th occupied molecular orbital) and the $^2(\psi_i, 3s^2)$ Feshbach resonance is about the same (4.5 eV) for a wide range of molecules and even for rare gases (references 22, 27, 28 and references therein). This observation is rationalized by the large spatial extent of the doubly occupied 3s Rydberg-like orbital which consequently does not strongly penetrate the positive ion core. The bands in

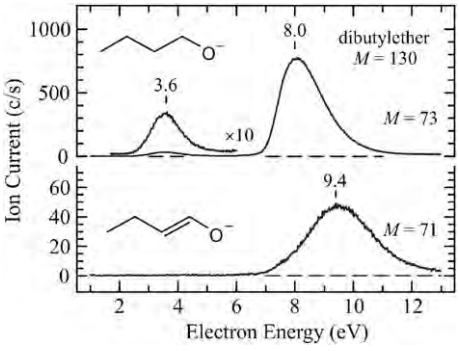

Fig. 2 DEA spectra of dibutyl ether.

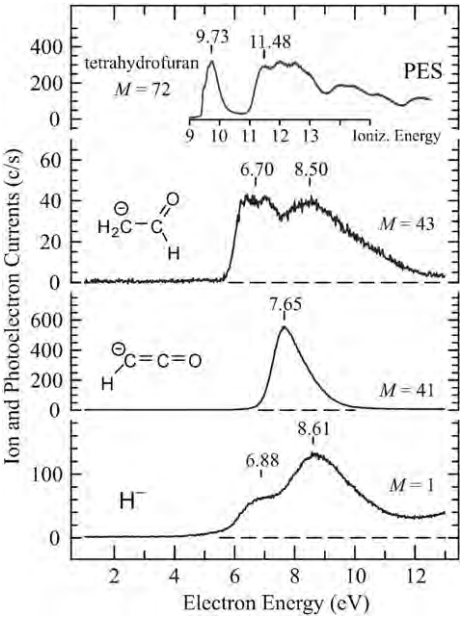

Fig. 3 The HeI photoelectron spectrum (top, shown shifted by −4.5 eV) and DEA spectra of tetrahydrofuran.

the shifted PE spectrum in Fig. 1 and 3 thus indicate the expected positions, and also Franck–Condon widths, of the Feshbach resonances of the type $^2(\psi_i, 3s^2)$, with a hole in the normally occupied ψ_i valence orbital and a double occupation of a Rydberg-like 3s orbital.

The 9.21 eV band in Fig. 1 is at a much higher energy, and is much wider, than would be expected for the low-lying Feshbach resonances $^2(\psi_O, 3s^2)$ or $^2(\bar{n}_O, 3s^2)$, associated with the 9.76 and 11.63 eV bands in the PE spectrum shown in the same figure. At the position in the PE spectrum corresponding to the 9.21 eV DEA band there is the 'σ-mountain', consisting of many broad overlapping bands corresponding to ionizations from σ orbitals localized on the C–C and C–H bonds, and we assign the 9.21 eV band to one or several of the corresponding Feshbach resonances. High-lying shape resonances are also expected in this energy range, but these resonances generally have an autodetachment rate too fast to permit dissociation and we consequently favor the assignment to Feshbach resonances, although a varying degree of mixing of shape and Feshbach configurations, analogous to mixing of valence and Rydberg states in neutral molecules[29,30] is probable.

There is little doubt that $^2(n_O, 3s^2)$ or $^2(\bar{n}_O, 3s^2)$ Feshbach resonances, with holes in the oxygen lone pair orbitals, occur around 5.2 and 7 eV in diethyl ether—but they do not lead to observable dissociation, in contrast to the H-loss from the alcohols. This indicates that they are, in contrast to the corresponding resonances in the alcohols, not suitably predissociated by a repulsive valence resonance with an antibonding σ* orbital occupation (shape or valence core excited). It is interesting to note that a related observation has been made for the parent Rydberg states. Robin[29,30] analyzed term energies and band shapes in VUV spectra and recognized that in water and the alcohols the lowest $^1(n_O, 3s)$ parent Rydberg states are unusually low in energy and the bands are broad and structureless—whereas the corresponding photoelectron bands are narrow with sharp vibrational structure. In contrast, the lowest Rydberg bands in the ethers behaved normally. Robin concluded that the $^1(n_O, 3s)$ Rydberg states are strongly perturbed by the conjugate $^1(n_O, \sigma^*)$ valence promotions in the alcohols and water, but that this perturbation is not significant in the ethers.

The fragment with mass 43 is probably formed by loss of H_2 from the initially formed (hot) ethanolate anion. The H^- band is very broad and hard to assign to individual Feshbach resonances.

The weak band at 3.89 eV (mass 45) is too low for a Feshbach resonance and must be due to a σ* shape resonance. We calculated the threshold for this process to be 1.7 eV, using the model validated on alcohols.[22] The facts that the 3.89 eV band peaks far above the threshold and that it does not have a vertical onset indicate that, in contrast to the similar low-energy bands found for alcohols,[22] there is an activation barrier on the dissociation path.

The DEA spectra of dibutyl ether in Fig. 2 are similar to those of diethyl ether and indicate an efficient cleavage of the C–O bond with both the low energy (3.6 eV) and the high energy (8 eV) bands. We calculate the threshold for the $M = 73$ ion formation to be 1.6 eV, indicating an energy barrier on the dissociation path leading to the 3.6 eV band, similarly to the diethyl ether case. The 9.4 eV $M = 71$ band is probably due to a subsequent loss of an H_2 molecule from the primary $M = 73$ anion. There is one important difference, however, the energy of the upper RO^- band dropped by 1.2 eV (from 9.2 to 8 eV) with respect to diethyl ether, indicating a fairly strong dependence on the size of the alkyl substituent. The 1.2 eV energy difference is similar to the difference of the ionization energies of ethane and *n*-butane (about 1 eV),[31] in line with the assignment of the ether DEA bands to Feshbach resonances associated with ionizations from orbitals of the alkyl groups.

The most intense fragment from THF has the mass of 41 with a peak at 7.65 eV, in agreement with the previous work of Sulzer *et al.*[7] A fragment with this mass is frequently found in DEA (see, for example, reference 32) and probably has the stable structure of deprotonated ketene. We did not find the ions with masses 70 and 72 reported at 1.25 eV,[7] however. The $m/e = 72$ ion corresponds to the full molecular mass, and detection of ions with the full molecular mass is very rare in DEA at non-thermal energies, because such ions tend to thermally lose the electron or to dissociate as will be detailed further below.

Comparison with the absolute (but not mass resolved) spectrum of Aflatooni *et al.*[8] is less straightforward. The two DEA bands at 6.2 and 8 eV which they report resemble the two bands which we observe for the fragments with masses 1 and 43. The present 7.65 eV, mass 41 band could contribute to the second band in the spectrum of Aflatooni *et al.*,[8] which could be reduced in intensity in their spectrum by the onset of the positive ion current. Finally, our instrument could underestimate the H^- intensity. With these points in mind, the present spectra are compatible with the results of Aflatooni *et al.*

The two bands in the yield of H^- in Fig. 3 could have the same origin as the 10 eV band and 7.3 eV shoulder in the H^- yield from frozen THF reported by Antic *et al.*[1] It is plausible to assume that the present two bands are shifted to higher energies and broadened by the action of the condensed media on the spatially large Rydberg-like orbitals of the Feshbach resonances. Finally a fragment with mass 43, whose structure could

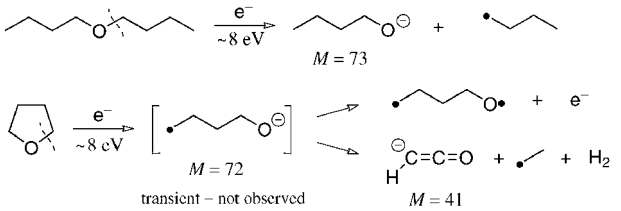

Fig. 4 Hypothetical electron-induced reactions. The butanolate anion formed in the upper reaction may be cooled by depositing part of the excess energy into vibrations of the neutral butyl fragment and the kinetic energy of the products. The $M = 72$ fragment in the lower scheme does not have this possibility and the high internal energy makes it too short-lived to be detected mass-spectrometrically—only the $M = 41$ fragment is observed.

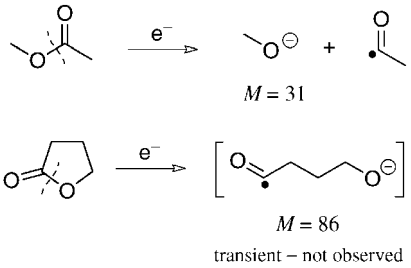

Fig. 5 Electron-induced reactions of methyl acetate and γ-butyrolactone. The methanolate anion was observed with a large intensity whereas the $M = 86$ anion from γ-butyrolactone was not observed.[20,32]

be deprotonated acetaldehyde, is observed with weak intensity. Its spectrum has two bands with energies similar to those in the H^- spectrum. It could thus be that the same resonant mechanisms which lead to H^- also lead to H and a hot $(M - 1)^-$ ion, which then dissociates further to the mass 43 fragment.

The present spectra of diethyl ether and dibutyl ether show that the C–O bond is not inert to cleavage by electron impact but breaks to yield the $R–O^-$ anion, both at low energy, *via* a shape resonance, and at high energy, *via* a Feshbach resonance. The process resembles the cleavage of the O–H bond in the alcohols with the difference that activation energy is necessary at the low energy band and dissociation occurs only from the higher excited Feshbach resonances for the high energy bands.

There is no plausible reason why the C–O bond in THF should not break in the same way as in the linear ethers—as proposed in the scheme in Fig. 4. In fact, the 7.65 eV (mass 41) band in THF is very similar to the 8.0 eV (mass 73) band of dibutyl ether both in terms of energy and of band shape, suggesting that the initial step of the resonant dissociation is essentially the same in both cases. The principal difference is that in the linear ethers the products may be cooled by transferring part of the excess energy into the kinetic energy of the fragments and the internal degrees of freedom (vibrational and possibly even electronic excitation) of the neutral fragment, whereas in THF the entire excess energy remains in the negative ion product. An excess energy of 6.4 eV is obtained for 7.7 eV incident electrons using our calculated threshold for the $^•CH_2(CH_2)_3O^-$ ion formation of 1.3 eV. The $^•CH_2(CH_2)_3O^-$ ion thus necessarily has enough energy to either dissociate further or to lose an electron by autodetachment. It is consequently too short-lived to be observed in a mass spectrometer which involves a flight time of the order of 10 μs.

The present lack of observation of the $(M)^-$ ion from THF is in line with the fact that there are only few known cases where the attachment of a non-thermal electron leads to an anion with the full molecular mass M sufficiently long-lived to be detected in a mass spectrometer. A notable example is the *p*-benzoquinone where the attachment of 1.4 eV electrons leads to a long-lived anion with the full molecular mass.[33,34] A more recently discovered case is C_{60} (reference 35 and references therein)—but it is not comparable to the present case because the long-term electron attachment occurs over a very wide range of energies, not *via* a specific resonance. A relevant example where a search for a long-lived anion with the full molecular mass failed is γ-butyrolactone,[20,32] illustrated in the scheme in Fig. 5. It is related to the present case in the sense that the ester bond was shown to break readily in the linear esters and that the cleavage of the ester bond in the cyclic γ-butyrolactone should lead to an open-chain anion with the full molecular mass. Such an $(M)^-$ ion was, however, not observed in the experiment, with the same explanation being invoked as in the present case for THF.

The 3.8 eV band of diethyl and dibutyl ethers does not have an analogy in the THF spectrum in our measurements, although it is energetically possible. Even at this energy there is no plausible reason why the C–O bond should behave very differently in the cyclic and the open-chain ethers. We presume that the C–O bond does break in THF, but the resulting $^•CH_2(CH_2)_3O^-$ ion is metastable in respect to autodetachment, which would in this case require that the ring is re-closed. The initial $^•CH_2(CH_2)_3O^-$ ion could be stabilized in the condensed phase, however, and give rise to the weak process reported around 3 eV by Breton *et al.*[4]

4. Conclusions

Dissociative electron attachment to the linear diethyl and dibutyl ethers on the one hand and the cyclic ether THF on the other hand yield very different types of fragments in the Feshbach resonance energy region (6–12 eV)—but we conclude that the primary step, a cleavage of the C–O bond, is the same in both cases.

We propose that the different appearance of the detected fragmentation patterns stems from the fact that the primary fragment from, for example, dibutyl ether, the butanolate anion $CH_3(CH_2)_3O^-$, can be 'cooled' by depositing part of the excess energy of the reaction (which is about 6.4 eV for an attachment of an 8 eV electron) into the kinetic energy of the fragments and the internal energy of the neutral fragment, the butyl radical. At least some of the butanolate anions are produced with sufficiently low internal energy and consequently long lifetime to be detected in the mass spectrometer. (Part of the anions fragment further by losing an H_2 molecule, another part may thermally detach an electron and not be detected at all.)

In contrast, cleavage of the C–O bond in THF does not lead to two fragments, but only one ion, $^•CH_2(CH_2)_3O^-$, which necessarily retains all of the excess energy, making it too short-lived with respect to further dissociation, and probably also thermal autodetachment, to be detected in a mass spectrometer. The

subsequent dissociation appears to lead primarily to a fragment with a mass of 41, probably deprotonated ketene.

These findings imply that the fragmentation pattern of THF in the condensed phase could be quite different from the gas phase, because the initially formed $^{\bullet}CH_2(CH_2)_3O^-$ fragment could be cooled sufficiently rapidly in the condensed phase to quench further dissociation and autodetachment. The small value of the electron trapping cross section in the 6–9 eV range measured by Park *et al.*[6] indicates that this process does not have a very large cross section even in the condensed phase, however.

The C–O bond is cleaved also by $\sim$3.5 eV electrons in the linear ethers, *via* a σ^* shape resonance, and an energy barrier is involved. It is well possible that this $\sim$3.5 eV cleavage occurs also in THF but the resulting anion is metastable toward the reverse reaction of ring-closure and subsequent autodetachment.

The indications of metastability of the fragment anions are indirect in the present work, but it may be worth noting that there is a known case where metastability of a CH_3^- fragment anion, formed by DEA to acetaldehyde *via* a Feshbach resonance, has been measured directly by delayed coincidence of detached electrons.[36] A direct observation of metastability of negative ion fragments was recently reported in DEA to amino acids.[37]

The metastability of the fragment anions could have the consequence that different instruments, with different time intervals between ion formation and detection of the anions, could yield different DEA cross section values, and possibly even different DEA spectra shapes.

The present work further reveals an important difference in the dissociation patterns of Feshbach resonances in alcohols and in ethers. Whereas the O–H bond cleavage in alcohols proceeds already from the lowest Feshbach resonance (with hole in the oxygen lone pair orbital), the C–O bond cleavage in ethers proceeds only from higher-lying Feshbach resonances with holes in the σ_{C-C} and σ_{C-H} orbitals. From this observation we conclude that the lowest Feshbach resonance in the alcohols is predissociated by a repulsive resonant state with a σ^* orbital occupation, but no such suitable repulsive surface is available in the ethers. An interesting related conclusion was made for the parent states of the Feshbach resonances, the Rydberg states of the neutral molecules, where strong Rydberg–σ^* valence mixing was deduced for alcohols (and water) but not for ethers.[29,30]

A difference in the dissociation pattern of ethers and alcohols is also observed in the low energy region (1–5 eV), where alcohols dissociate without an activation barrier, whereas substantial barrier is found in the ethers.

Acknowledgements

This research is part of project No. 200020-113599/1 of the Swiss National Science Foundation.

References

1 D. Antic, L. Parenteau, M. Lepage and L. Sanche, *J. Phys. Chem. B*, 1999, **103**, 6611.
2 M. Lepage, S. Letarte, M. Michaud, F. Motte-Tollet, M.-J. Hubin-Franskin, D. Roy and L. Sanche, *J. Chem. Phys.*, 1998, **109**, 5980.
3 D. Antic, L. Parenteau and L. Sanche, *J. Phys. Chem. B*, 2000, **104**, 4711.
4 S.-P. Breton, M. Michaud, C. Jäggle, P. Swiderek and L. Sanche, *J. Chem. Phys.*, 2004, **121**, 11240.
5 C. Jäggle, P. Swiderek, S.-P. Breton, M. Michaud and L. Sanche, *J. Phys. Chem. B*, 2006, **110**, 12512.
6 Y. S. Park, H. Cho, L. Parenteau, A. D. Bass and L. Sanche, *J. Chem. Phys.*, 2006, **125**, 074714.
7 P. Sulzer, S. Ptasińska, F. Zappa, B. Mielewska, A. R. Milosavljević, P. Scheier, T. D. Märk, I. Bald, S. Gohlke, M. A. Huels and E. Illenberger, *J. Chem. Phys.*, 2006, **125**, 044304.
8 A. Aflatooni, A. M. Scheer and P. D. Burrow, *J. Chem. Phys.*, 2006, **125**, 054301.
9 A. Zecca, C. Perazzolli and M. Brunger, *J. Phys. B: At., Mol. Opt. Phys.*, 2005, **38**, 2079.
10 P. Możejko, E. Ptasińska-Denga, A. Domaracka and C. Szmytkowski, *Phys. Rev. A*, 2006, **74**, 012708.
11 A. R. Milosavljević, A. Giuliani, D. Šević, M.-J. Hubin-Franskin and B. P. Marinković, *Eur. Phys. J. D*, 2005, **35**, 411.
12 C. J. Colyer, V. Vizcaino, J. P. Sullivan, M. J. Brunger and S. J. Buckman, *New J. Phys.*, 2007, **9**, 41.
13 M. Dampc, A. R. Milosavljević, I. Linert, B. P. Marinković and M. Zubek, *Phys. Rev. A*, 2007, **75**, 042710.
14 M. Dampc, I. Linert, A. R. Milosavljević and M. Zubek, *Chem. Phys. Lett.*, 2007, **443**, 17.
15 M. Allan, *J. Phys. B: At., Mol. Opt. Phys.*, 2007, **40**, 3531.
16 C. S. Trevisan, A. E. Orel and T. N. Rescigno, *J. Phys. B: At., Mol. Opt. Phys.*, 2006, **39**, L255.
17 C. Winstead and V. McKoy, *J. Chem. Phys.*, 2006, **125**, 074302.
18 S. Tonzani and C. H. Greene, *J. Chem. Phys.*, 2006, **125**, 094504.
19 D. Bouchiha, J. D. Gorfinkiel, L. G. Caron and L. Sanche, *J. Phys. B: At., Mol. Opt. Phys.*, 2006, **39**, 975.
20 M. Stepanoviæ, Y. Pariat and M. Allan, *J. Chem. Phys.*, 1999, **110**, 11376.
21 R. Dressler and M. Allan, *Chem. Phys.*, 1985, **92**, 449.
22 B. C. Ibănescu, O. May, A. Monney and M. Allan, *Phys. Chem. Chem. Phys.*, 2007, **9**, 3163.
23 A. Stamatovic and G. J. Schulz, *Rev. Sci. Instrum.*, 1968, **39**, 1752.
24 M. J. Frisch, G. W. Trucks, H. B. Schlegel, G. E. Scuseria, M. A. Robb, J. R. Cheeseman, J. A. Montgomery, Jr., T. Vreven, K. N. Kudin, J. C. Burant, J. M. Millam, S. S. Iyengar, J. Tomasi, V. Barone, B. Mennucci, M. Cossi, G. Scalmani, N. Rega, G. A. Petersson, H. Nakatsuji, M. Hada, M. Ehara, K. Toyota, R. Fukuda, J. Hasegawa, M. Ishida, T. Nakajima, Y. Honda, O. Kitao, H. Nakai, M. Klene, X. Li, J. E. Knox, H. P. Hratchian, J. B. Cross, V. Bakken, C. Adamo, J. Jaramillo, R. Gomperts, R. E. Stratmann, O. Yazyev, A. J. Austin, R. Cammi, C. Pomelli, J. Ochterski, P. Y. Ayala, K. Morokuma, G. A. Voth, P. Salvador, J. J. Dannenberg, V. G. Zakrzewski, S. Dapprich, A. D. Daniels, M. C. Strain, O. Farkas, D. K. Malick, A. D. Rabuck, K. Raghavachari, J. B. Foresman, J. V. Ortiz, Q. Cui, A. G. Baboul, S. Clifford, J. Cioslowski, B. B. Stefanov, G. Liu, A. Liashenko, P. Piskorz, I. Komaromi, R. L. Martin, D. J. Fox, T. Keith, M. A. Al-Laham, C. Y. Peng, A. Nanayakkara, M. Challacombe, P. M. W. Gill, B. G. Johnson, W. Chen, M. W. Wong, C. Gonzalez and J. A. Pople, *GAUSSIAN 03 (Revision C.01)*, Gaussian, Inc., Wallingford, CT, 2004.
25 M. G. Curtis and I. C. Walker, *J. Chem. Soc., Faraday Trans.*, 1992, **88**, 2805.
26 A. Kühn, H. P. Fenzlaff and E. Illenberger, *J. Chem. Phys.*, 1988, **88**, 7453.
27 T. Skalický and M. Allan, *J. Phys. B*, 2004, **37**, 4849.
28 A. M. Scheer, P. Możejko, G. A. Gallup and P. D. Burrow, *J. Chem. Phys.*, 2007, **126**, 174301.
29 M. B. Robin, *Higher Excited States of Polyatomic Molecules*, Academic Press, New York, 1974, vol. 1.
30 M. B. Robin, *Higher Excited States of Polyatomic Molecules*, Academic Press, Orlando, 1985, vol. 1.
31 K. Kimura, S. Katsumata, Y. Achiba, T. Yamazaki and S. Iwata, *Handbook of HeI Photoelectron Spectra of Fundamental Organic Molecules*, Japan Scientific Societies Press, Tokyo, 1981.
32 Y. Pariat and M. Allan, *Int. J. Mass Spectrom. Ion Processes*, 1991, **103**, 181.
33 L. G. Christophorou, J. G. Carter and A. A. Christodoulides, *Chem. Phys. Lett.*, 1969, **3**, 237.
34 C. D. Cooper, W. T. Naff and R. N. Compton, *J. Chem. Phys.*, 1975, **63**, 2752.
35 M. Lezius, *Int. J. Mass Spectrom.*, 2003, **223–224**, 447.
36 R. Dressler and M. Allan, *J. Electron Spectrosc. Relat. Phenom.*, 1986, **41**, 275.
37 H. D. Flosadóttir, S. Denifl, F. Zappa, N. Wendt, A. Mauracher, A. Bacher, H. Jónsson, T. D. Märk, P. Scheier and O. Ingólfsson, *Angew. Chem., Int. Ed.*, 2007, **46**, 8057.

4.2 Selective cleavage of the C−O bonds in alcohols and asymmetric ethers by DEA

The reprint of the article starts on the next page. This article is to be submitted to *Physical Chemistry Chemical Physics*.

Selective cleavage of the C−O bonds in alcohols and asymmetric ethers by dissociative electron attachment

Bogdan C. Ibănescu and Michael Allan*
Department of Chemistry, University of Fribourg, Chemin du Musée 9, CH-1700 Fribourg, Switzerland
(Dated: February 10, 2009)

Dissociative electron attachment spectra of 20 saturated compounds containing ether and hydroxyl groups are presented. Two groups of fragmentation processes are identified: (i) one or two bands mediated by shape resonances in the 1-5 eV range and (ii) three bands (often overlapping) in the 5-12 eV range, assigned to Feshbach resonances with a hole in either the oxygen 'nonbonding' orbitals n_O or $\bar{n}_O$, or in a σ orbital. The main result of this paper is the discovery of unexpected selectivity of the cleavage of C−O bonds in asymmetric ethers R_1−O−R_2, *within* the range of the σ-Feshbach resonances, where a neutral alkyl group R_1 is lost at a given energy (9.1, 8.4, 8.0 and 8.8 eV for R_1=ethyl, propyl, butyl and *t*-butyl, resp.), independent of R_2, in all compounds under study. This empirical rule indicates that the excitation (a hole and two excited electrons) of Feshbach resonances responsible for the fragmentation are spatially localized on one or the other alkyl group. This interpretation is supported by correlation with ionization energies of the alkanes R_1H. The methyl group behaves differently from the larger alkyl groups, it is not split off at all (except in methanol), thus acting as a 'protective group'. A number of other observations were made: The previously observed lack of cleavage of C−O bonds (in contrast to O−H bonds) in the n_O and $\bar{n}_O$ Feshbach resonance bands was confirmed in all compounds containing one oxygen atom, but it is now shown that the C−O bond can be broken under certain circumstances in compounds with two oxygen atoms, in cyclic hydrogen-bonded structures or when the neutral fragment contains oxygen.

I. INTRODUCTION

Dissociative electron attachment (DEA),

$$e^-(E_i) + \mathrm{AB} \rightarrow \{\mathrm{AB}\}_j^- \rightarrow \mathrm{A}^- + \mathrm{B},$$

is a primary process causing chemical changes in collisions of low-energy ($E_i < 15$ eV) electrons with molecules. DEA on isolated molecules is consequently of key importance in the chemistry of natural and technological plasmas [1]. DEA also occurs, in a somewhat modified but closely related form, in condensed phase where it plays an important role in radiation-induced damage to living tissue [2] and in technologies like electron-beam induced polymerization and nano-fabrication by focused electron beam induced processing (FEBIP) [3].

A significant cross section results only when the DEA proceeds resonantly, that is, at suitable electron energies E_i where an intermediate short-lived anion $\{\mathrm{AB}\}_j^-$ (also called a resonance) is formed in its ground state or in an electronically excited state j.

The present paper is concerned with the assignment of such resonances and with clarification of their dissociation mechanisms. It focuses on Feshbach resonances [4], which involve core excitation and temporary occupation of Rydberg-like [5, 6] orbitals, lie in the $5 - 15$ eV energy region, and which, because of their autodetachment lifetime, which is typically longer than that of shape resonances, often make a substantial contribution to the overall DEA. The understanding of these resonances is more complicated, and generally less advanced, than the understanding of the shape resonances (with the core in the electronic ground state) at lower energies.

To facilitate the assignment and understanding of the DEA bands we choose to work with saturated compounds, thus avoiding the complications due to the often very pronounced shape resonances that are associated with the temporary occupation of π^* orbitals, and with core excited resonances associated with valence (π, π^*) excited states.

Previously published results related to the present work concern primarily small alcohols, in particular the work on methanol by Kühn *et al.* [7] and Curtis and Walker [8], and the work on methanol and ethanol by Prabhudesai *et al.* [9], including a recent measurement of absolute cross sections [10, 11], and on ethanol by Orzol *et al.* [12]. This work revealed, mainly through the study of partially deuterated compounds, various kinds of selectivity. This selectivity can be found, in a slightly weakened form, also in condensed phase [13]. A more detailed account of the previous work can be found in our earlier publications [14–17].

Our own earlier work on a series of larger alcohols and ethers had already yielded a number of conclusions:

- Two groups of fragmentation processes are identified in all the compounds: (i) One or two bands in the 1-5 eV range, mediated by shape resonances [15] and (ii) three bands, at around 6.5, 7.5, and 8-11 eV, respectively. Following the early assignment in methanol [6, 18] and using the energies of the grandparent cation states [14, 15], the latter three bands were assigned to Feshbach resonances with a hole in either the oxygen 'nonbonding' orbitals n_O or $\bar{n}_O$ (subsequently called n- and $\bar{n}$-Feshbach

*E-mail:bogdancatalin.ibanescu@unifr.ch

resonances, respectively), or in one of the many σ orbitals (σ-Feshbach resonances). The prototypes of the n_O and $\bar{n}_O$ orbitals are the $1b_1$ and $3a_1$ orbitals of H_2O [19].

- Metastable $(M\text{-}1)^-$ ions were identified, which subsequently lost one or two H_2 molecules. Deuteration studies revealed that the hydrogens are lost in a 1,2- fashion, that is, HD is lost from CD_3CH_2OH [20].

- A general rule was observed, whereby the C−O bond (in contrast to the C−H bond) is not broken *via* the n- and $\bar{n}$-Feshbach resonances, it is cleaved only *via* the σ-Feshbach resonances.

- The shape resonance bands are weak and exhibit a dramatic isotope effect in the small alcohols, but become stronger and may even dominate the spectra for dialcohols.

The present work extends the earlier efforts, primarily to higher energies, and is concerned with assignments and phenomena within the manifold of the σ-Feshbach resonances.

II. EXPERIMENTAL AND THEORETICAL METHODS

The dissociative electron attachment spectrometer used to measure the yield of mass-selected stable anions as a function of the electron energy has been described previously [15, 21, 22]. It employs a magnetically collimated trochoidal electron monochromator [23] to prepare a beam of quasi-monoenergetic electrons, which is directed into a target chamber filled with a quasi-static sample gas. Fragment anions are extracted at 90° by a three-cylinder lens and directed into a quadrupole mass spectrometer. The energy scale was calibrated on the onset of the O^-/CO_2 signal at 4.0 eV. The electron current was around 100 nA and the resolution about 150 meV.

All the substances presented in this article are commercially available, except dibutoxy methane which was synthesized in Fribourg. The commercial samples were supplied by Sigma-Aldrich and were used as delivered, without any further purification.

The calculations presented in this article were performed with the quantum chemical package Gaussian 03 [24]. Threshold energies for various fragmentations were calculated as the differences of the total energies of the products and the targets at 0 K, corrected for the zero point vibrational energy, using the density functional theory (DFT) B3LYP/6−311+G(2df,2p) model, used also for geometry optimizations. The molecular orbitals were calculated at HF/6−31g(d) level of theory, the ionization energies with the Outer Valence Green's Function method.

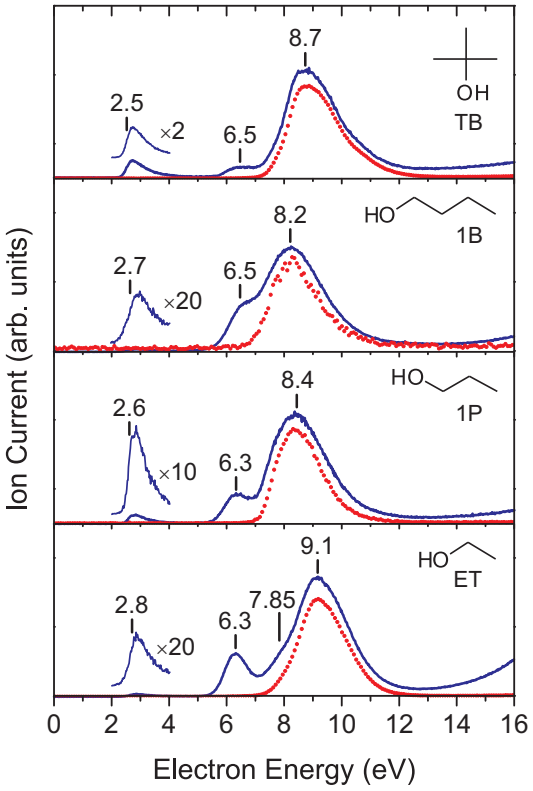

FIG. 1: Comparison between the DEA spectra for OH^- (dotted line) and $(M\text{-}1)^-$ anions (solid line) for ethanol (ET), 1-propanol (1P), 1-butanol (1B) and *t*-butyl alcohol (TB).

III. RESULTS AND DISCUSSION

A. Cleavage of the C−O and the O−H bonds in alcohols

Fig 1 shows the yields of the OH^- ion (cleavage of the C−O bond) and the $(M\text{-}1)^-$ ion (cleavage of the O−H bond) for ethanol, 1-propanol, *n*-butanol and *t*-butanol. The $(M\text{-}1)^-$ yield from ethanol, at the bottom of the figure, is consistent with our previous work [15] and exemplifies the processes mentioned in the Introduction – the shape resonance band at 2.9 eV, and the n-, $\bar{n}$- and σ-Feshbach resonance bands, at 6.35, 7.85, and 9.1 eV, respectively. The $\bar{n}$-Feshbach resonance appears only as a shoulder on the low-energy side of the 9.15 eV band in Fig. 1, but the yield of D^- from C_2H_5OD [15] shows this band very clearly, distinct from the 9.1 eV band.

Our results for ethanol are not fully consistent with those of Orzol *et al.* [12], all DEA bands in their work appear at energies about 1 eV lower than ours (ref. [15] and this work). We further do not observe the broad O^- band which they reported at 5.5 eV. Our energy-scale calibration receives support from the fact that our energies of the H^- and D^- bands from ethanol (in ref. [15], not shown here) are consistent with those of Prabhudesai *et al.* [9, 10].

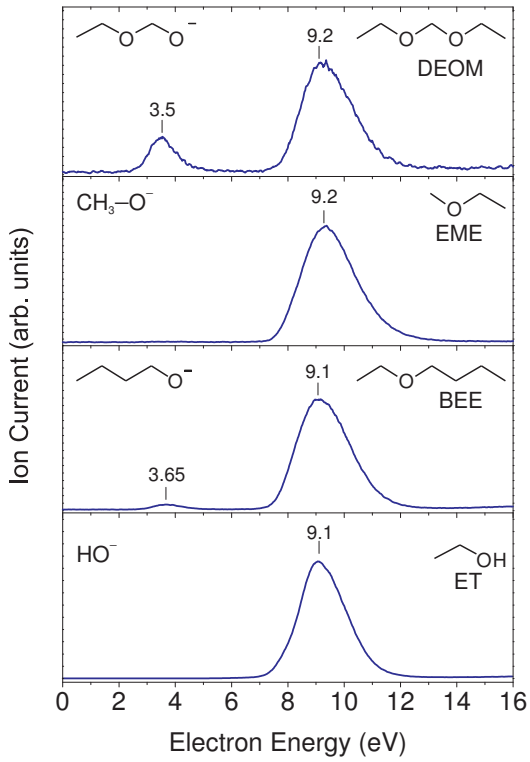

FIG. 2: DEA spectra for the loss of neutral ethyl radical from ET, butyl ethyl ether (BEE), ethyl methyl ether (EME) and diethoxy methane (DEOM). The initial molecule is shown in the right corner, the resulting anion in the left corner of each spectrum.

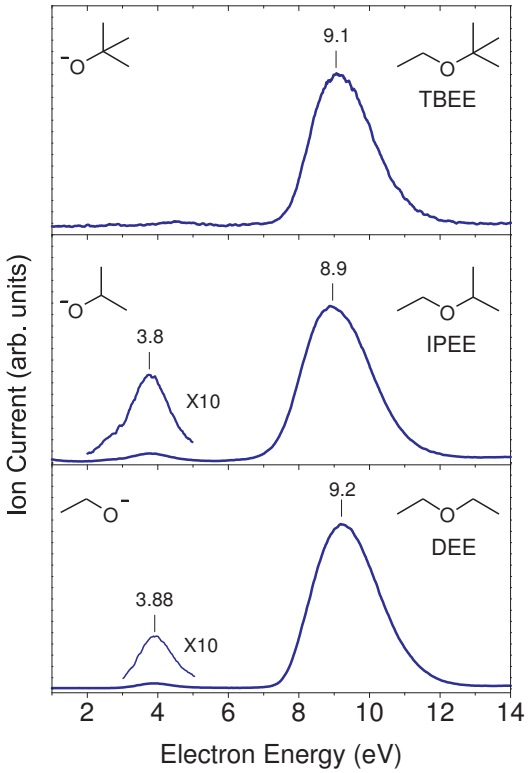

FIG. 3: DEA spectra for loss of ethyl neutral fragment from diethyl ether (DEE), isoptopyl ethyl ether (IPEE) and *t*-butyl ethyl ether. (continuation of Fig. 2)

The absence of the shape resonance and of the n- and $\bar{n}$-Feshbach resonances in the OH^- yield, shown by the dotted line at the bottom of Fig. 1, shows that cleavage of the C−O bond is not permitted *via* these resonances. This observation was reported and rationalized in our earlier work [17]. The present work is concerned primarily with the band assigned to σ-Feshbach resonances, which is at 9.1 eV in ethanol.

The remaining spectra in Fig. 1 show that the energy of this band is sensitive to the size of the alkyl group – it drops in energy, by nearly 1 eV, when going from ethyl to butyl. The energy of the lower-lying bands remain essentially unchanged, only their relative intensities change. The shape resonance band does not shift substantially because its energy is determined by the thermochemical threshold, given by the O−H bond dissociation energy and the electron affinity of the alkoxy radical, none of which changes appreciably when going from ethyl to butyl. The n-Feshbach resonance band remains essentially unchanged at 6.3 eV, its localization on the oxygen atom makes it insensitive to the size of the alkyl substituent. The $\bar{n}$-Feshbach resonance is obscured by the σ-Feshbach resonances in the upper three spectra.

B. Loss of neutral alkyl radicals in ethers and alcohols

The cleavage of the C−O bond in ethers follows the same rules as the cleavage of the C−O bond in alcohols in the Feshbach resonance region, in the sense that the n- and the $\bar{n}$-Feshbach resonances do not cleave this bond, and only the band due to σ-Feshbach resonances appears in the spectra [16, 17]. This section studies trends and regularities in the latter band in a long series of compounds, both alcohols and ethers. The result is an unexpected observation – that the energy of the σ-Feshbach resonance band depends on the neutral fragment which is formed in the DEA, and not on the target molecule. This is best illustrated when spectra are presented grouped not in the usual way, sorted by a given target molecule, but when spectra resulting in the same neutral fragment, from a range of targets, are presented in one picture.

The first example is the formation of the ethyl radical from ethanol and six different ethers, shown in Figs. 2 and 3, where the band due to σ-Feshbach resonance(s) is at the same energy of about 9.1 eV, despite the widely varying structures of the precursors. Two more examples of ethyl radical loss from more complex targets will be presented in Section III D.

Fig. 4 shows DEA spectra where the neutral fragment

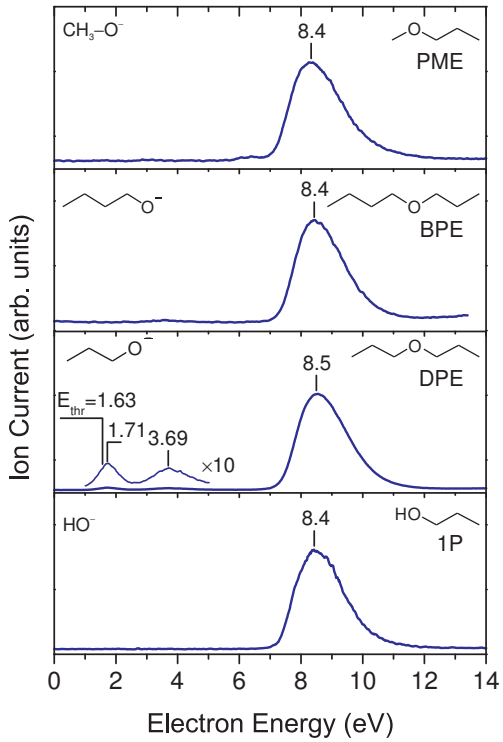

FIG. 4: DEA spectra for loss of propyl neutral fragment from 1P, dipropyl ether (DPE), butyl propyl ether (BPE) and propyl methyl ether (PME). The calculated threshold energy $E_{\rm thr}$ is indicated for DPE.

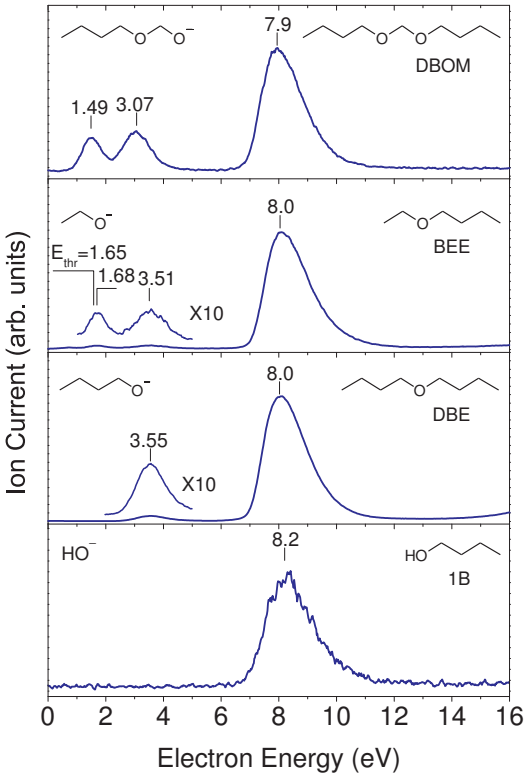

FIG. 5: DEA spectra for loss of n-butyl neutral fragment from 1B, dibutyl ether (DBE), BEE and dibutoxy methane (DBOM). The calculated threshold energy $E_{\rm thr}$ is indicated for BEE.

is n-propyl radical, with propanol and two different ethers as precursors. The bands are again at the same energy for all precursors, but this energy is about 0.7 eV lower than when ethyl is the neutral fragment! Since the propyl chain is the only chemical similarity between these three molecules, we conclude that the Feshbach resonances associated with the 8.5 eV band has a positive core that is localized on the propyl moiety (but delocalized over the length of the propyl chain).

The results for the loss of the n-butyl radical are shown in Fig. 5 and the bottom two spectra of Fig. 6. The energies of the bands are again about the same and are about 0.4 eV lower than those for loss of n-propyl radical. Two more examples of a loss of n-butyl radical will be presented in Section III D.

Finally the top two spectra in Fig. 6 show the loss of t-butyl radical. The band is at an energy about 0.7 eV higher than that for the loss of the n-butyl radical.

Note that some targets are shown twice in the above figures, for example butyl ethyl ether BEE in Figs. 2 (loss of ethyl) and 5 (loss of butyl). A band due to σ-Feshbach resonances appears in both spectra, but its energy is different: 8 eV for loss of butyl and 9.1 eV for loss of ethyl. This suggests that two different resonances are responsible for the bands in the two spectra and that these resonances are localized on different alkyl moieties of the molecule. This energy difference of about 1 eV also raises the possibility of controlling the dissociation of this molecule by changing the energy of the electron.

The above mentioned extensive data indicates an empirical rule whereby the σ-Feshbach resonance band appears at nearly the same energy for a given neutral fragment, independent of the structure of the precursor. This rule is very unexpected. It can not be due to different threshold energies – all processes are high above threshold.

In our earlier work we attempted to assign bands in the 8-11 eV range to specific σ-Feshbach resonances, guided by comparison with the grandparent states in the photoelectron spectrum [14, 15, 17], but this approach does not allow to rationalize the selectivity presented here. The photoelectron spectra reveal many closely spaced, strongly overlapping bands (in jargon sometimes called 'the σ-mountain'), associated with ionization from $\sigma_{\rm C-C}$ and $\sigma_{\rm C-H}$ orbitals. The number of these orbitals and thus the number and the density of the states of the cation increase rapidly with the size of the alkyl groups. The energy range of the σ-Feshbach resonances thus very likely contains a large number of closely spaced, strongly overlapping resonances whose number and density increase with the size of the molecule. The energies of these res-

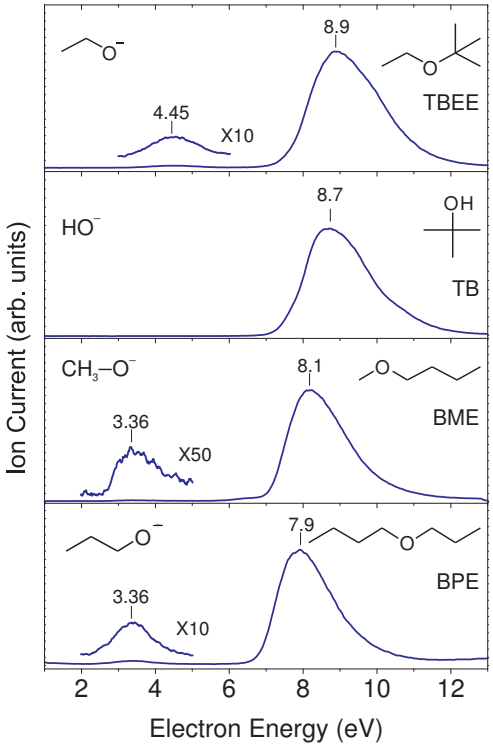

FIG. 6: DEA spectra for loss of n-butyl (bottom two panes) and t-butyl (top two panes) neutral fragments from BPE, butyl methyl ether (BME), TB and t-butyl ethyl alcohols (TBEE).

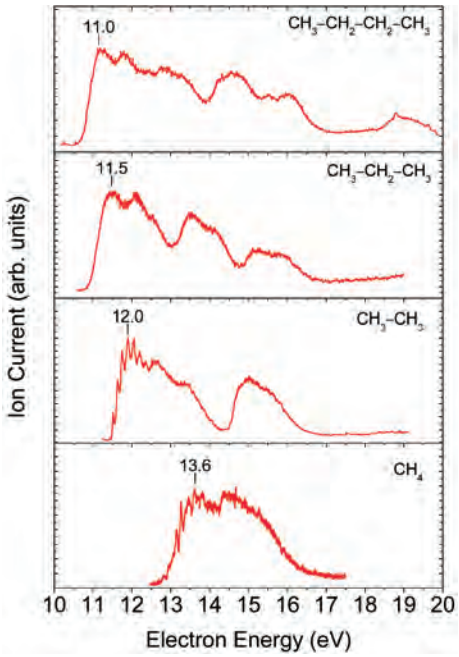

FIG. 7: HeI photoelectron spectra of several n-alkanes. The spectra are reproduced from ref. [19]

onances are expected to depend on the structure of the target molecule – in contrast to the rule described above.

The conjecture that the holes associated with the Feshbach resonances responsible for the above fragmentations are localized on a given alkyl fragment (and surrounded by two electrons in Rydberg-like spatially diffuse orbitals, whose binding energy is to a large degree constant) would imply that the energies of the DEA bands should correlate with the energies of the holes in alkyl moieties (bound to an oxygen atom). A good indication of these energies should be the ionization energies of the corresponding alkanes. The difference is that the alkyl residue is bound to a hydrogen atom in the alkanes, and to an oxygen atom in the ethers, but this should have only a weak influence on ionization from predominantly σ_{C-C} and σ_{C-H} orbitals. The photoelectron spectra shown in Fig. 7 and the ionization energies given in Table I correlate very well with the resonant energies – the energy difference is nearly constant 3 eV – providing additional support for the above conclusions. The only deviation is the value $\Delta E = 2.4$ eV for t-butyl. It could be related to the reduction of the term values of Rydberg states of alcohols when changing from linear to branched alkyl groups, reported by Robin [25] (pages 258-259).

We conclude that out of the many possible densely spaced Feshbach resonances in the 7-10 eV range some are localized on a given alkyl moiety (and simultaneously delocalized over that moiety). Their energy is dictated by the energy of the hole and thus to a large degree independent of the rest of the molecule. And it appears that out of the many possible resonances, it is only these which give rise to fragmentations. The fragment lost is the one on which the excitation (*i.e.*, the hole and the two associated diffuse electrons) were localized. The charge finally resides on the oxygen-containing fragment, not the alkyl fragment on which the original excitation resided.

C. Molecular orbitals

Calculations of ionization energies and the shapes of SCF orbitals give useful insight into the present subject. Selected results for both are shown in Fig. 8.

Assuming that ionizations occur from individual orbitals implies that the shapes of these orbitals gives an indication of the shape and spatial extension of the resulting hole. The indication is crude because of electron redistribution which accompanies ionization, and in our case more such redistribution could be caused by the two excited electrons in the Feshbach resonance. Despite these caveats we wish to pursue this approach on one example, that of butyl ethyl ether, and show its 5 topmost (and one more at lower energy) occupied SCF orbitals in Fig. 8.

The $7a''$ HOMO, the n_O lone pair MO, is calculated to be largely localized on the oxygen atom. The following four ionization energies are closely spaced (and this

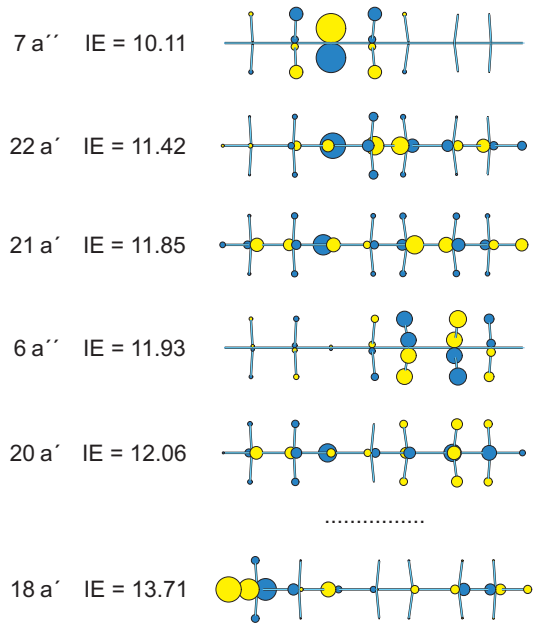

FIG. 8: Diagrams of the top 5 (plus the lower-lying $18a'$) occupied molecular orbitals in butyl ethyl ether within C_s symmetry, drawn with the MOPLOT program [26]. The ionization energies are calculated with the Outer Valence Green's Function method.

TABLE I: Summary of results for the band due to σ-Feshbach resonances in molecules of the type R_1OR_2. Given are, for each R_1, the position of the σ-Feshbach resonance (E_{FR}) as observed in the yield of the fragment R_2O^-, that is, the loss of neutral R_1. These values are, for a given R_1, nearly independent of R_2, and their mean is given. The first vertical ionization energies, IE, of the hydrocarbons R_1H [19] are given in the next column and the last column lists the differences $\Delta E = IE - E_{FR}$. All values are in eV.

R_1	E_{FR}	IE	ΔE
Methyl	10.5	13.6	3.1
Ethyl	9.1	12.0	2.9
Propyl	8.5	11.5	3.0
Butyl	8.0	11.0	3.0
t-Butyl	8.7	11.1	2.4

continues to higher energies, not shown in the figure), emphasizing the high density of states in this energy range, the 'σ-mountain'. The $6a''$ MO is localized on the butyl moiety (and delocalized over its entire length), and has thus the correct properties to rationalize the 8.0 eV butyl loss band in the butyl ethyl ether (BEE) spectrum of Fig. 5. A second such MO, $18a'$, localized on the ethyl moiety, is also shown in Fig. 8, with a calculated ionization energy of 13.71 eV. On the other hand the usefulness of these findings is limited by the fact that the majority of the calculated MOs, for example $20a'$ and $21a'$ in Fig. 8, are delocalized over the entire molecule and thus not suited to explain the observed exclusive selectivity in DEA. Also, the difference of the two ionization energies for ionization from the two localized orbitals, $6a''$ and $18a'$, 1.8 eV, is larger than the difference of the two DEA bands, 1.1 eV.

At this point we can only speculate about possible reasons. It could be that the Feshbach resonances associated with localized holes have longer autodetachment lifetimes and give rise to fragmentations, wheereas the Feshbach resonances associated with the delocalized holes have short autodetachment lifetimes. It is also possible, and perhaps more probable, that the two excited electrons in the Feshbach resonance cause an additional electron redistribution, *e.g.*, a spontaneous hole localization, driven by the effect that the two diffuse electrons are more attracted by a more localized positive hole.

D. Compounds with two oxygen atoms

The study of the breaking of the C−O bond in ethers is completed by extending it to more complex compounds whose structures, experimentally observed reactions, and resulting fragments, are listed in Figs. 9 and 10. These compound are discussed separately because they reveal certain extensions of the rules and regularities described in the above sections, which are best discussed when the basis of the above rules is already given.

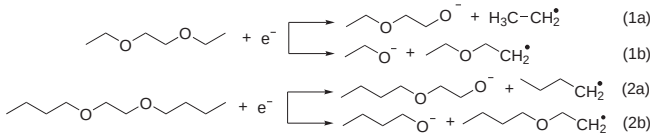

FIG. 9: Reaction scheme for the dissociation of EGDE (1a and 1b) and EGDB (2a and 2b).

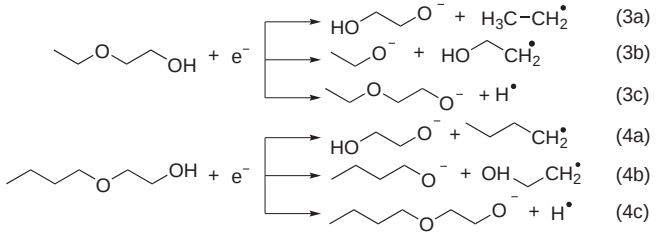

FIG. 10: Reaction scheme for the dissociation of 2EE (3a, 3b and 3c) and 2BE (4a, 4b and 4c).

Fig. 11 shows the DEA spectra for the reactions (1a), (2a), (3a) and (4a). The top two spectra correspond to a loss of a neutral ethyl radical and belong in this sense to the same category as the spectra in Figs. 2 and 3. Similar to those figures, the band for this reaction appears at 9.0 eV, providing further support for the conclusions

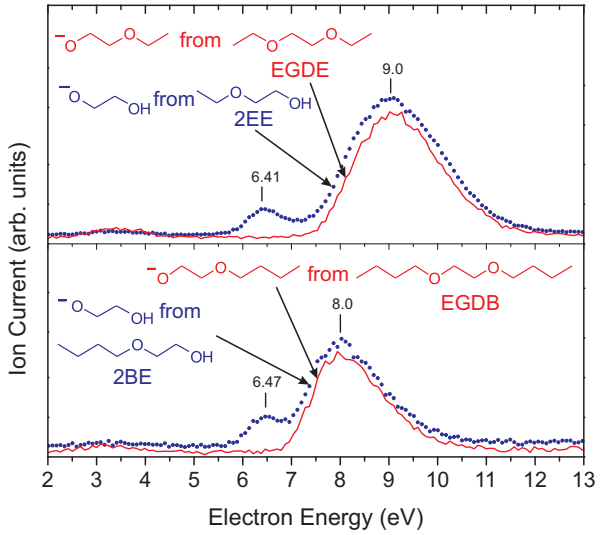

FIG. 11: DEA spectra of ethylene glycol diethyl ether (EGDE) (top, solid line), 2-ethoxy ethanol (2EE) (top, dots), ethylene glycol di-*n*-butyl ether (EGDB) (bottom, solid line), and 2-butoxy ethanol (2BE) (bottom, dots).

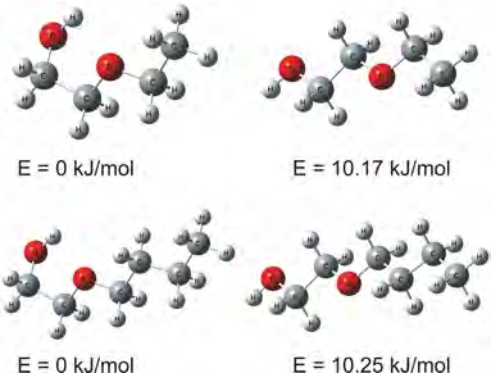

FIG. 12: The two most stable conformations of 2EE (top row) and of 2BE (bottom row).

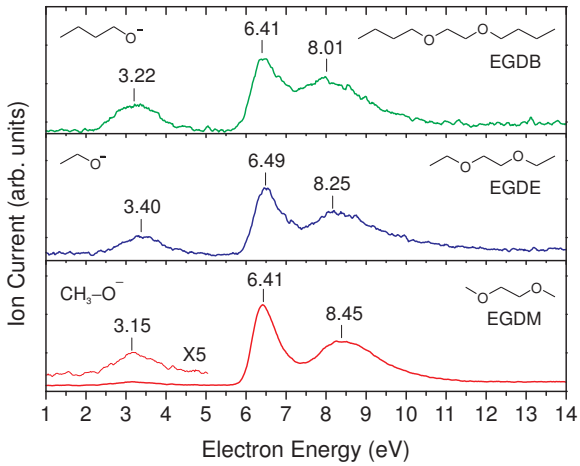

FIG. 13: DEA spectra of EGDB, EGDE, and of ethylene glycol dimethyl ether (EGDM). The anions are indicated on the left side of the panel.

made in section III B. The same applies for the loss of a neutral butyl radical in the bottom part of Fig. 11, with a band at 8.0 eV, to be compared with bands at the same energies in Figs. 5 and 6.

More surprising are the bands at 6.41 and 6.47 eV in Fig. 11, because they indicate that the *n*-Feshbach resonance causes a cleavage of C−O bond, in contrast to what has been observed with alcohols and simple ethers (Fig. 1 and ref. [17]). The fact that this process occurs only in the compounds with a hydroxyl group, 2EE and 2BE in Fig. 11, indicates that it is the hydroxyl group which mediates the cleavage of the ether bond. A decisive point is presumably the intramolecular hydrogen bridge which holds the hydroxyl and the ether oxygens in close proximity in the lowest energy conformation. Our DFT calculations predict, for both molecules, that the hydrogen-bridged cyclic conformations are 10 kJ/mol more stable than their open chain counterparts, as shown in Fig. 12. The cycle is maintained even more in the anions formed through the reactions (3a) and (4a). The presence of a hydrogen bridge appears to reduce or to remove the activation barrier which prevents the cleavage of the C−O bond *via* the 6.5 eV resonance in simple alcohols and ethers.

Fig. 13 shows the DEA spectra for the reactions (1b), (2b), and an analogous reaction of ethylene glycol dimethyl ether EGDM. The particularity of these reactions, which were not possible with monoethers, is a cleavage of the C−O bond to form a neutral fragment which is not a simple alkyl radical as discussed in Sec. III B, but which contains an oxygen atom. An example is the 2-butoxy ethyl radical in reaction reaction (2b). Its formation is depicted in the DEA spectrum in the top panel of Fig. 13. DEA spectra involving the formation of other oxygen containing neutral fragments from ethylene glycol dimethyl and diethyl ethers are shown in the lower panels of Fig. 13. All three spectra in this figure are very similar, and unexpected in the sense that the 6.4 eV *n*-Feshbach resonance is responsible for cleavage of a C−O bond, in contrast to the observations made with simple alcohols and ethers (ref. [17] and the present work). in this case it appears that the presence of an oxygen atom in the neutral fragment is responsible for the reduction or the removal of the activation barrier which prevents the cleavage of the C−O bond *via* the 6.4 eV resonance in simple alcohols and ethers [17].

The energy of the 8.0-8.5 eV band in Fig. 13 decreases slightly with increasing size of the neutral fragment, an observation made already for the pure alkyl neutral fragments in Sec. III B. The relatively small shift of about 0.2 eV in each step indicates that the effect approaches its asymptotic value – the neutral fragment chains are 4,

5 and 7 atoms long here, longer than the ethyl, propyl and butyl fragments discussed in Sec. III B. The fact that the band does shift suggests that the Feshbach resonance is delocalized over the entire butoxy ethyl radical.

For EGDM, the formation of CH_3O^- (bottom of Fig. 13) is the only fragmentation pathway. In particular a reaction where a neutral methyl fragment is lost is missing. This further supports the conclusion reached above for simple methyl ethers, *i.e.*, that methyl radical is not lost as a neutral fragment.

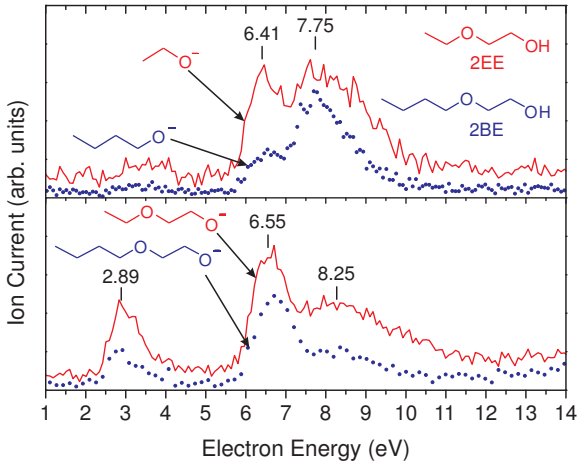

FIG. 14: DEA spectra of 2EE and 2BE. The top panel refers to the reactions (3b) and (4b), while the bottom panel refers to the reactions (3c) and (4c).

The bottom part of Fig. 14 shows the yields of the $(M-1)^-$ ions from ethoxy- and butoxy- ethanol. They are best discussed in comparison with the $(M-1)^-$ ion yield from unsubstituted ethanol, the solid line in the bottom panel of Fig. 1. The bands near 2.8 and 6.5 eV are nearly identical in all three cases, compatible with their interpretation. The onset of the former band corresponds to the threshold energy, which does not change appreciably. The Feshbach resonance near 6.5 eV is localized on the oxygen and is not affected by changes in substitution far from it. On the other hand the 9.1 eV band of ethanol shifts down to 8.25 eV upon substitution, also in line with the interpretation that the excitation in the Feshbach resonance is delocalized over the ethoxy and butoxy moieties.

The top part of Fig. 14 shows breaking of the C−O bond such that the same $^{\cdot}CH_2CH_2OH$ neutral fragment is released for both targets. If the rules reported above for the release of neutral alkyl fragments were valid even for the release of this fragment, then the 7.75 eV band should be at the same energy for both targets – which is within experimental error the case.

E. Shape resonances

This paper is primarily concerned with Feshbach resonances, but a brief discussion of the shape resonance bands observed in many of the spectra appears appropriate. In alcohols the shape resonance bands are narrow, with a nearly vertical onset at the threshold energy. They may thus be understood as a dissociation of a σ^* resonance which proceeds without an activation barrier – in agreement with our earlier discussion [15].

A brief discussion of the shape resonance bands in diethyl and dibutyl ether was given in our earlier publication [16]. The main conclusions, that the bands do not have a vertical onset, and peak well above the threshold for dissociation (indicating an activation barrier), are confirmed in the present work. The details of these bands are difficult to rationalize, however. One band around 3.5 eV is often observed, but two bands appear in some cases (Figs. 4 and 5). The lower of these two bands are at a surprisingly low energy for saturated compounds. The dissociations appear to occur at threshold as indicated by the calculated threshold values in Figs. 4 and 5. This fact may help to explain the unexpected cleavage of ethers by dissociative attachment of an photoexcited trapped electron in a cryogenic γ-irradiated 3-methylpentane glass [27]. The ether used there was dimethyl ether, which does not show low energy bands in the gas phase, but it is possible that solvation stabilizes the resonance, decreasing it autodetachment width and permitting dissociation even in dimethyl ether.

F. Comparison with unsaturated ethers

The present data can be compared to the results on unsaturated ethers of Bulliard *et al.* [28]. The major difference with the present compounds is the presence of a very pronounced π^* shape resonance at 1-2 eV. Their results fall into two categories:

a) Compounds where the ether oxygen and the π system are separated by a methylene group, that is methyl allyl ether, CH_2=CH-CH_2-O-CH_3, and the benzyl methyl ether C_6H_5-CH_2-O-CH_3. In these cases the C-O bond to be broken does not lie in the plane of the π system, the π system can conjugate with the σ^* orbital of the C-O bond to be broken, the dissociation of the π^* shape resonance is symmetry-allowed, occurs rapidly and completely dominates the DEA spectra. Feshbach resonances are not visible in the DEA spectra of these compounds, and there is no evident relation to the processes presented in this work.

b) Compounds where the ether oxygen and the π system are directly linked, methyl vinyl ether, CH_2=CH-O-CH_3, ethyl vinyl ether CH_2=CH-O-C_2H_5 and anisole C_6H_5-O-CH_3. In these cases the C-O bond to be broken lies in the plane of the π system, the π system cannot conjugate with the σ^* orbital of the C-O bond to be broken, the dissociation of the π^* shape resonance is

symmetry-forbidden. DEA spectra of these compounds have only relatively weak shape resonance bands in the 2-4 eV range, and prominent Feshbach resonance bands similar to those in the present work.

A $(n, 3s^2)$ resonance is observed around 6.5 eV, but, unlike in saturated ethers, this resonance appears to cleave the C−O bond when the C atom is an sp^2-hybridized carbon of the allyl group. This resonance does not, however, cleave the C−O bond when the C atom is sp^3-hybridized in the ethyl group, confirming the conclusions reached in ref. [17] and in this work.

A loss ot ethyl radical from ethyl vinyl ether has a broad band around 9.1 eV, the same energy as loss of ethyl radical in numerous saturated alcohols and ethers presented in this work.

Finally, the loss of the neutral methyl radical has not been observed in methyl vinyl ether, reinforcing the conclusion that the methyl group can be used as a "protective group" and steer the fragmentation in a controlled manner.

IV. CONCLUSIONS

Dissociative electron attachment processes in saturated oxygen containing compounds are mediated by shape resonances, which lead to generally weak fragmentations below 5 eV, and by Feshbach resonances in the 5-11 eV range. The Feshbach resonances have electronic configurations of the type $^2(\psi_i^-1, 3s^2)$, and give rise to DEA bands around 6.5 eV (where ψ_i is n_O), 7.5 eV (where ψ_i is $\bar{n}_O$), and 8-11 eV (where ψ_i is one of the many available σ orbitals). The $\bar{n}$-Feshbach band often overlaps with the σ-Feshbach band and cannot be discerned as a separate band.

The primary result of the present work is the observation of a marked selectivity *within* the dense manifold of the σ-Feshbach resonances. In the reaction

$$e^-(E_i) + R_1OR_2 \rightarrow R_1^{\cdot} + R_2O^-,$$

with R_1 and R_2 being alkyl or H, the energy of the σ-Feshbach band is the same for a given R_1 in many compounds – it is independent of the nature of R_2. The band was observed at 9.1, 8.5 and 8.0 eV for R_1 being ethyl, propyl and butyl radicals, and at 8.7 eV for the *t*-butyl radical, for a wide variety of target molecules.

This has the interesting consequences that one or the other C−O bond can be selectively cleft in asymmetric ethers by choosing the appropriate electron energy, and that a given alkyl radical is lost when electrons of a given energy impact on a wide range of compounds.

$R_1 = CH_3$ behaves differently from other alkyl moieties, dissociations involving methyl radical as a neutral product are too weak to be detected, except in the case of methanol, where the OH^- ion is observed. This means that methyl can be used as a "protective group", to inhibit certain fragmentations.

These observations are surprising because one would expect that the energy of a Feshbach resonance depends on the nature of the entire target molecule, not only on which neutral radical is formed in the fragmentation. One would also not expect such pronounced selectivity within a dense manifold of very highly excited states of the intermediate negative ion, as the individual states should be strongly vibronically coupled, allowing thee system to jump between the different through numerous conical intersections and breakdown of the Born-Oppenheimer approximation.

The interpretation proposed here is that the 7-12 eV region contains many closely spaced Feshbach resonances, which overlap because of their Franck-Condon widths, with holes in the many σ orbitals available in large molecules. Certain of these Feshbach resonances are localized on a given alkyl moiety, one resonance at R_1 and another at R_2, and at the same time delocalized over the entire length of that moiety. The energy of these selected resonances thus depends only on R_1 or R_2, but not on the remainder of the target molecule. Localized means that the hole in the core, and hence the two diffuse electrons bound by the positive charge of the hole, are spatially localized on a given part of the target molecule.

Next one needs to assume that these localized Feshbach resonances cause the fragmentation, and that they dissociate is such a way, that the charge finally resides on the fragment with the higher electron affinity, which is the one containing the oxygen atom, and not on the alkyl fragment on which the Feshbach resonance was initially localized.

This interpretation is based on the empirically observed selectivity and the fact that the observed resonance energies depend only on R_1 and not on R_2. The interpretation is further supported by a correlation between the resonance energies and the experimental ionization energies of the hydrocarbons R_1H.

The interpretation is thus not based on quantum chemical calculations – in fact, theoretical methods applicable to our observations are not available. The problems are the large size of the molecules, the necessity to calculate highly excited Feshbach resonances, and to understand the nuclear dynamics on a dense manifold of closely spaced electronic states of the transient anion.

We used theory in an attempt to gain more insight into the problem by inspecting the shapes of the occupied SCF orbitals of butyl ethyl ether, which may be taken as representative of the charge distributions of the positive holes in the core of the Feshbach resonances. Among the many σ orbitals we found indeed two which are localized in the desired way, one on the butyl, the other on the ethyl moieties. The majority of the many σ orbitals in the same energy range were delocalized over the entire molecule, however, so that the orbital pictures alone do not provide a complete rationalization of the observations.

To explain the observations, we have to assume that

a spontaneous localization of the excitation (*i.e.*, of the hole in the core and of the two diffuse electrons) occurs in the Feshbach resonances. This concept could have important implications for localization of damage caused by 8-12 eV electrons in large molecules like DNA or proteins.

We extended the study to compounds of the type $R_1OCH_2CH_2OR_2$ which offer more fragmentation channels, in particular ones where the neutral fragment is not a simple alkyl radical, but also contains an oxygen atom. The above conclusions could be extended even to these cases.

This class of compounds also led to conclusions which are slightly outside of the main focus of this paper, but also interesting. They represent an extension of the rule which states that the ~ 6.5 eV resonance with a hole in the n_O nonbonding MO mediates cleavage of the O−H but not the C−O bond in alcohols and ethers containing only one oxygen atom [17]. The present study reveals that this rule is relaxed under certain circumstances in the compounds of the type $R_1OCH_2CH_2OR_2$, with two oxygens, where the ~ 6.5 eV resonance was found to break also the C−O bond. It was in two cases: (i) when the neutral fragment contained an oxygen atom or (ii) in molecules with $R_2 = H$, when the neutral fragment was a simple alkyl radical but when the most stable conformation of the target molecule had a hydrogen-bonded cyclic structure bringing the hydroxyl and the ether oxygens into close proximity.

V. ACKNOWLEDGMENT

This research is part of project No. 200020-113599/1 of the Swiss National Science Foundation and of the COST Action CM0601 (ECCL). We thank to T. Bally for critical reading of the manuscript. We thank to Anne Schuwey for the synthesis of dibutoxy methane.

[1] L. G. Christophorou and J. K. Olthoff, *Fundamental Electron Interactions with plasma processing gases*, Kluwer Academic, New York, Boston, Dordrecht, London, Moscou, 2004.
[2] B. Boudaiffa, P. Cloutier, D. Hunting, M. A. Huels, and L. Sanche, *Science*, 2000, **287**, 1658.
[3] I. Utke, V. Friedli, M. Purrucker, and J. Michler, *J. Vac. Sci. Technol.*, 2007, **25**, 2219.
[4] G. J. Schulz, *Rev. Mod. Phys.*, 1973, **45**, 423.
[5] F. H. Read, *J. Phys. B*, 1977, **10**, 449.
[6] M. B. Robin, *Higher Excited States of Polyatomic Molecules*, Vol. 3, Academic Press, Orlando, 1985.
[7] A. Kühn, H. P. Fenzlaff, and E. Illenberger, *J. Chem. Phys.*, 1988, **88**, 7453.
[8] M. G. Curtis and I. C. Walker, *J. Chem. Soc. Faraday Trans.*, 1992, **88**, 2805.
[9] V. S. Prabhudesai, A. H. Kelkar, D. Nandi, and E. Krishnakumar, *Phys. Rev. Lett.*, 2005, **95**, 143202.
[10] V. S. Prabhudesai, D. Nandi, A. H. Kelkar, and E. Krishnakumar, *J. Chem. Phys.*, 2008, **128**, 154309.
[11] V. S. Prabhudesai, N. B. Ram, G. Aravind, P. Rawat, and E. Krishnakumar, *Journal of Physics: Conference Series*, 2007, **80**, 012016 (8pp).
[12] M. Orzol, I. Martin, J. Kocisek, I. Dabkowska, J. Langer, and E. Illenberger, *Phys. Chem. Chem. Phys.*, 2007, **9**, 3424.
[13] L. Parenteau, J. P. Jaygerin, and L. Sanche, *J. Phys. Chem.*, 1994, **98**, 10277.
[14] T. Skalický and M. Allan, *J. Phys. B*, 2004, **37**, 4849.
[15] B. C. Ibănescu, O. May, A. Monney, and M. Allan, *Phys. Chem. Chem. Phys.*, 2007, **9**, 3163.
[16] B. C. Ibănescu, O. May, and M. Allan, *Phys. Chem. Chem. Phys.*, 2008, **10**, 1507.
[17] B. C. Ibănescu and M. Allan, *Phys. Chem. Chem. Phys.*, 2008, **10**, 5232.
[18] M. Jungen, J. Vogt, and V. Staemmler, *J. Phys. B*, 1979, **37**, 49.
[19] K. Kimura, S. Katsumata, Y. Achiba, T. Yamazaki, and S. Iwata, *Handbook of HeI Photoelectron Spectra of Fundamental Organic Molecules*, Japan Scientific Societies Press, Tokyo, 1981.
[20] B. C. Ibanescu *Electron-driven chemistry of saturated compounds containing oxygen and nitrogen atoms.* PhD thesis, University of Fribourg, 2009.
[21] M. Stepanović, Y. Pariat, and M. Allan, *J. Chem. Phys.*, 1999, **110**, 11376.
[22] R. Dressler and M. Allan, *Chem. Phys.*, 1985, **92**, 449.
[23] A. Stamatovic and G. J. Schulz, *Rev. Sci. Instrum.*, 1968, **39**, 1752.
[24] M. J. Frisch, G. W. Trucks, H. B. Schlegel, G. E. Scuseria, M. A. Robb, J. R. Cheeseman, J. A. Montgomery, Jr., T. Vreven, K. N. Kudin, J. C. Burant, J. M. Millam, S. S. Iyengar, J. Tomasi, V. Barone, B. Mennucci, M. Cossi, G. Scalmani, N. Rega, G. A. Petersson, H. Nakatsuji, M. Hada, M. Ehara, K. Toyota, R. Fukuda, J. Hasegawa, M. Ishida, T. Nakajima, Y. Honda, O. Kitao, H. Nakai, M. Klene, X. Li, J. E. Knox, H. P. Hratchian, J. B. Cross, V. Bakken, C. Adamo, J. Jaramillo, R. Gomperts, R. E. Stratmann, O. Yazyev, A. J. Austin, R. Cammi, C. Pomelli, J. W. Ochterski, P. Y. Ayala, K. Morokuma, G. A. Voth, P. Salvador, J. J. Dannenberg, V. G. Zakrzewski, S. Dapprich, A. D. Daniels, M. C. Strain, O. Farkas, D. K. Malick, A. D. Rabuck, K. Raghavachari, J. B. Foresman, J. V. Ortiz, Q. Cui, A. G. Baboul, S. Clifford, J. Cioslowski, B. B. Stefanov, G. Liu, A. Liashenko, P. Piskorz, I. Komaromi, R. L. Martin, D. J. Fox, T. Keith, M. A. Al-Laham, C. Y. Peng, A. Nanayakkara, M. Challacombe, P. M. W. Gill, B. Johnson, W. Chen, M. W. Wong, C. Gonzalez, and J. A. Pople, Gaussian 03, Revision C.01.
[25] M. B. Robin, *Higher Excited States of Polyatomic Molecules*, Vol. 1, Academic Press, New York, 1974.
[26] R. V. Olkhov and T. Bally, Moplot version 1.83 `http://www-chem.unifr.ch/tb/moplot/moplot.html`.
[27] H. Yoshida, M. Irie, O. Shimada, and K. Hayashi, *J. Phys. B*, 1972, **76**, 3747.
[28] C. Bulliard, M. Allan, and S. Grimme, *Int. J. of Mass Spectr. and Ion Proc.*, 2001, **205**, 43.

Chapter 5

Dissociative electron attachment of amines

In this chapter the dissociative electron attachment to amines is presented. Trends like those observed for saturated compounds with oxygen, namely the use of methyl as a protective group, the dependence of the energy for the observed DEA band on the alkyl group and the non-dissociative nature of the $^2(n, 3s^2)$ resonance with respect to the heteroatom−C bond, are also found in amines. Amendments to these trends are provided by the study of primary and secondary amines. This chapter is written as a draft for a paper that will be submitted at a later time.

5.1 Introductions

Dissociative electron attachment (DEA) represents one of the many processes that can occur when a molecule, AB, in gas phase collides with an electron:

$$e^-(E_i) + \mathrm{AB} \rightarrow \{\mathrm{AB}\}^- \rightarrow \mathrm{A}^- + \mathrm{B}$$

where E_i is the energy of the incident electron and $\{\mathrm{AB}\}^-$ is an intermediate short-lived anion also called a resonance.

The interest in this process has increased due to emerging applications in technology [6] and the need to understand radiation-induced damage to living tissue [3]. An important role in biology and technology is played by heteroatom-containing compounds, primarily alcohols and ethers, but also amines and thioalcohols.

For saturated compounds DEA fragmentations are observed at electron energies in the 6-15 eV range, sometimes with substantial cross sections, but very little is generally known about the assignment of the resonances responsible for the corresponding bands in the DEA spectrum, and even less is known about the mechanisms of the dissociation. These DEA bands are generally assigned to Feshbach resonances, with two excited electrons, but only rarely has a specific assignment been given for large polyatomic molecules. At the same time DEA bands in the 6-15 eV range are often responsible for a significant fraction of the electron-induced chemistry. Bands

in this energy range have been reported in the context of electron-induced damage in DNA [3, 33], suggesting that Feshbach-type resonances may be responsible even for electron-induced chemistry in condensed-phase biomolecules.

Previously we discovered that the presence of lone pairs of electrons in saturated compounds with heteroatoms leads to Feshbach resonances with interesting properties [32, 35, 36]. In the 6-15 eV region the spectra of alcohols [22, 32, 57] shows the presence of three types of Feshbach resonances with a hole in either the oxygen 'nonbonding' orbitals n_O or $\bar{n}_O$, or in the σ orbitals manifold. They were designated as n-, $\bar{n}$- and σ-Feshbach resonances. In ethers and alcohols the resonances localized on the heteroatom are not dissociative with respect to the O−C and they do not lead to any observable DEA signal, indicating the presence of an activation barrier on their potential energy surface. Additionally, the energy of the detected σ-Feshbach resonance depends on the size of alkyl group, being 9 eV for ethyl and 8 eV for butyl.

The trends observed for alcohols and ethers need to be amended in the case of compounds with two oxygen atoms such as monoethers and diethers of ethylene glycol. [36]. In monoethers of ethylene glycol, with one hydroxyl group and one ether group, the presence of an hydrogen bond between the the two mentioned groups leads to the observation of a DEA band at 6.5 eV indicating a lowering of the activation barrier otherwise present on the potential surface of the $^2(n, 3s^2)$ resonance. Further insight is provided by diethers of ethylene gylcol where loss of radicals containing an oxygen atom also leads to the observation of a band at 6.5 eV, energy associated with the $^2(n, 3s^2)$ resonance localized on the oxygen atom. This suggests that the breaking of the O−C bond may be enabled by suitable chemical environment. In the simplest case, ethers, the O−C is dissociated only by the σ-Feshbach resonance, while the additional presence of hydrogen bonds or of a second oxygen atom, as in ethers of ethylene glycol, leads to the dissociation of this bond even by n-Feshbach resonance [36].

The current chapter extends the observation previously made for saturated compounds with oxygen to another class of compounds with biological relevance – amines. As in the case of ethers the bond breaking occurs only at specific energies, dependent on the alkyl fragment that is lost irrespective of the target molecule.

5.2 Results and discussion

The study of ethers where methyl is one of the alkyl groups have shown that this group can be used as a protective group [36]. Thus the selective methylation of a molecule can be used as a tool to study the dissociation patterns upon electron collision. One such example is provided by the study of DEA in thymine [58]. Ptasinska *et al.* have shown that the selective methylation of the amino groups can be used to determine the site-selective breaking of the bonds, depending on the electron energy used.

Fig. 5.1 shows the DEA spectra of dimethylbutyl amine (DMBA) and diethylmetylamine (DEAM). Both molecules have methyl group and butyl or ethyl respec-

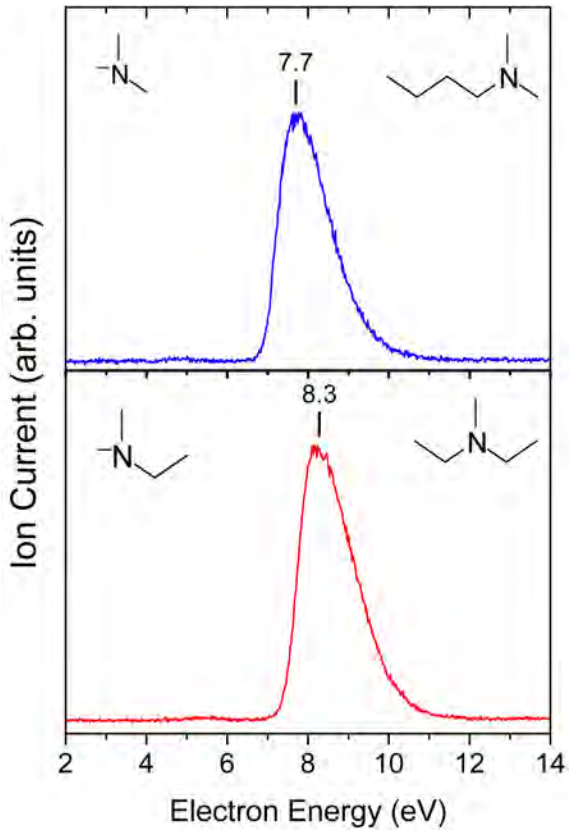

Figure 5.1: DEA spectra of dimethylbutylamine (DMBA, top), and diethylmethylamine (DEAM, bottom).

tively attached to the nitrogen atom. The only anions that were detected in this case corresponded to loss of alkyl chain but not methyl. This indicates that O−Methyl bond cannot be broken by electrons with energies up to 16 eV and, indeed, methyl can be used as a protective group when studying saturated compounds with either oxygen or nitrogen.

In the Introduction we have presented several trends that were observed for saturated compounds with oxygen [36]. The O−C bond was broken selectively only by σ-Feshbach resonance resonance and not by n-Feshbach resonance, indicating the presence of an activation barrier on the potential surface of the latter resonance. A special case is presented by molecules with more than one oxygen atom where the presence of hydrogen bonds or of an oxygen atom in the lost radical lowers the activation barrier sufficiently so even the $^2(n, 3s^2)$ resonance can break the O−C bond. Additionally the energy at which the O−C bond was broken by the $^2(\sigma, 3s^2)$ resonance were dependent on the lost alkyl radical and not on the target molecule. It is interesting to know if similar trends are valid for amines or if they are restricted to compounds with oxygen.

Fig. 5.2 shows the DEA spectra of diethylamine (DEA), diethylmethylamine (DEMA), triethylamine (TEA) and ethylbutylamine (EBA). All these amines lose an ethyl radical upon electron collision, as indicated by the solid line in fig. 5.2.

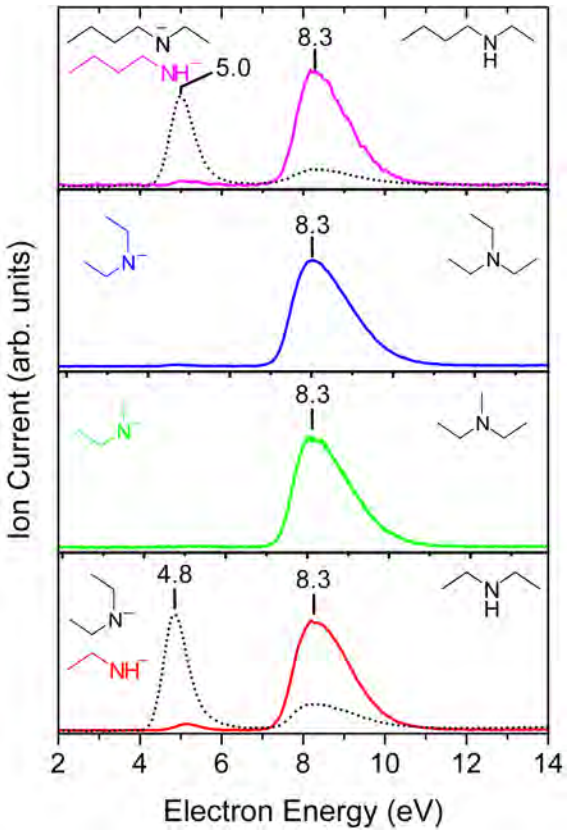

Figure 5.2: Loss of ethyl radical from various amines. The resulting anion is shown in the left corner of each spectrum, while in the right corner the initial molecule is shown. For comparison loss of an H-atom is included as dotted lines.

Additionally DEA and EBA can also lose an H-atom forming the $(M\text{-}1)^-$ anion. This is shown by the dotted DEA spectra in fig. 5.2. DEA has been previously reported in the literature by Skalický and Allan [22]. They have observed two distinct bands in the DEA spectra, at 4.7 eV and 8.4 eV. Using a comparison with the HeI photoelectron spectrum they have assigned the bands to Feshbach resonances, the 4.7 eV band was assigned to $^2(n_N, 3s^2)$ Feshbach resonance where n_N is the a' nonbonding lone pair orbital, while the 8.7 eV band was assigned to the $^2(\pi_{CH_3}, 3s^2)$ Feshbach resonance, where π_{CH_3} is the a'' pseudo π orbital, contributing primarily to the C−H bonds. Our spectra presented in fig. 5.2 is in agreement with this assignment within the experimental error limits.

Fig 5.2 shows that the loss of an ethyl radical occurs mostly at 8.3 eV irrespective of the target molecule. Similar to the above case encountered in DEA, in EBA ethyl radical can also be lost through a resonance at 5.0 eV albeit significantly less than the other resonance detected at 8.3 eV. As in DEA, we assign the resonances at 5.0 eV to $^2(n_N, 3s^2)$ Feshbach resonance localized on the heteroatom. In all 4 amines we assign the 8.3 eV resonance as being a Feshbach resonance where the hole is predominately localized on the ethyl fragment.

Loss of butyl radical offers similar insight as the loss of the ethyl fragment.

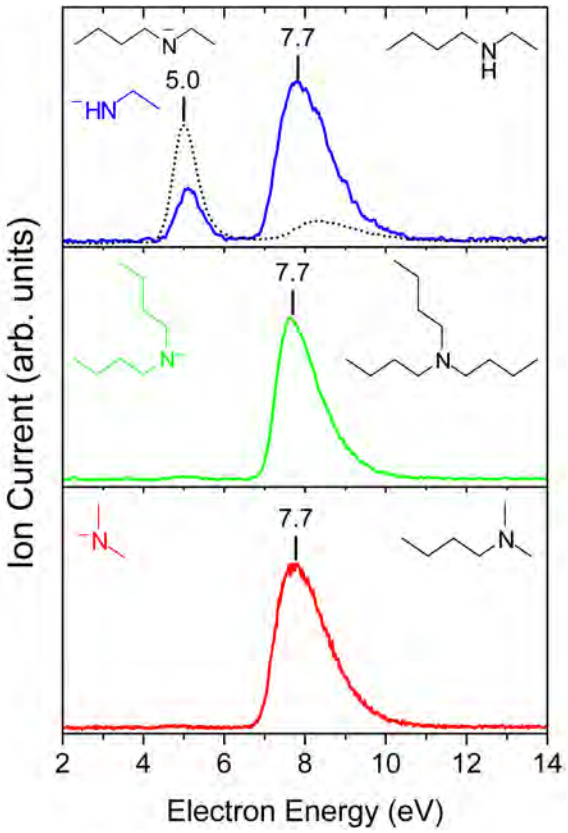

Figure 5.3: Same as 5.2 but for loss of butyl radical.

Fig. 5.3 shows the DEA spectra of dimetylbutylamine (DMBA), tributylamine (TBA) and EBA. The loss of butyl radical is represented by solid line while loss of an H-atom is represented by dotted lines. The DEA spectra from fig. 5.3 show that loss of butyl radical occurs mainly through a resonance located at 7.7 eV irrespective of the target molecule. As in the previous cases we assign this band to a Feshbach resonance, where a pair of electrons are in a $3s$ Rydberg type orbital and a hole is in an orbital mainly localized on the butyl chain.

Figs. 5.2 and 5.3 shows DEA spectra of tertiary amines able either to lose an ethyl or a butyl radical. An inspection of these spectra reveals that the breaking of the N−C bond occurs only at 8.3 eV for the loss of an ethyl and at 7.7 eV for loss of butyl. In all cases these band have been assigned to a resonance localized on the respective alkyl group. There is no doubt that there must be a resonance at a lower energy, around 4.5-5 eV, localized on the nitrogen atom, similar to the secondary amines presented in figs. 5.2 and 5.3. But the fact that no DEA band has been detected at these energies for tertiary amines is an indication for the presence of an activation barrier on the potential energy surface for the $^2(n_N, 3s^2)$ resonance.

A dependence on the alkyl chain can be noticed for the observed Feshbach resonance in the 7-14 eV energy range. The energy of this resonance is 7.7 eV when it is localized on a butyl chain and 8.3 eV for an ethyl chain. This situation is very similar to that previously observed for ethers [36] where the energy of Feshbach

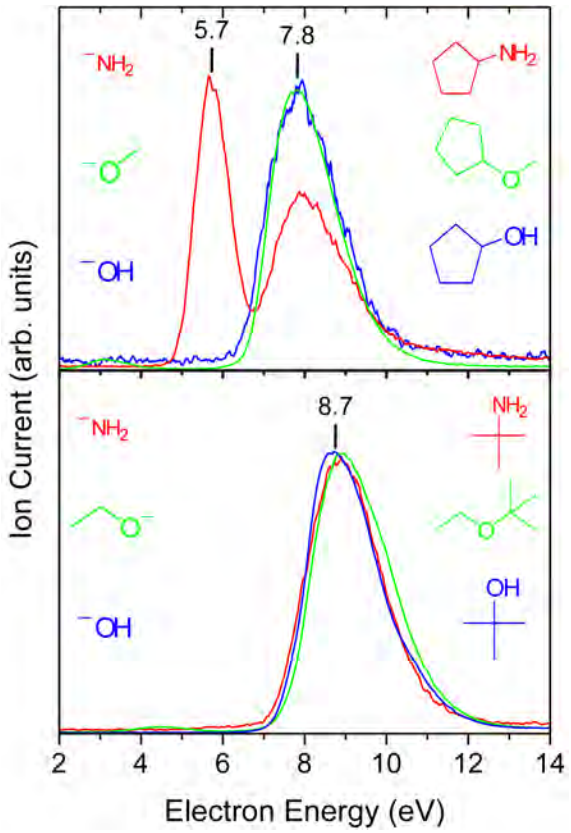

Figure 5.4: Comparison between loss of cyclopentyl radical (top) and *tert*-butyl radical (bottom) from various compounds. Amines are represented in red, ethers in green and alcohols in blue.

resonance dropped from 9 eV when it was localized on an ethyl chain to 8 eV when it was localized on the butyl chain.

Fig 5.4 shows a comparison of the loss of cyclopentyl radical (top) and *tert*-butyl radical (bottom) from alcohols, ethers and amines. In substances that can lose *tert*-butyl radical this process happens at the same energy, at 8.7 eV independent on the class of the compound. This suggests that the resonance is localized on the same fragment in all the cases, *tert*-butyl chain. A similar conclusion can be drawn for compounds with cyclopentyl, where this group is lost through a resonance at 7.8 eV. Cyclopentylamine (CPA) is a special case because the N−C bond breaking also occurs at 5.7 eV. In other amines presented in this work the DEA band at energies around 5 eV has been assigned to a $^2(n_N, 3s^2)$ Feshbach resonance. In a similar manner we assign the 5.7 eV, although a little bit high in energy since the 1st ionization energy is the same as in all other amines at 9.1 eV, to a similar Feshbach resonance. In all compounds we assign the 7.8 eV band in compounds with cyclopentyl and the 8.7 eV band in molecules with *tert*-butyl to a Feshbach resonance localized on cyclopentyl chain in the first case and on *tert*-butyl chain in the latter.

5.3 Conclusions

The dissociation of amines upon electron collision occurs mainly through the breaking of either N−H or N−C bonds in the molecule. This can lead to the loss of an alkyl chain or to the formation of the $(M-1)^-$ ion (in primary or secondary amines).

Two Feshbach resonances have been detected in the DEA spectra of amines. The first resonance is located at 4.8-5.0 eV while the second one is placed at energies higher than 7 eV. The first resonance is a $^2(n_N, 3s^2)$ Feshbach resonance, primarily localized around the nitrogen atom. This assignment is supported by the energy relation with the grandparent cation observable in the photoelectron spectrum [22] and the fact that its energy does not change with the length of the alkyl chain. The energy of the second observed Feshbach resonance shows a particular dependence on the alkyl chain that is present in the molecule, being at 7.7 eV for butyl chain and at 8.3 eV for ethyl chains. The energy dependence suggests that this resonance is localized on the particular alkyl chain. This is particularly visible for EBA, an amine that can lose both an ethyl radical and a butyl radical. In this case, in the 7-14 energy range, the breaking of the N−Ethyl bond occurs only through the 8.3 eV resonance while breaking of N−Butyl bond is detected only at 7.7 eV, even though both Feshbach resonances are present in the molecule.

The dependence of the energy of the Feshbach resonance on the alkyl chain is reminiscent of the trend observed for ethers and alcohols. In oxygen containing compounds the Feshbach resonance localized on the ethyl chain is at 9 eV while the resonance localized on butyl chains is at 8 eV. This suggests that such trends could be present other classes of saturated compounds such as thiols or thioethers. In some case such as the case of cyclopentyl or *tert*-butyl radical presented in this work the loss of the radical occurs at the same energy independent on the heteroatom to which the group is linked. But for other radicals such as linear alkyl chains, like ethyl or butyl, the energy of the resonance depends on the heteroatom. When the heteroatom is oxygen then ethyl is lost at 9 eV while in the case of nitrogen it is lost at 8.3 eV. A similar shift is observed for butyl radical that is lost at 8.0 eV in oxygen containing compounds and at 7.7 eV in the case of amines.

The shift to lower energies when the heteroatom in the molecule is changed from oxygen to nitrogen depends on the size of the alkyl chain involved. For relatively small chains, such as ethyl the shift is 0.7-0.8 eV and, as the chain size is increased, it drops to 0.3 eV for butyl chains and, finally for very bulky chains such as *tert*-butyl or cyclopentyl, it is not observable. A similar situation has been observed by Robin when he studied term energies and band shapes in VUV spectra [27]. He has observed that the term value that links the positive core observed in photoelectron spectroscopy and the Rydberg states observed in VUV spectra decreases as the molecular volume of the group is increased from ethyl to *tert*-butyl [27]. At this point we can only speculate about the possible reasons. It could be that the positive core from the Feshbach resonance is affected by the size of the electronic cloud next to positive core and by the size of the positive core.

We observe that in molecules with oxygen or nitrogen two different types of

Feshbach resonances have been observed, depending on the site where the resonance is localized. In the first case the resonance is localized on the heteroatom and is characterized by the fact that is breaks only the O−H or the N−H bond. This resonance is usually found at an energy of 6-6.5 eV in compounds with oxygen for the first pair lone pair of electrons and 7-8 eV for the second pair of electrons. In nitrogen containing compounds the resonance is usually at 4.5-5.0 eV. The selectivity of the bond breaking in oxygen containing compounds is a result of an activation barrier being present on the potential energy surfaces of the parent Rydberg states and their daughter Feshbach resonances.

The second type of Feshbach resonance is localized on an alkyl group present in the molecule. Usually it breaks both O−H or N−H bond and O−C or N−C bond respectively. The energy of this resonance is above 8 eV and it depends on the alkyl group where the resonance is localized. This resonance is located in a region that contains many closely spaced Feshbach resonances that overlap. These resonances have holes in the many σ orbitals available in the large polyatomic molecules. Out of these resonances only those where the resonance is localized on a given alkyl group seem to mediate the dissociation.

We have determined some special cases of the Feshbach resonances of the first type that break even the O−C or N−C bond respectively. In oxygen containing compounds they are found in molecules with intra-molecular hydrogen bonds and where the lost radical includes an oxygen atom [36]. For molecules with nitrogen the special case is encountered in secondary of primary amines, that contain at least one N−H bond. In these molecules the N−C bond is broken by the resonances of the first type, the $^2(n_N, 3s^2)$ resonance, indicating a lowering of the activation barrier otherwise present on the potential surface of this resonance. This case is particular for nitrogen containing compounds and it has not been encountered in alcohols, where the presence of an O−H bond attached to the oxygen does not lead to a lowering of the activation barrier and thus to an observable DEA band in the 6-7 eV range.

The lowering of the activation barrier in amines and not in ethers or alcohols is most likely the result of different geometries of the primary molecule. In oxygen containing compounds the C−O bonds are located in the same plane (a planar geometry) while in amines the starting geometry is pyramidal. This allows for more energy to be stored in the structure of the molecule. This energy is not available in oxygen but in amines can be used to surpass the activation barrier present on the potential energy surface of the resonance. A consequence of this hypothesis would be a dependence of the least energy path followed by the system as it evolves toward dissociation on the pyramidal angle. Calculations are underway at the moment to verify this hypothesis and preliminary calculations presented in section 6.3.4 seem to indicate the validity of this hypothesis.

A final trend observed in saturated molecules with either oxygen or nitrogen is the fact that the O−CH_3 bond or the N−CH_3 bonds do not break upon electron collision. An important practical application of this observation is the possibility to use the methyl group as a protective group.

Chapter 6

Potential Surfaces of Rydberg States of Alcohols and Ethers

In this chapter, we attempt to offer a rationale for the striking difference between the dissociative electron attachment processes of alcohols and those of ethers. To explain these differences, the relation between the Feshbach resonaces and their parent Rydberg states, defined in section 1.1, is used. First, the potential energy surfaces of Rydberg states are modelled using the TD−DFT method. These surfaces could explain the experimental observations under the assumption that the potential energy surfaces of Feshbach resonances are similar to those of their parent Rydberg states. In the last section an attempt to directly calculate the Feshbach resonances is presented, in order to verify the above mentioned assumption. The main results from this chapter are published in ref. [37], reprinted as section 6.2 below.

6.1 Introduction

The extensive use of potential energy surfaces throughout this chapter requires the introduction of the notion of avoided crossing.

According to IUPAC [59], in the Born-Oppenheimer approximation, two electronic states ($|1\rangle$, $|2\rangle$) can change their energy ordering as the molecular geometry is changed continuously along a path (see fig. 6.1(a)). In the process their energies may become equal at some points (the surfaces are said to cross, dotted lines in the figure), or only come relatively close (the crossing of the surfaces is said to be avoided). If the electronic states are of the same symmetry, the surface crossing is always avoided in diatomics and usually avoided in polyatomics.

An examples of this situation is represented in fig. 6.1(a). Here $|1\rangle$ and $|2\rangle$ represent the diabatic components of the adiabatic electronic eigenfunctions $|\phi_1\rangle$ and $|\phi_2\rangle$(a diabatic function describes the energy of a particular spin-coupling, while the adiabatic function represents the surface of the real state).

Herzberg *et al.* [60] discussed the possible intersections in potential energy surfaces of polyatomic molecules and found the conditions necessary for an avoided

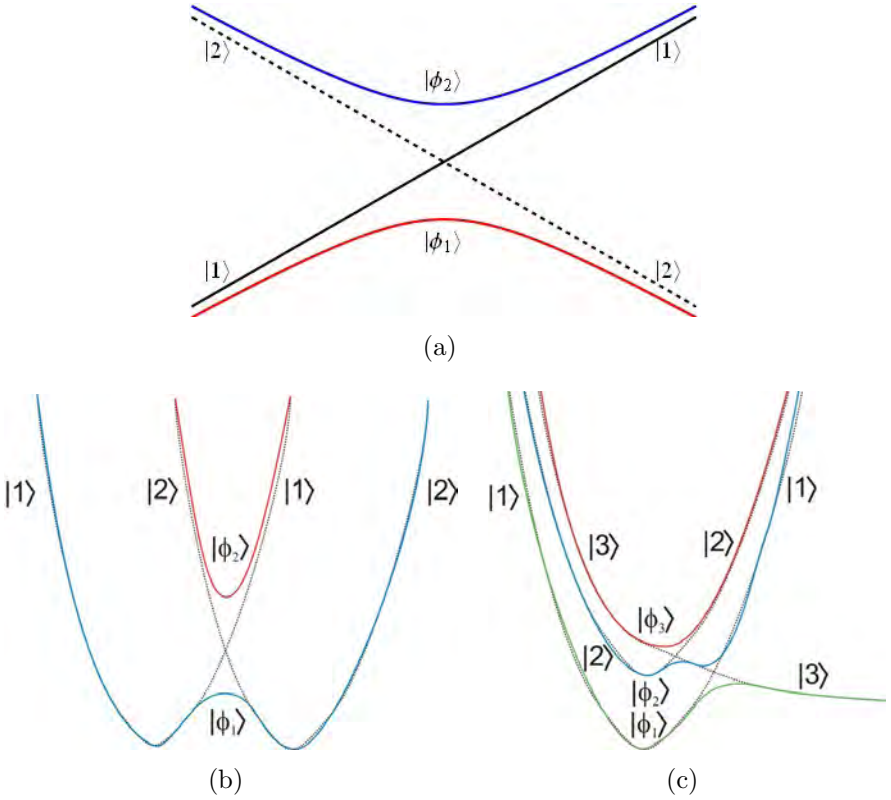

Figure 6.1: Schematic diagram of avoided crossings for various situations. a) A general representation of avoided crossing between two different electronic states; b) An avoided crossing between two states leading to an adiabatic potential curve with two minima; c) An avoided crossing between three states leading also to an adiabiatic potential curve with two minina (the situation encountered in this work). $|1\rangle$, $|2\rangle$, $|3\rangle$ represent the diabatic states (dotted lines), while $|\phi_1\rangle$, $|\phi_2\rangle$, $|\phi_3\rangle$ represent the adiabatic states (solid colored lines).

crossing. Two independent conditions need to be satisfied, namely:

$$\begin{aligned} H_{11} &= H_{22} \\ H_{12}(= H_{21}) &\neq 0 \end{aligned} \tag{6.1}$$

where H represent the electronic Hamiltonian and:

$$\begin{aligned} H_{11} &= \langle 1|H|1\rangle \\ H_{22} &= \langle 2|H|2\rangle \\ H_{12} &= H_{21} = \langle 1|H|2\rangle \end{aligned} \tag{6.2}$$

Let's have a closer look at eq. (6.1). It says that the crossing condition (real or avoided) is fulfilled when the energies of the two diabatic potentials (H_{11} is the energy for the diabatic function $|1\rangle$ and H_{22} is the energy for the diabatic function $|2\rangle$) are the same. Then at crossing of the diabatic functions, the expressions for the

energies of the two real states become:

$$\begin{aligned} E_1 &= H_{11} - H_{12} \\ E_2 &= H_{11} + H_{12} \end{aligned} \tag{6.3}$$

The energy gap between the two real states is

$$E_2 - E_1 = 2H_{12} \tag{6.4}$$

Thus, if the exchange term H_{12} is *not zero*, the crossing will be avoided and the potential surfaces of the two real states will *diverge*, *i.e.* one of the two adiabatic energies is lower and the other is higher than the diabatic energy H_{11}. Moreover, the value of the exchange term H_{12} determines the gap between the diabatic surfaces (small values will generate a small gap and a *narrow* potential trough on the upper surface ($|\phi_2\rangle$ in fig. 6.1(a)), large values a big gap and a *wide* potential trough). In general, H_{12} is *zero* (and the crossings will be real) when the two electronic states have a different (spatial or spin) symmetry, while it is usually assumed to be *non-zero* for states of the same symmetry (which will generate avoided crossings).

The analysis of adiabatic curves is most of the time not as straightforward as presented above. Such a situation is presented in fig. 6.1(b) and 6.1(c) where double minimum on the potential curves of adiabatic states can be obtained in different ways. Here, $|1\rangle$ - $|3\rangle$ are diabatic states with the same symmetry that generate avoided crossings, $|\phi_1\rangle$ - $|\phi_3\rangle$ are the resulting adiabatic states. Both figures show the presence of a double minimum (in fig. 6.1(b) for $|\phi_1\rangle$ state and in fig. 6.1(c) for $|\phi_2\rangle$ state). In the first case the double minimum is the result of an avoided crossing between two diabatic states (this case is often encountered in electron transfer processes), while in the second case it is the result of avoided crossings between three diabatic states, one of them being repulsive (this is the case encountered in this chapter).

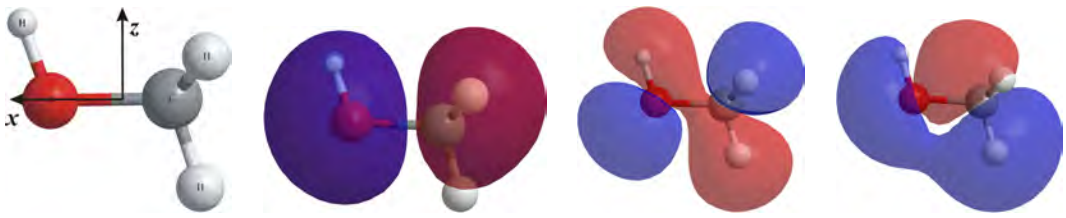

(a) Axis orientation (b) n (HOMO) (c) $\bar{n}$ (d) $\sigma_{\mathrm{O-C}}$

Figure 6.2: The highest three occupied molecular orbitals of methanol. The axis orientation is indicated on the left.

Other concepts, important for this chapter, are the notation and the symmetry of molecular orbitals (MO). Methanol which has C_s symmetry, has been chosen to illustrate this. The highest three occupied MOs are presented in figs. 6.2 and 6.3, while figs. 6.4 and 6.5 show the four lowest unoccupied MOs. The choice of the axes is shown in figs. 6.2(a) and 6.3(a).

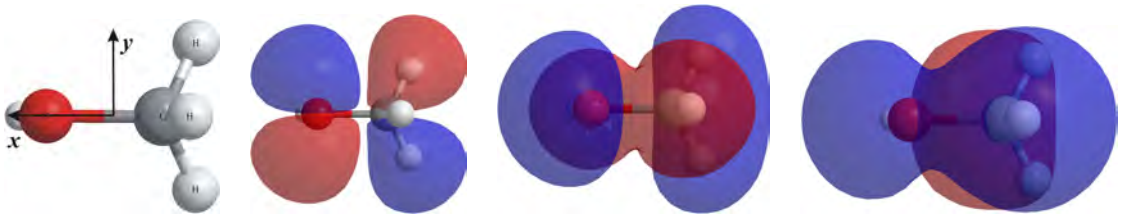

(a) Axis orientation (b) n (HOMO) (c) $\bar{n}$ (d) $\sigma_{\mathrm{O-C}}$

Figure 6.3: The same orbitals as in fig. 6.2, rotated by 90° around the x-axis.

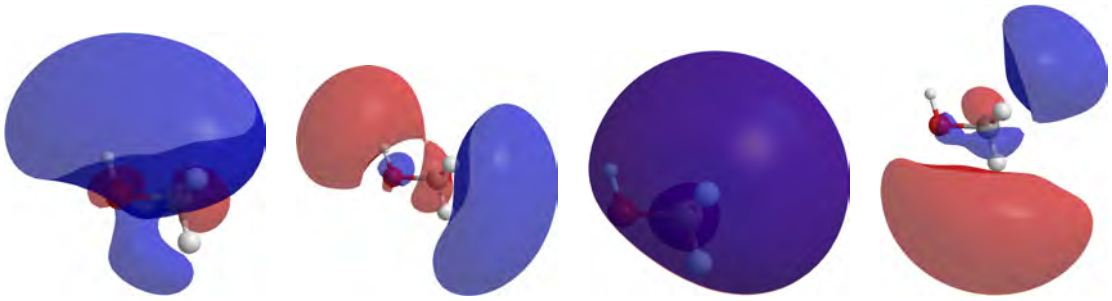

(a) $3s$ (LUMO) (b) $3p_x$ (c) $3p_z$ (d) $3p_y$

Figure 6.4: The lowest four unoccupied MOs of methanol. The axis orientation is the same as in fig. 6.2(a).

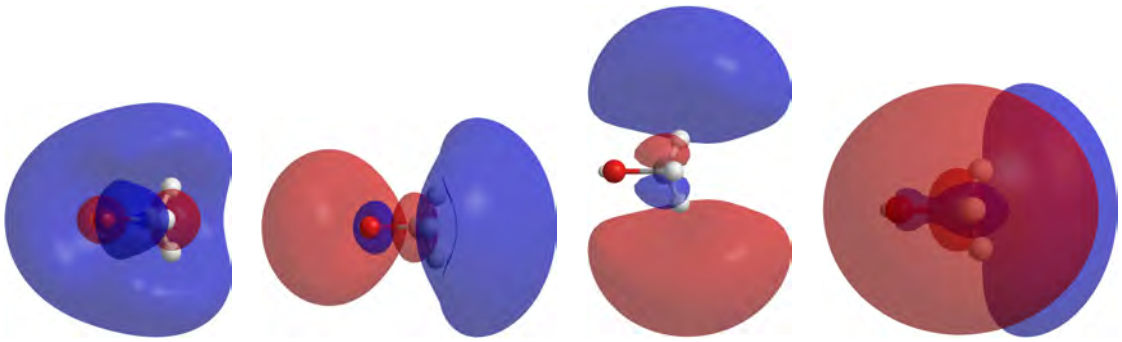

(a) $3s$ (LUMO) (b) $3p_x$ (c) $3p_z$ (d) $3p_y$

Figure 6.5: The same unoccupied MOs of methanol as in fig. 6.4, shown rotated by 90° around the x-axis. The axis orientation is shown in fig. 6.3(a).

The highest occupied molecular orbital (HOMO) is an antibonding combination of the 1st lone pair of the oxygen atom with a pseudo-π MO of the methyl group. It will be labeled as n and it has a'' symmetry. The next occupied MO, in the order of decreasing energy, is the second lone pair of the oxygen atom combined with the other component of the pseudo-π MO of the methyl group. It is labeled as $\bar{n}$, and has a' symmetry. The last MO shown in fig. 6.2 is a σ orbital with a' symmetry.

Table 6.1: Symmetry of the excited states in methanol. The state are of (i, f) type, where i is the initial MO in the rows header and f is the final MO in the column header.

Orbital	$3s$	$3p_x$	$3p_z$	$3p_y$
n	A''	A''	A'	A''
$\bar{n}$	A'	A'	A''	A'

An examination of the unoccupied MOs of methanol reveals that all the MOs shown in fig. 6.4 have some degree of Rydberg character. This is due to the fact that Rydberg orbitals are diffuse and thus the selected basis set for these calculations includes diffuse functions. This aspect will be discussed in more detail in section 6.3.1. The lowest unoccupied MO has $3s$ character. The spherical symmetry is perturbed by the non-spherical core and the outer layer does not entirely enclose the core (the degree to which it encloses it depends on the *iso* value chosen for the rendition), but the tendency of the outer cloud to enclose the core is unmistakable. The symmetry of this orbital is a'. The next highest orbital is clearly $3p_x$-like and it has a' symmetry. Similarly, the following orbital has a $3p_z$ character with a'' symmetry. The last orbital shown in fig. 6.4 is $3p_y$ with a' symmetry.

The symmetry of the MOs plays an important role in determining the symmetry of the states and also which crossings are true and which are avoided. For methanol, the symmetry of the excited states resulting from electron promotion between the MOs shown in figs. 6.2 and 6.4 is presented in table 6.1. In this table the excited states are of (i, f) type, where i is the orbital from where the electron is promoted (the rows header) and f is the orbital where the electron is promoted (the columns header).

6.2 A dramatic difference between the electron-driven dissociation of alcohols and ethers and its relation to Rydberg states

The reprint of the article starts on the next page.

A dramatic difference between the electron-driven dissociation of alcohols and ethers and its relation to Rydberg states

Bogdan C. Ibănescu* and Michael Allan

Received 18th April 2008, Accepted 29th May 2008
First published as an Advance Article on the web 30th June 2008
DOI: 10.1039/b806578k

A difference was observed in the reactivity of alcohols and ethers toward free electrons. Whereas the lowest core-excited state of the negative ion—a $^2(n,3s^2)$ Feshbach resonance—of the alcohols readily dissociates by losing a hydrogen atom, ethers show no observable signal from this resonance. This difference in reactivity has a parallel in the anomalous shapes and energies of the parent states of the Feshbach resonances, the $^1(n,3s)$ Rydberg states of the neutral alcohols. We explained this anomaly using potential surfaces of the alcohols and ethers calculated using the TD-DFT method as a function of the dissociation coordinate. The lowest excited state of alcohols was found to be repulsive, whereas a barrier to dissociation was found in the ethers. Rydberg-valence mixing and avoided crossings are decisive in determining the shapes of the potential surfaces. It is concluded that the reactivities of alcohols and ethers toward free electrons are rationalized by assuming that the potential surfaces of the daughter Feshbach resonances closely follow those of the parent Rydberg states, *i.e.*, the lowest Feshbach resonance is repulsive, but a barrier occurs in ethers. The potential surfaces of both the Rydberg states and the Feshbach resonances thus differ dramatically from the non-dissociative surface of the grandparent $^2(n^{-1})$ positive ions, despite the nominally non-bonding character of the Rydberg electrons.

I. Introduction

Interest in chemical processes induced by free electrons is motivated by emerging applications in technology, for example focused electron beam induced processing (FEBIP),[1] and the need to understand radiation-induced damage to living tissue.[2] An important primary electron-induced process leading to chemical change is dissociative electron attachment (DEA), an example being the dissociation of methanol,

$$e^-(E_i) + CH_3OH \rightarrow \{CH_3OH\}^- \rightarrow CH_3O^- + H$$

where E_i is the energy of the incident electron and the intermediate short-lived anion is called a resonance.

The present paper is concerned with DEA mediated by Feshbach resonances, situated generally between about 5 and 15 eV, where the incident electron causes a Rydberg excitation of the target molecules and is itself temporarily captured in a Rydberg-like orbital. Despite the somewhat exotic electronic structure of these core-excited resonances, they often represent the dominant path for DEA, particularly in saturated compounds.[3,4] They appear to carry their signature even in the electron-induced damage to DNA in condensed phase.[2] Despite the very large body of experimental results on DEA,[5,6] including many bands attributable to Feshbach resonances, virtually nothing is known about the detailed mechanism of the dissociation, in particular in polyatomic molecules. A notable exception is the recent calculation on the small molecule H_2O.[7,8]

Department of Chemistry, University of Fribourg, chemin du Musée 9, Fribourg, CH-1700, Switzerland

In the present work we gain insight into the mechanism of dissociation of the Feshbach resonances in one particular case, that of alcohols and ethers. We first report a striking experimental observation, a difference of fragmentation patterns of the alcohols and the ethers, whereby the lowest Feshbach resonance $^2(n,3s^2)$ yields strong $(M-1)$ signal in the alcohols, but no DEA signal at all in the ethers. We then note that this difference between the properties of the $^2(n,3s^2)$ Feshbach resonances in the ethers and alcohols has an analogy in the spectroscopic properties of the parent $^1(n,3s)$ Rydberg states. Finally, we calculate the potential surfaces of the Rydberg states along the O–H and O–C bond stretching coordinate and show that they explain the Rydberg spectra and also the differences observed in the DEA spectra, under the assumption that the Feshbach resonance surfaces follow those of the parent Rydberg states.

II. Methods

A Experimental

The dissociative electron attachment spectrometer used to measure the yield of mass-selected stable anions as a function of electron energy has been described previously.[4,9,10] It employs a magnetically collimated trochoidal electron monochromator[11] to prepare a beam of quasi-monoenergetic electrons, which is directed into a target chamber filled with a quasi-static sample gas. Fragment anions are extracted at 90° by a three-cylinder lens and directed into a quadrupole mass spectrometer. The energy scale was calibrated on the onset of the O^-/CO_2 signal at 4.0 eV. The electron current was around 200 nA and the resolution about 150 meV. Photoelectron

spectra were recorded with a modified Perkin Elmer PS18 HeI photoelectron spectrometer. Electron energy loss spectrum (EELS) was recorded with a spectrometer using hemispherical electron-energy selectors.[12]

B Calculations

The excited state calculations were performed using the time-dependent density functional theory (TD-DFT) PBE0/6-311++G(3df,3p) model, the geometry optimizations using the DFT B3LYP/6-311+G(2df,2p) model, as implemented in the Gaussian 03 package.[13] This model has been tested and found to satisfactorily reproduce both valence and low-lying Rydberg states of a number of molecules.[14] We confirmed this conclusion, since our calculated transition energies agree well with the experimental values. The calculated results for the 3s and $3p_x$ states of methanol lie 0.12 and 0.36 eV below our experimental values from the electron energy loss spectrum and a similar agreement is obtained for dimethyl and diethyl ethers when compared to the absorption spectra.[15]

Potential curves were obtained by calculating the transition energies over a range of O–H and O–C distances and adding them to the ground state energy calculated with the same model. Only the O–H and O–C distances were varied, the remaining geometrical parameters were not re-optimized (a rigid scan). The energy of the positive ion was calculated using the same model and used to plot the potential curve of the ground electronic state of the cation.

Rydberg states with large spatial extension can be poorly described by TD-DFT.[16] One way to alleviate this problem[16] is to increase the admixture of nonlocal Hartree–Fock (HF) exchange in hybrid functionals to values up to 50% as, *e.g.*, in the BHLYP functional.[16,17] We tested whether this problem effects our conclusions by repeating all calculations using the BHLYP functional, with the same basis set. The energies were calculated about 0.5 eV higher than with the PBE0 model. Since the latter values were slightly lower than the experiment, BHLYP were somewhat higher, but satisfactorily close. The shapes of the potential energy curves were nearly identical with both methods.

Finally, we estimated the increase of the size of the electronic wave function upon excitation as the difference of the electronic spatial extents of a given excited state and the electronic ground state, $\Delta\langle r^2\rangle = \langle r^2\rangle - \langle r_0^2\rangle$. This calculation was done with the CIS model.

III. Results and discussion

Fig. 1 illustrates the well known[20] relation between the grandparent cation, parent Rydberg state and daughter Feshbach resonance, on the example of the argon atom.[21,22] Adding an electron into a Rydberg orbital around a positive ion core releases about 4 eV of energy—the term value. Another about 0.4 eV, the electron affinity of the Rydberg state, is released when a second electron is added to an 3s Rydberg state, leading to a short-lived Feshbach resonance involving two strongly correlated electrons localized on a potential-energy ridge.[23] Both energies are to some degree independent of the molecule because of the weak penetration of the core by the diffuse Rydberg electron cloud, and this fact will be used to

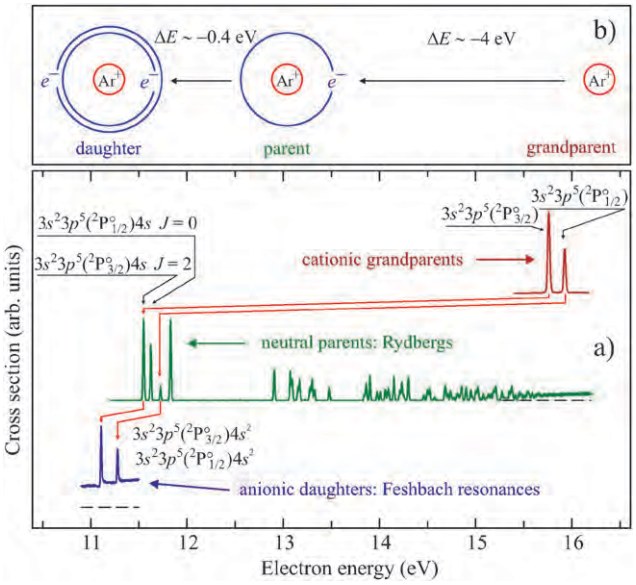

Fig. 1 Figure illustrating the descendancy relations between the grandparent cation, parent Rydberg and Feshbach anion states on the example of Ar. (a) The photoelectron spectrum (top), the electron energy loss spectrum (center), and the elastic cross section[18] (bottom) of argon. (The energy-loss spectrum was recorded at a scattering angle of $\theta = 135°$ and a residual energy of 1 eV, the elastic cross section at $\theta = 117°$.) (b) Schematic diagram of the electron configurations, with the daughter Feshbach resonance having two highly correlated electrons moving in a Rydberg-like orbital.

predict the energies of the Feshbach resonances from ionization energies determined by He–I photoelectron spectra. The method is important in the present case of polyatomic molecules with Feshbach resonances without sharp structures, which can not be detected in elastic cross section or by other means.

A more detailed investigation of many molecules revealed that the 3s term values are not entirely constant for different molecules, but decrease with increasing degree of alkylation, because bulky substituents penetrate even a large Rydberg orbital.[15] As an example, the 3s term value of ethanol is 3.8 eV, and this value decreases with increasing alkylation until it reaches a limiting value of about 2.8 eV for very bulky alkyl substituents.[15] Likewise, the energy relation between the Rydberg states and the Feshbach resonances has been studied in detail for a number of atoms and molecules,[21,24–27] and is not entirely independent of the target.

Even with these limitations, the energy relation between the grandparent and the daughter represents a useful tool for assigning DEA bands to Feshbach resonances, as illustrated in Fig. 2. Ethanol and the two amines represent a series of compounds with gradually decreasing first ionization energy, and DEA bands closely following this trend are observed. They are situated below the 1st photoelectron band, by an amount of energy compatible with the above reasoning, permitting their assignment to the $^2(n,3s^2)$ Feshbach resonances. The observations are not limited to the compounds shown in Fig. 2, but were made in all hydroxyl and amino group containing compounds which we studied.[3,4] The relation permits even to assign the next DEA band to a Feshbach

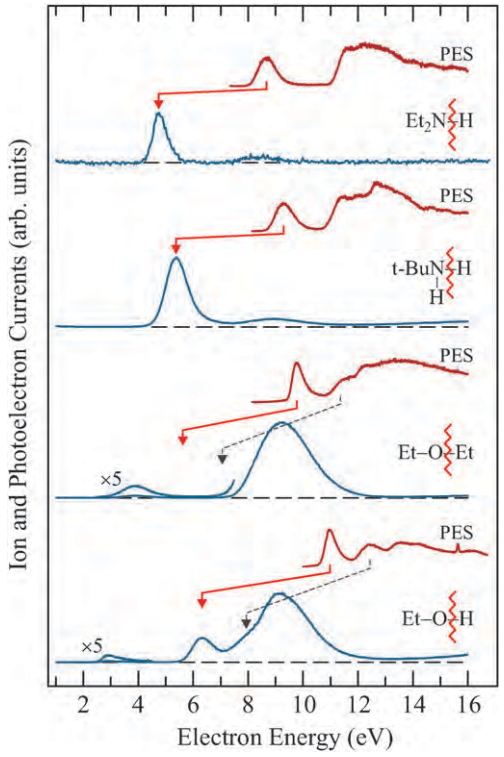

Fig. 2 Photoelectron spectra (PES) and DEA spectra of the compounds indicated. The bonds being broken are indicated in the formulas, the charge remains on the O or N containing fragment. Arrows indicate the relation between the grandparent $^2(n^{-1})$ positive ion states and the daughter $^2(n,3s^2)$ Feshbach resonances, dashed arrows the $^2(\bar{n},3s^2)$ resonances. These two resonances apparently do not dissociate in diethylether, since no bands appear at the arrow positions. (The weak bands at 3 eV in ethanol and 4 eV in diethyl ether are due to shape resonances.[4,19])

resonance associated with the second ionization energy in alcohols, $^2(\bar{n},3s^2)$, as indicated for ethanol by the dashed arrow in Fig. 2. These resonances, belonging to deeper ionizations, were discussed in more detail earlier[3,4] and are not of primary concern in this work.

The main experimental result of the present work is that no DEA bands corresponding to breaking a bond attached to the O atom appear around 5.2 and 7 eV in diethyl ether, where Feshbach resonances are predicted by the analogy with the alcohols and the amines (the continuous and the dashed arrows above the Et–O–Et DEA spectrum in Fig. 2). There is little doubt that the $^2(n,3s^2)$ and the $^2(\bar{n},3s^2)$ Feshbach resonances, with holes in the oxygen lone pair orbitals, occur at these energies.

It is unlikely that the absence of DEA bands from these resonances is due to a very large autodetachment width Γ and, thus, an unfavorable competition between dissociation and autodetachment in the ether. The autodetachment widths of Feshbach resonances are generally narrow, substantially narrower than a typical vibrational spacing, both in atoms (Fig. 1) and in molecules (for example in acetylene[28] or acetaldehyde[29]). The large width of the spectral bands in the present molecules must be due to wide Franck–Condon profiles with many overlapping vibrations or to a repulsive potential surface. We thus expect the Feshbach resonances to have a narrow Γ in both alcohols and ethers.

In this case the absence of $^2(n,3s^2)$ DEA band in the ether must indicate that this resonance is, in contrast to the corresponding resonances in the alcohols and amines, not dissociative. This conclusion is not limited to diethyl ether shown in Fig. 2, but applies to all ethers which we have studied so far, including dibutyl ether.[19]

In search for the explanation of this experimental result we note that a related observation has been made for the parent Rydberg states—it is illustrated for the case of methanol in Fig. 3 (see also ref. 30). Robin analyzed term energies and band shapes in VUV spectra and recognized that in water and the alcohols the lowest $^1(n,3s)$ Rydberg states are anomalous in the sense that they are broad and structureless—whereas they may be expected to be narrow and have a sharp vibrational structure like the corresponding photoelectron bands (this expectation is fulfilled for the higher-lying $^1(n,3p)$ bands in Fig. 3).[15] In contrast, the lowest Rydberg bands in the ethers behave normally—they have a sharp vibrational structure, similar to that of the grandparent ion in the photoelectron spectrum. Robin concluded that the $^1(n,3s)$ Rydberg states are strongly perturbed by the conjugate $^1(n,\sigma^*)$ valence promotions in the alcohols and water, but that this perturbation is not significant in the ethers. It is interesting to note that G. Herzberg already realized in 1931 that in the model compound H_2O the absence of structure indicates that the 3s state is repulsive, in contrary to an initial expectation for a Rydberg state (see the comment by G. Herzberg in the general discussion at the end of ref. 31).

We gain further insight into the causes for this behavior of the Rydberg states by calculating the potential energy curves along the dissociation coordinates. To simplify the calculation and the orbital diagrams, we present the curves for the smaller molecules methanol and methyl ethyl ether instead of ethanol and diethyl ether shown in Fig. 2—this does not affect the argument since the observations appear to apply to all alcohols and ethers. The results are shown in Fig. 4 and 5.

The potential energy curves are compatible with the energy-loss spectrum of Fig. 3 in the sense that the structureless 3s

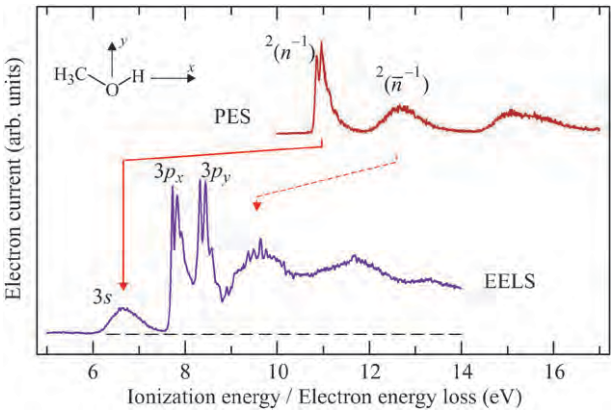

Fig. 3 The photoelectron (top) and the electron energy loss spectrum of methanol (the latter recorded at a scattering angle of 0° and a residual energy of 10 eV).

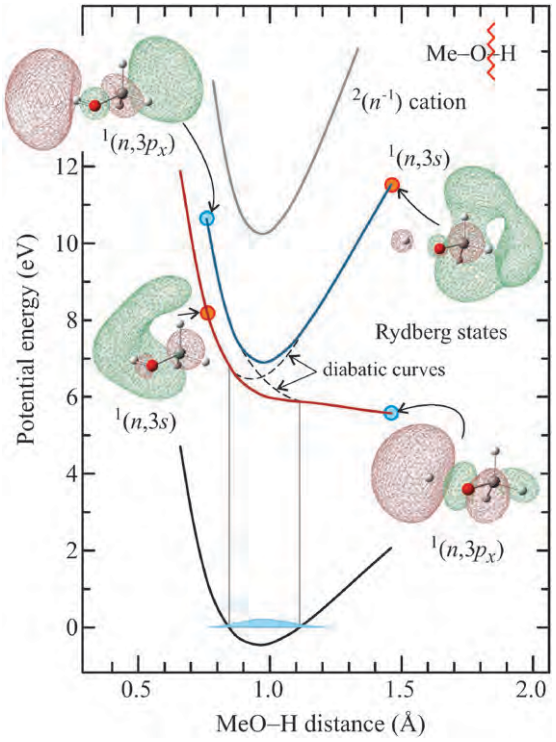

Fig. 4 Potential energy surface of methanol (bottom curve), its two lowest excited states, and the ground state of the cation (top curve), shown as a function of the O–H distance.

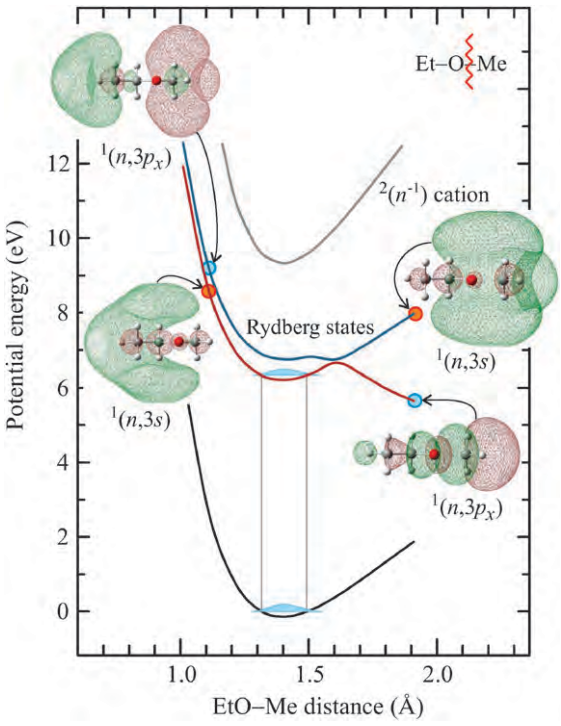

Fig. 5 Same as Fig. 4, but for methyl ethyl ether.

band indicates a dissociative potential whereas the structured $3p_x$ band indicates that the $3p_x$ potential is not dissociative. Calculation of the next excited states, $3p_y$ and $3p_z$, yields potential curves with shapes similar to that of the positive ion (shown at the top of Fig. 4). The $3p_y$ and $3p_z$ curves are not shown in the Figure to improve clarity. The calculated $3p_y$ state explains well the $3p_y$-labeled band in Fig. 3. The $3p_z$ state has an energy only slightly higher than that of the $3p_y$ state and a very low oscillator strength, and is consequently not easily visible in the energy-loss spectrum.

The important difference between the curves of the alcohol in Fig. 4 and the ether in Fig. 5 is that in the latter there is a barrier to dissociation on the lower curve. This explains why the 3s VUV absorption band of ethers does have, in contrast to the alcohols, vibrational structure.[15]

The behavior of these potential energy surfaces follows the same fundamental pattern studied in detail for the $^1(\pi,\sigma^*)$ states of a number of molecules of biological relevance,[32,33] with the difference that the present molecules do not have a π,π^* chromophore. These studies revealed that the $^1(\pi,\sigma^*)$ state can be classified as a 3s Rydberg state that collapses in terms of size upon the stretching of the OH bond (for example in phenol) or the NH bond (for example in pyrrole and indole). This Rydberg-to-valence orbital transformation was reflected by a double-well shape of the $^1(\pi,\sigma^*)$ potential energy function in some molecules.[32,33] A diffuse $^1(\pi,\sigma^*)$ state was also invoked in the photodissociation of the C–O bond in aromatic compounds.[34] Related π^*–σ^* potential energy surfaces were invoked by Barrios *et al.*[35] to interpret the dissociation of a portion of DNA following an attachment of an electron, albeit *via* a shape resonance.

The present curves, particularly for the ether (Fig. 5) are also remarkably similar to those of the $^3\Pi_u$ manifold of O_2.[36] The shapes of the O_2 curves were explained as a consequence of predissociation of the nominally bound Rydberg curves by a strongly repulsive valence curve, that is, a consequence of avoided crossings resulting from Rydberg–valence coupling. This suggests that also in the present case the repulsive nature of the nominally 3s states, the barrier to dissociation in the ether, and the double minimum on the upper state in the ether, can all be understood as a result of avoided crossings.

The excited state orbitals are informative about the nature of the excited state and are shown in Fig. 4 and 5 for two O–H and O–C bond distances, one shorter and one longer than the equilibrium bond length. For both compounds the orbitals of the lower states on the left, at short bond distances, are reminiscent of 3s orbitals. The spherical symmetry is perturbed by the non-spherical core and the outer layer does not entirely enclose the core (the degree to which it encloses it depends on the iso value chosen for the rendition), but the tendency of the outer cloud to enclose the core is unmistakable. The orbitals of the second excited states on the left are clearly $3p_x$-like (see Fig. 3 for the orientation of the coordinates). This ordering corresponds to the spectroscopic assignment of the Rydberg bands in the UV and energy-loss spectra and is also compatible with the values of the quantum defects derived from the experimental energies.[15] They are $\delta = 1.2$ and $\delta = 0.84$ for the 3s states, and $\delta = 0.95$ and $\delta = 0.56$ for the $3p_x$ states, for methanol and diethyl ether, respectively.

The Rydberg nature of the states was further confirmed by the calculated (see section IIB) spatial extent of the electronic wave function, $\Delta\langle r^2\rangle$, which was $17a_0^2$ for the 3s and $33a_0^2$ for the $3p_x$ state in methanol. For the lower state, $\Delta\langle r^2\rangle$ decreased

to about $7a_0^2$ as the O–H bond was stretched, reflecting a Rydberg-valence conversion. In contrast, for the upper, nominally $3p_x$ state, $\Delta\langle r^2\rangle$ remained constant at a value characteristic for a Rydberg state, around $30a_0^2$. For methyl ethyl ether the $\Delta\langle r^2\rangle$ were $30a_0^2$ for the 3s and $41a_0^2$ for the $3p_x$ state. As for the alcohol, the spatial extent of the 3s state decreased to about $10a_0^2$ when the O–Me bond was stretched onto the repulsive section of the potential, beyond the activation barrier (Fig. 5), whereas that of the $3p_x$ state remained above $30a_0^2$.

The nature of the orbitals at large O–H bond lengths, on the right in Fig. 3, appears reversed, the upper orbital resembles more 3s and the lower $3p_x$ (or σ^*). This could be understood as an indication an avoided crossing of the 3s and $3p_x$ states (both have the A'' symmetry), as tentatively indicated in the Figure. Note that the $3p_x$ orbital in methanol has a pronounced node across the O–H bond (Fig. 4)—for this low principal quantum number the nominally Rydberg orbital has a partial σ^* character.

The details of the potential curve of the 2nd excited state of the ether (Fig. 5) are more complicated than in methanol. The $3p_x$ orbital in the ether appears less antibonding across the O–C bond than was the case in methanol across the O–H bond. The potential curve of the 2nd excited state has a shallow double minimum indicative of another avoided crossing with a strongly repulsive σ^* state. (This repulsive state can be followed to higher energies, where avoided crossings with higher-lying A'' Rydberg states—not shown in Fig. 5—appear.) These details of the potential, however, do not affect our main conclusion that the 1st excited state is dissociative in the alcohols, but bound in the ethers.

As a final step of our reasoning we note that the main experimental observation of this paper, namely the fact that the $^2(n,3s^2)$ Feshbach resonance gives rise to a strong DEA signal in the alcohols, but no detectable DEA signal in the ethers, can be explained by assuming that the main features of the Rydberg potential curves shown in Fig. 4 and 5 apply also to the Feshbach resonances. Since the additional electron in a Feshbach resonance is in a diffuse orbital and is only weakly bound, it is not unreasonable to assume that it does not substantially contribute to bonding and consequently does not appreciably change the shape of the potential curves, except for lowering them by about 0.4 eV.

We also calculated the potential curves for the higher-lying Rydberg states, the $A'\ ^1(\bar{n},3s)$ and $^1(\bar{n},3p_x)$ where $\bar{n}$ is the $2p_y$-like a' lone pair orbital on the O atom. The results were similar in terms of the shapes to the curves discussed above, the nominally 3s states being dissociative in the alcohol and not dissociative in the ether. These results are in line with the observation of a DEA band assigned as $^2(\bar{n},3s^2)$ in the alcohols and its absence in the ethers (see Fig. 2).

IV. Conclusions

The present work reveals a qualitative difference in the dissociation patterns of Feshbach resonances in alcohols and in ethers. Whereas the O–H bond cleavage in alcohols already proceeds from the lowest Feshbach resonance (with a hole in the oxygen lone pair orbital), the C–O bond cleavage in ethers proceeds only from the higher-lying Feshbach resonances with holes in the σ_{C-C} and σ_{C-H} orbitals. From this observation we conclude that the lowest Feshbach resonance, $^2(n,3s^2)$, is dissociative in the alcohols, but bound in the ethers.

We further point out the spectral evidence that the same behavior is found for the parent states of these Feshbach resonances, the $^1(n,3s)$ Rydberg states.

We then calculated the potential curves for the Rydberg states along the dissociation coordinate and found that they explain the observed spectral properties, a broad structureless band in the alcohols, and a band with vibrational structure in the ethers. Finally we conclude that, under the assumption that an additional electron in a diffuse orbital does not appreciably change the shape of the potential curves, these potential curves also explain the observations for DEA to these molecules.

These calculations provide an insight into a situation which is *a priori* surprising. A simple view of the Rydberg electron is that it is in a spatially large, diffuse cloud, does not penetrate the positive ion core, and does not contribute to chemical binding. This view would result in an expectation that the potential surfaces of the $^2(n,3s^2)$ Feshbach resonances follow those of the $^2(n^{-1})$ positive ion core, which are not dissociative. No DEA signal would thus be expected from the $^2(n,3s^2)$ Feshbach resonances. Our study suggests that a σ^* orbital, which has, in terms of its nodal structure, partially a $3p_x$ character, is responsible for the dissociative behavior. An avoided crossing has then the consequence that it is the nominally $^2(n,3s^2)$ Feshbach resonance which is predissociated by the repulsive state, explaining the DEA signal. The difference between the alcohols and the ethers is the absence or presence of an energy barrier on the lower state potential energy surface.

Although not discussed in detail in this work, similar behavior was found also for higher excited states and Feshbach resonances, with occupation of the same 3s, $3p_x$ and σ^* orbitals, but a hole in the next deeper lying orbital $\bar{n}$ (essentially a $2p_y$ orbital, with a considerable σ_{C-O} character).

The principal finding of this work, the dissociative nature of Feshbach resonance centered on a hydroxyl oxygen and nondissociative nature of Feshbach resonance centered on a ether oxygen, is preserved even in compounds having hydroxyl and ether oxygens in one molecule. Based on photoelectron spectra, two distinct Feshbach resonances, $^2(n_{ether},3s^2)$ at lower energy and $^2(n_{OH},3s^2)$ at higher energy, were identified in tetrahydrofuran-3-ol and (tetrahydrofuran-2-yl)methanol, but only the hydroxyl-centered $^2(n_{OH},3s^2)$ Feshbach resonance resulted in DEA signal.[4]

As an outlook, it would be interesting to calculate directly the potential curves of the Feshbach resonances using a scattering calculation such as the R-matrix theory yielding both their energy and the autodetachment width.

Acknowledgements

We thank to Olivier May for assistance in recording the photoelectron spectra and acknowledge helpful discussions with W. Domcke, H. Hotop and S. Grimme. This research

is part of project No. 200020-113599/1 of the Swiss National Science Foundation.

References

1 I. Utke, V. Friedli, M. Purrucker and J. Michler, *J. Vac. Sci. Technol., B*, 2007, **25**(6), 2219.
2 B. Boudaiffa, P. Cloutier, D. Hunting, M. A. Huels and L. Sanche, *Science*, 2000, **287**, 1658.
3 T. Skalický and M. Allan, *J. Phys. B*, 2004, **37**, 4849.
4 B. C. Ibănescu, O. May, A. Monney and M. Allan, *Phys. Chem. Chem. Phys.*, 2007, **9**, 3163.
5 L. G. Christophorou, D. L. McCorkle and A. A. Christodoulides, in *Electron–Molecule Interactions and their Applications*, ed. L. G. Christophorou, Academic Press, Orlando, 1984, vol. 1, p. 477.
6 E. Illenberger and J. Momigny, *Gaseous Molecular Ions*, Steinkopff Verlag, Darmstadt and Springer Verlag, New York, 1992.
7 D. J. Haxton, T. N. Rescigno and C. W. McCurdy, *Phys. Rev. A*, 2007, **75**, 012711.
8 D. J. Haxton, T. N. Rescigno and C. W. McCurdy, *Phys. Rev. A*, 2007, **76**, 049907 (erratum).
9 M. Stepanović, Y. Pariat and M. Allan, *J. Chem. Phys.*, 1999, **110**, 11376.
10 R. Dressler and M. Allan, *Chem. Phys.*, 1985, **92**, 449.
11 A. Stamatovic and G. J. Schulz, *Rev. Sci. Instrum.*, 1968, **39** 1752.
12 M. Allan, *J. Phys. B*, 1992, **25**, 1559.
13 M. J. Frisch, G. W. Trucks, H. B. Schlegel, G. E. Scuseria, M. A. Robb, J. R. Cheeseman, J. A. Montgomery, Jr., T. Vreven, K. N. Kudin, J. C. Burant, J. M. Millam, S. S. Iyengar, J. Tomasi, V. Barone, B. Mennucci, M. Cossi, G. Scalmani, N. Rega, G. A. Petersson, H. Nakatsuji, M. Hada, M. Ehara, K. Toyota, R. Fukuda, J. Hasegawa, M. Ishida, T. Nakajima, Y. Honda, O. Kitao, H. Nakai, M. Klene, X. Li, J. E. Knox, H. P. Hratchian, J. B. Cross, V. Bakken, C. Adamo, J. Jaramillo, R. Gomperts, R. E. Stratmann, O. Yazyev, A. J. Austin, R. Cammi, C. Pomelli, J. Ochterski, P. Y. Ayala, K. Morokuma, G. A. Voth, P. Salvador, J. J. Dannenberg, V. G. Zakrzewski, S. Dapprich, A. D. Daniels, M. C. Strain, O. Farkas, D. K. Malick, A. D. Rabuck, K. Raghavachari, J. B. Foresman, J. V. Ortiz, Q. Cui, A. G. Baboul, S. Clifford, J. Cioslowski, B. B. Stefanov, G. Liu, A. Liashenko, P. Piskorz, I. Komaromi, R. L. Martin, D. J. Fox, T. Keith, M. A. Al-Laham, C. Y. Peng, A. Nanayakkara, M. Challacombe, P. M. W. Gill, B. G. Johnson, W. Chen, M. W. Wong, C. Gonzalez and J. A. Pople, *GAUSSIAN 03 (Revision C.01)*, Gaussian, Inc., Wallingford, CT, 2004.
14 I. Cioffini and C. Adamo, *J. Chem. Phys.*, 2007, **111**, 5549.
15 M. B. Robin, *Higher Excited States of Polyatomic Molecules*, Academic Press, New York, vol. 1, 1974.
16 S. Grimme and F. Neeseb, *J. Chem. Phys.*, 2007, **127** 154116.
17 A. D. Becke, *J. Chem. Phys.*, 1993, **98**, 1372.
18 K. Franz, T. H. Hoffmann, J. Bömmels, A. Gopalan, G. Sauter, W. Meyer, M. Allan, M.-W. Ruf and H. Hotop, *Phys. Rev. A*, 2008, in preparation.
19 B. C. Ibănescu, O. May and M. Allan, *Phys. Chem. Chem. Phys.*, 2008, **10**, 1507.
20 G. J. Schulz, *Rev. Mod. Phys.*, 1973, **45**, 423.
21 L. Sanche and G. J. Schulz, *Phys. Rev. A*, 1972, **5**, 1672.
22 D. Spence, *Phys. Rev. A*, 1977, **15**, 883.
23 U. Fano and A. R. P. Rau, *Comments At. Mol. Phys.*, 1985, **16**, 241.
24 L. Sanche and G. J. Schulz, *Phys. Rev. A*, 1972, **6**, 69.
25 L. Sanche and G. J. Schulz, *J. Chem. Phys.*, 1973, **58**, 479.
26 D. Spence, *J. Phys. B*, 1975, **12**, 721.
27 D. Spence, *J. Chem. Phys.*, 1977, **66**, 669.
28 R. Dressler and M. Allan, *J. Chem. Phys.*, 1987, **87**, 4510.
29 R. Dressler and M. Allan, *J. Electron Spectrosc. Relat. Phenom.*, 1986, **41**, 275.
30 M. B. Robin and N. A. Kuebler, *J. Electron Spectrosc. Relat. Phenom.*, 1972, **1**, 13.
31 C. F. Goodeve and N. O. Stein, *Trans. Faraday Soc.*, 1931, **21**, 393.
32 A. L. Sobolewski, W. Domcke, C. Dedonder-Lardeux and C. Jouvet, *Phys. Chem. Chem. Phys.*, 2002, **4**, 1093.
33 A. L. Sobolewski and W. Domcke, *J. Phys. Chem. A*, 2007, **111**, 11725.
34 S. Grimme, *Chem. Phys.*, 1992, **163**, 313.
35 R. Barrios, P. Skurski and J. Simons, *J. Phys. Chem. B*, **106**(33), 7991.
36 B. R. Lewis, J. P. England, S. T. Gibson, M. J. Brunger and M. Allan, *Phys. Rev. A*, 2001, **63**, 022707.

6.3 Excited States of Alcohols and Ethers

6.3.1 Choice of the level of theory

The potential energy surfaces of excited states were calculated using the time-dependent density functional theory (TD-DFT) as implemented in Gaussian 03 package [47]. TD-DFT offers two parameters for the control of the theory level: the basis-set and the functional used by the DFT. Consequently it is necessary to study how these two parameters affect the potential energy surfaces.

6.3.1.1 Basis-set effects on the excited states of methanol

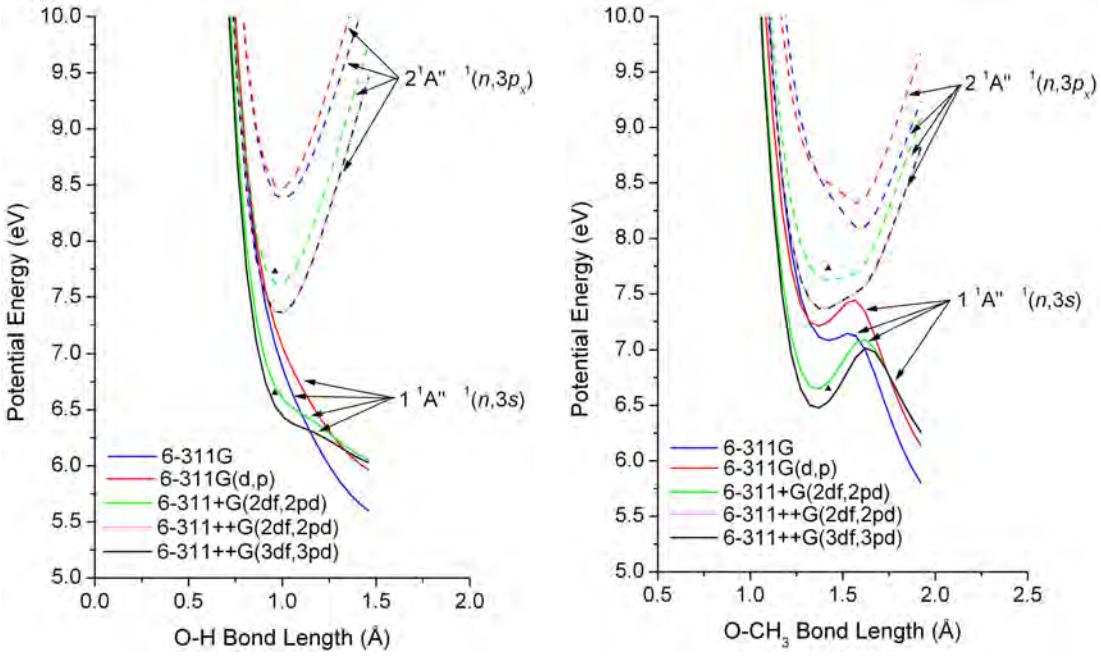

(a) For the O−H Stretch (b) For the O−C Stretch

Figure 6.6: Variation of the potential curves for the lowest two A'' singlet excited states of methanol calculated with different basis-sets (solid line: the potential curves corresponding to the 1 $^1A''$ $^1(n, 3s)$ state; dashed line: the potential curves for the 2 $^1A''$ $^1(n, 3p_x)$). The experimental vertical transition energies are represented by triangles, the lower one for the 1 $^1A''$ $^1(n, 3s)$ state and the upper one for the 2 $^1A''$ $^1(n, 3p_x)$ state. The results for the 6−311++G(2df,2pd) and 6−311++G(3df,3pd) basis-set are nearly identical and the corresponding lines overlap, –only those for 6−311++G(3df,3pd) are visible. Calculations were performed using the PBE0 functional.

Only Pople-type basis-sets have been selected for the test. These basis-sets belong to the category of split-valence basis-sets together with correlation consistent basis sets. The usual notation for Pople-type basis-sets is *X-YZWg*. In this case *X*

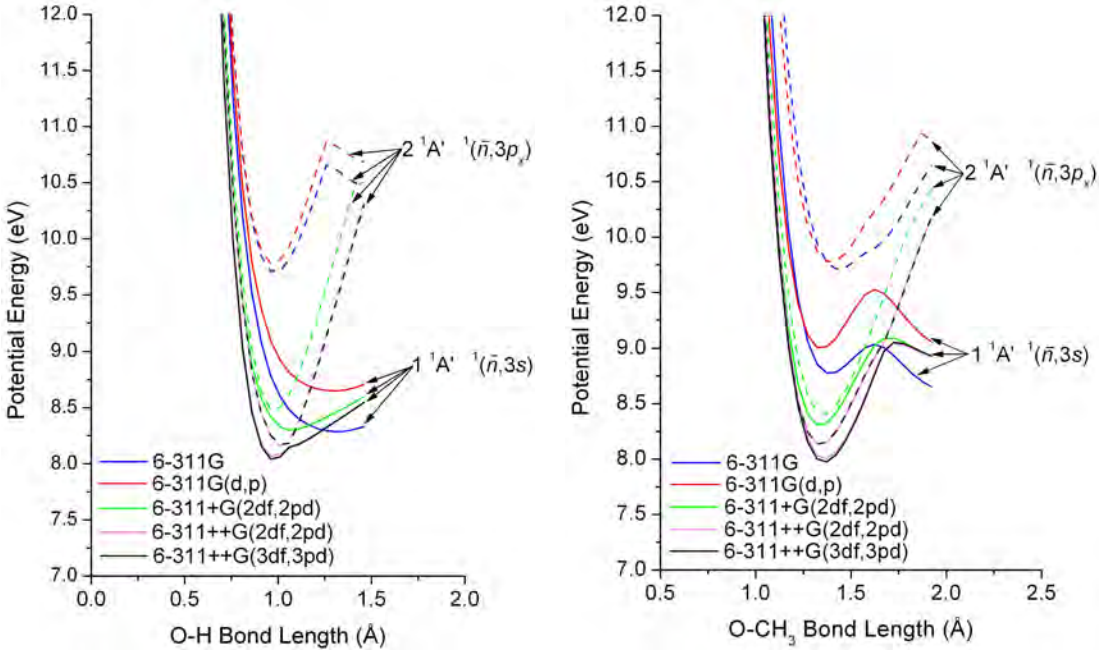

(a) For the O−H Stretch

(b) For the O−C Stretch

Figure 6.7: Same as Fig. 6.6 but for the lowest two A' singlet excited states of methanol

represents the number of primitive Gaussians comprising each core atomic orbital basis function. The Y, Z and W indicate that the valence orbitals are composed of three basis functions each, the first one composed of a linear combination of Y primitive Gaussian functions, the second and the third being also composed of a linear combination of Z and of W primitive Gaussian functions respectively. The plus sign indicate the presence of diffuse functions, while the polarization functions are specified in parenthesis. The selected basis sets are: 6−311G, 6−311G(d,p), 6−311+G(2df,2pd), 6−311++G(2df,2pd), 6−311++G(3df,3pd). The results are presented in fig. 6.6 for the A'' excited states and in fig. 6.7 for the A' excited states. A discussion about the shape of the potential curve for the O−C stretch is presented later in the chapter in section 6.3.2.

Robin has analyzed the VUV spectra of alcohols [61] and concluded that the first excited states have a Rydberg character. Consequently it is expected that diffuse functions are required to properly describe the excited states of alcohols. Also increasing the number of Gaussian functions included in the basis-set should improve the results.

Several trends can be observed in figs. 6.6 and 6.7. All basis-sets yield the same qualitative conclusions for the A'' excited states. In all cases the $^1(n, 3s)$ state is dissociative as the O−H bond length is increased, and it shows an activation barrier as the O−C bond is elongated. It is in the details of the potential curves for the first two excited state where the differences between the basis-sets can be observed.

As expected, the 6−311G basis-set leads to potential curves with vertical tran-

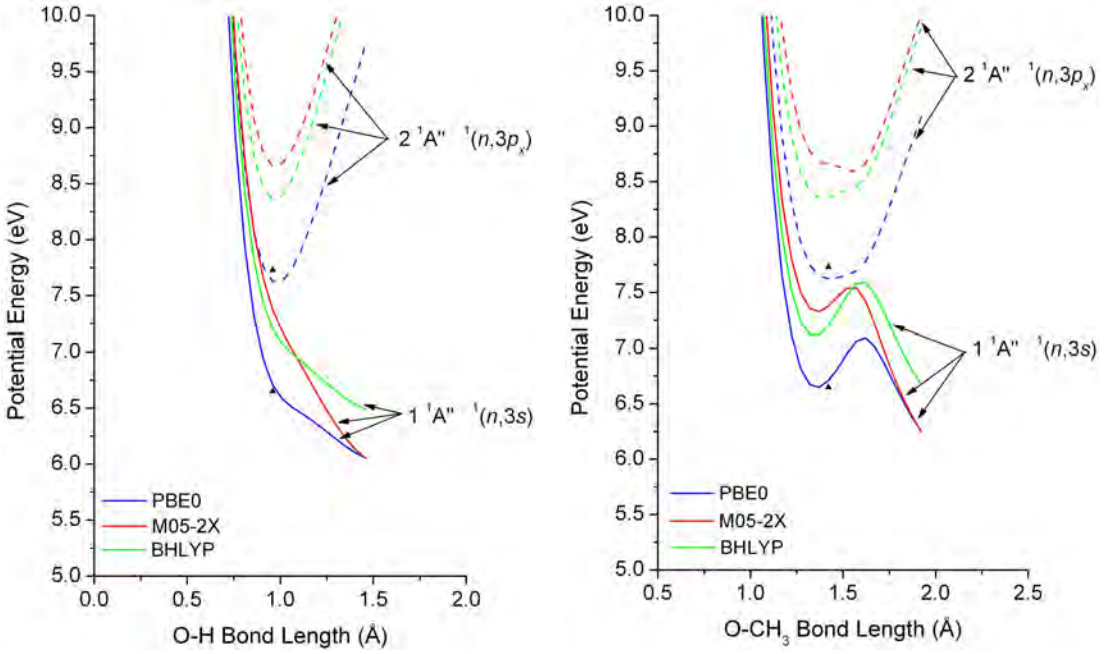

(a) For the O−H Stretch

(b) For the O−C Stretch

Figure 6.8: Variation of the potential curves for the lowest two A'' singlet excited states of methanol calculated with different functionals (solid line: the potential curves corresponding to the 1 $^1A''$ $^1(n, 3s)$ state; dashed line: the potential curves for the 2 $^1A''$ $^1(n, 3p_x)$). The experimental vertical transition energies are represented by triangles, the lower one for the 1 $^1A''$ $^1(n, 3s)$ state and the upper one for the 2 $^1A''$ $^1(n, 3p_x)$ state. Calculations were performed using the 6−311+G(2df,2pd) basis-set.

sition energies at equilibrium geometry that are high above the experimental values, since it does not include any diffuse or polarization functions. Surprisingly, the inclusion of some polarization function (the 6−311G(d,p) basis-set) into the basis-set increases the energy of the potential curves. When diffuse functions are added to the basis-set (a change from the red curve to the green curve in figs. 6.6 and 6.7) the vertical transition energies start to approach the experimental values and the results obtained with the 6−311+G(2df,2pd) basis-set are the closest, being only 0.05 eV and 0.11 eV higher than the experimental transition energies. The inclusion of additional diffuse function (the 6−311++G(2df,2pd) basis-set) lowers the energies of the excited states only slightly, and additional polarization functions (the 6−311++G(3df,3pd) basis-set) do not change the shape nor the position of the excited states.

The height of the activation barrier observed at elongated O−C bond distances is also affected by the size of the basis-set. The observed trend indicates that the bigger the basis-set the higher the activation barrier is for $^1(n, 3s)$ and $^1(\bar{n}, 3s)$ states.

Since the excited states of methanol have a pronounced Rydberg character [61] it is not surprising that the inclusion of diffuse functions has the biggest influence

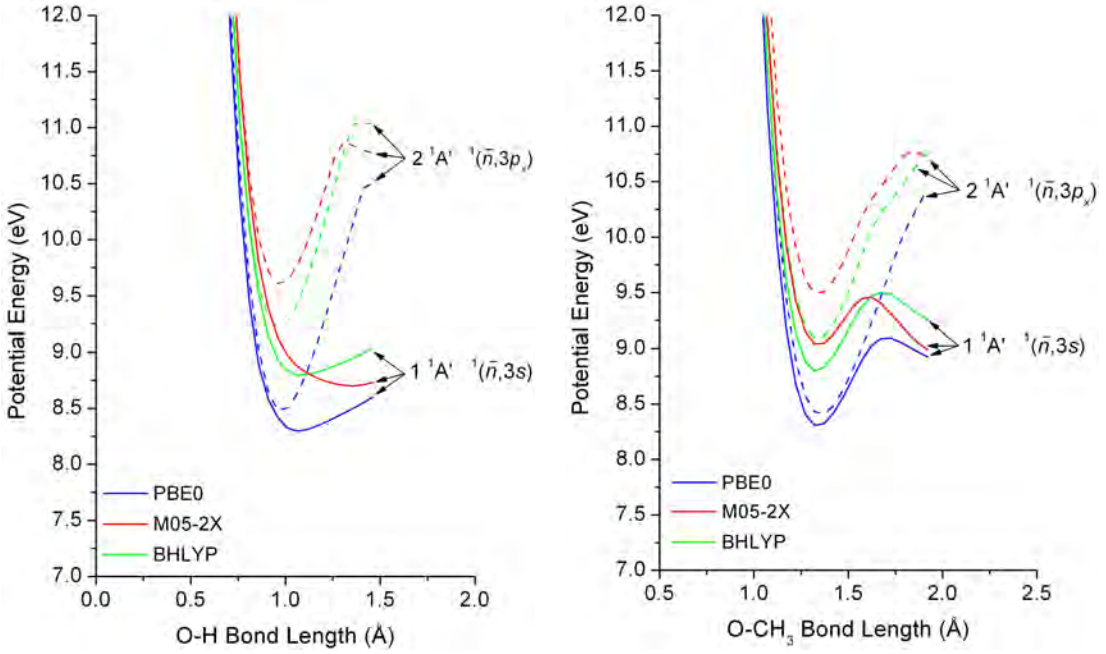

(a) For the O−H Stretch (b) For the O−C Stretch

Figure 6.9: Same as Fig. 6.8 but for the lowest two A' singlet excited states of methanol.

on the description of the states. The inclusion of polarization functions in the basis set has a lesser impact than diffuse functions. Additionally, it is not necessary to include more that 2 sets of d functions, one set of f function on the heavy atoms and 2 sets of p functions and one set of d function on the hydrogen atoms.

6.3.1.2 Influence of the functional on the excited states of methanol

TD-DFT can poorly describe excited states with large spatial extension [62]. A possible correction is to increase the amount of Hartee-Fock (HF) exchange included in the functional. We tested how are potential curves for the excited states affected by this problem and the results are presented in fig. 6.8 for the A'' excited states and in fig. 6.9 for the A' excited states. Three functionals have been selected: PBE0 [63] (with 25% HF exchange), BHLYP [64, 65] (with 50% HF exchange) and MO5-2X [66] (with 57% HF exchange).

An examination of the results for the selected excited states reveals that the choice of functional has a small effect on the shape of the potential curves. The main difference between the potential curve of the $^1(n, 3s)$ state as a function of the O−H bond distance and as a function of the O−C bond distance, namely the presence of an activation barrier in the latter case and the lack of any barrier in the first case, remains the same regardless of the functional. However, the position of the potential curves and the height of the activation barrier are influenced by the choice of the functional.

PBE0 functional gives, for the present case, the energetically lowest excited states and also the vertical transition energies of these states are the closest to the experimental values. The potential curves obtained with the BHLYP functional have the same shape as those obtained with the PBE0 functional but are at higher energies. MO5-2X is a highly parametrized functional and the potential curves obtained with this functional are worse then BHLYP in terms of vertical transition energy. They also have different shape than those obtained with the previous functional indicative of the increased degree of parametrization.

6.3.1.3 Selection of the theory level

When choosing the basis-set for the calculations a good strategy is to use the biggest basis-set from a given family since it incorporates the smaller ones and the algorithm has the possibility to include or to exclude certain functions. This is the strategy that has been chosen in ref. [37]. The convergence of the models shown in figs. 6.6 and 6.7 supports this strategy. When computer time becomes a factor, then a certain compromise needs to be reached between the size of the basis-set and the accuracy of the results. This is the strategy that has been chosen for the generation of the two dimensional potential energy surfaces of the excited states in this chapter. Consequently, the 6−311+G(2df,2pd) basis-set has been selected since it offers an optimal balance between the CPU time and the accuracy of the results.

The selection of the functional is a straightforward procedure. PBE0 has been selected due to several reason. First of all, the vertical transition energies obtained with this functional agree best with the experimental values. Secondly, it has been tested in the literature (ref. [63] and all references therein) and found to give reasonable accuracy. The importance of the major objection, the wrong asymptotic behavior of the potential, has been tested by the BHLYP calculations and it was found that the shape of the curve is not particularly sensitive to this problem.

Of course there are better basis-sets and better functionals (M06 class of functionals are likely candidates) in the literature but PBE0 appears suitable for the purpose of the calculations presented in this chapter, to offer insight on how the Rydberg states can be used to qualitatively explain the DEA results, and an extensive test of the functionals was not aimed at.

Other methods have also been tested: single-excitation CI (CIS) method [67] and the related CIS(D) method [68]. The shape of the potential curves for the excited states obtained with these methods is similar to that obtained with the other methods, increasing the confidence in the selected model. But the energies of the excited states are dramatically higher (more than 2 eV) than those obtained with the DFT method described above.

However, the CIS method offers the possibility to calculate the electronic spatial extent ($\langle R^2 \rangle$). The $\langle R^2 \rangle$ gives informations concerning the size of the molecular volume, indicative of Rydberg/valence character. The results concerning the $\langle R^2 \rangle$ are presented in section 6.3.2.2 and 6.3.3.2.

6.3.2 Potential Energy Surfaces of Alcohols

This sections presents the potential surfaces for the excited states of alcohols. The main results are published in ref. [37], reprinted in section 6.2. Additional results concern the two dimensional potential surfaces of $^1(n, 3s)$ and $^1(n.3p_x)$ states as a function of the O−H and O−C bond distances, and potential curves as a function of the C−O−H angle. The conclusions are extended to higher alkyl alcohols (ethanol and 1-propanol) and subsequently to all alcohols.

6.3.2.1 Methanol

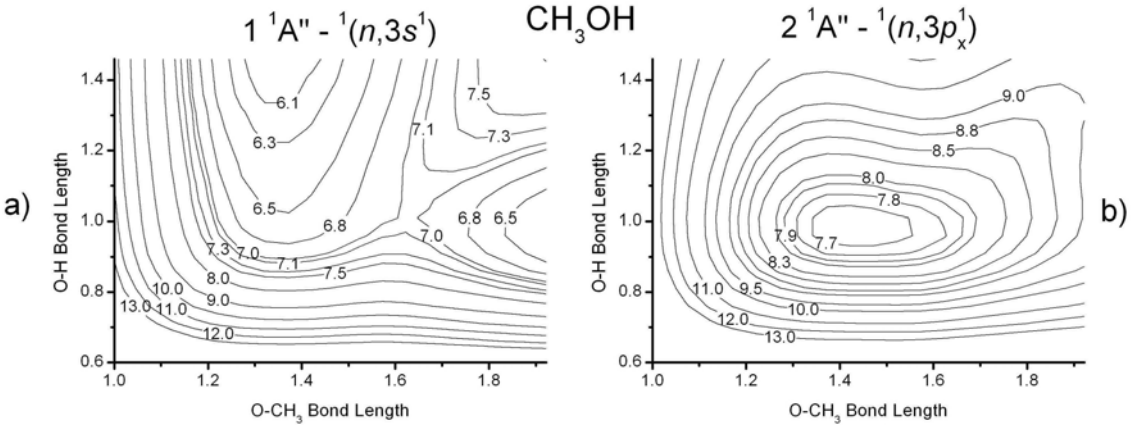

Figure 6.10: Contour plots of selected excited states for methanol. The contour values are in eV (the intervals between the contour lines are smaller around the minimum and higher in the steep sections). a) $^1(n, 3s)$ excited state; b) $^1(n, 3p_x)$ excited state.

A deeper understanding is provided by the potential surfaces in function of both O−H and O−C bond lengths. Fig. 6.10 shows the contour plots for two dimensional potential energy surfaces of the first two excited states for methanol.

While the $^1(n, 3s)$ potential surface is repulsive along the O−H stretch, a barrier to dissociation on the potential energy surface of the $^1(n, 3s)$ excited state is encountered along the O−C coordinate. The $^1(n, 3p_x)$ has a shape similar to that of the positive ion. The shape of the surfaces along the O−C stretch in methanol is similar to that of the O−C bond in ethers [37], but there are some differences between the two cases. While in ethers the $^1(n, 3p_x)$ state presented a shallow double minimum (see fig. 5 in ref. [37]), indicative of the presence of two avoided crossings between the two excited states and an additional repulsive σ^*, following the general shown in fig. 6.1(c), in methanol a plateau has been identified. The plateau is stretched more along the O−C coordinate. Similar to ethylmethylether, we suggest that the plateau is an indication for the presence of an additional avoided crossing. There is no reason why the second avoided crossing with a repulsive σ^* state should be missing from methanol since the two bonds are so similar. We conclude that in methanol the double minimum is very shallow, such as to become a plateau.

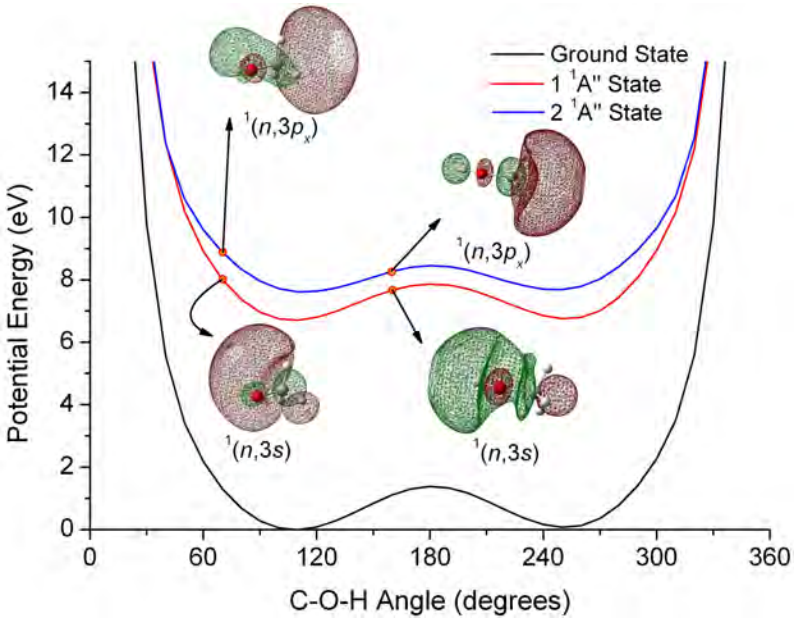

Figure 6.11: Potential energy surface of the ground state of methanol (bottom curve, in black) and the two lowest A'' singlet excited states shown as a function of the C−O−H angle.

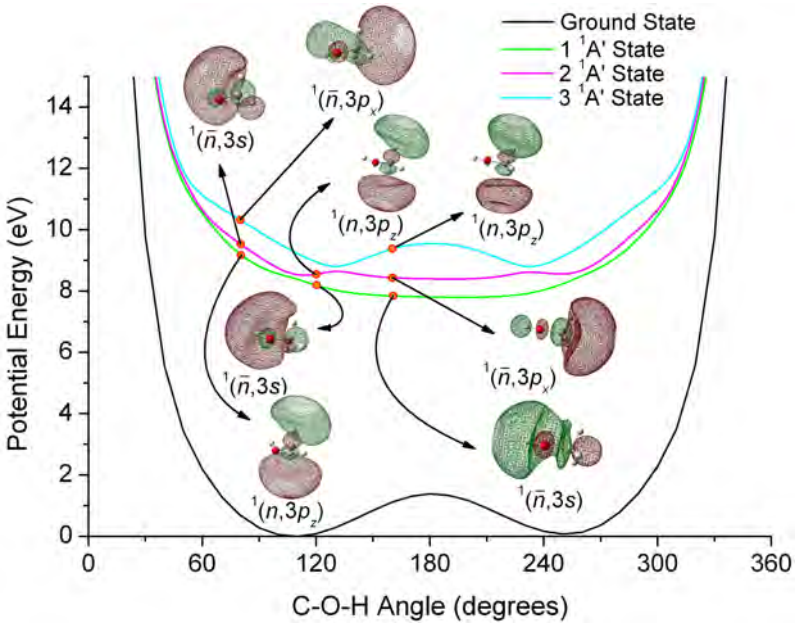

Figure 6.12: Same as fig. 6.11 but for the three lowest A' singlet excited states.

The presence of a barrier along the O−C coordinate in fig. 6.10 explains one more experimental observation. Dissociation in methanol proceeds also through the O−C bond breaking, with the generation of the OH^- anion. The first OH^- band is observed at 10.7 eV and the bands corresponding to the $^2(n, 3s^2)$ and $^2(\bar{n}, 3s^2)$ res-

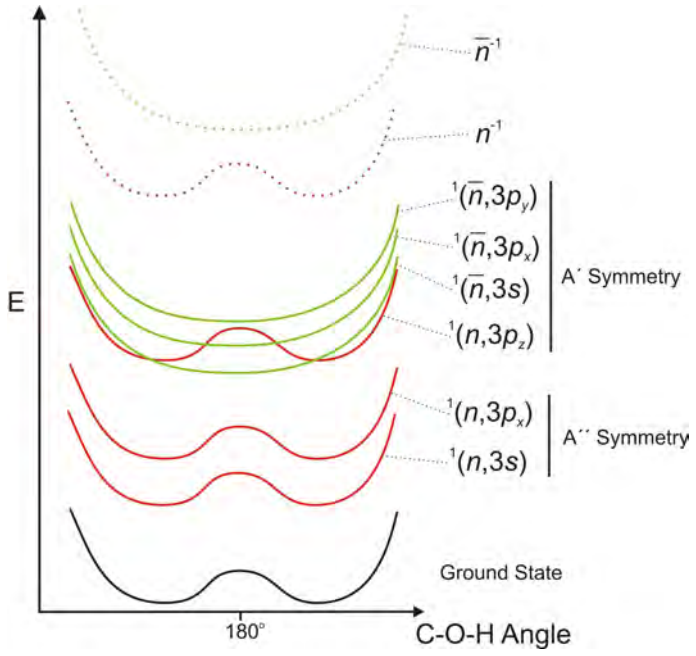

Figure 6.13: General diagram for the diabatic states of methanol as a function of the C−O−H angle. The ground state is shown in black, the $^2(n^{-1}$ and $^2(\bar{n}^{-1})$ states of the ion are shown in dashed red and green, respectively. The Rydberg states converging to the $^2(n^{-1}$ limit are shown in red, those converging to $^2(\bar{n}^{-1})$ green.

onances are missing [57, 22, 32]. It is similar to the observation that has been made between dissociation of the O−H bond in alcohols and dissociation of the O−C bond in ethers (section 6.2). In that case an activation barrier on the $^2(n, 3s^2)$ potential surface along the O−C coordinate has been suggested to explain the experimental differences. In the same way, we conclude that the presence of an activation barrier along the O−C stretch in methanol could explain why the first two Feshbach resonances do not lead to any observable OH^- signal.

Fig. 6.11 shows the energies of the lowest two Rydberg states as a function of the angle between the two oxygen bonds. The potential curves for the $^1(n, 3s)$ and $^1(n, 3p_x)$ states have a shape similar to that of the potential curve of the ground state, they are bent. This is the result of the lack of overlap of the n orbital with the other atomic orbitals and thus it does not contribute to the bonding. It is an indication that the least energy path on the entire surface involves changing the O−H or O−C bond lengths but does not involve changing the C−O−H angle. Thus it was justified to keep the angle at the value from the equilibrium geometry when performing the rigid scan to obtain the two dimensional surfaces from fig. 6.10.

Fig. 6.12 shows the lowest three A' Rydberg states as a function of the C−O−H angle. It shows the presence of several avoided crossings. They suggest that, in contrast to the A'' manifold, for the A' manifold the least energy path also involves changing the C−O−H angle. Consequently, the study of the potential surfaces of the A' states required the inclusion of the angle into the scan.

There is a phenomenon in the A' manifold which is absent in the A'' manifold. This difference between the two manifold is represented schematically in fig. 6.13. In the A'' manifold, the avoided crossings are only between states converging to the same ionization limit $^2(n^{-1})$. But, in the A' manifold, the avoided crossing can take place between states converging to two different states of the ion. One is converging to the $^2(\bar{n}^{-1})$ ionization limit (with A' final MO, see figs. 6.4 and 6.5 for the unoccupied MOs of methanol). The other one is converging to the $^2(n^{-1})$ ionization limit (with A'' final MO). Thus, we have avoided crossings between states with configurations with a completely different orbital occupation. This means that the exchange term between these states is expected bo be very small, resulting in avoided crossing that are very close to true crossings.

The $^2(n^{-1})$ state of the cation is bent since the n MO of the methanol is localized on the oxygen atom and is perpendicular to the molecular plane. Consequently it does not contribute to bonding. But the $^2(\bar{n}^{-1})$ state of the cation is linear since the $\bar{n}$ MO contributes to bonding. Thus the diabatic Rydberg states that converge to the $^2(n^{-1})$ ionization limit are bent, while those converging to the $^2(\bar{n}^{-1})$ ionization limit are linear. Consequently, there is a dramatic change in the geometry of the molecule between Rydberg states converging to the $^2(n^{-1})$ limit and those converging to the $^2(\bar{n}^{-1})$ limit around the avoided crossing point, indicating small exchange terms between diabatic Rydberg states of different symmetry.

6.3.2.2 Spatial extent of the excited states in methanol

The Rydberg nature of the excited states of methanol is also confirmed by the electronic spatial extent of the electronic wave function ($\langle R^2 \rangle$). $\langle R^2 \rangle$ is a single number that is computed as the expectation value of electron density times the distance from the center of mass [69]:

$$\langle R^2 \rangle = \int_0^\infty R^2 \cdot \rho(\vec{r}) d\vec{r} \tag{6.5}$$

where $\vec{r}$ is the coordinate vector (x, y, z), $R = |\vec{r}|$ and $\rho(\vec{r})$ is the electron density

$\langle R^2 \rangle$ gives information about the molecular volume. For our purposes, it is more important to compare the electronic spatial extent of a given excited state to the electronic spatial extent of the ground state. We calculate the difference between the two values:

$$\Delta\langle R^2 \rangle = \langle R^2 \rangle_{excited\ state} - \langle R^2 \rangle_{ground\ state} \tag{6.6}$$

$\Delta\langle R^2 \rangle$ gives information about how diffuse a given excited states is compared to the ground state. Rydberg states are known to be diffuse states and thus have high $\Delta\langle R^2 \rangle$ values (around 30-100 a_0^2 for $n = 3$) [70]. Valence states are more compact than Rydberg states and their spatial extent is similar to the spatial extent of the ground state. Consequently, they have low $\Delta\langle R^2 \rangle$ values (around 3-10 a_0^2) [70].

Fig. 6.14 shows the variation of the $\Delta\langle R^2 \rangle$ as a function of O−H bond distance for the $^1(n, 3s)$, $^1(n, 3p_x)$, $^1(\bar{n}, 3s)$, $^1(\bar{n}, 3p_x)$ excited states for methanol. The $\Delta\langle R^2 \rangle$

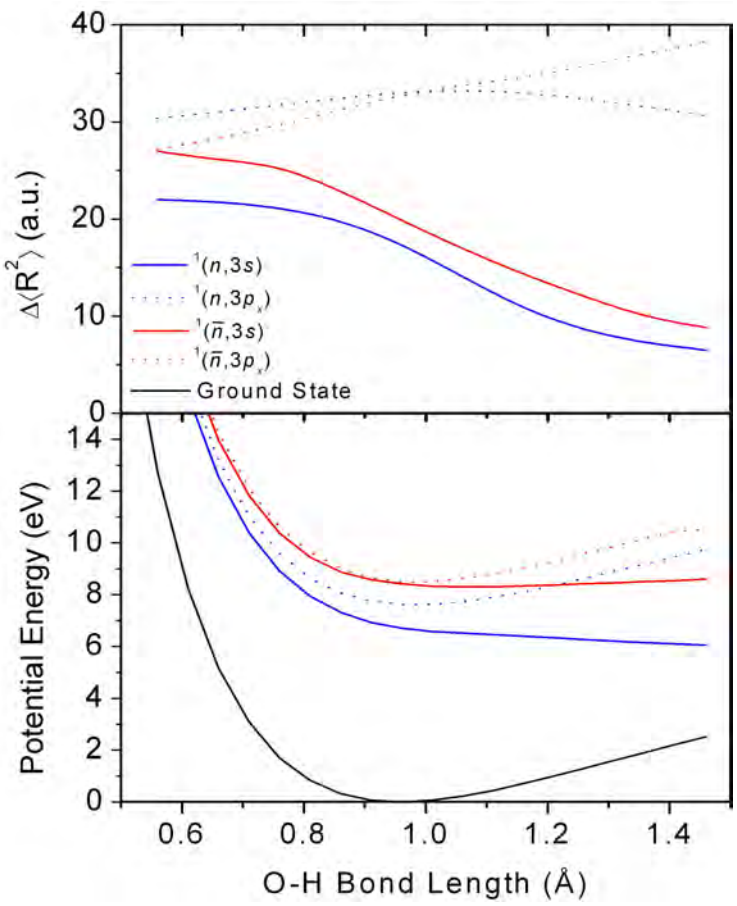

Figure 6.14: (Top) Electronic spatial extent for the first two excited states of A'' and A' symmetry of methanol as a function of the O−H bond distance. (Botton) Potential energy curves for the same states as a function of the O−H bond length.

value for the $^1(n, 3s)$ and $^1(\bar{n}, 3s)$ states has a value of 30 a_0^2 at short O−H bond distances and it decreases as the bond is elongated down to 10 a_0^2. This suggests that these two states collapse in terms of size, changing from Rydberg to valence. For the $^1(n, 3p_x)$ state the $\Delta\langle R^2\rangle$ value remains around a value of 35 a_0^2, value characteristic for a Rydberg state. In the case of the $^1(\bar{n}, 3p_x)$ state the $\Delta\langle R^2\rangle$ value increases as the O−H bond is stretched, but remains in the domain of values specific to Rydberg states.

All these observations are an indication for the presence of an avoided crossing. As a consequence of this avoided crossing the $^1(n, 3p_x)$ and $^1(\bar{n}, 3p_x)$ states maintain their Rydberg character, remaining bound as the bond length is varied. But the $^1(n, 3s)$ and $^1(\bar{n}, 3s)$ states change from bound Rydberg to repulsive valence and consequently they become dissociative, in agreement with the experimental observations presented in section 6.2.

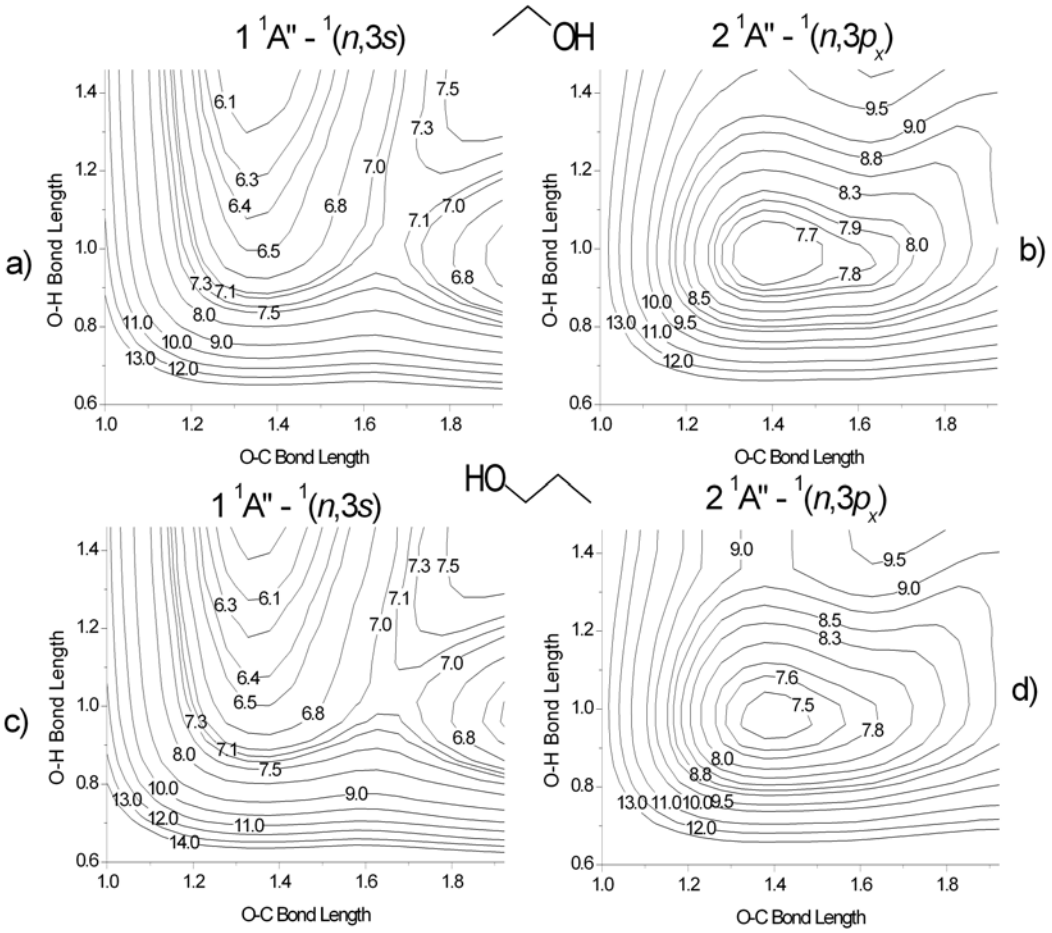

Figure 6.15: Contour plots of the first two excited states for ethanol and 1-propanol. The contour values are in eV. Top row: ethanol, bottom: 1-propanol; left side: $^1(n, 3s)$ excited state, right: $^1(n, 3p_x)$ excited state.

6.3.2.3 Ethanol and 1-Propanol

One of the objectives of this work is to observe general trends that are applicable to entire classes of compounds. It is thus important to know if the observations made for methanol are applicable to other alcohols and by extension to all OH-containing compounds. Fig. 6.15 shows the two dimensional potential energy surfaces for the lowest two excited states $^1(n, 3s)$ and $^1(n, 3p_x)$ of the next two alcohols: ethanol and 1−propanol.

A comparison between the $^1(n, 3s)$ state of the three alcohols (fig. 6.10 for methanol and fig. 6.15 for the other alcohols) reveals their similarities. All three surfaces are dissociative when the O−H bond is elongated. Also all three surfaces show the presence of a barrier at longer O−C bonds. Moreover, there is no clear dependence of the position of activation barrier on the type of the alkyl fragment. A similar comparison for the potential surfaces for the $^1(n, 3p_x)$ state between the selected alcohols indicates that they are repulsive as both bonds are stretched alter-

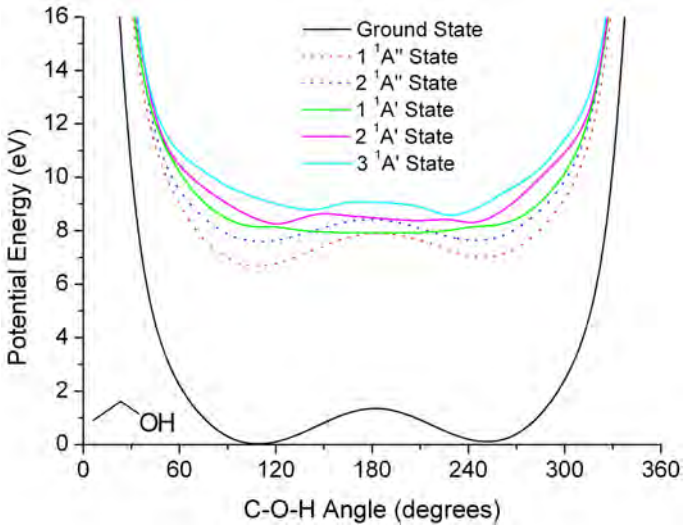

(a)

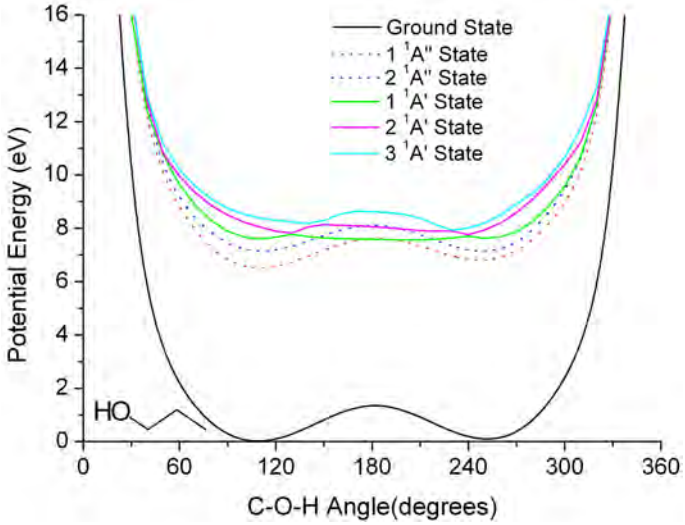

(b)

Figure 6.16: Potential energy surface of ground state (bottom curve, in black) and the lowest excited states shown as a function of the C−O−H angle, for ethanol (a) and 1-propanol (b).

natively.

The potential curves for several excited states for ethanol and 1-propanol as a function of the C−O−H angle are presented in fig. 6.16. They show several similarities with those obtained for methanol. The potential curves for the $1\ ^1\mathrm{A}'' - ^1(n, 3s)$ and $2\ ^1\mathrm{A}'' - ^1(n, 3p_x)$ states for all alcohols show the presence of two minima, at 110 ° and 250 °, consistent with a bent geometry at equilibrium for the molecule, while the curves for the A' excited states show the presence of avoided crossings. These avoided crossings are between Rydberg states converging to different states of the ion and, consequently, are expected to have small exchange terms as it was

discussed in more detail for methanol. But there are minor differences between the alcohols. The exchange terms for A' states decrease as the size of the alkyl fragment is increased. For 1−propanol they are the smallest and the avoided crossings in this case are almost true crossings.

We conclude that the observations made for methanol can be extended to the entire class of alcohols and most likely to all OH-containing compounds. But the study of more complex ethers with more than one oxygen atom in the molecule presented in section 4.2 shows the limitations of these observations to the OH-containing compounds. For the monoethers of glycol presented in section 4.2 the $^2(n, 3s^2)$ Feshbach resonance breaks the O−C bond leading to a DEA band at 6.5 eV. This is due the the presence of hydrogen bonds in the molecule between the hydroxyl group and the second oxygen atom, that closes a 5 atom cycle. Another exception is provided by molecules that can lose radicals with an heteroatom in the chain.

6.3.3 Potential Energy Surfaces of Ethers

This sections presents the potential surfaces for the Rydberg states of ethers. They are compared with the potential surfaces of the excited states of alcohols and it is concluded that the reactivities of alcohols and ethers toward free electrons can be rationalized by assuming that the potential surfaces of the daughter Feshbach resonances closely follow those of the parent Rydberg states. The main results are published in ref. [37], reprinted in section 6.2.

6.3.3.1 Methylethylether

Figs. 6.17 and 6.18 show the potential surfaces for the first four singlet excited states of A'' and A' symmetry respectively of methylethylether. Methylethylether has been selected as representative because it is the smallest ether with the same symmetry as methanol, simplifying the calculations.

For A'' symmetry the surfaces have been identified as $^1(n, 3s)$, $^1(n, 3p_x)$, $^1(n, 3p_y)$ and $^1(n, 3d)$ respectively. An inspection of the potential surface of $^1(n, 3s)$ state reveals the presence of an activation barrier as the O−Methyl or O−Ethyl bonds are stretched. For the surface of the $^1(n, 3p_x)$ state a double minimum can be observed when the O−Methyl bond is elongated. When the O−Ethyl bond is elongated then the surface shows a plateau. Since the two alkyl bond are similar we interpret the presence of the plateau as two minina that have coalesced into a single minimum. In section 6.2 the potential curves of these two states are presented as a function of the O−Methyl bond distance. Their features were interpreted as a result of a series of avoided crossings between the two states and a strongly repulsive σ^* state. Consequently, we conclude that the features observed on the potential surfaces of the $^1(n, 3s)$ and $^1(n, 3p_x)$ states can also be rationalized as resulting from a series of avoided crossing between the two states and a σ^* state.

The plateau in the $^1(n, 3p_y)$ surface in fig. 6.17 could be due to an avoided crossing with the previously identified σ^* state. The 4^{th} state of A'' symmetry has

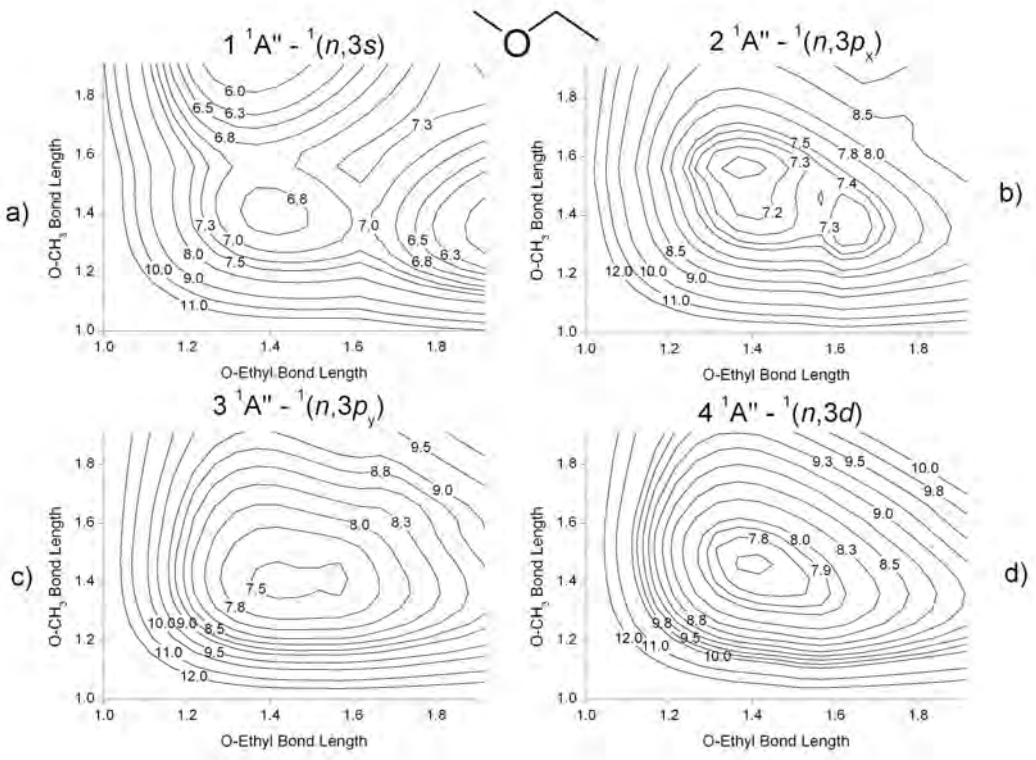

Figure 6.17: Contour plots of the first four A'' excited states for methylethylether. The contour values are in eV.

a only one minimum and its shape is similar to that of the cationic core, suggesting that, in contrast to the previous A'' states, it is unaffected by the presence of a repulsive σ^* state.

The A' excited states (shown in fig. 6.18) have several similarities with the A'' excited states. The 1 $^1A'$ state shows the presence of an activation barrier as the O−C bonds are stretched, similar to the $^1(n, 3s)$ state. Also, a triple minimum can be observed on the 2 $^1A'$ and 3 $^1A'$ potential surfaces, similar to those on the corresponding states of A'' symmetry. The features of the A' states are more pronounced than for their counterparts of the A'' states. But, the assignment of these states is more difficult because, at this energy, configurations arising from the n and $\bar{n}$ molecular orbitals (the two lone pairs of the oxygen) can be observed. This case is similar to the case presented in section 6.3.2.1, where the lowest three A' states are presented as a function of the C−O−H angle. In that case the presence of excited states with the same symmetry, but with completely different orbital occupations lead to small exchange terms between the states and, consequently, avoided crossings that resemble true crossings. An inspection of the states reveals that, at equilibrium geometry of the ground state, the ordering of the states with A' symmetry is $^1(n, 3p_z)$, $^1(\bar{n}, 3s)$ followed by $^1(\bar{n}, 3p_x)$.

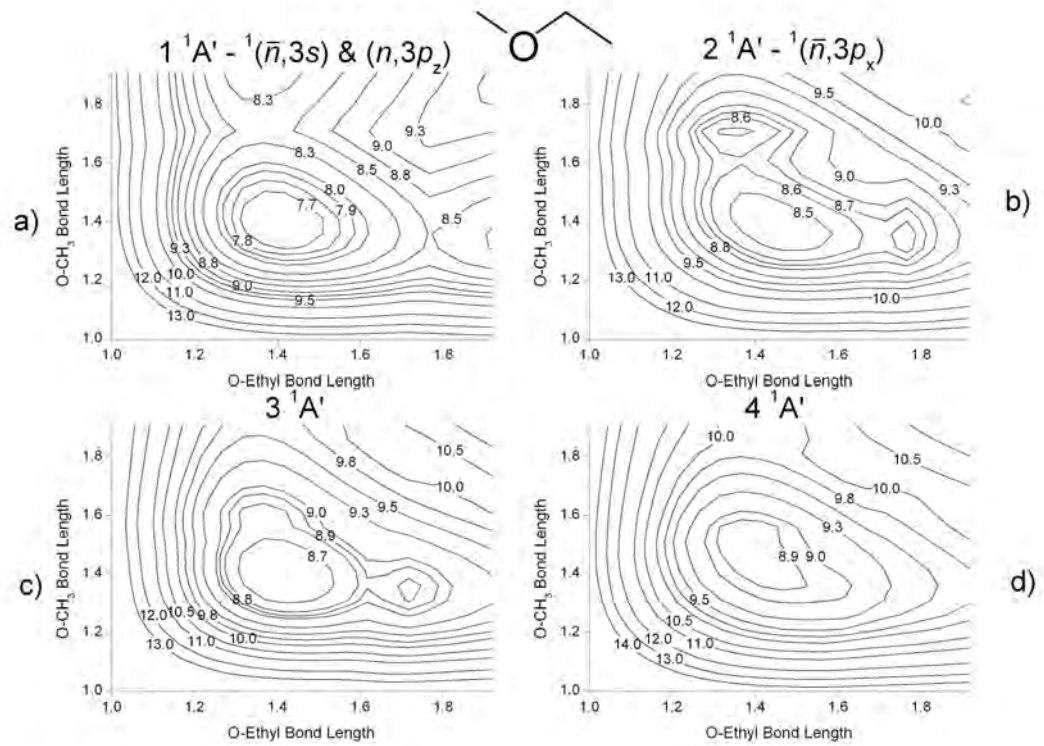

Figure 6.18: Contour plots of the first four A' excited states for methylethylether. The contour values are in eV.

We conclude that in the case of the A' states of the methylethylether, the situation that has been observed for the A'' states (an avoided crossing between the $^1(n, 3s)$ and $^1(n, 3p_x)$ states) is reproduced for the $^1(\bar{n}, 3s)$ and $^1(\bar{n}, 3p_x)$ Rydberg states. But this is complicated by the presence of the $^1(n, 3p_z)$ state, leading to additional avoided crossings with presumably very small exchange terms, since they resemble true crossings.

6.3.3.2 Spatial extent of excited states of methylethylether

The analysis of the electronic spatial extent revealed interesting effects in the case of alcohols. It showed that, as the O−H bond is stretched, the $^1(n, 3s)$ state collapses in terms of size from a Rydberg state to a valence state, while the $^1(n, 3p_x)$ remained a Rydberg state.

Similar effects can be observed for the methylethylether. The $\Delta\langle R^2\rangle$ values as a functions of the two O−C bonds for the lowest two excited states of the ether are presented in fig. 6.19. The curves for the two states are similar for both bonds. They show that $\Delta\langle R^2\rangle$ for the $^1(n, 3s)$ state is around 30 a_0^2 at equilibrium bond length and decreases to about 10 a_0^2 at longer O−C bond lengths, reflecting a Rydberg-

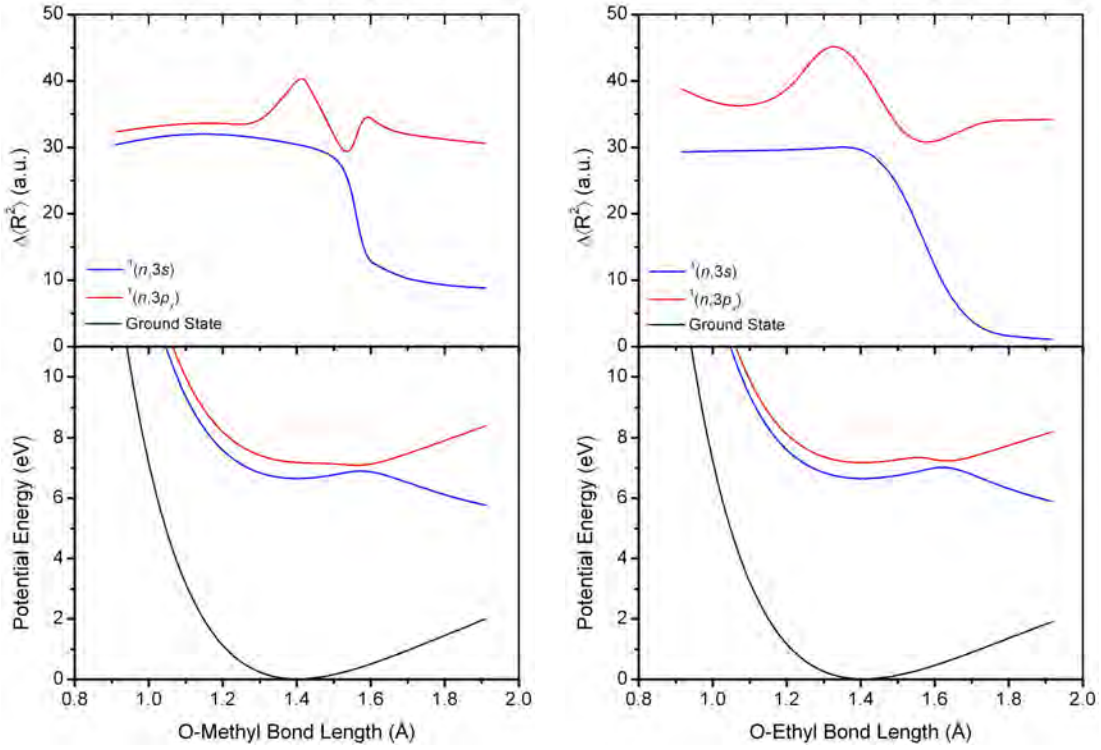

(a) (b)

Figure 6.19: (Top) Electronic spatial extent for the $^1(n, 3s)$ (red) and $^1(n, 3p_x)$ (blue) excited states of methylethylether as a function of the O−Methyl bond distance (a) and O−Ethyl bond distance (b) respectively. (Bottom) The potential energy curves for the two excited states as a function of the O−Methyl bond distance (a) and O−Ethyl bond distance (b) respectively.

valence conversion. At the same time the values for the $^1(n, 3p_x)$ state remain above 30 a_0^2.

A comparison with the case of methanol (fig. 6.14) and that of methylethylether (fig. 6.19) indicated that for the $^1(n, 3s)$ state $\Delta\langle R^2\rangle$ decreases from 30 a_0^2 at equilibrium bond length to much lower values as the bonds are stretched. This is an indication that in all cases the state changes from Rydberg to valence. But, for the $^1(n, 3p_x)$ state the comparison is not as straightforward as for the previous state. While for methanol $\Delta\langle R^2\rangle$ values remain around 30 a_0^2 for all O−H bond lengths, for methylethylether the $\Delta\langle R^2\rangle$ values first increase, then decrease, and finally stabilize as the O−C bonds are stretched. The variation is more significant for the O−Ethyl bond. These variation take place in an interval of bond lengths where two avoided crossing have been identified for the $^1(n, 3p_x)$ (section 6.2). The maximum of $\Delta\langle R^2\rangle$ is at a bond length where the first avoided crossing has been observed, while the minimum corresponds to a bond length where a second avoided crossing with a strongly repulsive σ^* state has been detected on the potential energy curves. These sharp variations in the $\Delta\langle R^2\rangle$ values for the $^1(n, 3p_x)$ state occur in the bond-length range between the two minima and are indicative that this state, while $\Delta\langle R^2\rangle$ values

remain in the interval associated with Rydberg states, changes from one diabatic state to another, as a result of avoided crossings. Interestingly, the structure in the $\Delta\langle R^2\rangle$ is broader for the O−Ethyl stretch then for the O−Methyl stretch. These results are in agreement with our previous observation (section 6.2) that the $^1(n, 3p_x)$ state is affected by an avoided crossing with a repulsive σ^* state.

6.3.3.3 Other ethers

We have tried to extend the results to other ethers but unfortunately CPU times longer than 1 month prevented us to calculate potential energy surfaces of excited states for ethers bigger that methylethylether. The only other ether for which the potential surfaces could be calculated is dimethylether.

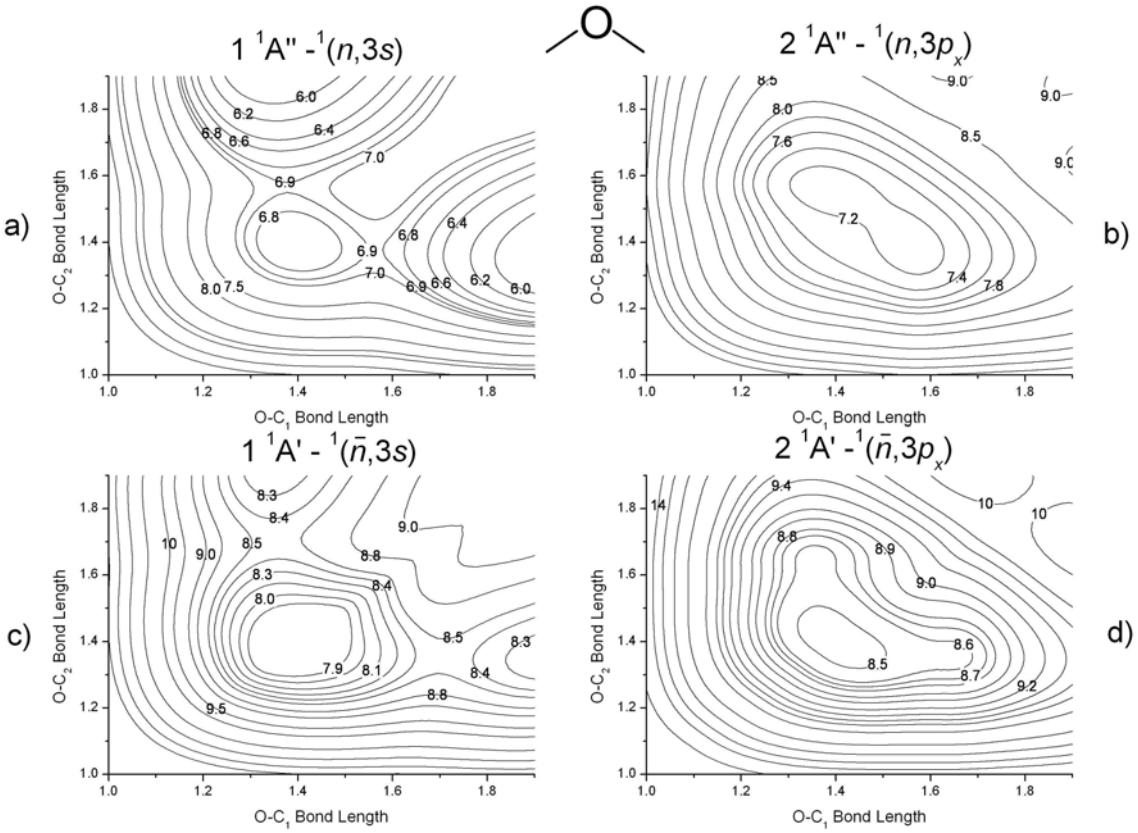

Figure 6.20: Contour plots of the selected excited states for dimethylether. The contour values are in eV. a) $^1(n, 3s)$ state; b) $^1(n, 3p_x)$ state; c) $^1(\bar{n}, 3s)$ state; d) $^1(\bar{n}, 3p_x)$ state;

The situation is more complicated for dimethylether. This is because at equilibrium geometry it has C_{2v} symmetry while methylethylether and the alcohols have C_s symmetry. But at geometries where the lengths of the two O−C bonds are not equal, the symmetry of dimethylether changes to C_s. To preserve the same notation, all the calculations for dimethylether were performed imposing a C_s symmetry at all geometries.

The results obtained for dimethylether are shown in fig. 6.20. Only the first two excited states of each symmetry are presented. A comparison between the excited states for dimethylether and those of methylethylether (shown in figs. 6.17 and 6.18) reveals some similarities. For both ethers, the $^1(n, 3s)$ state shows an activation barrier as one or the other of the O−C bond is elongated. Also, for the $^1(n, 3p_x)$ state, a double minimum can be observed for the stretching of both O−C bonds. The situation is reproduced for the A' states but here an activation barrier is created, just as for methylethylether, by the avoided crossing between the $^1(n, 3p_z)$ and $^1(\bar{n}, 3s)$ states, states with the same symmetry but completely different orbital occupations. This is expected to lead to small exchange terms between the states and thus avoided crossings resembling a true crossing.

The striking similarity observed for the two ethers, coupled with the observation made for alcohols, leads us to the conclusion that, in the case of O−C bond, for the $^1(n, 3s)$ Rydberg state, an activation barrier is present in all compounds where this bond in present. An exception is provided by compounds with two oxygen atoms in the molecule, where the presence of hydrogen bonds leads to the absence of an activation barrier (section 6.2). The presence of this activation barrier prevents the dissociation along this coordinate and, ultimately, the absence of any experimental DEA band in these compounds.

6.3.4 Potential Energy Surfaces of Amines

The TD-DFT method has been successfully applied in alcohols and ethers to explain the different reactivity of alcohols and ethers toward free electrons using the parent Rydberg states. The lowest excited state of alcohols was found to be dissociative, whereas a barrier to dissociation was found in the ethers. Rydberg-valence mixing and avoided crossings were decisive in determining the shapes of the potential surfaces. These results encouraged us to apply the same methodology to calculate the excited states for the simplest two amines: methylamine and ethylamine.

There are several differences between the alcohols and amines. At equilibrium geometry both have C_s symmetry. But as the N−H bond is varied, the symmetry changes to C_1, while for the O−H stretch in alcohols the symmetry remains C_s. For the N−C bond the symmetry of the molecule remains unchanged, C_s, symmetry at the equilibrium geometry, as the bond length is varied. Another distinct difference between alcohols and amines is the fact that the nitrogen atom has only one non-bonding electron pair compared to two pairs for the oxygen. The non-bonding electron pair of the nitrogen is labeled with n.

High resolution UV-VUV photon absorption spectra of methylamine and ethylamine have been reported in the literature [71]. Three bands have been observed for methylamine centered at 5.7, 7.2, and 8.7 eV, respectively. For ethylamine the band centers are at 5.8, 7.0, and 7.9 eV, respectively. All the observed bands show vibrational structure that comes from progressions involving excitation of an amino wag vibration.

The potential energy surfaces for methylamine are presented in fig. 6.21. They

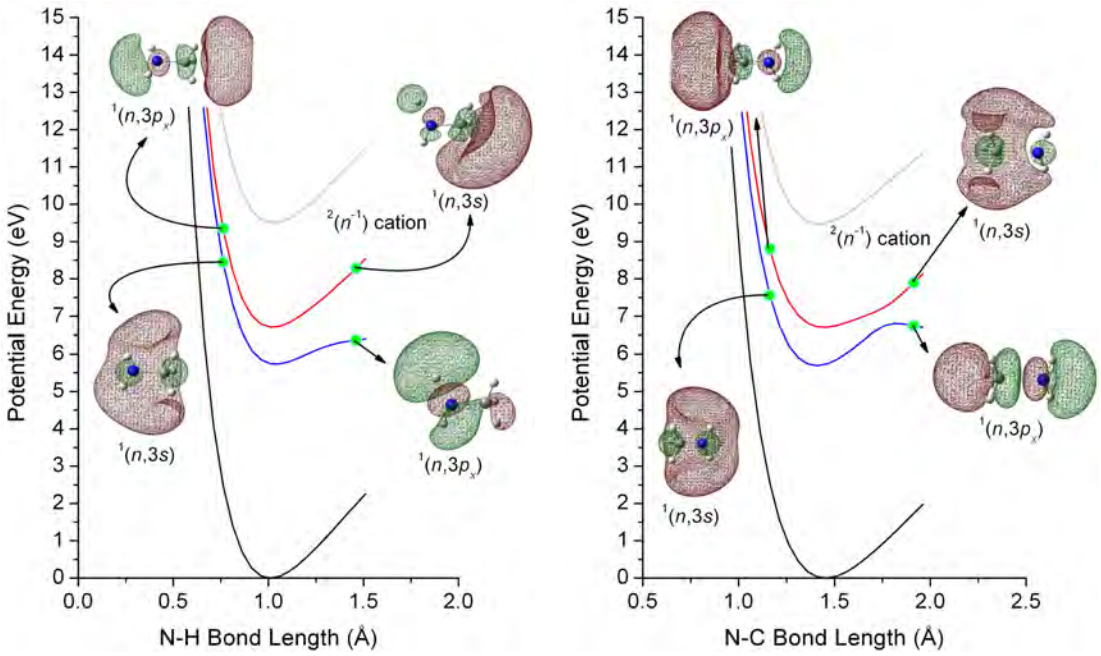

Figure 6.21: Potential energy surface of methylamine (black, bottom curve), its two lowest excited states, and the ground state of the cation (light gray, top curve), shown as a function of the NH distance (a) and as a function of the N−C distance (b).

are in agreement with the observed VUV spectra in the sense that for both bonds stretches the obtained potential curves can support vibrations. For the N−H stretch the energy of the two lowest excited states increase at different rates with respect to the bond distance, the $^1(n, 3s)$) curve being steeper. A pronounced activation barrier is observed at longer N−C bond distances than for the N−H bond.

As presented in ref. [37], the excited state orbitals are informative about the nature of the involved excited state. Similarly, in fig. 6.21 we present the upper orbitals for two different bond lengths, one shorter and one longer than equilibrium. For both bonds the final orbitals associated with the lower excited state have a distinct resemblance to an atomic $3s$ orbital (for more details see the molecular orbitals of methanol in figs. 6.2 and 6.4). Also the final orbital of the next excited state is $3p_x$-like. The situation is reversed at longer bond lengths when the lower one resembles a $3p_x$ orbital and the higher one a $3s$ orbital.

We interpret all these observations, similar to the case of methanol, as indications for the presence of an avoided crossing. But there are marked differences between methylamine and methanol. If, in methanol, the avoided crossing in the O−H bond stretch occurred very close to the equilibrium geometry, for methylamine the corresponding avoided crossing occurs at N−H bond lengths longer than equilibrium. The result is that, in methanol, the lowest excited state is dissociative while in methylamine it is not.

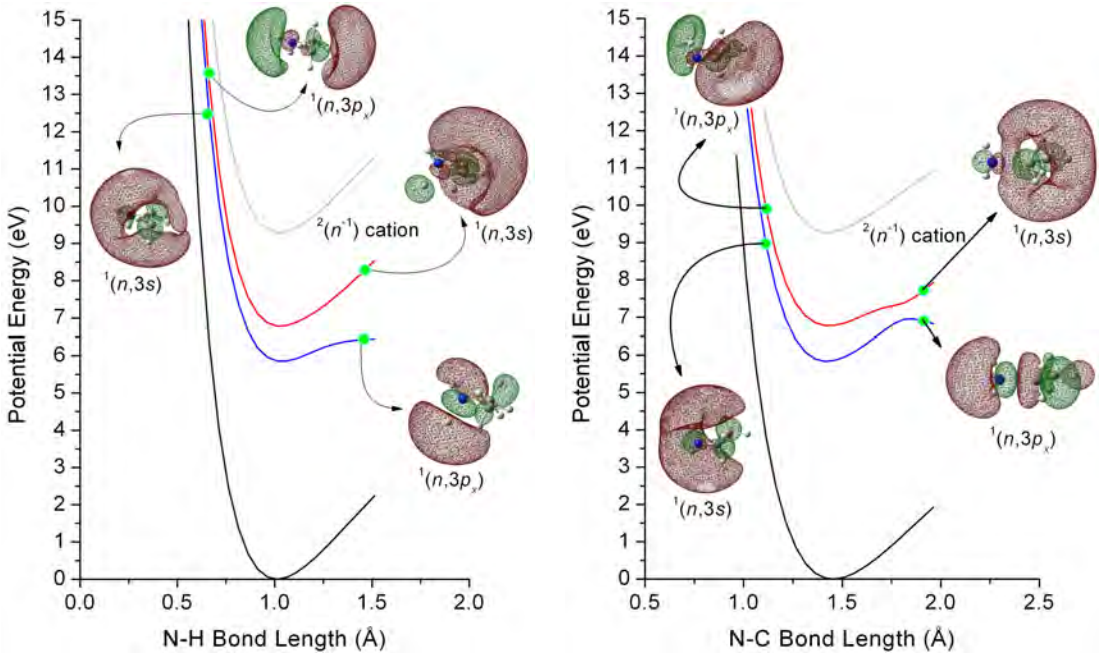

Figure 6.22: Same as fig. 6.21 but for ethylamine

A similar observation can be made for the stretch of the N−C bond. The comparison with the potential curves for the O−C stretch (fig. 6.10 for methanol) reveals that an activation barrier is present in both cases. But for methylamine there are no indications for the presence of a second avoided crossing with a repulsive σ^* state, as for methanol and ethers.

The similarities between methanol (and all alcohols) and methylamine stop here. Negative ion formation in electron-molecule collision in methylamine has been reported [72]. Collin *et al.* have reported that NH_2^- (N−C bond breaking) has been detected mainly at an energy that would correspond to a Feshbach resonance arising from the lone pair of the nitrogen. Also the CH_3NH^- (loss of an H atom) anion has been detected from the same resonance.

The detection of these two anions at energies corresponding to the lowest $^2(n, 3s^2)$ Feshbach resonance suggests that the link between the potential surfaces for the Rydberg states and those for the daughter Feshbach resonances is not as straightforward as it seems to be for oxygen containing compounds. It is also possible that using the *rigid scan* method does not offer the same insight for methylamine as it has provided for alcohols and ethers. The geometry of the grandparent cation is planar as revealed by the fact that the 1st band in the PE spectrum in H_2O is sharp while that of NH_3 and amines is broader due to pyramidal vibrations. This suggests that the minimum energy path through which the system evolves requires the variation of two or more molecular parameters at the same time, one of which needs to be the pyramidal angle on N.

It is important to know if the conclusions for methylamine can be extended to

other amines. The potential curves of ethylamine at its two lowest excited states are presented in fig. 6.22. There is a certain degree of similarity between the potential curves of the first two excited states for both amines. In all cases the $^1(n, 3s)$ and $^1(n, 3p_x)$ states are non-dissociative in agreement with the VUV photon absorption spectra. Also the potential curves for ethylamine are affected by the same problem as those for methylamine.

We conclude that this preliminary study on amines indicates that methylamine can be used as a model compound for amines since the conclusions for the Rydberg states can be extended to all amines. It has the advantages that it is the smallest amine and consequently it is very feasible for calculations with various methods, such as R-matrix method.

6.4 Study of Feshbach resonances for methanol calculated using the R-Matrix method

6.4.1 General considerations about R-matrix method

The R-matrix method first was introduced in the mid 1940s to describe nuclear reactions, dominated by compound state formation. In the early 1970s this method was further developed to describe a broad range of atomic processes including electron-atom scattering [73, 74]. And also, within this period, the method was extended to treat electron molecule collisions [75, 76]. First it was shown how the scattered electron can be represented by analytic basis orbitals. In 1977 the ideas were developed further by Burke *and coworkers* to describe electron scattering by diatomic molecules [77]. Later the R-matrix method was extended to treat electron collisions with polyatomic molecules by Tennyson and Morgan [78].

R-matrix theory is based on the splitting of coordinate space into two regions by a spherical boundary at $r = 15a_0$ centered on the center of mass of the molecule: the inner region and the outer region (fig. 6.23). The boundary is placed so that the inner region contains most of the electronic charge cloud of the target molecule. In the inner region ($r < 15a_0$) the scattering electron lies within the molecular charge cloud and it is necessary to accurately account for all short-range interactions, such as exchange and correlation. The target molecule plus scattering electron are similar to a bound state, and quantum chemistry methods can be used to find the wavefunctions. In the outer region ($r > 15a_0$) the particles are still interacting but the forces are direct and multi-polar in character, the exchange and correlation are negligible, the scattering electron moves in the long-range multipole potential of the target and the single-center expansion of the total wavefunction can be used. Thus it is possible to reduce the scattering problem in the external region to the solution of a set of coupled, ordinary differential equations which are much easier to handle than when the particles are close together and the interactions are non-local.

The R-matrix approach to electron atom and electron molecule scattering is well documented by Burke and Berrington [79]. The general application of the R-

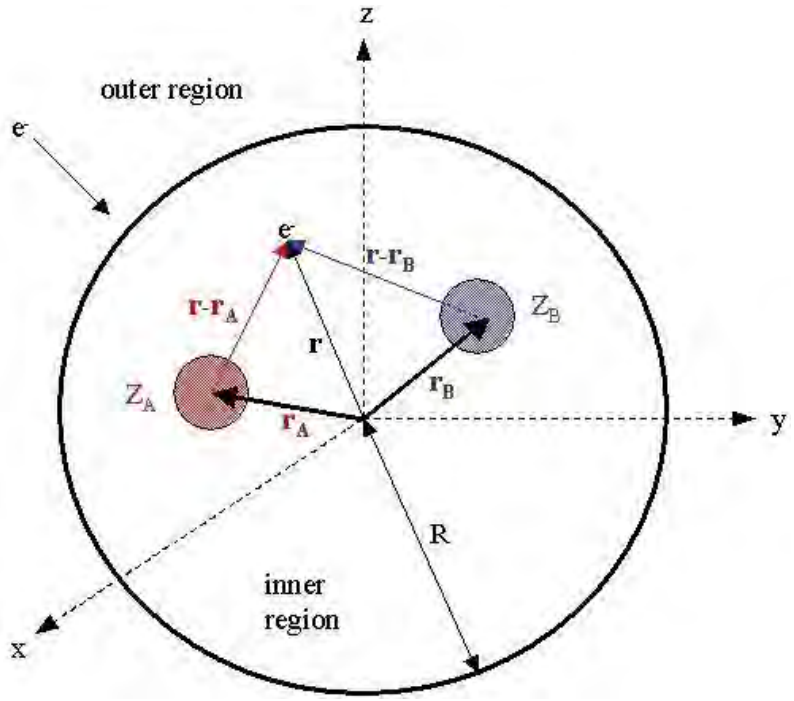

Figure 6.23: Division of space in the R-Matrix theory.

matrix method to polyatomic molecules employing the UK R-matrix code has been described in the literature [80, 81].

6.4.2 The UK R-matrix code

The UK Molecular R-matrix scattering package has been developed over many years by many researchers. R-matrix calculations can be broken down in a number of basic computational steps. They are presented in fig. 6.24. These are the generation of integrals, the generation of a set of molecular orbitals, the construction and diagonalization of the inner Hamiltonian matrix, calculation of the target parameters and solutions of the outer-region scattering equations.

The input required from the user are the geometry, the basis set, the weights used in the averaging of the natural orbitals and the CAS model (on the right side in fig. 6.24). Optionally the orbitals can be calculated with an external package and they can be used directly. Unfortunately the exchange of data is not optimized and the user input needs to be introduced manually at different stages. Additional to the user input when executing these scripts one needs to take care of the different files exchanged between them since this process is not performed automatically and can be a source of errors.

A more detailed description of the UK R-matrix codes and their usage can be found in ref. [82].

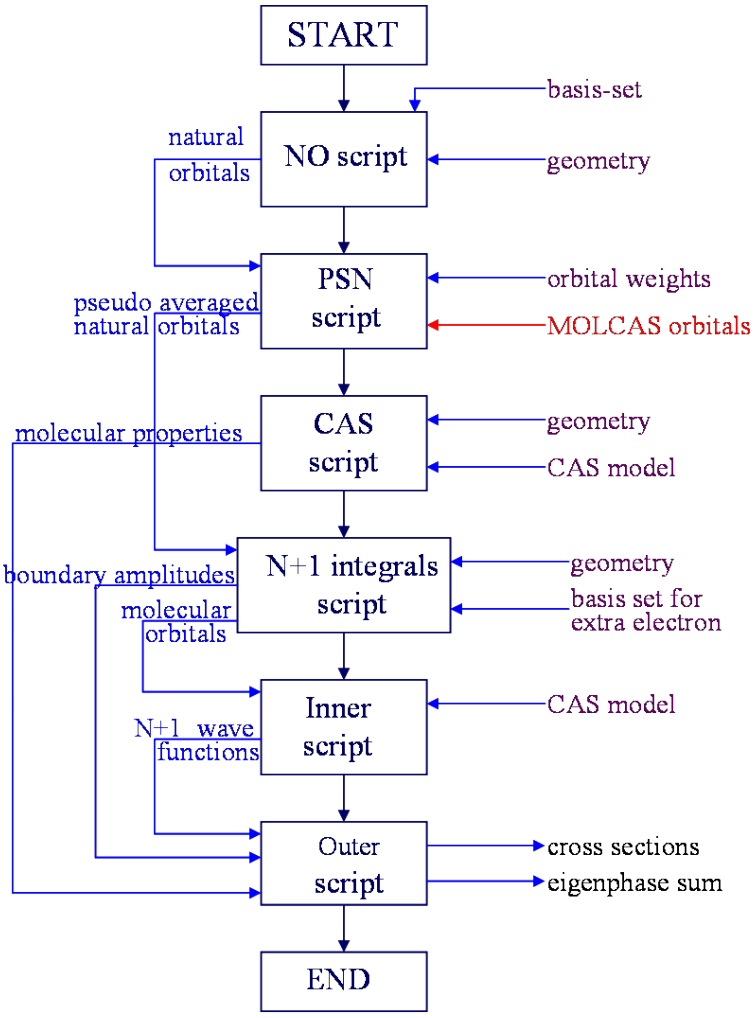

Figure 6.24: The UK R-matrix code.

6.4.3 R-matrix applications to methanol

In section 6.2, a striking difference was observed between the dissociative electron attachment of alcohols and that of ethers. To explain this difference the potential surfaces of Rydberg states for alcohols and ethers, calculated with TD-DFT method, were used. But, the Rydberg states are only the parent states for the observed Feshbach resonances. Consequently we assumed that the potential surfaces of the daughter Feshbach resonances are similar in shape to those of the parent Rydberg states, only shifted to a different energy. This hypothesis is tested in this section calculating the potential curves of Feshbach resonances for methanol as a function of the O−C and O−H bond distance, using the R-matrix method.

It is not unreasonable to assume that the addition of an electron (leading from Rydberg states to Feshbach resonances) will not influence the shape of the potential curves, since this electron is added in a diffuse orbital and as such does not contribute to bonding. This assumption can already be tested for another molecule: water. For this molecule the potential surfaces of both parent and daughter states are available

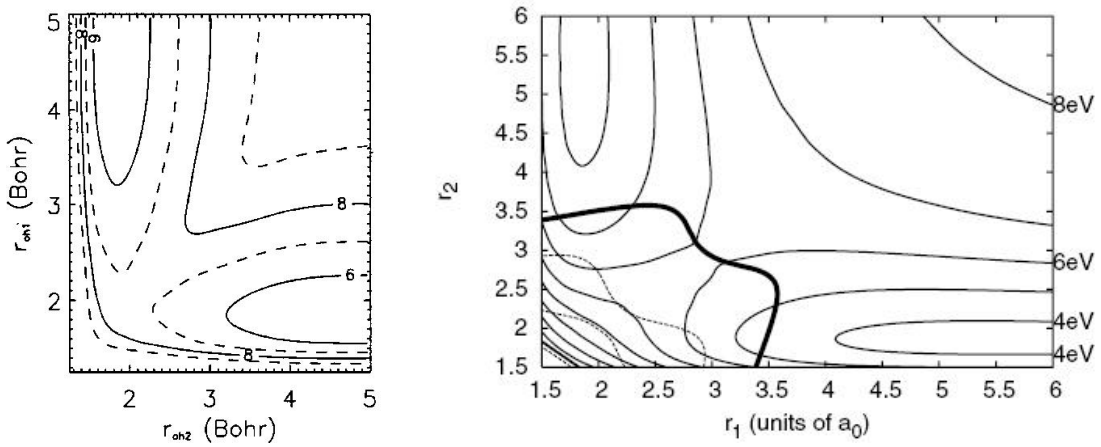

(a) (b)

Figure 6.25: The potential surface for the lowest Rydberg state (a) (ref. [83]) and for the lowest Fesbach resonance (b) (ref. [1]) in the case of water. The imaginary part of the potential surface are represented in dashed line with the bold line representing the lowest contour line. For more details see ref. [1]

in literature [1, 84, 83] and are reproduced in fig. 6.25. As it can be observed both potential surfaces are dissociative when one of the O−H bonds is stretched.

The analysis of the potential surfaces for the parent Rydberg state and the daughter Feshbach resonance in fig. 6.25 reveals that, for both surfaces, the least energy path along one of the dissociation coordinates is not influenced by the value of the other coordinate, meaning that when stretching one bond the geometry can be kept fixed. The same conclusion is also valid for methanol (see fig. 6.10). This conclusion allows for the comparison of the potential surfaces of the lowest Rydberg state as a function of the O−H distance for water and for methanol. The comparison reveals the fact that the potential surfaces for $^1(n, 3s)$ Rydberg state are similar as the O−H bond is stretched, in the sense that it is dissociative, for both substances. Consequently, it is not unreasonable to expect that the potential surface for the 1^{st} Feshbach resonance of methanol will be similar to that of the parent Rydberg state, situation already encountered for water. But there are reasons to expect possible differences. In methanol it is possible that crossings between shape resonances and Feshbach resonances in the 6-16 eV range could play a bigger role. Therefore verification of the assumption made above is desirable.

The calculations for the Feshbach resonances for methanol were performed using the UK R-matrix code at the Open University, UK, with the help of Prof. Jimena Gorfinkiel. A set of R-matrix calculations for the equilibrium geometry were already performed and they are presented in ref. [85]. These calculations where the starting point for the present set of calculations.

6.4.3.1 Target representation of the methanol molecule

A necessary precursor to scattering calculations with the UK R-matrix code is the verification of the target parameters (*e.g.*, vertical excitation energies and the ground state dipole moment). The quality of the scattering model depends on a satisfactory representation of the target. This raises the question what does one do if the target parameters are not satisfactory, particularly for electronically excited states. One of the possibilities is to change the basis-set used to construct the natural orbitals. Another possibility is to modify the complete active space (CAS) model used to calculate the electronic structure of the molecule. The third option is to change the set of averaging parameters used to calculate the natural orbitals. Finally, one can use molecular orbitals generated with an external program, for example, using the MOLCAS method from the quantum chemistry program MOLPRO.

Table 6.2: Number of CSFs as a function of different CAS models.

CAS Model	Number of CSFs				
	$^1A'$	$^3A'$	$^1A''$	$^3A''$	Total
(3-9)A' (1-4)A''	16430	25340	16240	25480	83490
(3-10)A' (1-4)A''	85212	141380	84672	141760	453024
(3-9)A' (1-5)A''	85142	141470	84742	141670	453024
(3-11)A' (1-3)A''	85590	141534	84294	141606	453024

Modification of the basis-set has not been attempted since it requires the optimizations of all other parameters and consequently the same basis set as that described in ref. [85] was used.

To determine the feasibility of changing the CAS model, a calculation to determine the required CPU time was performed. The number of configuration state functions (CSF) was calculated since it is in direct correlation with the CPU time. The results are presented in table 6.2. In all the presented cases the first two states from the A' manifold were frozen. The model noted (3-9)A' (1-4)A'' represents a CAS model where the first two states of A' symmetry are frozen and the next seven states from the A' manifold and the first four states of A'' symmetry are included. This model represents the model chosen as a reference and it is similar to the model used in ref. [85]. The following models presented in table 6.2 represent different combinations where an additional state has been added to the total number of the states included in the construction of the wavefunction, since it should improve the description of the molecule.

As it can be observed from table 6.2 the inclusion of an additional state, either in the A' or in the A'' manifold, increases dramatically the number of configurations that need to be calculated and thus the computational time required for the construction of the wavefunction increases dramatically. If, for the first model the CPU time required to compute the target properties was around 60 minutes, then for the other models the CPU time was around 540 minutes, representing a 9-fold increase in time. Considering the fact that computing the wavefunction for the anion takes about 1400 minutes when the first CAS model is used then a 9-fold increase in

the CPU time becomes not feasible from a practical point of view. Thus only the first CAS model from those presented in table 6.2 was used to describe the target molecule.

Table 6.3: Different models used in the R-matrix calculations.

R-matrix Model	Weight on state						
	Ground	$1\,^1A'$	$1\,^3A'$	$1\,^1A''$	$2\,^1A''$	$1\,^3A''$	$2\,^3A''$
Model 1	3	1	3	4	0	4	0
Model 2	3	0	0	1	4	1	4
Model 3	3	0	0	4	2	4	2

The last parameter to be modified was the set of averaging values used in the calculation of the pseudo-averaged natural orbitals. Ten models with different averaging values were tested. In the end only three models were selected. The values for each of these models are presented in table 6.3. Model 1 represent the model chosen as a reference and it is the same model as the one presented in ref. [85]. In this model a higher emphasis was placed on the A' states than on those from A'' manifold. In the models 2 and 3 the emphasis was shifted from the states of A' symmetry to those of A'' symmetry, since the lowest excited states are of this symmetry.

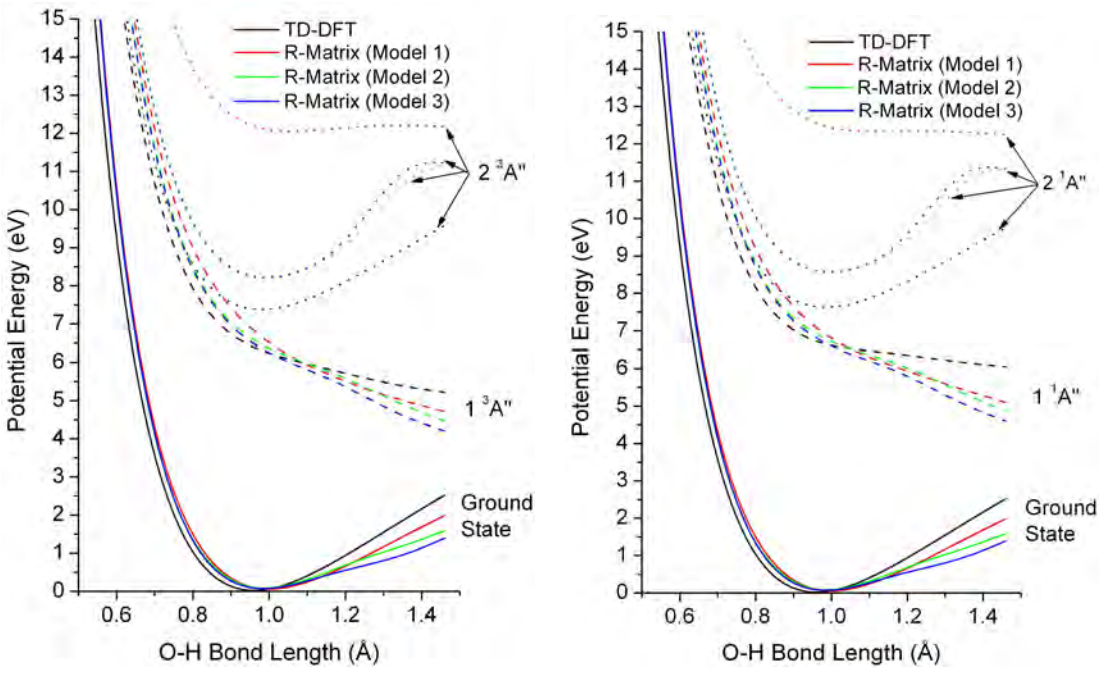

(a) (b)

Figure 6.26: The first excited states of methanol as calculated with TD−DFT (black line) and with the R-Matrix suite using three different models for the target molecule in the case of O−H stretch. Triplet states are presented in (a) while the singlet excited state are shown in (b)

The potential energy surface for the first singlet and triplet excited states as a function of O−C or O−H bond stretch are presented in figs. 6.26 and 6.27. They were performed using the models presented in Table 6.3. To judge the quality of the methods, potential surfaces are compared to those calculated with TD-DFT method (see section 6.3 for more details on TD-DFT), surfaces that are used as a reference for the R-matrix calculations.

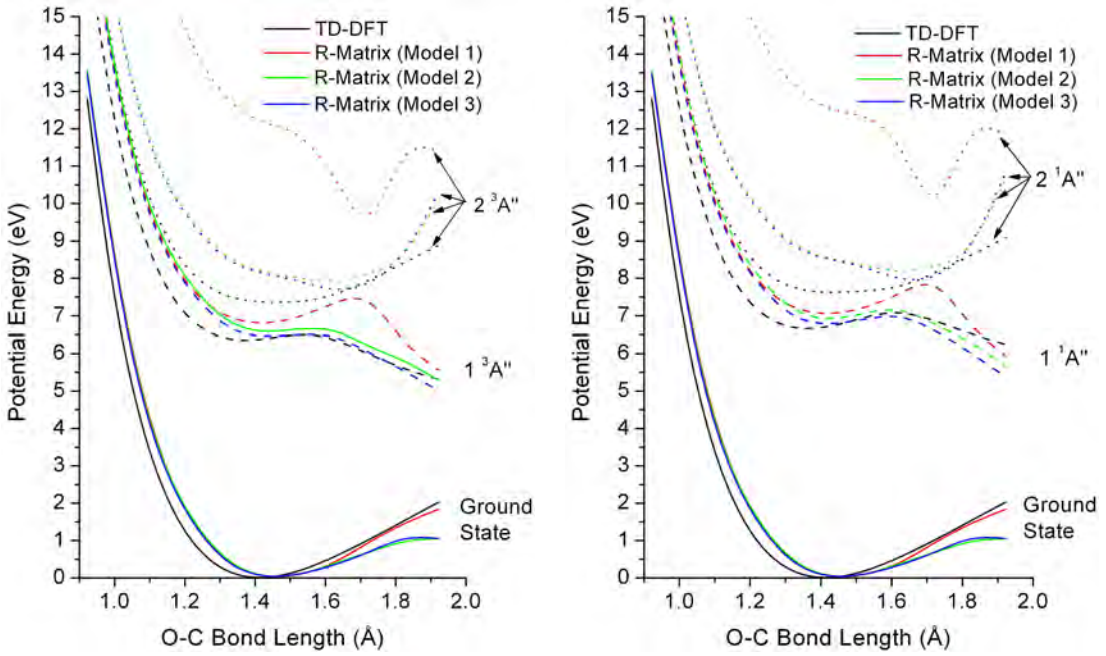

(a) (b)

Figure 6.27: As fig. 6.26 but for the O−C stretch.

For the O−H bond stretch the potential energy surfaces for both the 1 $^3A''$ and the 1 $^1A''$ state with the three selected models present the same dissociative behavior as that obtained with the TD-DFT model. The energy difference between these states is negligible, but as the bond is elongated the decrease in energy is bigger for the states calculated with R-matrix models than those with the reference model.

In the case of 2 $^1A''$ and 2 $^3A''$ states all the R-matrix models reproduce the behavior of the TD-DFT model. But the difference in energy between the states calculated with R-matrix and those calculated with the reference model are bigger than those for the previous A'' states. Models 2 and 3 are the closest to the reference with only negligible difference between them. The energy separation between the first two singlet states or between the first two triplet states, calculated with the R-matrix model 1 is bigger than in the reference model. The possible consequence of this is that an eventual avoided crossing between these states will be taken into account with a lesser degree of accuracy in model 1, since the exchange terms between the states depends on the energy separation.

In the case of the O−C bond stretch an activation barrier can be observed on

the potential energy surface of the 1 $^1A''$ state calculated with all three R-matrix models similar to the situation obtained with the TD-DFT model. For the models 2 and 3 the deviation from reference is small for all the points, increasing as the bond is elongated. But, for model 1, the height of the activation barrier is significantly bigger than in the reference.

The non dissociative character of the 2 $^1A''$ state calculated with the TD-DFT model is also reproduced with the R-matrix models 2 and 3. But the behavior for the potential energy surface calculated with model 1 is different. The same features can be observed as in the case of other models but for this model the features are dramatically enhanced. Also the 2 $^1A''$ state is, in this model, at significantly higher energy than with all other models.

Beside singlet excited states there are also triplet excited states. The lowest triplet states are presented in figs. 6.26 and 6.27. The potential energy surfaces obtained for the 1 $^3A''$ and 2 $^3A''$ states are similar in shape to those of the singlet counterparts with the difference that they are situated about 0.4 eV lower in energy.

In conclusion, the R-matrix model 1 gives a poor description of the electronic spectrum for methanol since the potential energy curves obtained with this model are at significantly higher energies and have quite different shapes from those obtained with the TD-DFT model. But, the other two models (model 2 and 3) reproduce qualitatively well the reference model, although they disagree quantitatively. For these models the deviation is bigger for the second singlet and triplet A'' state that for the lower one. The difference between these two models is negligible so both can be considered valid to use in the next step: the calculation of the Feshbach resonances.

6.4.3.2 Feshbach resonances

To calculate the resonances in the R-matrix model one needs to supplement the orbitals used with a set of continuum orbitals, centered on the center of gravity of the molecule. These orbitals are of longer range than the orbitals centered on the nuclei, as they represent the scattering electron and do not vanish on the R-matrix boundary.

The next step is the calculation of the Ψ_k^{N+1} from the diagonalization of the Hamiltonian matrix. The R-matrix on the boundary can now be determined from the solution of the $\mathcal{H}^{N+1}$. This is a sum over quantities related to the overlap integrals of the internal and external wavefunctions evaluated at the surface of the sphere and the eigenenergies of the internal states [77]. The R-matrix contains a complete description of the collision problem in the inner region and provides the boundary conditions necessary to match the inner and the outer regions wavefunctions, and solve the problem in the outer region. Then, the R-matrix is propagated to an asymptotic region where the radial wavefunctions describing the scattering electron can be matched to analytical expressions. From the latter, the K-matrix elements are determined and subsequently the resonance positions and widths and the cross sections (*via* the generation of the T-matrix) are computed.

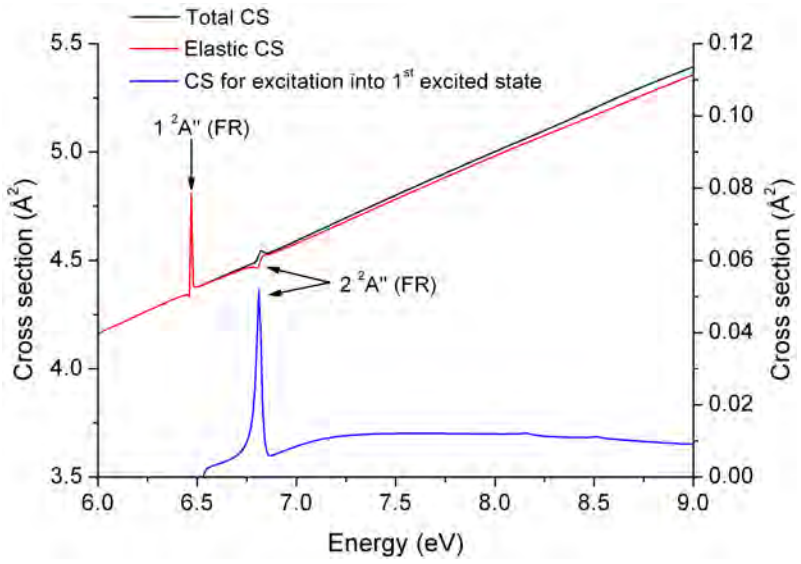

(a)

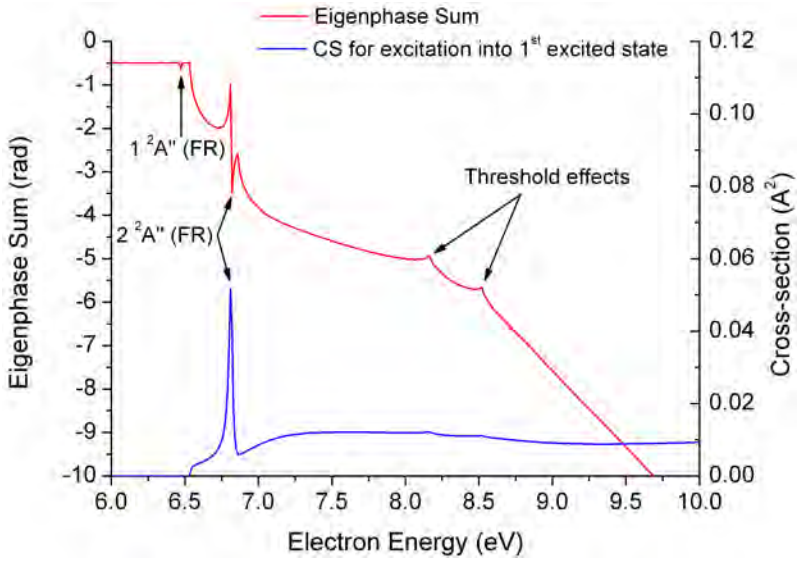

(b)

Figure 6.28: Cross sections(CS) (a, b) and eigenphase sum (b) for the equilibrium geometry. The position of the 1 $^2A''$ and 2 $^2A''$ resonances are marked.

In the UK R-matrix package the resonances are identified by dramatic changes in the eigenphase sum and the corresponding partial cross section in the respective energy range. The resonances are detected and fitted automatically using the RESON module [86]. This module uses a Breit-Wigner profile [87] to fit the eigenphase sum to a resonance characterized by its position E_i^r and width Γ_i^r:

$$\eta(E) = \sum_i \tan^{-1}\left[\frac{\Gamma_i^r}{E - E_i^r}\right] + \sum_j a_j (E)^j \tag{6.7}$$

where $a_j(E)$ is the background eigenphase (from other non-resonant partial waves) and $\eta(E)$ is the eigenphase sum as calculated by the R-matrix package and is used by the RESON module to fit the position and the width of the resonances.

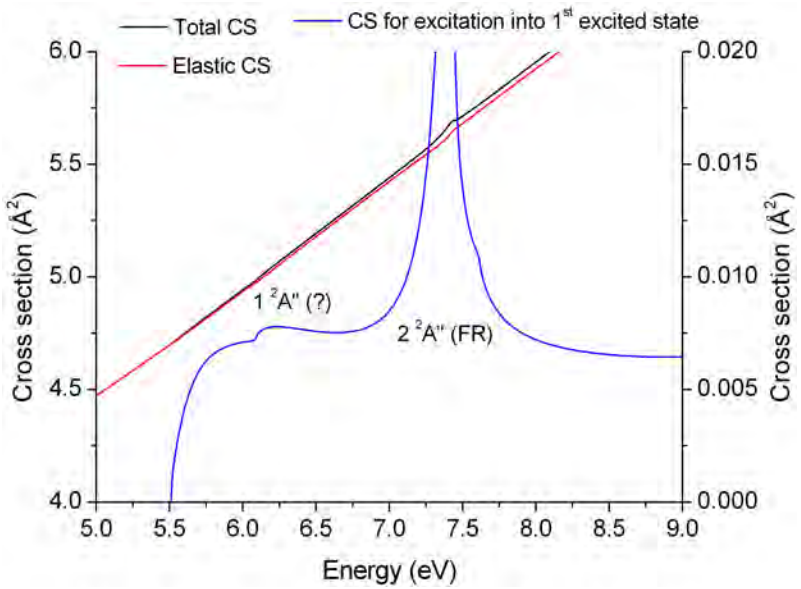

(a)

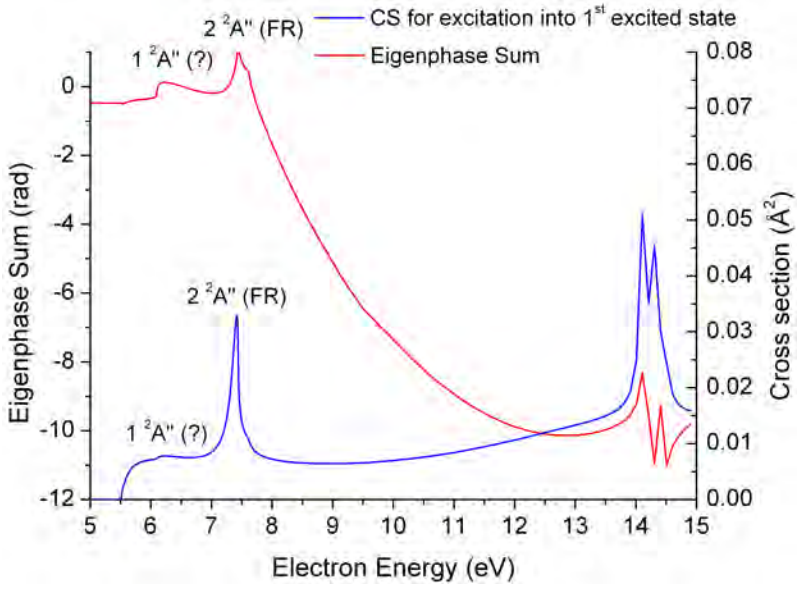

(b)

Figure 6.29: Cross sections (a, b) and eigenphase sum (b) for the geometry with elongated O−C bond, where r(O−C)=1.72 Å. The position of the 1 $^2A''$ and 2 $^2A''$ resonances are marked.

In fig. 6.28 this process is exemplified for the equilibrium geometry using the R-matrix model 2. Two Feshbach resonances have been identified using the coincidence between the features observed in the eigenphase sum and different cross sections (CS). The first Feshbach resonance is below the threshold energy for the first excited

state and consequently can be observed only in the total CS or in the elastic CS as a sharp peak. But the second Feshbach resonance appears more distinctly in the CS for excitation into the first excited state ($1\ ^3A''$) and only slightly in the other two CS and as such is identified by the coincidence of structures between the eigenphase sum and the CS for excitation into $1\ ^3A''$.

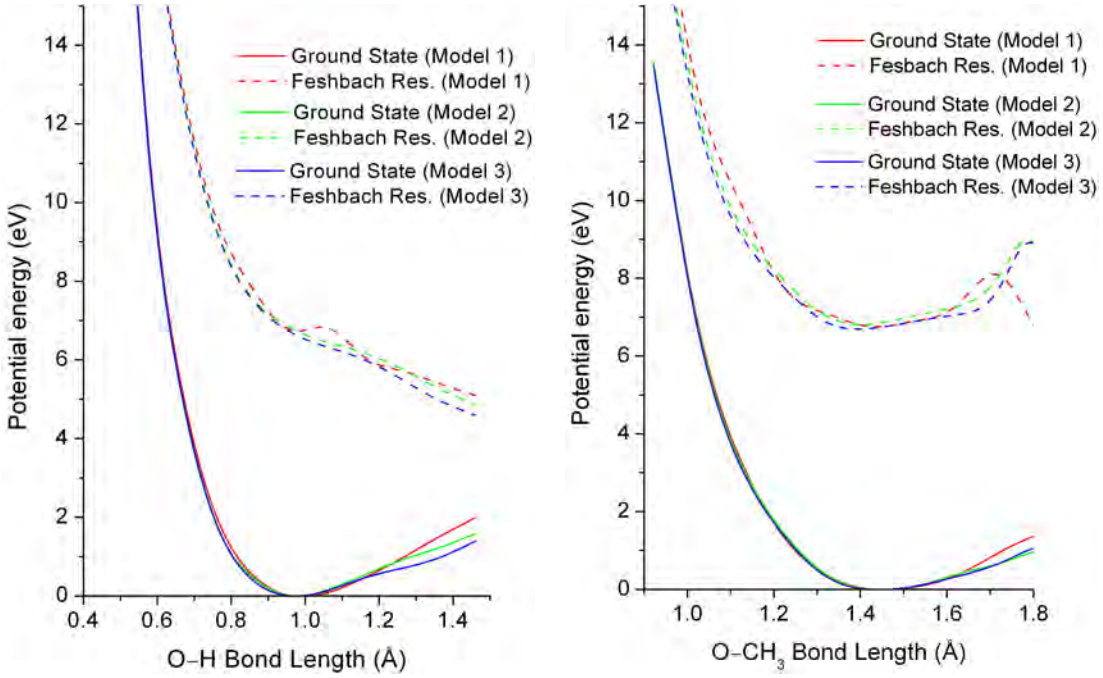

(a) (b)

Figure 6.30: The potential energy surfaces for ground state and 2nd Feshbach resonance as a function of the O−H bond distance (a) and O−C bond distance (b) calculated with the three R-matrix models.

One added difficulty with the R-matrix code is the fact that resonances can often appear exactly at a threshold and then can have the effect of distorting the resonance or of cutting off some part of it. This makes the resonance difficult to fit by the RESON module and thus harder to identify by the present codes. This problem is encountered in the present case, particularly when the O−H bond is elongated.

Besides resonances, the eigenphase sum and the CS presented in fig. 6.29 reveal the presence of other structures. They are called *threshold effects* since they appear when a new parent state becomes available for decay. These effects must not be confused with the Feshbach resonances, since resonances usually lead to a π jump in the eigenphase sum, and care must be taken when assigning different features present in eigenphase sum.

A feature that appears to be a resonance has been observed for O−C bond lengths greater than 1.72 Å. This is shown in fig. 6.29 and it is labeled as $1\ ^2A''$. An examination of both eigenphase sum and cross section for excitation into the

1st excited state reveals a feature at 6.1 eV. In the eigenphase sum this feature is better observed and resembles a resonance with the exception that is not a π jump but rather seems cut off by a threshold before reaching the expected π value. At the moment it is unclear if this feature is a *true* resonance or it is an artifact of the various approximations introduced in the calculation.

The 1st Feshbach resonance is difficult to identify for bonds lengths bigger than 1.72 Åand thus it is unsuitable for testing the various models. Thus the potential energy surfaces for the 2nd Feshbach resonance have been calculated using the three models tested in the previous section. Even though the results with R-matrix model 1 are less accurate than with the other models, they have been included as a verification of the codes. The results are presented in fig. 6.30. For the O−H bond all the models indicate a dissociative surface, while stretch of the O−C bond leads to a non-dissociative surface in all cases. But, there are some quantitative differences between the models. The first model leads to the presence of a small activation barrier when the O−H bond is stretched. The potential energy surface obtained with the 2nd model is slightly higher in energy than that obtained with the 3rd model.

There is a distinct difference between the potential energy surface obtained with model 1 and the potential energy surfaces obtained with the other two models, for the O−C bond. In the case of model 1 an activation barrier is observed while the other two models indicate a bound potential energy surface. This difference in behavior between the two models is most likely due to the fact that in model 1 the 1st pair of singlet and triplet excited states is better separated from the 2nd pair of excited states.

An examination of the cross sections obtained at different geometries reveals that the change in cross section associated with the first two Feshbach resonances decreases as the two bonds are elongated. Consequently it becomes harder to track and identify these resonances. The first resonance is affected to a higher degree by this and, already at 1.2 Å for the O−H bond and at 1.52 Å for the O−C bond, they are impossible to distinguish from the background.

Fig. 6.31 shows a comparison between the potential surfaces of the two lowest singlet and triplet excited states and the Feshbach resonances. A correlation can be observed between the 1 $^2A''$ state (the first Feshbach resonance) and the 1 $^3A''$ state (the first triplet excited state). A similar correlation is found between the 2 $^2A''$ state and the 1 $^1A''$ state (the first singlet excited state). The Feshbach resonances are lower in energy than their counterparts, with the 1 $^2A''$ resonance being 0.06 eV lower and the 2 $^2A''$ resonance 0.05 eV lower at equilibrium geometry. This correlation emphasizes a parent-daughter relation between the two states in the pair.

When the O−H bond is stretched the two Feshbach resonances remain below their parent states initially. The energy difference between the parent and daughter states diminishes as the bond is elongated. For the O−C bond, after 1.62 Å , the 2 $^2A''$ state is above its parent state. This can be interpreted in two ways: either the resonance changes from a Feshbach resonance to a core excited shape resonance, or the present calculations underestimate the electron affinity of the resonance, up to

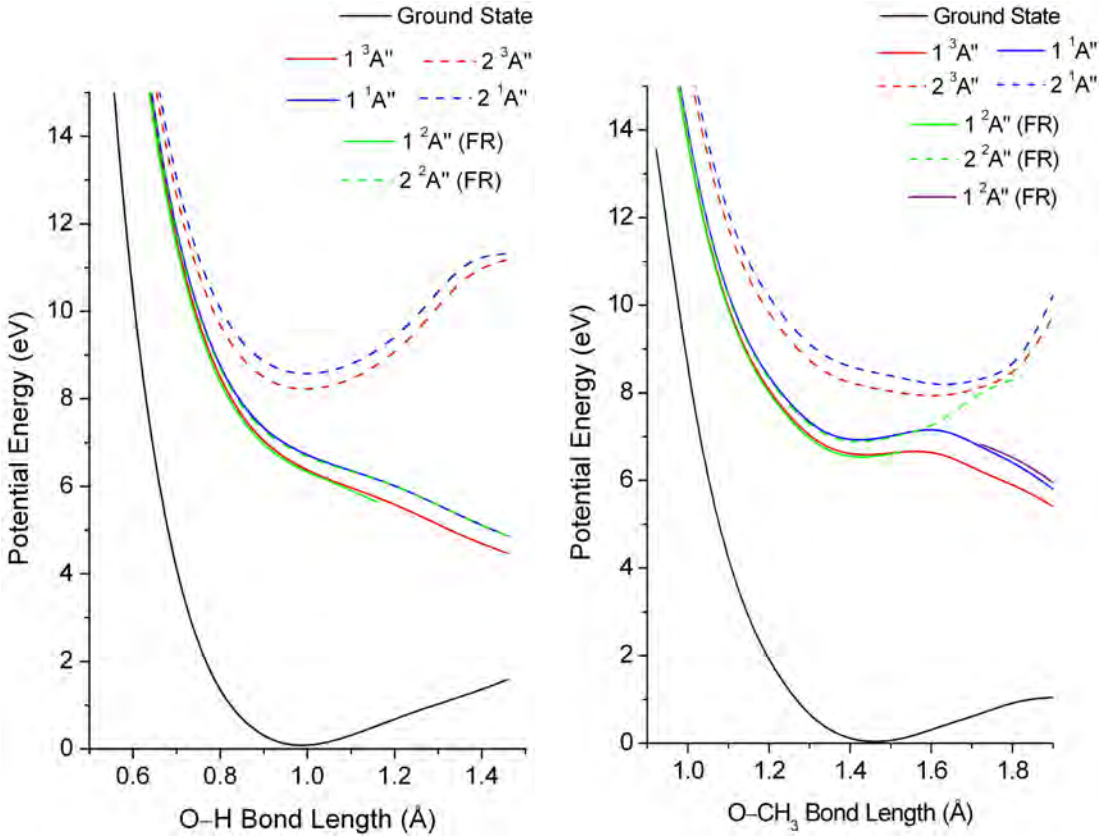

(a) (b)

Figure 6.31: The potential energy surfaces for ground state, lowest two singlet and triplet excited states and the first two Feshbach resonances as a function of the O−H bond distance (a) and O−C bond distance (b) calculated with the R-matrix model 2. The first member of each series is drawn in solid line while the second member is drawn with dotted line. The feature observed in fig. 6.29 is labeled as $1\ ^2A''$ and is shown in solid violet line.

the degree of placing it above its parent state.

At present it is unclear why the R-matrix calculations indicate the presence of two Feshbach resonances for bond lengths shorter than equilibrium and also a range of bond lengths bigger than the equilibrium value. Experimentally only one Feshbach resonance has been detected in DEA, but this does not exclude the existence of such a resonance with a low DEA cross section.

For the case where the O−C bond length is varied the results obtained are less clear than for the O−H bond. The study of the eigenphase sum and of the cross sections reveals the presence of a resonance, shown in fig. 6.31. The excited states show the presence of an avoided crossing around r(O−C) = 1.62 Å. This avoided crossing is between a strongly repulsive σ^* surface and a nominally bound Rydberg state (section 6.3.2.1). Consequently it is expected that the potential energy surface of the daughter Feshbach resonance is also affected by an avoided crossing.

Unfortunately we have not been able to accurately determine the 1 $^2A''$ resonance beyond 1.62 Å since the cross section becomes very small and thus impossible to distinguish from the background. One of the possible scenarios is presented in fig. 6.31. The 2 $^2A''$ resonance changes the parent state as the O−C bond is stretched, from 1 $^1A''$ to 2 $^1A''$ and as a result it is nominally bound. But the 1 $^2A''$ resonance shows a discontinuity around 1.62 Å and it cannot be accurately followed beyond this value and in this scenario is considered to be an artifact. Still, this scenario explains reasonably well the experimental observation that the Feshbach resonance is not dissociative since the potential energy surface for the more reliable resonance (2 $^2A''$) is bound.

There is another scenario. It is possible that the feature observed in the cross sections for O−C bond lengths bigger that 1.72 Å is a section of the 1 $^2A''$ resonance. Thus in fig. 6.31 the 1 $^2A''$ resonance is represented by the solid green line up to 1.52 Å and by the solid violet line beyond this value. This would make this resonance non dissociative since the potential curve shows an activation band and would still explain the experimental observation concerning the lack of DEA signal. In this scenario the 2 $^2A''$ resonance remains identical as in the previous scenario and would still change the parent state.

It is disconcerting that the current R-matrix results are not able to distinguish between the two scenarios presented above. This could be the result of the fact that the parent state changes character from Rydberg to valence and this most likely would affect the resonance. The manner in which the resonance would be affected in such a case is unclear at the moment. It could remain a Feshbach resonance or it could change to a core excited shape resonance.

Despite these problems, there are some positive aspects shown by the present set of R-matrix calculations. Even though we cannot distinguish between the two cases, both cases indicate that the first resonance should be non-dissociative when the O−C bond is stretched, in agreement with the experimental observation. In addition, for the dissociation of the O−H bond the potential energy surface of the resonances are distinctly different, being repulsive and thus supporting the experimental observation. Another positive aspect shown by these results is that, with the exception of the longer O−C bond lengths, the potential energy curves for the Feshbach resonances follow those of their parent Rydberg states. This is an indication that the assumption made at the beginning of this section is true.

The results reported here indicate a need for further testing and development of the R-matrix method since one of the major deficiencies of this method is that the calculated electron affinity of Rydberg states is wrong. The experimental value for the Rydberg states discussed in this chapter are around 0.4-0.5 eV while the calculated value is on the order of 0.01 eV. A consequence of this is that the Feshbach resonances are in most cases at the threshold making their identification more difficult. The results obtained with the R-matrix method could be the basis for new calculations with a different method such as the complex Kohn variational method used for water [1] and acetylene [34].

Chapter 7

Dissociative electron attachment of thiols

In this chapter we present the first results of a study on the dissociative attachment of compounds with S−H bond. Interestingly, the DEA spectra of ethanethiol, the first such compound which was analyzed, proved to be completely different from the spectra recorded for alcohols or ethers. For oxygen containing compounds the spectra are dominated by Feshbach resonances, while for thiols it seems that shape resonances are the main dissociation channel. Thus, thiols are likely candidates for site and state selective chemistry similar to aminoalcohols [88].

7.1 Introduction

In the previous chapters we have analyzed the DEA of oxygen containing compounds and we have observed that their spectra are dominated by Feshbach resonances with occupation of Rydberg-like orbitals. These resonances are highly localized and seem to follow a precise set of empirical rules when dissociating. Additionally the analysis of amino-alcohols [88] revealed a case of state and site selective chemistry where the Feshbach resonances are localized on a particular functional group even though experimental evidence shows the presence of a hydrogen bond between the two groups.

The thiol group is a saturated functional group that offers the same possibility as amines and alcohols to control chemical reactions with electrons. Additionally thiols are employed in surface science to attach large molecules to a solid substrate, *i.e.*, in the case of self-assembled monolayers. The SH group plays an important role in biochemistry, being vital in the structure of proteins. Thus it is important to know how molecules with sulfur bonds react with electrons.

Little experimental data is available concerning dissociative electron attachment. H_2S has received the most attention and low energy electron collisions with H_2S have been treated both experimentally [89, 90, 91, 92, 93] and theoretically [94, 95, 96, 97, 98], suggesting several resonant states. R-matrix calcu-

lations [97] have focused on the elastic scattering and electronic excitation, while, using the local complex potential model, the H^- dissociative attachment channel has also been investigated [98].

In H_2S the DEA process gives rise to HS^-, S^- and H^- ions. The recent work of Abouaf *et al.* [93] reveals marked differences between the DEA processes in H_2S and H_2Se on the one hand and H_2O on the other hand. They observed the presence of three separated bands in the S^- spectrum and suggested the occurrence of at least three resonant states. The lowest resonance at 2.2 eV was attributed to a shape resonance, involving an attractive resonance state. The higher resonances are most likely Feshbach resonances but the corresponding parent states were not identified. Abouaf *et al.* also observed sharp structure on the lowest DEA band in the S^- and HS^- spectra. This structure is attributed to interference oscillations as in the case of N_2.

The aim of our current work is to establish a general DEA spectrum of molecules containing a thiol group. A similar approach has been successful in alcohols (chapter 3) and amines (chapter 5) and has led to the discovery of state and site selective chemistry in amino-alcohols [88].

7.2 Ethanethiol

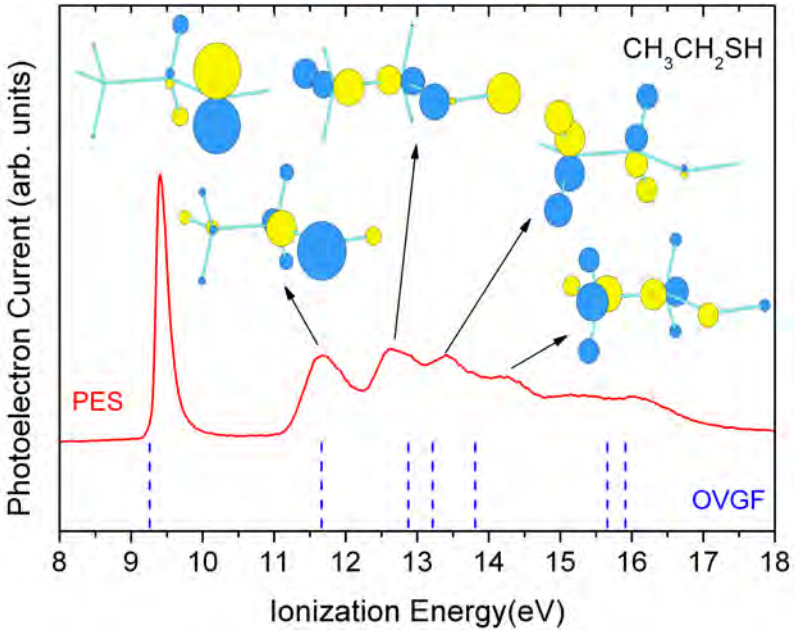

Figure 7.1: HeI Photoelectron spectrum of ethanethiol. IPs calculated with OVGF method are shown with bars. The MOs associated with the IPs are displayed using the Moplot software.

Our work on alcohols (chapter 3) reveals that the DEA spectra of higher mass alcohols (propanols and butanols) are more similar to ethanol than to methanol and

H_2O. It is not unreasonable to consider that a similar relation exists for thiols. Thus ethanethiol could be used as a model molecule for larger or more complex molecules containing SH group.

Photoelectron spectrum of ethanethiol (fig. 7.1) offers valuable information concerning the grandparent states of Feshbach resonances. To obtain the ionization potentials (IP) we have performed *ab initio* calculations using the Outer Valence Green's Function (OVGF) method as implemented in Gaussian 03 [47] package. The results are shown in fig. 7.1. They offer important informations concerning the molecular orbitals (MO) from where the electron is ejected. Our spectrum is in perfect agreement with the spectrum previously recorded by Kimura *et al.* [45].

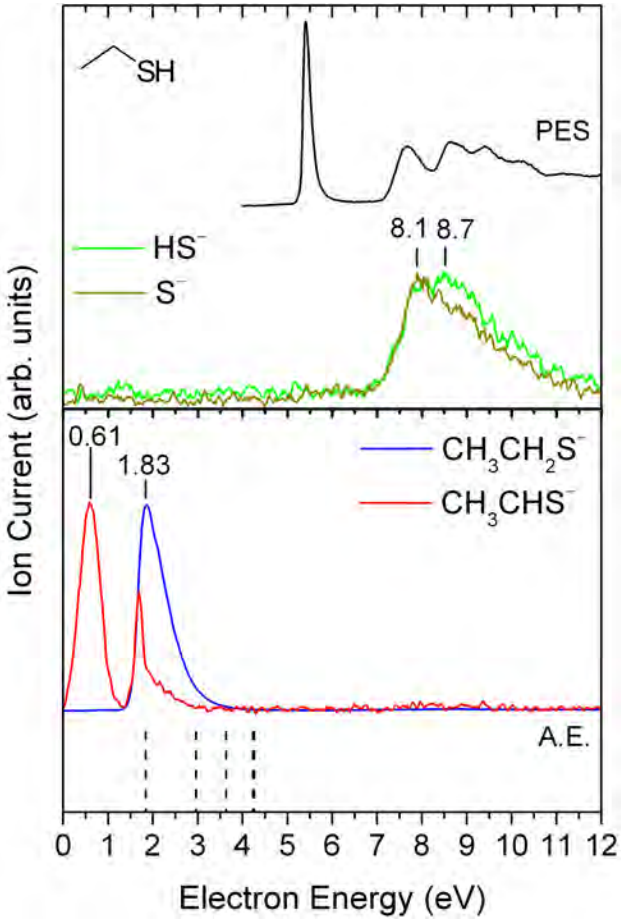

Figure 7.2: DEA spectra of ethanethiol. The photoelectron spectrum is displayed on the top (shifted by -4.0 eV). The calculated attachment energies for the $(M-1)^-$ ion are displayed on the bottom.

A comparison between the calculated IPs and the bands in the PE spectrum reveals a good agreement between theory and experiment. The first two bands are assigned to ionizations from the lone pairs of electrons of sulfur, while the next one is ionization from an orbital that is delocalized over the entire molecule. The fourth MO is localized on the alkyl fragment. A comparison with the MOs of ethanol reveals several similarities, with the first two MOs being the lone pairs of electrons,

the 3rd MO being delocalized over the entire molecule, and the 4th one on the ethyl fragment.

The following ions were detected as a result of various DEA processes: S^-, SH^-, $(M-2)^-$ and $(M-1)^-$. Their DEA spectra are shown in fig. 7.2. The most probable structure for $(M\text{-}2)^-$ ion is CH_3CHS^- while for $(M\text{-}1)^-$ is $CH_3CH_2S^-$, as shown in fig. 7.3. To explain these spectra we have calculated the attachment energies where the resonances are located using the following formula fitted by Chen and Gallup [99]:

$$E(A.E.) = \frac{E(V.O.) - 2.33}{1.31} \tag{7.1}$$

where E(A.E.) represents the attachment energy of the shape resonance and E(V.O.) is the energy of the virtual orbital associated with this resonance. This formula is valid of only for orbital energies calculated with Hartree-Fock method and using the 6−31G basis-set.

The attachment energies are presented as dashed bars in figs. 7.2 and 7.4.

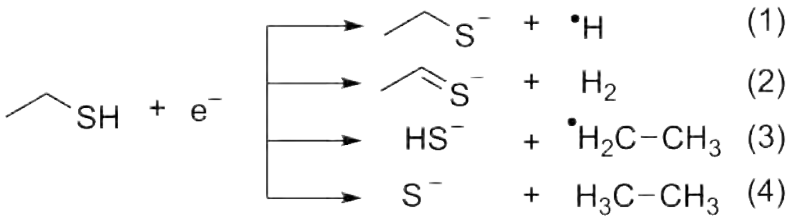

Figure 7.3: Reaction schema for the generation of the detected ions.

The most likely reactions to obtain the observed ions are presented in fig. 7.3. A comparison with the fragmentation of ethanol upon electron collision reveals several differences. In both molecules we observe the loss of a H-atom, the breaking of the C−S or C−O bond respectively, with formation of the ethyl radical. Another similarity is the formation of the heteroatomic ion S^- and O^-, respectively, which takes place in both molecules. But the formation of the $(M-2)^-$, *i.e.* the loss of a hydrogen molecule, is recorded only for the thiol, while in ethanol the concurrent loss of a H-atom and a hydrogen molecule are characteristic, leading to the $(M-3)^-$ ion.

Table 7.1: Threshold energies for reactions (1) and (2) in fig. 7.3, in eV. The DFT values were calculated as described in section 2.2.1. The onset of the DEA bands (taken at 75% of peak height) were taken from the present spectra.

Reaction	E_{thr}	
	DFT	Onset of DEA
(1)	1.74	1.71
(2)	0.64	0.43

The DEA spectrum of $CH_3CH_2S^-$ shown in fig. 7.2 reveals the presence of only one band at 1.83 eV. This energy is too low to allow the assignment to a Feshbach resonance. The band is most likely due to a shape resonance. An examination of the threshold energy calculated using the method developed for alcohols [32] reveals that the 1.83 eV band corresponds to a resonance occurring at the thermodynamical threshold. Most likely the electron is captured into the lowest unoccupied molecular orbital (LUMO), as indicated by the attachment energy of this orbital, and forms the fragment ion as soon as the channel becomes thermodynamically available.

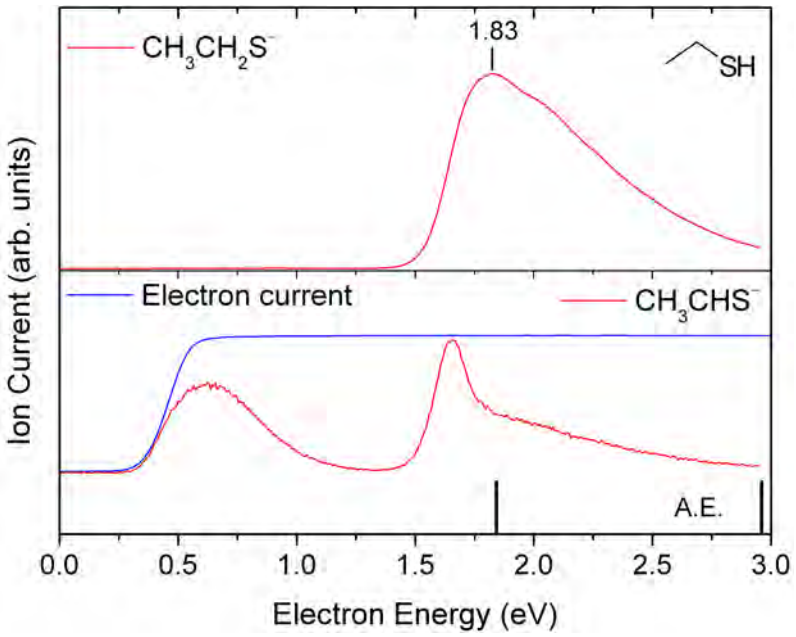

Figure 7.4: Details of DEA spectra the high mass fragments from ethanethiol. The calculated attachment energies are shown in the bottom panel.

Another interesting aspect about the DEA spectrum of $CH_3CH_2S^-$ is the lack of any other bands at higher energies. This is contrast to ethanol where the spectrum of the $(M-1)^-$ ion is dominated by Feshbach resonances. For ethanethiol, the spectrum for $(M-1)^-$ shows the presence of only shape resonances. It is unclear why Feshbach resonances are missing in this case. A comparison with the situation encountered for ethers (chapter 4) indicates that most likely there must be an activation barrier on the potential surface of the Feshbach resonances. But there are no theoretical calculations to confirm this assumption.

Another ion formed in the dissociation of the ethanethiol is CH_2CHS^-. The DEA spectrum for this anion reveals two bands at 0.61 eV and 1.66 eV. The 0.61 eV band is very close to the calculated thermodynamical threshold for formation of this ion. Also, it is too low in energy to be considered as a Feshbach resonance. All this, and the similarity to the band in the $(M-1)^-$ spectrum indicate that the band is a shape resonance occurring at the thermodynamic threshold.

A closer examination of the 0.6 eV band shown in fig. 7.4 reveals that the band is at the onset of the electron current. This indicates the possibility that the band

can be cut-off by the electron curent and the maximum of the band could be at a lower value than it appears in the DEA spectrum. This indicates that this band may be a 0 eV band, similar to SF_6.

The contour of the 1.66 eV band is distinct from those of the bands encountered so far. It has an onset at 1.37 eV with a maximum at 1.66 eV. But there are several distinctive features: the onset of the band corresponds to that of the the band at 1.81 eV in the $(M-1)^-$ spectrum. Additionally, at 1.82 eV it shows a dramatic change in the slope that corresponds to the maximum in the $(M-1)^-$ spectrum. The coincidence in the onset of the band indicates that the same process is responsible for both bands. But the change in the slope at 1.82 eV is indicative that another process is becoming dominant. These processes are not pressure dependent and thus they are not a possible result of ion-molecule reactions. We conclude that, initially, the electron is trapped in a shape resonance. The newly formed temporary negative ion dissociates initially through the $(M-2)^-$ channel. But as soon as a new channel ($CH_3CH_2S^-$) becomes available the dissociation in the old channel decreases significantly, indicative of interchannel coupling.

Fig. 7.2 shows the spectra of two more fragments: S^- and HS^-. They are the result of breaking of the C−S bond either alone or accompanied by the breaking of the S−H bond. In both situations this process shows a remarkable energy selectivity since it occurs at energies above 7 eV. This suggests that the primary process for the formation of both ions is cleavage of the C−S bond *via* a Feshbach resonance, in contrast to the breaking of the S−H bond which in ethanethiol occurs through a shape resonance.

The DEA spectrum of S^- shows the presence of a single asymmetric band with a maximum at 8.1 eV. The energy of this band can be associated with the second band in the PE spectrum shifted by -4.0 eV. This is an indication that the resonance associated with the band could be a Feshbach resonance with a hole in the in-plane *sp* lone pair of the S-atom. It is unclear why there is no band associated with the *p* lone pair from the S-atom, but most likely an activation barrier on the potential surface of the Feshbach resonances could inhibit dissociation during the lifetime of the resonance.

The DEA spectrum of HS^- ion consists of two resonances as indicated by the additional signal observed when the spectrum of HS^- is compared to that of S^-. As explained above, the 8.1 eV is most likely a Feshbach resonance where the hole is localized in the in-plane *sp* lone pair of the S-atom, while the 8.7 eV resonance could be another Feshbach resonance that could be associated with the third band in the PE spectrum.

However, the parentage of the Feshbach resonances that appear in the S^- and HS^- spectra is uncertain. It is unclear why the first PE band has no resonance associated with it whereas the next two do. In oxygen containing compounds both Feshbach resonances associated with the lone pairs of electrons from the oxygen displayed the same behavior: they were dissociative with respect to the O−H bond and non-dissociative with respect to the O−C bond. Conversely, in ethanethiol, there is no detectable signal from Feshbach resonance associated with *p* lone pair of

electrons but it seems that there is a resonance associated with the in-plane *sp* lone pair.

In conclusion, the DEA spectra for the loss of H-atom and H_2 from thiols seem to be dominated by shape resonances in the 0-3 eV region. The capture mechanism of the electron to form the shape resonances is unclear at the moment, but these resonances are responsible for breaking of the S−H bond. In the case of the C−S bond the main mechanism of dissociation most likely involves Feshbach resonances. This leads to a clear separation of the type of dissociation, with the S−H bond being broken preferentially in the 0-3 eV range and C−S bond in the 7-15 eV region. Unfortunately the selectivity is not restricted to the formation of one ion, but rather to the bond that is broken in the dissociation.

Considering the fact that the spectra of the thiols are different from those of alcohols or amines, this makes the SH group a perfect candidate for state and site selectivity, similar to the one observed in aminoalcohols.

Chapter 8

Dissociative electron attachment of acetylene and diacetylene

In this chapter we present the determination of the absolute cross sections for dissociative electron attachment in the case of acetylene and diacetylene. These results are obtained using two mutually complementary instruments: a dissociative electron attachment spectrometer and a newly constructed total ion collection tube. The author's contribution to this work is the determination of relative cross sections in the case of acetylene and diacetylene. These results are published as ref. [38] and are reprinted as section 8.1. Additionally pressure tests have been performed to determine the influence of the calibrating gas on the studied molecules.

8.1 Absolute cross sections for dissociative electron attachment to acetylene and diacetylene

The reprint of the article starts on the next page.

PHYSICAL REVIEW A **77**, 040701(R) (2008)

Absolute cross sections for dissociative electron attachment to acetylene and diacetylene

Olivier May, Juraj Fedor, Bogdan C. Ibănescu, and Michael Allan
Department of Chemistry, University of Fribourg, Fribourg, Switzerland
(Received 1 February 2008; published 14 April 2008)

Absolute cross sections for the production of the two astronomy-relevant negative ions H—C≡C$^-$ and H—C≡C—C≡C$^-$ by dissociative electron attachment to acetylene C_2H_2 and diacetylene C_4H_2 were measured (with a ±25% error bar). Acetylene yielded the C_2H^- ion at an electron energy of 2.95 eV with a cross section of 3.6 ± 0.9 pm^2 and also the C_2^- ion at 8.1 eV with a cross section of 4.1 ± 1 pm^2. Diacetylene yielded the C_4H^- ion at 2.5 eV with a cross section of 3.0 ± 0.8 pm^2 and at 5.25 eVwith a cross section of 73 ± 17 pm^2. Weaker C_4^-, C_2H^-, and C_2^- signals were also observed from diacetylene. The identity of the negative ion resonances mediating the dissociation and the consequences for the production of these ions in discharges are discussed. An alternate path for C_4H^- formation, from the O^--C_4H_2 ion-molecule reaction, was also observed.

DOI: 10.1103/PhysRevA.77.040701 PACS number(s): 34.80.Ht, 52.20.Fs, 52.20.Hv

The identifications of the negative ions C_6H^- [1], C_4H^- [2] and C_8H^- [3,4] in outer space are among the most exciting recent discoveries in astronomy. A necessary prerequisite for the assignment of the observed astronomical bands were laboratory microwave spectra [1,5]—recorded with negative ions prepared in discharges containing acetylene H—C≡C—H and diacetylene H—C≡C—C≡C—H. The knowledge of electron-induced chemistry of the $C_{2n}H_2$ class of compounds is thus of great interest if we wish to address the question of how the $C_{2n}H^-$ ions are formed, primarily in laboratory discharges.

The most important primary electron-induced process leading to negative ion fragments is dissociative electron attachment (DEA), and the present work reports experimental absolute cross sections for this process in acetylene and diacetylene. These two compounds were found also in the upper layers of planetary atmospheres [6,7] and in flames [8]. Both environments contain free electrons and the present electron-induced processes could consequently also play a role there.

The desired quantitative cross sections were obtained by combining the results from two mutually complementary instruments.

(a) A dissociative electron attachment spectrometer described previously [9]. It employs a trochoidal electron monochromator to prepare a magnetically collimated beam of quasi-monoenergetic electrons, which is directed into a target chamber filled with a quasistatic sample gas. Fragment anions are extracted at 90° and directed into a quadrupole mass spectrometer.

(b) A newly constructed total ion collection tube having the same basic principle of operation as that of Rapp and Briglia [10]. Fragment ions were collected at electrodes surrounding the electron beam in a collision chamber. A smoothly varying background of scattered electrons also reached the ion collecting electrodes after multiple collisions with the gas, and was subtracted. The cross section was calculated from the ion current, the incident electron beam intensity, and the sample gas pressure measured with a capacitance manometer. The electron current varied between 50 nA and 2 μA, and the sample pressure between 0.05×10^{-3} and 0.3×10^{-3} mbars. Measurements were performed in two modes: (1) In a field-free target chamber and (2) with an ion extraction field of up to 6 V/cm. The former mode is similar to that employed by Aflatooni and Burrow [11]. The results, over the range of pressures and beam currents, agreed within about ±20% and we report the average value, with an error bar of ±25%. The instrument was tested on the O^- yield from O_2, CO_2, and N_2O, and a good agreement with the results of Rapp and Briglia [10] was obtained (Table I).

The dashed curve in Fig. 1 shows the absolute data, without mass resolution, obtained from the magnitude of the ion current in instrument (b). Earlier work [14–16] showed that the 2.95 eV band is due to C_2H^- and the 8.1 eV band to C_2^-. The present value of the cross section at 2.95 eV is higher than the value of Azria and Fiquet-Fayard [15] (Table I), with the difference being about equal to the combined error limits. Our value is also higher for the 8.1 eV band although here the values are within the combined error limits. The present value at 2.95 eV is in an excellent agreement with the calculated result of Chourou and Orel [12]. (The degree of agreement is presumably to some degree fortuitous in view of the 25% error bar of the experiment.) Figure 1 shows also the yield of the C_2H^- fragment measured by the mass resolved experiment, normalized to the absolute measurement at 2.95 eV. It reveals a second, weaker band peaking at 7.45 eVwhich is obscured by background variations in the absolute measurement. The earlier work [14,15] revealed also H^- production.

TABLE I. DEA cross sections (pm^2).

Target	Energy	Product	This work	Lit.[a]
C_2H_2	2.95	C_2H^-	3.6	2.2 ± 0.3
	8.1	C_2^-	4.1	3.1 ± 0.4
C_4H_2	2.50	C_4H^-	3.0	
	5.25	C_4H^-	73	
O_2	6.5	O^-	126	140
CO_2	8.1	O^-	37.4	42.4
N_2O	2.2	O^-	830	860

[a]References [10] (O_2, CO_2 and N_2O) and [15] (C_2H_2).

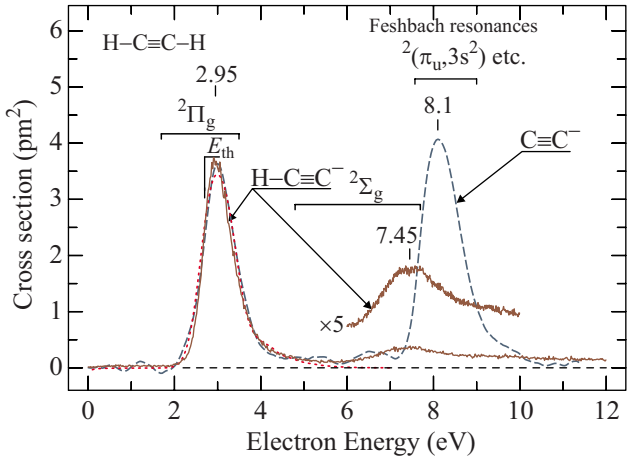

FIG. 1. (Color online) Dissociative electron attachment cross sections of acetylene. The dashed curve shows the absolute data, without mass resolution; the continuous curve is the yield of mass 25 fragment from the relative but mass resolved measurement, normalized to the absolute data. The dotted curve is the calculated cross section of Chourou and Orel [12]. The threshold energy E_{th}, and the positions of the $^2\Pi_g$, $^2\Sigma_g$, and the Feshbach resonances derived from earlier vibrational excitation [13] and electron transmission [14] work are indicated.

Dissociative electron attachment is nearly always a resonant process, it proceeds *via* a "resonance," a given state of a negative ion of the target molecule, which is generally very short-lived (of the order of a classical vibrational period) because of fast autodetachment. Independent information on acetylene resonances was obtained from vibrational excitation [13] and electron transmission [14]. These methods identified a $^2\Pi_g$ shape resonance, due to a temporary occupation of the π_g (π^*) LUMO of acetylene, extending from about 1.7 to 3.5 eV and peaking at 2.6 eV, as indicated in Fig. 1.

Shape resonances with temporary occupation of $\sigma^*_{C—H}$ orbitals have been identified by vibrational excitation in many hydrocarbons, for example propane [17] or ethene [18]. They peak around 7.5 eV and are several eV wide. A similar resonance may also be present in acetylene, but is unlikely to play a substantial role in dissociative electron attachment around 3 eV because of its high energy and extremely large autodetachment width. We therefore prefer the assignment of the present C_2H^- band to the $^2\Pi_g$ resonance.

The onset of the C_2H^- production coincides with the energetic threshold of the process (Table II). This indicates that the C_2H^- ion is produced with little excess energy, in its $^1\Sigma$ electronic ground state, and that the dissociation proceeds without an activation barrier.

The dissociation of the $^2\Pi_g$ resonance is symmetry-forbidden in the linear geometry, but is made possible by vibronic coupling between the π^* and the σ^* resonances which makes it bent [12–14]. The situation, where vibronic coupling in negative ion resonances leads to symmetry lowering which opens a barrier-free path for a nominally forbidden dissociation, is quite common. It was encountered for example in chlorobenzene [19]. The large autodetachment width of the $^2\Pi_g$ shape resonance, revealed by the absence of vibrational (boomerang) structure in the vibrational excitation cross section [13], and the necessity of the hydrogen atom to move out of the linear geometry in the course of the dissociation result in an unfavorable dissociation-autodetachment competition and explain the small magnitude of the cross section and the large observed H or D isotope effect of $\geq$11 [15].

TABLE II. Threshold energies (eV).

Target	Products	Calc.[a]	Expt.
C_2H_2	C_2H^-+H	2.70	2.744 ± 0.007[b]
	$C_2^-+H_2$	2.81	
	C_2^-+H+H	7.4	
C_4H_2	C_4H^-+H	2.07	1.94 ± 0.08[c]
	$C_4^-+H_2$	3.50	
	C_4^-+H+H	8.1	
	$C_2H^-+C_2H$	4.0	
	$C_2^-+C_2H_2$	2.93	
	$C_2^-+C_2H+H$	8.7	

[a]Using the Beeke three-parameter Lee-Yang-Parr hybrid functional 6–311 and Gaussian $(2df,2p)$ model as in Ref. [9].
[b]Calculated from the electron affinity of C_2H and the C—H bond dissociation energy ([20] and references therein).
[c]Calculated from the experimental gas phase acidity [20].

Vibrational excitation revealed a broad $^2\Sigma_g$ core excited resonance extending from about 4.8 to 7.7 eV and peaking at 6.2 eV [13], as indicated in Fig. 1, but the observed 7.45 eV C_2H^- band is higher in energy and cannot be assigned to this resonance. The energy and width of the 7.45 eV C_2H^- band is reminiscent of the $^1\Delta_u$ (π,π^*) band in the energy-loss spectrum of acetylene [14]. Dissociative electron attachment bands which have nearly the same energy as, and resemble in shape, low-lying singlet valence excited states of the target molecule have been found in a number of unsaturated compounds and assigned to resonances where an *s*-like electron is weakly bound to a valence-excited core [21,22]. The 7.45 eV dissociative attachment band of acetylene is probably of this type—associated with the $^1\Delta_u$ excited state of C_2H_2.

The 8.1 eV C_2^- band has vibrational structure when recorded with higher resolution and has been assigned to several Feshbach resonances with a hole in the π_u orbital and two electrons in Rydberg-like 3*s* and/or 3*p* orbitals [14,16].

The dashed curve in Fig. 2 shows the absolute data, without mass resolution, for diacetylene. The figure shows also the yield of the C_4H^- fragment measured by the mass resolved experiment and normalized to the absolute measurement. It reveals a lower-lying band peaking at 2.5 eV which is too weak to be visible in the absolute measurement.

Independent information on the diacetylene resonances was obtained from transmission and vibrational excitation spectra [23]. These methods identified a $^2\Pi_u$ shape resonance due to a temporary occupation of the π_u LUMO of diacetylene, peaking at 1.0 eV and extending from about 0.6 to 2.2 eV, as indicated in Fig. 2. This resonance has a longer

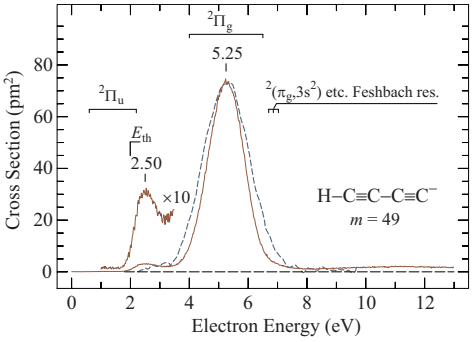

FIG. 2. (Color online) Yield of the mass 49 fragment from diacetylene. The dashed curve is the absolute data, the continuous curve is the relative, mass resolved measurement, normalized to the absolute measurement at 5.25 eV. The threshold energy E_{th}, and the positions of the $^2\Pi_u$, $^2\Pi_g$, and the Feshbach resonances are indicated.

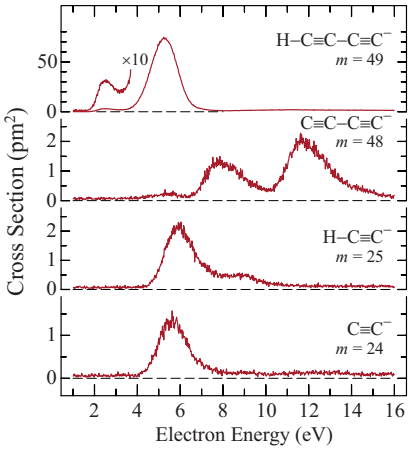

FIG. 3. (Color online) Yields of fragment of various masses from diacetylene. The data was normalized to the absolute measurement shown in Fig. 2 using the relative count rates.

lifetime (slower autodetachment) than $^2\Pi_g$ resonance of acetylene, as indicated by boomerang (vibrational) structure [23]. A second, broader resonance has been found in the transmission spectrum, peaking at 5.6 eV and assigned as a predominantly shape $^2\Pi_g$ resonance. The singly occupied orbitals of these two resonances are approximately the in-phase and out-of-phase combinations of the acetylene LUMO.

The onset of the C_4H^- production (Fig. 2) coincides with the energetic threshold of the process (E_{th}=2.07 eV, Table II), which is about 1 eV above the peak of the $^2\Pi_u$ resonance. The influence of this resonance extends well above its peak, however, because of its Franck-Condon and autodetachment widths, and the 2.5 eV C_4H^- band can be assigned as being mediated by the high-energy tail of the $^2\Pi_u$ resonance. As in the case of acetylene, the C_4H^- ion is produced in its $^1\Sigma$ electronic ground state and the dissociation is symmetry-forbidden in the linear geometry. It is made possible by vibronic coupling between the π^* and the σ^* resonances which makes the $^2\Pi_u$ resonance bent. Evidence for the bent geometry was obtained already from the fact that it caused strong excitation of bending vibration [23].

The peak value of the cross section at 2.5 eV is comparable to that of the 2.95 eV band in acetylene. This is presumably the result of compensation of two effects: (i) The longer autodetachment lifetime of the $^2\Pi_u$ resonance in diacetylene as compared to the $^2\Pi_g$ resonance of acetylene tends to increase the cross section. (ii) The fact that the center of the $^2\Pi_u$ resonance in diacetylene is situated well below the dissociative electron attachment threshold decreases the cross section.

The assignment of the 5.25 eV band is less certain. In terms of energy the band coincides with the expected position of the $^2\Pi_g$ shape resonance, with a temporary occupation of a MO consisting essentially of the out-of-phase combination of the two acetylene π^* MOs. Because of its high energy this shape resonance is expected to have a large autodetachment width, however, and the large magnitude of the dissociative electron attachment cross section indicates a resonance with a slower autodetachment, such as a core excited resonance. In fact, the $^2\Pi_g$ shape resonance is energetically close to low-lying electronically excited states which could serve as parent states for core excited resonances. In particular, it nearly coincides with the $^1\Delta_u$ (HOMO→LUMO) valence-excited state with a vertical transition energy of 5.5 eV [24]. Two core-excited resonances, one consisting of an *s*-like electron around the $^1\Delta_u$ excited state, the other having the configuration $^2(\pi_g,\pi_u^2)^2\Pi_g$, are consequently expected near 5.5 eV. The latter of these two resonances has the right symmetry to mix with the $^2\Pi_g$ shape resonance configuration, so that the nominally shape resonance probably involves mixing of a "single particle" and a core excited "two particles–one hole" configurations.

About 3.25 eV excess energy are available at the 5.25 eV band and part of the C_4H^- ions could thus be formed in an excited state, in particular the $^1A'$ dipole bound state studied by Pino *et al.* [25] and Pachkov *et al.* [26]. Their rotationally resolved spectra showed that the C_4H^- ion in this state is non-linear and consists of an electron loosely bound to the $C_4H^{\cdot}$ radical in its A $^2\Pi$ excited state which has a large dipole moment of 5D. The ground vibrational level lies about 70 cm^{-1} (9 meV) below the detachment threshold (which is equal to the electron affinity, 3.56 eV [25,27,28]).

Spectra of other fragments formed in electron collisions with diacetylene are shown in Fig. 3. The cross sections were too low for direct measurement of the absolute values with the instrument (b), but the relative count rates from instrument (a) were normalized to the absolute value of the C_4H^- production at 5.25 eV. The energetic thresholds (Table II) indicate that the acetylene molecule (and not C_2H+H) must be formed as the neutral fragment to accompany C_2^-. This is surprising because a long shift of a hydrogen atom is required. Similarly, the formation of C_4^- below 8.1 eV requires that H_2 is the neutral fragment and not two H atoms. A broad H^- band peaking at about 8.5 eV, about 5× weaker than the highest C_4^- band, was also observed but is not shown in Fig. 3.

In conclusion, dissociative electron attachment to acetylene and diacetylene yields the C_2H^- and C_4H^- ions at energies below about 3.5 eV, relevant in discharge conditions.

The cross sections have similar magnitudes in both compounds, but this is a result of two opposing effects. In comparison with acetylene, the lowest shape resonance in diacetylene has a slower autodetachment rate, favoring dissociation, but it is at a lower energy, resulting in a less favorable overlap with the dissociative electron attachment threshold. The signals appear at their energetic thresholds, indicating absence of barrier along the dissociation path despite the fact that the dissociation of the $^2\Pi$ resonances is *a priori* forbidden in the linear geometry. The magnitudes of the cross sections at these low-energy bands are much smaller than, for example, that for the O^- production from N_2O (Table I). Ion-molecule reactions, such as proton abstraction by a strong base, may thus be an important alternate path for the formation of the C_4H^- ion in discharges. To test this possibility, we carried out the experiment in the instrument (a) with a mixture of diacetylene and CO_2 in the target chamber. In this way we prepared O^- ions *in situ* at 4.4 and 8.1 eV electron energy (Ref. [10] and Table I), and observed a strong C_4H^- signal at these energies, which must result from $O^-+C_4H_2$ collisions.

Diacetylene has a second band at 5.25 eV, with an about 20× larger cross section. The larger cross section at this band is probably a consequence of contribution of core-excited resonances, which are energetically lower in diacetylene because of the lower-lying parent excited states of the target molecule, and which typically have slower autodetachment rates. This band is less relevant under discharge conditions where electron energy distribution peaks at 1–2 eV, however.

We thank to John P. Maier and to Jacques Lecoultre for a generous sample of diacetylene. We also thank John P. Maier and Sandra Brünken for inspiring discussions. This research is part of the Swiss National Science Foundation Project No. 200020-113599/1 and of COST Action CM0601.

[1] M. C. McCarthy, C. A. Gottlieb, H. Gupta, and P. Thaddeus, Astrophys. J. Lett. **652**, L141 (2006).
[2] J. Cernicharo, M. Guelin, M. Agundez, K. Kawaguchi, M. McCarthy, and P. Thaddeus, Astrophys. J. Lett. **467**, L37 (2007).
[3] S. Brünken, H. Gupta, C. A. Gottlieb, M. C. McCarthy, and P. Thaddeus, Astrophys. J. Lett. **664**, L43 (2007).
[4] K. Kawaguchi, R. Fujimori, S. Aimi, S. Takano, E. Y. Okabayashi, H. Gupta, S. Brünken, C. A. Gootlieb, M. C. McCarthy, and P. Thaddeus, Publ. Astron. Soc. Jpn. **59**, L47 (2007).
[5] H. Gupta, S. Brünken, F. Tamassia, C. A. Gottlieb, M. C. McCarthy, and P. Thaddeus, Astrophys. J. Lett. **655**, L57 (2007).
[6] D. E. Shemansky, A. I. F. Stewart, R. A. West, L. W. Esposito, J. T. Hallett, and X. Liu, Science **308**, 978 (2005).
[7] M. Burgdorf, G. Orton, J. van Cleve, V. Meadows, and J. Houck, Icarus **184**, 634 (2006).
[8] H. Gueniche, P. Glaude, R. Fournet, and F. Battin-Leclerc, Combust. Flame **151**, 245 (2007).
[9] B. C. Ibănescu, O. May, A. Monney, and M. Allan, Phys. Chem. Chem. Phys. **9**, 3163 (2007).
[10] D. Rapp and D. D. Briglia, J. Chem. Phys. **43**, 1480 (1965).
[11] A. Aflatooni and P. D. Burrow, J. Chem. Phys. **113**, 1455 (2000).
[12] S. T. Chourou and A. E. Orel, Phys. Rev. A (to be published).
[13] L. Andrić and R. I. Hall, J. Phys. B **21**, 355 (1988).
[14] R. Dressler and M. Allan, J. Chem. Phys. **87**, 4510 (1987).
[15] R. Azria and F. Fiquet-Fayard, J. Phys. (Paris) **33**, 663 (1972).
[16] R. Abouaf, L. Andrić, R. Azria, and M. Tronc, in *Proceedings of the 12th International Conference on the Physics of Electronic and Atomic Collisions*, edited by S. Datz (North-Holland, Amsterdam, 1981), p. 409.
[17] M. Allan and L. Andrić, J. Chem. Phys. **105**, 3559 (1996).
[18] I. C. Walker, A. Stamatovic, and S. F. Wong, J. Chem. Phys. **69**, 5532 (1978).
[19] T. Skalický and M. Allan, J. Phys. B **37**, 4849 (2004).
[20] Y. Shi and K. M. Ervin, Chem. Phys. Lett. **318**, 149 (2000).
[21] R. A. Dressler, M. Allan, and M. Tronc, Chem. Phys. **20**, 393 (1987).
[22] V. I. Khvostenko, A. S. Vorob'yov, and O. G. Khvostenko, J. Phys. B **23**, 1975 (1990).
[23] M. Allan, Chem. Phys. **86**, 303 (1984).
[24] M. Allan, J. Chem. Phys. **80**, 6020 (1984).
[25] T. Pino, M. Tulej, F. Güthe, M. Pachkov, and J. P. Maier, J. Chem. Phys. **116**, 6126 (2002).
[26] M. Pachkov, T. Pino, M. Tulej, F. Güthe, K. Tikhomirov, and J. P. Maier, Mol. Phys. **101**, 538 (2003).
[27] T. R. Taylor, C. Xu, and D. M. Neumark, J. Chem. Phys. **108**, 10018 (1998).
[28] J. Zhou, E. Garand, and D. M. Neumark, J. Chem. Phys. **127**, 154320 (2007).

8.2 Ion molecule reactions between O^- and diacetylene

This section is devoted to the study of an alternative path of generating the C_4H^- ion, by an ion-molecule reaction. The very small value of the DEA cross section reported in the previous section indicates that ion - molecule reactions may represent the dominant path of $H{-}C{\equiv}C{-}C{\equiv}C^-$ formation in plasmas. Ion-molecule reaction were observed in an earlier version of the present instrument, whereby a proton was abstracted from acetaldehyde by O^- [100]. Since the diacetylene hydrogen is weakly acidic, it could be abstracted by a strong base like the O^- ion, as indicated by the reaction scheme shown in fig. 8.1.

$$O^- + HC{\equiv}C{-}C{\equiv}CH \longrightarrow OH^{\cdot} + HC{\equiv}C{-}C{\equiv}C^-$$

Figure 8.1: Reaction Scheme for the ion-molecule reaction in the CO_2 - C_4H_2 system.

We prepared the O^- ion *in situ*, in the target chamber, by DEA to CO_2. The two channels of $H{-}C{\equiv}C{-}C{\equiv}C^-$ formation are distinguished by electron energy: direct DEA has a weak band at 2.5 eV and a stronger band at 5.25 eV, whereas O^- formation from CO_2 has bands at 4.2 and 8.2 eV.

The experiment consists of measuring the yields, as a function of electron energy, of the O^- ion and the $H{-}C{\equiv}C{-}C{\equiv}C^-$ ion from gas mixtures with a constant diacetylene pressure and an increasing pressure of CO_2, as shown in fig. 8.2.

Table 8.1: Pressure measured with the Penning gauge. The pressure in the target chamber is inferred from the value measured by the penning gauge. The partial pressure of CO_2 is calculated as a difference between the pressure in the target chamber when CO_2 is present and when it is missing. The values are in mbar.

Condition	Penning Gauge	Pressure in the target chamber	Pressure of CO_2
(a)	$1 \cdot 10^{-7}$	$3 \cdot 10^{-4}$	0
(b)	$5 \cdot 10^{-7}$	$1.5 \cdot 10^{-3}$	$1.2 \cdot 10^{-3}$
(c)	$1 \cdot 10^{-6}$	$3 \cdot 10^{-3}$	$2.7 \cdot 10^{-3}$
(d)	$2.5 \cdot 10^{-6}$	$7.5 \cdot 10^{-3}$	$7.2 \cdot 10^{-3}$
(e)	$4.7 \cdot 10^{-6}$	$1.41 \cdot 10^{-2}$	$1.38 \cdot 10^{-2}$

The experiment is not quantitative because the instrument is not equipped for measurements of absolute pressures in the target chamber. At the time when this experiment was performed, the pressure could be measured by a Penning gauge in the main vacuum chamber (*i.e.*, a reading $3 \cdot 10^3$ lower than in the target chamber, determined based on the geometrical characteristics of the target chamber), and by a capacitance gauge in the gas inlet system (*i.e.*, a reading higher than in the target chamber because of the pressure drop along the gas line). Further complication is the gas-type dependence of the readings of the Penning gauge and the fact that the correction factors are not known for diacetylene. The pressure reading of the

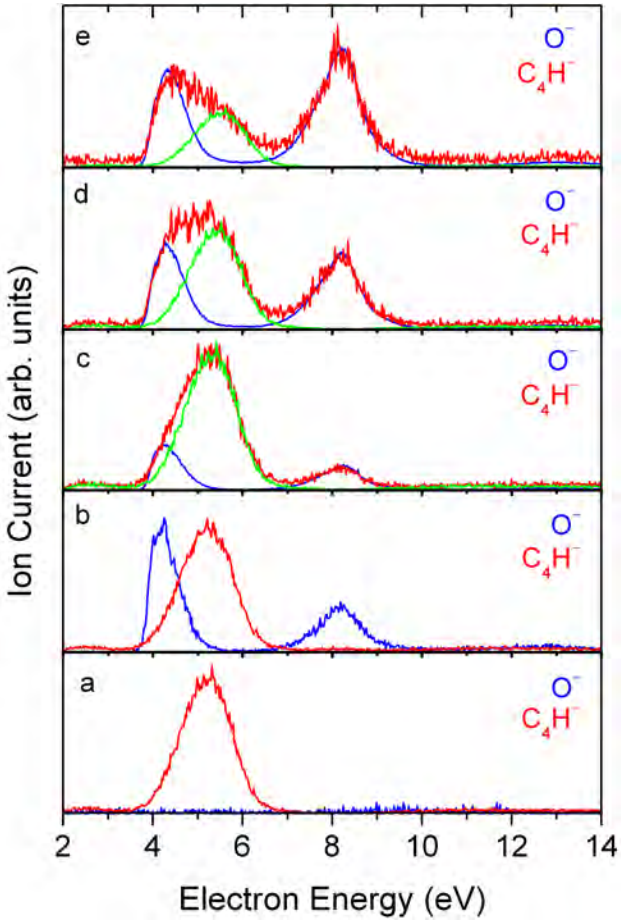

Figure 8.2: Yields of O^- (blue) and C_4H^- (red) from pure diacetylene (a) and diacetylene/CO_2 mixtures with increasing partial pressures of CO_2 (b)-(e). As a guide to the eye, the C_4H^- yield from pure diacetylene is repeated as a green line in the sections (c)-(e) of the figure.

Penning gauge together with the inferred pressure in the target chamber and the partial pressure of CO_2 are indicated in table 8.1.

Diacetylene and CO_2 were introduced into the target chamber through two separate needle valves. Diacetylene needle valve was opened first until the DEA spectrum of C_4H^- was obtained. The pressure in the target chamber is estimated to be around $3 \cdot 10^{-4}$ mbar at this point (case (a) in table 8.1 and fig. 8.2). The corresponding spectrum of the C_4H^- ion, fig. 8.2(a), is characteristic of pure diacetylene and is identical to that shown in fig. 3 of the article in the preceding section. It was verified that no O^- is observed under these conditions (blue line in Fig 8.2(a)).

The diacetylene needle valve was left in a constant position, so that the diacetylene partial pressure was constant in the subsequent experiments. The CO_2 needle valve was then opened in four steps, resulting in gas mixtures with increasing CO_2 partial pressures, as indicated by the reading (b)-(e) of table 8.1. The partial pressure of CO_2 were calculated as the difference between the pressure in the target chamber when CO_2 is introduced and the pressure in the target chamber when only

diacetylene is present.

In the case (b) the CO_2 pressure and consequently the amount of O^- are low, and there is no evidence for an ion-molecule reaction – the C_4H^- spectrum is that of pure diacetylene and the O^- spectrum that of pure CO_2. At the highest CO_2 pressure, in the case (e), the C_4H^- spectrum is dominated by ion-molecule reaction – the strongest C_4H^- band coincides with the formation of O^- from CO_2. C_4H^- from direct DEA to diacetylene appears only as a shoulder at 5.5 eV in the red line in Fig. 8.2(e). The spectra (c) and (d) are intermediate between the cases (b) and (e).

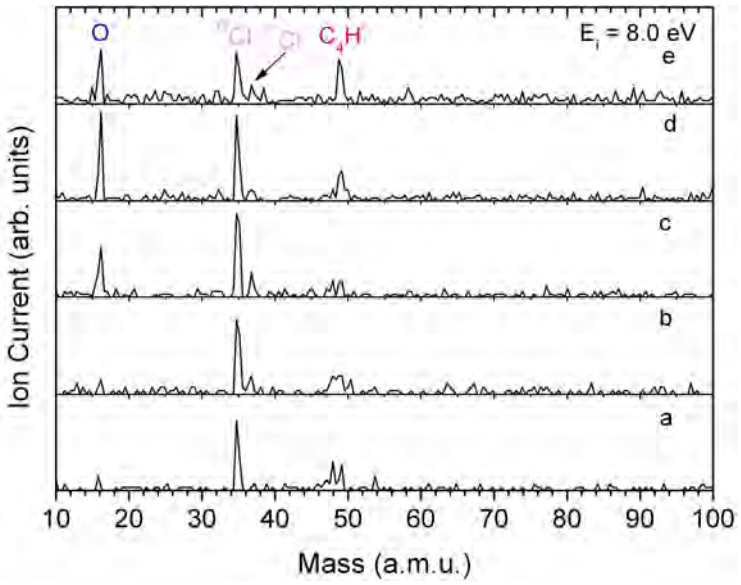

Figure 8.3: Mass spectra recorded at an incident energy of 8.0 eV and with various mixtures. The pressures are indicated in table 8.1. The ions of interest are marked on the top panel.

We have not been able to identify other ion - molecule reactions in our system. This can be observed from the mass spectra recorded at various pressures as shown in fig. 8.3. The mass spectra reveal only the presence of the O^-, $^{35}Cl^-$, $^{37}Cl^-$ and C_4H^- ions. The two chlorine ions are, unfortunately, impurities in our experimental setup and, although our system has been pumped out for several months, due to the high cross section for the formation of these ions the ion signal for the chlorine ions remains quite high even at these very low concentrations.

The O^-/CO_2 cross section is about 40 pm^2 (see the preceding section). This means that at a CO_2 pressure of $7.2 \cdot 10^{-3}$ mbars in the target chamber, and an electron beam current of 26 nA, we generate an O^- current of about 30 pA over a length of 2 mm (which is approximately the length from which ions are collected by the ion extractor). That means, that the O^- current is about $10^3\times$ weaker than the electron current. The ion-molecule reaction cross section must be roughly $10^3\times$ larger than the C_4H^-/C_4H_2 DEA cross section for the direct and ion/molecule processes yielding comparable C_2H^- currents as observed in Fig 8.2. Its value must

thus be of the order of $75 \cdot 10^3$ pm^2. It is most likely dependent on the kinetic energy of the O^- ion.

We conclude that ion - molecule reactions occur in the $CO_2-C_4H_2$ mixture. This indicates that, despite the fact that the magnitudes of the cross sections for DEA of diacetylene [38] are much smaller when compared to that for the O^- production from N_2O or CO_2, the formation of the C_4H^- can be increased in discharge experiments through ion - molecule reactions, such as the proton abstraction by a strong base.

Chapter 9

Conclusions

Dissociative attachment processes were studied for more than 60 saturated compounds ranging from alcohols to ethers, thiols. These studies were complemented by *ab initio* calculations giving insight into the dissociation mechanism in alcohols and ethers. Two different theoretical methods were used: TD-DFT method was used to calculate the parent excited states of the molecule and R-matrix method was used for the calculation of the Feshbach resonances.

In the case of alcohols, our studies reveal new weaker processes at lower energies, around 3 eV. They have a steep onset at the dissociation threshold and show a dramatic D/H isotope effect. We assigned them as proceeding *via* shape resonances with temporary occupation of σ^*_{OH} orbitals. These low energy fragmentations become much stronger in the larger molecules and the strongest DEA process in the compounds with two hydroxyl groups, which thus represent an intermediate case between the behavior of small alcohols and the sugar ribose which was discovered to have strong DEA fragmentations near zero electron energy [101].

Above 6 eV, in the Feshbach resonance regime, the dominant process is a fast loss of a hydrogen atom from the hydroxyl group, leading to the formation of $(M-1)^-$ ion. In some cases the resulting $(M-1)^-$ anion is sufficiently energy-rich to further dissociate by loss of stable, closed shell molecules. The fast primary process is state- and site selective in several cases, the negative ion states with a hole in the n_O orbital losing the OH hydrogen, those with a hole in the σ_{CH} orbitals the alkyl hydrogen.

One frequent dissociation reaction undergone by alcohols is the loss of an hydrogen atom, followed by an additional loss of H_2 molecule with the formation of a $(M-3)^-$ anion. The DEA results obtained for the partially deuterated ethanol, ethanol-d_3, CH_3CH_2OH, and for *tert*-butanol reveal that one hydrogen is lost from α-carbon and the other from β-carbon. The conclusion is supported, for ethanol-d_3, by the mass of the detected fragments and by the remarkable similarity of the DEA spectra of fragments from ethanol-d_3 and those from undeuterated ethanol, resulting from an identical process.

The present experimental setup does not measure absolute cross-sections but the relative cross-sections can be determined for various methanol and ethanol iso-

topomers by recording signal intensities for the same pressure (same Penning gauge reading) and the same electron beam current. The analysis of the fragment yields, as a function of deuteration, reveals interesting isotope effects for the bands in the region where Feshbach resonances have been detected. For methanol, the DEA processes show an inverse isotope effect for the bands in the Feshbach resonance region, with the highest yield being observed for methanol-d_4. The relative intensities of the three methanolate bands in the 612 eV range (*i.e.*, the shape of the spectrum in this energy range) also depend to some degree on deuteration. For ethanol, we observe a strong isotope effect for the main fragments with the exception of H^- ion, for the 6-14 eV region.

As already discussed above, the DEA spectra of alcohols and of other polyatomic molecules, can be divided into a low energy domain, between zero and about 5 eV where dissociation is dominated by shape resonances, and a high energy domain, about $5 - 14$ eV where dissociation occurs mostly through Feshbach resonances. In the first energy domain a linear dependence exists between the ion yield for the $(M-1)^-$ anion and the pressure in the target chamber. We conclude that the band associated with the shape resonance is not affected by ion-molecule reactions. For the high energy domain our work reveals that the dependence of the ion yield of the $(M-1)^-$ fragment on pressure is non-linear already above $1.5 \cdot 10^{-4}$ mbar in the target chamber. We conclude that above this pressure there are secondary ion-molecule reactions that cause the dependence on pressure to deviate from linearity. In the case of methanol O^- abstracts a proton from the neutral methanol forming CH_3O^-, while for ethanol the removal of a proton is done by the OH^- fragment, with the formation of the ethanolate anion.

A striking difference is observed between the fragmentation pattern of cyclic ethers, such as tetrahydrofuran, and that of linear ethers, such as diethylether or dibutylether. The cleavage of the C−O bond by electron yielded $CH_3CH_2O^-$ at 9.1 eV in diethylether and $CH_3(CH_2)_3O^-$ at 8.0 eV in dibutylether. In contrast in tetrahydrofuran breaking of the C−O bond yielded mainly a fragment of mass 41, presumably deprotonated ketene, at 7.65 eV. The rationalization of this observation is based on the fact that in open-chain ethers the excess energy is partitioned between the (internal and kinetic) energies of two fragments, resulting in an ion cool enough to be observed. The ion resulting from cleavage of the CO bond in THF contains the entire excess energy (more than 6 eV at an electron energy of 7.65 eV) and is too short-lived with respect to further dissociation and thermal autodetachment to be detected in a mass spectrometer. These findings imply that there could be a substantial difference between the fragmentation in the gas phase described here and fragmentation in the condensed phase where the initially formed fragments can be rapidly cooled by the environment.

An analysis of the dissociation *via* Feshbach resonances is performed in various compounds with C−O bonds. In these substances the O−C bond breaking is one of the major pathway of dissociation. The bond breaking occurs only at specific energies, dependent on the alkyl fragment that is lost and not on the target molecule. This empirical rule indicates that the Feshbach resonances responsible for the fragmentation are spatially localized on one or the other alkyl group. We observe that

the methyl group can be used as a protective group, to steer the fragmentation in a controlled manner. These conclusions are verified in more complex saturated compounds such as monoethers and diethers of ethylene glycol. A comparison with the published data on unsaturated ethers [102] reveals that conclusions derived from saturated ethers can be extended to the unsaturated ones when the ether oxygen and the π system are directly linked. A $(n, 3s^2)$ resonance is observed around 6.5 eV, but, unlike in saturated ethers, this resonance appears to cleave the C−O bond when the C atom is an sp^2-hybridized carbon of the allyl group. This resonance does not, however, cleave the C−O bond when the C atom is sp^3-hybridized in the ethyl group, confirming the conclusions reached in this work. A loss of ethyl radical from ethyl vinyl ether has a broad band around 9.1 eV, the same energy as loss of ethyl radical in numerous saturated alcohols and ethers presented in this work. Finally, the loss of the neutral methyl radical has not been observed in methyl vinyl ether, reinforcing the conclusion that the methyl group can be used as a protective group.

The study of alcohols revealed that DEA measurements can be affected by ion-molecule reactions above a certain pressure in the target chamber. A similar study is performed on a different molecule, diacetylene, where we determined an alternative path of generating the C_4H^- ion, by an ion-molecule reaction. We have detected additional C_4H^- ions formed at 4 eV due to the deprotonation of the diacetylene by the O^- ion. This can be clearly observed in the fitted DEA spectrum of C_4H^- ion. This spectrum allowed the calculation of the cross section for the deprotonation of the diacetylene. We conclude that, despite the fact that the magnitudes of the cross sections for the diacetylene [38] are much smaller when compared to that for the O^- production from N_2O or CO_2, the formation of the C_4H^- can be increased in discharge experiments through ion - molecule reactions, such as the proton abstraction by a strong base.

A qualitative difference was observed in the reactivity of alcohols and ethers toward free electrons. Whereas the lowest core-excited state of the negative ion, a $^2(n, 3s^2)$ Feshbach resonance, of the alcohols readily dissociates by losing a hydrogen atom, ethers show no observable signal from this resonance. This difference in reactivity has a parallel in the anomalous shapes and energies of the parent states of the Feshbach resonances, the $^1(n, 3s)$ Rydberg states of the neutral alcohols. We explained this anomaly using potential surfaces of the alcohols and ethers calculated using the TD-DFT method as a function of the dissociation coordinate. The lowest excited state of alcohols was found to be repulsive, whereas a barrier to dissociation was found in the ethers. Rydberg-valence mixing and avoided crossings are decisive in determining the shapes of the potential surfaces. It is concluded that the reactivities of alcohols and ethers toward free electrons are rationalized by assuming that the potential surfaces of the daughter Feshbach resonances closely follow those of the parent Rydberg states, *i.e.*, the lowest Feshbach resonance is repulsive, but a barrier occurs in ethers. The potential surfaces of both the Rydberg states and the Feshbach resonances thus differ dramatically from the non-dissociative surface of the grandparent $^2(n^{-1})$ positive ions, despite the nominally non-bonding character of the Rydberg electrons.

It was desirable to verify the central assumption required for the above conclu-

sion by calculation the potential surfaces of the Feshbach resonances. An attempt to calculate the Feshbach resonances is presented, using R-matrix method. The theoretical treatment of dissociative attachment processes is more complicated than of processes like photodissociation because they occur on a complex potential surface characterized by a width, Γ, and an energy, E_R, which are functions of the internuclear geometry, $\vec{q}$ [1]. Despite the very large body of experimental results on DEA virtually nothing is known about the detailed mechanism of the dissociation of Feshbach resonances, in particular in polyatomic molecules. A notable exception are the recent calculations on small molecules like H_2O [1, 2] and C_2H_2 [34]. Unfortunately the methods developed for these molecules are too time expensive and computational facilities powerful enough do not exist, to be applicable to larger molecules. We present *ab initio* calculations on larger molecules such as CH_3OH, or C_2H_5OH using the R-matrix method.

There are some positive aspects shown by the present set of R-matrix calculations, Despite the fact that they indicate two possible scenarios. Both cases indicate that the first resonance should be non-dissociative when the O−C bond is stretched, in agreement with the experimental observation. In addition, for the dissociation of the O−H bond the potential energy surface of the resonances are distinctly different, being repulsive and thus supporting the experimental observation. Another positive aspect shown by these results is that, with the exception of the longer O−C bond lengths, the potential energy curves for the Feshbach resonances follow those of their parent Rydberg states. This is an indication that the central assumption is true. The results reported here indicate a need for further testing and development of the R-matrix method and they could be the basis for new calculations with a different method such as the complex Kohn variational method used for water [1] and acetylene [34].

The DEA results presented in this work offer an overview over a wide range of saturated compounds with oxygen. Some trends are observed that are applicable to alcohols but also to all compounds with ether bonds. They offer the possibility of state and site selective chemistry and can be used to control the reactions with the help of electrons. This work can be continued by observing if similar trends exist in other classes of saturated compounds such as amines, thiols or disulfides.

The DEA spectra of compounds with oxygen show the presence of one or more shape resonances in the 0-4 eV energy range. In contrast, no shape resonance have been detected in the spectra of amines. For alcohols and ethers we observed n- and $\bar{n}$-Feshbach resonances, while for amines we detect only one n-Feshbach resonance. This resonance is lower in energy, to 4.5-5.0 eV, than in oxygen containing compounds.

There are also some similarities between compounds with oxygen and those with nitrogen. In both cases the energy relations exist between the positive core observed in photoelectron spectrum and the Feshbach resonances observed in DEA spectrum. The observation that the cleavage of the O−C bond is mediated only by σ-Feshbach resonances while the breaking the O−H bond is mediated by both n- and σ-Feshbach resonances. Similarly the N-H bond breaking is mediated by both types of Feshbach resonances while the cleavage of the N−C bond is mediated

by only σ-Feshbach resonances. In alcohols we have shown that most likely an activation barrier present on the potential surface of the parent Rydberg states is responsible for the selectivity. Accordingly in amines we assumed that a similar activation barrier must exist and be responsible for the selective breaking of the bonds.

An extension to this rule is provided by the study of amines that contain at least one N-H bond. In these amines the N-C bond is dissociated even by the n-Feshbach resonance, an indication for the lowering of the activation barrier otherwise present on the potential surface of this resonance. This case is particular for nitrogen containing compounds and it has not been encountered in alcohols, where the presence of an O−H bond in the molecule does not lead to a lowering of the activation barrier and thus to an observable DEA band in the 6-7 eV range.

Another similarity between the dissociation of alcohols and amines is the selectivity within the manifold of the σ-Feshbach resonance. In compounds with oxygen out of the many σ-Feshbach resonances present in the 7-16 eV region only the resonance that is localized on the alkyl group drives the dissociation. Thus the energy of the resonance depends only on the alkyl group and not on the primary molecule. A similar case is encountered in amines where loss of ethyl radical occurs preferentially through a Feshbach resonance at 8.3 eV, while the butyl radical is lost through a Feshbach resonance at 7.7 eV.

A preliminary study of dissociative attachment for compounds with S−H bond was performed on ethanethiol. The DEA spectra of this model molecule are completely different than the spectra of oxygen or nitrogen containing compounds. They seem to be dominated by resonances in the 0-3 eV region. The capture mechanism of the electron to form these resonances is unclear at the moment but they are responsible for breaking of the S−H bond. In the case of the C−S bond the main mechanism of dissociation is driven most likely by Feshbach resonances. This leads to a clear separation of the type of dissociation, with S−H bonds being broken preferentially in the 0-3 eV range and C−S are broken in the 7-15 eV region. Unfortunately the selectivity is not restricted to the formation of one ion, but rather to the bond that is broken in the dissociation.

Bibliography

[1] D. J. Haxton, T. N. Rescigno, and C. W. McCurdy, *Phys. Rev. A*, 2007, **75**, 012710/1–012710/25.

[2] D. J. Haxton, T. N. Rescigno, and C. W. McCurdy, *Phys. Rev. A*, 2007, **75**, 012711/1–012711/24.

[3] B. Boudaiffa, P. Cloutier, D. Hunting, M. A. Huels, and L. Sanche, *Science*, 2000, **287**, 1658.

[4] H. Tanaka and M. Inokuti, *Advances in At., Mol. and Opt. Phys.*, 2000, **43**, 1–17.

[5] S.-W. Hla, L. Bartels, G. Meyer, and K.-H. Rieder, *Phys. Rev. Lett.*, 2000, **85**, 2777 – 2780.

[6] I. Utke, V. Friedli, M. Purrucker, and J. Michler, *J. Vac. Sci. Technol.*, 2007, **25**(6), 2219–2223.

[7] A. Dalgano, *Adv. At. Mol. Phys.*, 1968, **4**, 381.

[8] K. Takayanagi and Y. Itikawa, *Space Science Review*, 1970, **11**, 380.

[9] A. Dalgano and R. McCray, *Annu. Rev. Astron. Astrophys.*, 1972, **10**, 379.

[10] P. Thaddeus, *Astrophys. J.*, 1972, **173**, 317.

[11] A. Dickinson, *J. Phys. B*, 1977, **10**, 967.

[12] M. Yan and A. Dalgarno, *Astrophys. J.*, 1998, **500**, 1049.

[13] K. Houfek, M. Cizek, and J. Horacek, *Czech. J. Phys.*, 2002, **52**, 29.

[14] E. Illenberger and P. Swiderek, *Eur. Phys. J. D*, 2005, **35**, 173176.

[15] J. McConkey, C. Malone, P. Johnson, C. Winstead, V. McKoy, and I. Kanik, *Physics Reports*, 2008, **466**, 1–103.

[16] J. Franck and G. Hertz, *Verh. Dtsch. Phys. Ges*, 1914, **16**, 457.

[17] M. Allan, *J. Electron Spectrosc. Relat. Phenom.*, 1989, **48**, 219.

[18] G. J. Schulz, *Rev. Mod. Phys.*, 1973, **45**, 423–486.

[19] H. Hotop, M.-W. Ruf, M. Allan, and I. I. Fabrikant, *Adv. At. Mol. Opt. Phys.*, 2003, **49**, 85–216.

[20] M. Allan and T. Skalický, *J. Phys. B*, 2003, **36**, 3397–3409.

[21] M. Stepanović, Y. Pariat, and M. Allan, *J. Chem. Phys.*, 1999, **110**, 11376–11382.

[22] T. Skalický and M. Allan, *J. Phys. B*, 2004, **37**, 4849.

[23] M. Stepanovic *Dissociative electron attachment in cyclopentanone γ-Butyrolactone and ethylene carbonate: Role of dipole-bound states* PhD thesis, University of Fribourg, 1998.

[24] K. Franz, T. H. Hoffmann, J. Bömmels, A. Gopalan, G. Sauter, W. Meyer, M. Allan, M.-W. Ruf, and H. Hotop, *Phys. Rev. A*, 2008, **78**(1), 012712/1–012712/16.

[25] L. Sanche and G. J. Schulz, *Phys. Rev. A*, 1972, **5**, 1672–1683.

[26] U. Fano and A. R. P. Rau, *Comm. At. Mol. Phys.*, 1985, **16**, 241–248.

[27] M. B. Robin, *Higher Excited States of Polyatomic Molecules*, Vol. 1, Academic Press, New York, 1974.

[28] L. Sanche and G. J. Schulz, *Phys. Rev. A*, 1972, **6**, 69.

[29] L. Sanche and G. J. Schulz, *J. Chem. Phys.*, 1973, **58**, 479–493.

[30] D. Spence, *J. Phys. B*, 1975, **12**, 721.

[31] D. Spence, *J. Chem. Phys.*, 1977, **66**, 669.

[32] B. C. Ibănescu, O. May, A. Monney, and M. Allan, *Phys. Chem. Chem. Phys.*, 2007, **9**, 3163–3173.

[33] F. Martin, P. D. Burrow, Z. Cai, P. Cloutier, D. Hunting, and L. Sanche, *Phys. Rev. Lett.*, 2004, **93**, 068101.

[34] S. T. Chourou and A. E. Orel, *Phys. Rev. A*, 2008, **77**, 042709/1–042709/10.

[35] B. C. Ibănescu, O. May, and M. Allan, *Phys. Chem. Chem. Phys.*, 2008, **10**, 1507–1511.

[36] B. C. Ibănescu and M. Allan, *submitted*, 2009.

[37] B. C. Ibănescu and M. Allan, *Phys. Chem. Chem. Phys.*, 2008, **10**, 5232 – 5237.

[38] O. May, J. Fedor, B. C. Ibănescu, and M. Allan, *Phys. Rev. A*, 2008, **77**, 040701(R).

[39] R. A. Dressler *The dissociative decay of short-lived polyatomic anions formed by electron impact* PhD thesis, University of Fribourg, 1985.

[40] A. Stamatovic and G. J. Schulz, *Rev. Sci. Instrum.*, 1968, **39**, 1752–1753.

[41] A. Stamatovic and G. J. Schulz, *Rev. Sci. Instrum.*, 1970, **41**, 423–427.

[42] R. Dressler and M. Allan, *Chem. Phys.*, 1985, **92**, 449.

[43] R. Abouaf, R. Paineau, and F. Fiquet-Fayard, *J. Phys. B*, 1976, **4**, 303–314.

[44] D. C. Harris and M. D. Bertolucci, *Symmetry and Spectroscopy: an introduction to vibrational and electronic spectroscopy*, Dover Publications, INC., New York, 1989.

[45] K. Kimura, S. Katsumata, Y. Achiba, T. Yamazaki, and S. Iwata, *Handbook of HeI Photoelectron Spectra of Fundamental Organic Molecules*, Japan Scientific Societies Press, Tokyo, 1981.

[46] J. Eland, *Photoelectron Spectroscopy: An introduction to ultraviolet photoelectron spectroscopy in the gas phase*, Butterworths, London, 1974.

[47] M. J. Frisch, G. W. Trucks, H. B. Schlegel, G. E. Scuseria, M. A. Robb, J. R. Cheeseman, J. A. Montgomery, Jr., T. Vreven, K. N. Kudin, J. C. Burant, J. M. Millam, S. S. Iyengar, J. Tomasi, V. Barone, B. Mennucci, M. Cossi, G. Scalmani, N. Rega, G. A. Petersson, H. Nakatsuji, M. Hada, M. Ehara, K. Toyota, R. Fukuda, J. Hasegawa, M. Ishida, T. Nakajima, Y. Honda, O. Kitao, H. Nakai, M. Klene, X. Li, J. E. Knox, H. P. Hratchian, J. B. Cross, V. Bakken, C. Adamo, J. Jaramillo, R. Gomperts, R. E. Stratmann, O. Yazyev, A. J. Austin, R. Cammi, C. Pomelli, J. W. Ochterski, P. Y. Ayala, K. Morokuma, G. A. Voth, P. Salvador, J. J. Dannenberg, V. G. Zakrzewski, S. Dapprich, A. D. Daniels, M. C. Strain, O. Farkas, D. K. Malick, A. D. Rabuck, K. Raghavachari, J. B. Foresman, J. V. Ortiz, Q. Cui, A. G. Baboul, S. Clifford, J. Cioslowski, B. B. Stefanov, G. Liu, A. Liashenko, P. Piskorz, I. Komaromi, R. L. Martin, D. J. Fox, T. Keith, M. A. Al-Laham, C. Y. Peng, A. Nanayakkara, M. Challacombe, P. M. W. Gill, B. Johnson, W. Chen, M. W. Wong, C. Gonzalez, and J. A. Pople, Gaussian 03, Revision C.01.

[48] E. Illenberger and J. Momigny, *Gaseous Molecular Ions*, Steinkopf Verlag, Darmstadt and Springer Verlag, New York, 1992.

[49] *NIST Chemistry webbook: http://webbook.nist.gov/chemistry.*

[50] J. I. Brauman and L. K. Blair, *J. Am. Chem. Soc.*, 1970, **92**, 5986–5992.

[51] R. Houriet, D. Stahl, and F. Winkler, *Environmental Health Perspectives*, 1980, **36**, 63–68.

[52] G. H. Hudson, J. C. McCoubrey, and A. R. Ubbelohde, *Trans. Faraday Soc.*, 1960, **56**, 1144 – 1151.

[53] T. L. Cottrell, R. A. Hamilton, and R. P. Taubinger, *Trans. Faraday Soc.*, 1956, **52**, 1310–1311.

[54] J. Hirschfelder, C. F. Curtiss, and R. B. Bird, *Molecular Theory of Gases and Liquids*, John Wiley & Sons, 1954.

[55] E. McLaughlin, *Trans. Faraday Soc.*, 1959, **55**, 28–38.

[56] G. A. Cummings, J. C. McCoubrey, and A. R. Ubbelohde, *J. Chem. Soc.*, 1952, **514**, 2725.

[57] A. Kühn, H. P. Fenzlaff, and E. Illenberger, *J. Chem. Phys.*, 1988, **88**, 7453.

[58] S. Ptasinska, S. Denifl, P. Scheier, E. Illenberger, and T. D. Mrk, *Angew. Chem. Int. Ed.*, 2005, **44**(42), 6941–6943.

[59] J. W. Verhoeven, *Pure & Appl. Chem.*, 1996, **68**, 2223–2286.

[60] G. Herzberg and H. C. Longuet-Higgins, *Discuss. Faraday Soc.*, 1963, **35**, 77–82.

[61] M. B. Robin and N. A. Kuebler, *J. Electron Spectrosc. Relat. Phenom.*, 1972, **1**, 13.

[62] M. Parac and S. Grimme, *Chem. Phys.*, 2003, **292**, 1121.

[63] I. Ciofini and C. Adamo, *J. Chem. Phys.*, 2007, **111**, 5549–5556.

[64] A. D. Becke, *J. Chem. Phys.*, 1993, **98**, 1372.

[65] S. Grimme and F. Neeseb, *J. Chem. Phys.*, 2007, **127**, 154116.

[66] Y. Zhao and D. G. Truhlar, *Journal of Physical Chemistry A Letters*, 2006, **110**, 13126–13130.

[67] J. B. Foresman, M. Head-Gordon, J. A. Pople, and M. J. Frisch, *J. Chem. Phys.*, 1992, **96**, 135–149.

[68] M. Head-Gordon, R. J. Rico, M. Oumi, and T. J. Lee, *Chem. Phys. Lett.*, 1994, **219**, 21–29.

[69] D. C. Young, *Computational Chemistry: A Practical Guide for Applying Techniques to Real-World Problems*, John Wiley & Sons, 2001.

[70] V. Huber, K. R. Asmis, A.-C. Sergenton, M. Allan, and S. Grimme, *J. Phys. Chem. A*, 1998, **102**(20), 3524–3531.

[71] M.-J. Hubin-Franskin, J. Delwiche, A. Giuliani, M.-P. Ska, F. Motte-Tollet, I. C. Walker, N. J. Mason, J. M. Gingell, and N. C. Jones, *J. Chem. Phys.*, 2002, **116**, 9261–9268.

[72] J.E.Collin, M. J. Hubin-Franskin, and L. D'Or, *Adv. Mass Spectr.*, 1968, **4**, 713–726.

[73] P. G. Burke, A. Hibbert, and W. D. Robb, *J. Phys. B*, 1971, **4**, 153–161.

[74] P. G. Burke and W. D. Robb, *Adv. At. Mol. Phys.*, 1975, **11**, 143–214.

[75] B. I. Schneider, *Chem. Phys. Lett.*, 1975, **31**, 237.

[76] B. I. Schneider and P. J. Hay, *Phys. Rev. A*, 1976, **13**, 2049.

[77] P. G. Burke, I. Mackey, and I. Schimamura, *J. Phys. B*, 1977, **10**, 2497–2512.

[78] L. A. Morgan, C. J. Gillan, and J. Tennyson, *J. Phys. B*, 1997, **30**, 4087.

[79] P. Burke and K. A. Berrington, *Atomic and Molecular Processes: An R-matrix Approach*, Institute of Physics Publishing, 1993.

[80] L. A. Morgan, J. Tennyson, and C. J. Gillan, *Comput. Phys. Commun.*, 1998, **114**, 120.

[81] J. Tennyson and L. A. Morgan, *Phil. Trans. R. Soc. Lond. A.*, 1999, **357**, 1161.

[82] I. Rozum *Electron collisions with CFx radicals using the R-matrix method* PhD thesis, University College London, 2003.

[83] R. van Harrevelt and M. C. van Hemert, *J. Chem. Phys.*, 2000, **112**, 5777–5787.

[84] D. J. Haxton, C. W. McCurdy, and T. N. Rescigno, *Phys. Rev. A*, 2007, **76**, 049906/1.

[85] D. Bouchiha, J. D. Gorfinkiel, L. G. Caron, and L. Sanche, *J. Phys. B*, 2007, **40**, 1259–1270.

[86] J. Tennyson and C. J. Noble, *Comput. Phys. Commun.*, 1984, **33**, 421–424.

[87] P. W. Atkins and R. Friedman, *Molecular quantum mechanics*, Oxford University Press, 1997.

[88] B. C. Ibănescu and M. Allan, *in preparation.*

[89] F. Fiquet-Fayard, J. P. Ziesel, R. Azria, M. Tronc, and J. Chiari, *J. Chem. Phys.*, 1972, **56**, 2540–2548.

[90] R. Azria, M. Tronc, and S. Goursaud, *J. Chem. Phys.*, 1972, **56**, 4234–4235.

[91] R. Azria, Y. L. Coat, G. Lefevre, and D. Simon, *J. Phys. B*, 1978, **12**, 679–687.

[92] K. Rohr, *J. Phys. B*, 1978, **11**, 4109–4117.

[93] R. Abouaf and D. Teillet-Billy, *Int. J. of Mass Spectr. and Ion Proc.*, 2008, **277**, 79–83.

[94] F. Gianturco and D. Thompson, *J. Phys. B*, 1980, **13**, 613.

[95] A. Jain and D. Thompson, *J. Phys. B*, 1983, **17**, 443.

[96] M. do N. Varella, M. Betega, M. Lima, and L. Ferreira, *J. Chem. Phys.*, 1999, **111**, 6396.

[97] M. Gupta and K. Baluja, *Eur.Phys.J.D.*, 2007, **41**, 475.

[98] D. Haxton, Z. Zhang, C. McCurdy, and T. Rescigno, *Phys. Rev. A*, 2006, **73**, 062724.

[99] D. Chen and G. Gallup, *J. Chem. Phys.*, 1990, **93**, 8893–8901.

[100] R. Dressler and M. Allan, *Journal of Electron Spectroscopy and Related Phenomena*, 1986, **41**(2), 275 – 287.

[101] S. Ptasińska, S. Denifl, P. Scheier, and T. D. Märk, *J. Chem. Phys.*, 2004, **120**, 8505.

[102] C. Bulliard, M. Allan, and S. Grimme, *Int. J. of Mass Spectr. and Ion Proc.*, 2001, **205**, 43–55.

Acknowledgments

I would like to thank my advisor Prof. Michael Allan for providing me with the opportunity to do my PhD work in his research group. His support and invaluable guidance, during the last four years, made my thesis work possible. He has been actively interested in my work and has always been available to advise me. I am very grateful for his patience, motivation, enthusiasm, and his profound knowledge of physical chemistry that, taken together, make him a great mentor. I am especially grateful for the freedom granted to pursue the scientific goals of my particular interest.

I am grateful to Prof. Thomas Bally, Prof. Petra Swiderek and Prof. Peter Belser for correcting and evaluating my thesis work.

I wish to express my gratitude to the members of the 4^{th} *floor* club, namely Matija Zlatar, Florian Senn, Oliver May, Dr. Juraj Fedor, Dr. Pawel Bednarek, Dr. Krzysztof Piech, Dr. Dmytro Dudenko, Mireille Elsen and to many others.

BOGDAN CATALIN IBANESCU

ibanescub@yahoo.co.uk

Married
28 years
Romanian
Place and date of birth:
Iasi, Romania, 12/08/1980

Formation

2005 – 2009	**Phd Student under the supervision of Prof. Michael Allan, Department of Chemistry**, University of Fribourg, Switzerland,
1999 – 2004 First in my series of students	**Diploma engineer**, Major in **Macromolecular Compounds Technology**, Faculty of Industrial Chemistry, "Gh. Asachi" Technical University Iasi, Romania
1995 – 1999	**Baccalaureate - computer programmer**, "Gr. Moisil" Computer High School, Iasi, Romania

Professional experience

06/2008	**Research visitor** at Open University UK, Department of Physics and Astronomy, group of Prof. N. Mason
02/2005 – present	**Teaching assistant** at University of Fribourg, Department of Chemistry, Switzerland
09/2001 – 02/ 2005	**Research technician** – "Petru Poni" Macromolecular Chemistry Institute Iasi, Romania
02/2003 – 08/2003	**Exchange student under the supervision of Prof. dr. Gérard Riess** University of Haute Alsace, Institute of Surfaces Chemistry and Interfaces, Group of Macromolecular Chemistry, Ecole Nationale Superieure de Chimie de Mulhouse (ENSCMu), France

Computer skills

Microsoft Office Suite, Gaussian, MathCAD, computer programming

Langues

Romanian- native
French- C1
English – C1

Research topics

Research areas	Experimental molecular physics, Electron Impact Spectroscopy, Mathematical Modeling of Chemical Structures and Processes, Experimental Design, Specific Equipment in Polymer Processing
Research projects:	Study of ageing process of polyurethanes, Mathematical modeling in polymer synthesis

Publications

1. A dramatic difference between the electron-driven dissociation of alcohols and ethers and its relation to Rydberg states, Bogdan C. Ibanescu and Michael Allan, *Phys.Chem.Chem.Phys.*, **2008**, DOI: 10.1039/b806578k

2. Absolute cross sections for dissociative electron attachment to acetylene and diacetylene, Olivier May, Juraj Fedor, Bogdan C. Ibanescu, Michael Allan, *Physical Review A: Atomic, Molecular, and Optical Physics* **2008**, *77(4, Pt. A)*

3. Differences in the cleavage of the ether bond by electron impact in linear ethers and in tetrahydrofuran, Bogdan C. Ibanescu, Olivier May and M. Allan, *Phys. Chem. Chem. Phys.* **2008**, *10*, 1507

4. Electron-induced chemistry of alcohols, Bogdan C. Ibanescu, Olivier May, Angèle Monney and Michael Allan, *Phys. Chem. Chem. Phys.* **2007**, *9*, 3163

5. Dissociative electron attachment and electron energy loss spectra of phenyl azide, S. Živanov, B. C. Ibanescu, M. Paech, M. Poffet, P. Baettig, A.-C. Sergenton, S. Grimme and M. Allan, *J. Phys. B: At. Mol. Opt. Phys.* **2007**, *40*, 101

6. The temperature dependence of dynamic viscosity for some vegetable oils used in alkyd resin synthesis, Constanta Ibanescu, C. Mihailescu, M. Daranga, Bogdan Catalin Ibanescu, Book of Proceedings a XVIII-a Conferinta internationala de inventică *"Cercetari si tehnologii inovative performante"* INVENT 2006, Iasi, Ed. Performantica 2006, pg. 415-421, ISBN (10) 973-730-231-1, ISBN (13): 978-973-730231-1

7. Controlled design of polymer materials based on poly[(N-acetylamino)ethylene] derivatives, Geta David, Bogdan Ibanescu, BRAMAT 2003, Book of Proceedings, vol. IV, Transilvania University Publishing House, 203-208

8. Modificatori reologici ai unor compoziţii de spălare (Rheological modifiers for some washing compositions), M.Lungu, C.Ibănescu, M.Dărangă, M.D.Vicol, C.Mihăilescu, B.C.Ibănescu, Revista Societăţii Române a Chimiştilor Cosmetologi (*RSSC Magazine*), Vol. 2, Nr. 4, 10-16 (2002); ISSN 1582-7011

Oral Presentations

1. Dissociative electron attachment in alcohools and ethers: Their relationship to Rydberg states, B.C. Ibanescu and M. Allan, 1st National Conference on Electronic, Atomic, Molecular and Photonic Physics – CEAMPP 2008, 15-18 May, Zaječar, Serbia

2. Electron-driven chemistry to ethers, Bogdan C. Ibanescu, Oliver May and Michael Allan, Swiss Chemical Society Fall Meeting, 12 September 2007, Lausanne

3. Site and selective chemistry in dea to compounds with amino and hydroxyl groups, EIPAM - Biomolecules, 24-29 June 2006, Obergurgl, Austria

Posters

1. Cleavage of the ether bond by electron impact: differences between linear ethers, tetrahydrofuran and alcohols, Bogdan Ibanescu, Olivier May and Michael Allan, LEEMI-EIPAM'08 -
Electron Induced Processes at Molecular Level Low-Energy Electron Molecule Interaction , 7-11 May 2008, Roscoff, France

2. Dissociative electron attachment of some cyclic diols, Bogdan Catalin Ibanescu, Olivier May, Michael Allan, ECAMP IX - 9th European Conference on Atoms, Molecules & Photons, 6-11 May 2007, Crete, Greece

3. Absolute angle-differential elastic and vibrational cross sections for electron collisions with tetrahydrofuran, Michael Allan and B. C. Ibanescu, ECAMP IX - 9th European Conference on Atoms, Molecules & Photons, 6-11 May 2007, Crete, Greece

4. Dissociative electron attachment to ethers, Bogdan C. Ibanescu, Olivier May and Michael Allan, XXV ICPEAC - XXV International Conference on Photonic, Electronic and Atomic Collisions, 25-31 July 2007, Freiburg, Germany

5. Electron-induced chemistry of alcohols, Oliver May, Bogdan C. Ibanescu and Michael Allan, XXV ICPEAC - XXV International Conference on Photonic, Electronic and Atomic Collisions, 25-31 July 2007, Freiburg, Germany

6. Dissociative electron attachment to ethers, Bogdan C. Ibanescu, Olivier May and Michael Allan, XV International Symposium on electron-molecule collisions and swarms, 1-4 August 2007, Reading, UK

7. Electron-induced chemistry of alcohols, Oliver May, Bogdan C. Ibanescu and Michael Allan, XV International Symposium on electron-molecule collisions and swarms, 1-4 August 2007, Reading, UK

8. Absolute angle-differential elastic and vibrational cross sections for electron collisions with tetrahydrofuran, Michael Allan and B. C. Ibanescu, XV International Symposium on electron-molecule collisions and swarms, 1-4 August 2007, Reading, UK

9. Elecron-driven chemistry of ethers, Bogdan C. Ibanescu, Oliver May and Michael Allan, Swiss Chemical Society Fall Meeting, 12 September 2007, Lausanne

10. State-selective chemistry, isotope effects, shape and feshbach resonances in dissociative electron attachment to alcohols and diols, Bogdan Catalin Ibanescu, Olivier May and Michael Allan, EIPAM - Biomolecules, 24-29 June 2006, Obergurgl, Austria

11. Site and state selective chemistry in dissociative electron attachment to compound containing the amino and the hydroxyl groups, Bogdan Catalin Ibanescu, Olivier May and Michael Allan, EIPAM - Biomolecules, 24-29 June 2006, Obergurgl, Austria

12. Site and state selective chemistry in dissociative electron attachment to 1-amino-2-hydroxyethane, Bogdan Catalin Ibanescu, Olivier May, Michael Allan, Swiss Chemical Society Fall Meeting, 13 October 2006, Zurich

13. Rydberg-like feshbach resonances in dissociative electron attachment, Bogdan Ibanescu, Svetlana Zivanov, Olivier May, Patric Oulevey and Michael Allan, 28th International Symposium on Free Radicals, 4-9 September 2005, Leysin, Switzerland